UNIVERSITY OF CALIFORNIA,
IRVINE

Synthesis of Chemically Modified TLR Agonists Used to Probe Innate and Adaptive Immune Responses

DISSERTATION

Submitted in partial satisfaction of the requirements
for the degree of

DOCTOR OF PHILOSOPHY

in Organic Chemistry

by

Janine K. Tom

Dissertation Committee:
Associate Professor Aaron Esser-Kahn, Chair
Associate Professor Jennifer Prescher
Professor Christopher Vanderwal

2016

DEDICATION

To

my Mom, Dad, and Family

for all of your love and support.

I could not have done it without you.

TABLE OF CONTENTS

LIST OF FIGURES

LIST OF SCHEMES

ACKNOWLEDGEMENTS

First, I would like to thank my Ph.D. advisor Prof. Aaron Esser-Kahn. It has been a great journey and exciting to see how the lab has grown from the beginning until now. I knew joining a new lab would be challenging, but also very rewarding. You challenged me to think outside of the box and put myself out there creatively. I have learned how to be a better scientist and have grown as a person. Thank you for your support, encouragement, and enthusiasm over the past five years. I cannot wait to see how the group and projects evolve in the years to come.

Next, I would like to thank Profs. Chris Vanderwal and Jennifer Prescher for sitting on my thesis committee. Both of you have helped and inspired me in ways that you cannot imagine. I greatly appreciate all of your time and support during my graduate career.

Thank you to the facilities, John, Beniam, and Phil for all of your help with analysis and characterization of our molecules.

I would like to thank the NSF, NIH, and DTRA for their financial support these past few years. Without funding, this research would not have been possible.

Thank you to the Esser-Kahn Group for all of your help scientifically as well as the fun times in and out of the lab. Thank you to the Dream Team, the original three; we have something special that I'll never forget. I would like to thank Hollie. You were my first undergraduate and a good friend. I appreciate all of your help, especially those first two years, and your positive and open attitude to learning. I would like to give a special thanks to Tyler for being an awesome bay mate and partner on this project. You will always be buddy number one (the o.g. buddy), and I will never forget all the good times and jokes we had. I will miss you very much and am excited to see all the great things you will do in the years to come. Thank you to Alfred for being my HPLC guru and friend. You were always there when I needed a good laugh. Seong-Min and Will, thank you for being good friends and part of our foodie family. Your positive attitudes were contagious, and I could always count on both of you when I needed support. I would like to thank Sam for all of your hard work and Arvind for the good laughs and conversations we had. Thank you to Troy and Beth for being amazing lab managers. You have been life savers on many occasions, and I cannot thank you enough for making things run smoothly in the lab. Thank you to Rachel, Alfred, and Tyler for taking time to read my thesis.

Thank you to all of my classmates that started in 2011. We survived that first year of classes and teaching together, and you all made it more bearable. I am especially thankful for Mariam and Emily. You were my besties through the good times and the tough times. We have been through a lot together, and I cannot wait to see where life takes us. Thank you to Dan, Udara, and Greg for all the good times and laughs. You always put a smile on my face and turned rough times into funny ones.

Thank you to Stan. We have been on this journey together for a good part of my time here. I appreciate all of your love and support, throughout all the good times as well as the hard times. You and your support mean the world to me.

Last, but certainly not least, I would like to express my deepest appreciation to my Mom, Dad, and family. You have supported me through everything. I could not imagine doing this without you. Thank you for listening to me when I needed to vent as well as celebrating all of my successes. You have always believed in me with your unconditional love and support. You taught me to be strong and do what makes me happy, and I thank you for that. I love you all so much. Thank you!

CURRICULUM VITAE

Janine K. Tom

EDUCATION

Ph.D. Organic Chemistry. University of California, Irvine. 2011-2016
Advisor: Aaron Esser-Kahn.
Thesis title: "Synthesis of Chemically Modified TLR Agonists Used to Probe Innate and Adaptive Immune Responses."

B.S. Chemistry and Minor in Art History. University of California, Santa Barbara. 2007-2011
High Honors, Phi Beta Kappa, and Dean's Honors. GPA: 3.77.
Advisor: Armen Zakarian.
Project title: "Synthesis of substrates for rhenium-catalyzed transposition of allylic alcohols."

RESEARCH EXPERIENCE

Esser-Kahn Lab. University of California, Irvine. Irvine, CA. 2011-2016
Graduate Student Researcher with Professor Aaron Esser-Kahn.

- Synthesize and characterize small molecule agonists and immune-stimulating bioconjugates to study the effect of immune agonist synergies on immune responses.
- Optimize synthetic routes and purifications of small molecules and bioconjugates.
- Test compounds *in vitro* (immune cell lines) and *in vivo* (mice) to examine effect on cytokine production and gene expression.
- Mentor two undergraduate researchers in synthetic organic chemistry and cell culture.

Centers for Disease Control and Prevention (CDC). Atlanta, GA. 2015
Oakridge Institute for Science and Education Intern with Dr. Carrie Pierce, Flu and Toxins Lab.

- Analyzed vaccine stability and antigen binding using immunocapture-isotope dilution mass spectrometry (IC-IDMS), under various physiochemical conditions.
- Performed protein digestions to isolate peptide antigen.
- Used LC-MS/MS to quantify the amount of antigen per stressed vaccine samples against isotope labeled peptide standards.

Zakarian Lab. University of California, Santa Barbara. Santa Barbara, CA. 2009-2011
Undergraduate Researcher with Professor Armen Zakarian.

- Synthesized oxazolidinone substrates for applications in total synthesis.
- Synthesized substrates for rhenium-catalyzed transposition of allylic alcohols method.

Goekjian Lab. Université Claude Bernard - Lyon 1, C.P.E. Lyon. Lyon, France. 2010
Undergraduate Summer Researcher with Professor Peter Goekjian.

- Worked on the total syntheses of natural products in the pyrrolizidine alkaloid family, Hyacinthacine A_3 and Broussonetine N.

Schimel Lab. University of California, Santa Barbara, Santa Barbara, CA. 2008-2010
Undergraduate Researcher with Professor Joshua Schimel.

- Studied carbon and nitrogen dynamics in California grassland and Alaskan soils.

SKILLS

- *Techniques:* synthetic organic chemistry, bioconjugation chemistry, purification (manual and automated column chromatography), analysis, and characterization of small molecules and bioconjugates, *in vitro* and *ex vivo* cell culture and assays, flow cytometry, ELISA, and gel electrophoresis (SDS-PAGE and agarose)
- *Instrumentation:* ^{1}H, ^{13}C, and 2D NMR, ESI-MS, FTIR, UV-Visible spectroscopy, high-performance liquid chromatography (HPLC), liquid chromatography mass spectrometry (LC-MS), matrix-assisted laser desorption ionization mass spectrometry (MALDI-TOF MS), and fast protein liquid chromatography (FPLC)

AWARDS

National Science Foundation Graduate Research Fellowship. 2012
Phi Lambda Upsilon Award 2011
University of California, Santa Barbara Honors Program Academic Excellence Award. 2011
Roche Bioscience Award. 2009

ADDITIONAL EXPERIENCES

Iota Sigma Pi-National Honors Society for Women in Chemistry. 2012-present
Vice President (2015), Secretary (2014), and Activities Coordinator (2013)

- Organize professional development seminars and events to promote women in STEM.
- Outreach: Ask-A-Scientist Night Mentor, Girls Inc. and National Chemistry Week Scientific Demonstration Leader

Safety Officer. Esser-Kahn Lab, University of California, Irvine. 2011-2016

- Maintain safety training for lab members, write chemical and process SOPs, and communicate with EHS about new safety protocols.

Organic Chemistry Laboratory Teaching Assistant. 2011-2012

- Taught six undergraduate organic chemistry lab courses.
- Topics included: Synthesis, purification, and analysis of organic compounds.

Family Ultimate Science Exploration Program Leader. 2010-2011

- Led scientific demonstrations for junior high school students to encourage interest in STEM fields.

PUBLICATIONS

1) **Tom, J.K.**; Dotsey, E.Y.; Wong, H.Y.; Stutts, L.; Moore, T.; Davies, D.H; Felgner, P.L; Esser-Kahn, A.P. Modulation of Innate Immune Responses *via* Covalently Linked TLR Agonists. *ACS Central Science,* **2015**, *1* (8), 439–448.

2) Lynn, G.M.; Laga, R.; Darrah, P.A.; Ishizuka, A.S.; Balaci, A.J.; Dulcey, A.E.; Pechar, M.; Pola, R.; Gerner, M.Y.; Yamomoto, A.; Buechler, C.R.; Quinn, K.M.; Smelkinson, M.G.; Vanek, O.; Cawood, R.; Hills, T.; Vasalatiy, O.; Kastenmuller, K.; Francica, J.R.; Stutts, L.; **Tom, J.K.**; Ryu, K.A.; Esser-Kahn, A.P.; Etrych, T.; Fisher, K.D.; Seymour, L.W.; Seder, R.A. Particle formation by polymer-bound TLR agonists is the principal physiochemical determinant for enhancing vaccine immunogenicity. *Nat. Biotech.*, **2015**, *33*, 1201-1210.

3) Ryu, K.A.; Stutts, L.; **Tom, J.K.**; Mancini, R.J.; Esser-Kahn, A.P. Stimulation of Innate Immune System by Light-Activated TLR7/8 Agonists. *J. Am. Chem. Soc.,* **2014**, *136*(31), 10823-10825.

4) Mancini, R.J.; Stutts, L.; Ryu, K.A.; **Tom, J.K.**; Esser-Kahn, A.P. Directing the Immune System with Chemical Structures. *ACS Chem. Bio.*, **2014**, *9*, 1075–1085.

5) Mancini, R.J.; **Tom, J.K.**; Esser-Kahn, A.P. Covalently Coupled Immunostimulant Heterodimers. *Angew. Chem. Int. Ed.*, **2014**, *53*, 189-192.
6) **Tom, J.K.**; Mancini, R.J.; Esser-Kahn, A.P. Covalent modification of cell surfaces with TLR agonists improves & directs immune stimulation. *Chem. Commun.*, **2013**, *49*, 9618-9620.
7) Herrmann, A.T.; Saito, T.; Stivala, C.E.; **Tom, J.**; Zakarian, A. Regio- and Stereocontrol in Rhenium-Catalyzed Transposition of Allylic Alcohols. *J. Am. Chem. Soc.*, **2010**, *132* (17), 5962–5963.

PATENTS

1) Mancini, R.J; **Tom, J.K.**; Esser-Kahn, A.P. Novel immunostimulants and synthesis thereof. U.S. Patent 20150050313, filed August 13, 2014, and issued February 19, 2015.

PRESENTATIONS

1) *Development of a tri-agonist compound library used to determine optimal adjuvanticity of a Q fever vaccine.* American Association of Immunologiest (AAI) 2016 National Meeting. Seattle, WA. May 2016. Poster Presentation.
2) *Synthesis of a tri-agonist compound library used to evaluate innate and adaptive immune responses.* American Chemical Society (ACS) Spring 2016 National Meeting. San Diego, CA. March 2015. Oral Presentation.
3) *H1N1 Hemagglutinin Temperature and pH Stability Studies Correlating IC-IDMS and SRID Methods*. Toxins and Flu Lab Seminar, Clinical Chemistry Branch, Division of Laboratory Sciences (DLS), Centers for Disease Control and Prevention (CDC), Atlanta, Georgia. August 2015. Oral Presentation.
4) *H1N1 Hemagglutinin Temperature and pH Stability Studies Correlating IC-IDMS and SRID Methods*. Division of Laboratory Sciences (DLS) Summer Symposium, Centers for Disease Control and Prevention (CDC), Atlanta, Georgia. August 2015. Poster Presentation.
5) *Analysis of Influenza Vaccines using Immunocapture Isotope Dilution Mass Spectrometry*. Division of Laboratory Sciences (DLS) Summer Symposium, Centers for Disease Control and Prevention (CDC), Atlanta, Georgia. August 2015. Poster Presentation.
6) *Application of multi-agonist scaffolds to modulate antigen presentation and adaptive immunity*. American Chemical Society (ACS) Spring 2015 National Meeting. Denver, CO. March 2015. Oral Presentation.
7) *A Multi-Agonist Core used to Study Synergies in Immune System Stimulation*. UC Irvine Immunology Fair 2014. University of California, Irvine. November 2014. Poster Presentation.
8) *Synthesis and application of a multi-agonist triazine core used to study synergies in immune system stimulation.* American Chemical Society (ACS) Fall 2014 National Meeting. San Francisco, CA. August 2014. Oral Presentation.
9) *Covalent Modification of Cell Surfaces with TLR Agonists Improves & Directs Immune Stimulation*. UC Irvine Immunology Fair 2013. University of California, Irvine. November 2013. Oral and Poster Presentations.
10) *Redirecting the Immune System Using Chemical Methods to Create an Agonist Façade on Lewis Lung Carcinoma*. Materials Research Society (MRS) Spring 2013 Meeting. San Francisco, CA. April 2013. Poster Presentation.
11) *Immune Programming: Using Polymeric Linkers to Create an Agonist Façade on Target Cell Surfaces*. Graduate Student Colloquium. University of California, Irvine. January 2013. Oral Presentation.

12) *Studies Toward the Synthesis of Hyacinthacines, Broussonetines, and their Analogues*. American Chemical Society (ACS) Fall 2010 National Meeting. Boston, MA. August 2010. Poster Presentation.

AFFILIATIONS

American Chemical Society
American Association of Immunologists

ABSTRACT OF THE DISSERTATION

Synthesis of Chemically Modified TLR Agonists
Used to Probe Innate and Adaptive Immune Responses

By

Janine K. Tom

Doctor of Philosophy in Organic Chemistry

University of California, Irvine, 2016

Associate Professor Aaron Esser-Kahn, Chair

The development of vaccines has resulted in a dramatic decrease in the number of cases of diseases, such as measles and smallpox. With the emergence of Ebola and the Zika virus, there is a greater need for the development of more effective and safer vaccines. However, the challenge with designing new immunotherapies is that little is still known about how vaccines work, since most have been empirically determined. Thus, our group is interested in using chemical tools to probe and understand the immune response with the goal of designing more effective vaccines. Dendritic cells, a vital part of the innate immune system, contain Toll-like receptors (TLRs) that are activated by components of pathogens, such as bacterial oligonucleotides and lipopeptides. These molecules are immune agonists that can act as adjuvants, which help elicit or enhance an immune response toward a non-immunogenic protein antigen, and are commonly used in vaccines. Recent studies indicate that vaccines containing multiple TLR agonists enhance the immune response toward a target pathogen compared to the use of a single ligand. A prime example is the Yellow Fever Vaccine, one of the most successful vaccines, which activates the immune system through four different TLRs. Due to this precedence, we hypothesized that activating specific receptors in a precise spatial manner could

modulate how the immune system responds by mimicking natural pathogens and therefore control downstream pathways. My research focuses on synthesizing multi-TLR agonist conjugates to study the spatial organization of multiple TLR agonists and how different combinations of agonists affect the immune response, as observed by cellular and antibody responses. To study the effect of multiple TLR agonists on the immune response, we chemically modified whole cell antigens with different TLR agonists as well as covalently conjugated multiple TLR agonists together to present them in a localized manner. As a result of chemical modification and linkage, we observed distinct changes in immune activation, *via* cytokine production and antibody responses, suggesting implications for downstream immune system signaling. We are applying our findings to more rationally develop safer and more effective vaccine adjuvants and immunotherapies.

CHAPTER 1

Introduction

1.1 Introduction

Vaccines are one of the most effective forms of immunotherapy for disease prevention, treatment, and elimination.[1] These treatments work by activating one's immune system toward a target pathogen. Traditionally, vaccines involve administration of the pathogen in one of the following forms: an attenuated or inactivated version of the pathogen *via* heat, UV, or formalin-inactivation, or as a subunit vaccine, in which a recombinant protein or peptide fragment associated with the pathogen is used.[2,3] However, with these vaccination methods, there are challenges with low immunogenicity, resulting in low efficacy of some vaccines. In addition, most vaccines are empirically derived, with little being known or understood about the mechanism of action, making it difficult to rationally and rapidly develop new vaccines. These challenges make it difficult to develop vaccines for prevalent diseases, including malaria and HIV, that do not have effective cures.

In the Esser-Kahn Lab, we are interested in probing the immune response using synthetic chemical tools to understand how the immune system responds to pathogens. Stimulation of multiple, different immune receptors enhances immune activation, and this type of immune activation is known as an "immune synergy." Utilizing chemical tools for immunological research, we can covalently conjugate different combinations of immune agonists together to chemically manipulate the immune response. Covalent conjugation of multiple agonists mimics natural pathogens better than a single ligand or multiple agonists unconjugated in solution, as pathogens contain multiple immune agonists in a distinct spatial arrangement. Different combinations of immunostimulatory molecules are sensed as distinct molecular "codes" that

result in a specific immune response. We can use these chemical tools or codes to determine how multiple molecular agonists affect the immune response, to understand the mechanism of action behind synergistic immune activation, and to aid in the more rational development of vaccines.

1.2 The Innate and Adaptive Immune Systems

To study the immune system, we are interested in synthetically modifying specific immune agonists to activate and control the immune response in order to understand how the immune system functions at the fundamental and applied levels. The immune system is comprised of the innate and adaptive immune responses, the body's rapid and long term responses to pathogens, respectively, which work together to protect one against bacteria and viruses (**Fig. 1.1**). Innate immune cells include antigen-presenting cells (APCs), such as dendritic cells and macrophages.[4–8] APCs express pattern recognition receptors (PRRs) that are activated by molecular components of pathogens called pathogen-associated molecular patterns (PAMPs).[9] PRRs are important targets for vaccine development because native pathogens activate PRRs, resulting in effective immune responses against a given target. Pathogen-associated molecules are immune agonists that range from single stranded DNA (ssDNA) to lipopeptides to small molecules. Our aim is to chemically modify these immune agonists, specifically Toll-like Receptor (TLR) agonists, to study how different molecular agonists affect innate immune system activation. By controlling how immune agonists stimulate the innate immune system using chemical modifications, we can alter the adaptive immune response and learn information that can be applied to designing more effective vaccines.

Figure 1.1 Innate and Adaptive Immune Systems and Responses

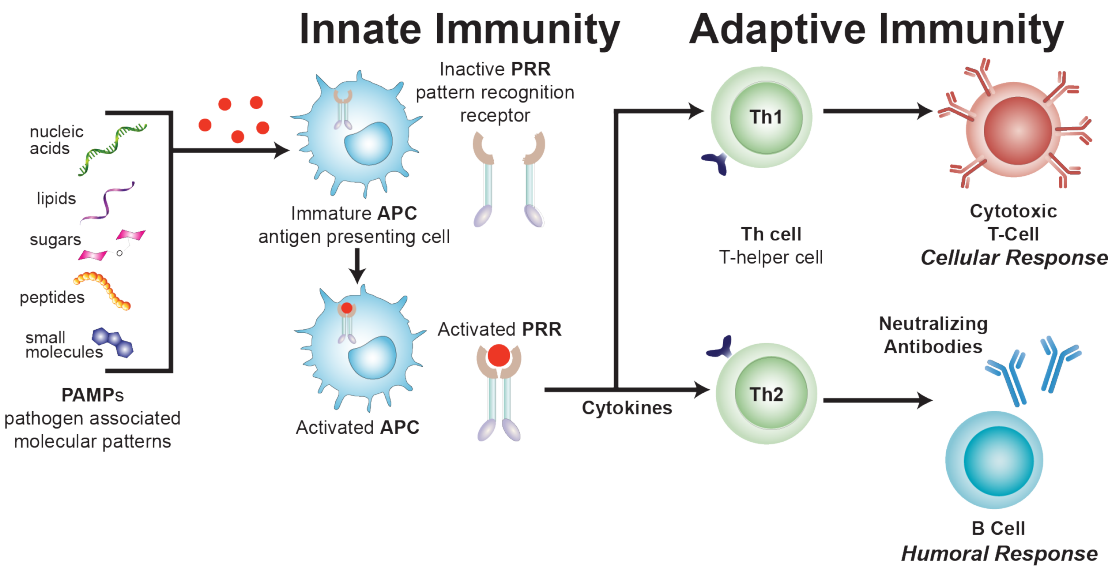

The interaction between innate and adaptive immune responses impacts the body's protective response to foreign pathogens. This immune response is affected by the chemical identity of the immune agonist and the corresponding receptor activated. Some classes of PAMPs, like TLR agonists, initiate the immune signaling cascade by activating a PRR, resulting in immune receptor dimerization with another PRR to form either a homo- or heterodimer.[10,11] The dimeric complex then recruits specific adaptor proteins, initiating an immune signaling cascade that leads to the activation of different transcription factors and subsequent upregulation of cell surface proteins and production of signaling cytokines.

These protein biomarkers and cell signaling molecules are used to communicate with the adaptive immune system, which is comprised of T and B cells and maintains the body's long term immune response through cytokine and antibody responses. T cells can be differentiated into several subsets, with different types of T cells polarizing the immune response down distinct pathways. Two major types of T cell responses are T_H1 and T_H2, which correspond to cellular and humoral or antibody responses, respectively (**Fig. 1.1**).[5,8] Cellular immune responses involve

activation of innate immune cells and T cells that respond to and attack foreign pathogens. In contrast, humoral responses entail B cell activation and the production of antibodies against the target pathogen. Depending on the bacteria or virus of interest, one or both types of immune responses are required to effectively combat the pathogen. Since distinct immune responses are necessary to fight off certain pathogens, the ability to activate specific immune cell populations and responses using chemically modified agonists is a powerful tool. Chemical tools provide a method to control the immune response at the molecular level, affecting the biochemical and physiological responses, and leading to the design of more targeted and effective therapies.

1.3 Toll-like Receptors (TLRs), TLR Agonists, and their Role as Adjuvants

Toll-like receptors (TLRs) are one of the most well characterized classes of PRRs, with 10 known TLRs in human and 12 in mice (**Fig. 1.2**).[12–17] The name "Toll-like" originates from the Toll gene in *Drosophila* in which the TLR homology of the human receptor is similar to that in the fruit fly. TLRs are composed of two main parts, the extracellular region and the cytoplasmic region.[12,14] The extracellular region contains leucine rich repeats (LRRs) and protrudes from the cell membrane in a question mark-like shape. The LRR region is where agonist binding occurs, and the binding motif varies between different TLRs.[18] In contrast, the cytoplasmic tail of the receptor, the Toll/IL-1R (TIR domain), is conserved among all TLRs. When an agonist binds to the ectodomain of a TLR, a structural change in the TIR domain occurs. Then, the TIR domains of two TLRs move closer in proximity to form a homo- or heterodimeric complex, which recruits adaptor proteins to initiate a signaling cascade.[12,14,15]

Figure 1.2 Toll-like Receptors, TLR Agonists, and Signaling Pathways

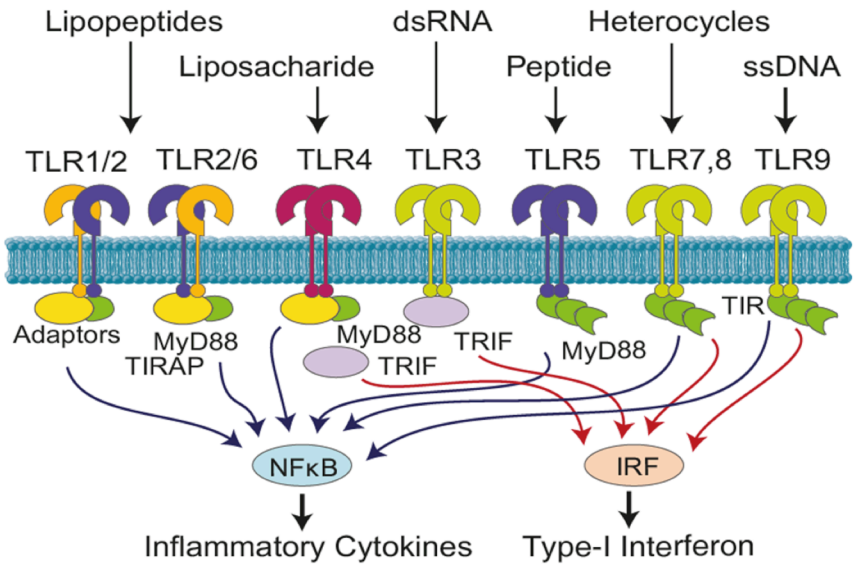

These receptors are interesting targets due to the wide range of agonists that activate the TLR signaling cascade, ranging from oligonucleotides to bacterial cell wall components. The first nine TLRs are the most studied and best characterized, where TLRs 1, 2, 4, 5, and 6 are located on the cell surface and TLRs 3, 7, 8, and 9 are in the endosome.[13,16,19] The cellular location of the TLRs corresponds to the types of ligands recognized. Cell surface TLRs recognize bacterial cell wall components (lipids, lipopeptides, and proteins) and endosomal TLRs bind to pathogen-derived nucleic acids (ssDNA, ssRNA, and dsRNA). Different TLR agonists are associated with specific signaling pathways and transcription factors, resulting in distinct cellular and antibody immune responses.

Many PAMPs, including TLR agonists, are used as vaccine adjuvants to enhance and elicit specific immune responses against a co-administered antigen. Adjuvants are needed because an attenuated or inactivated pathogen may not induce an effective or complete immune response against the target pathogen compared to the native pathogen.[20–25] In addition, the peptide antigens used in subunit vaccines tend to be minimally immunogenic or non-

immunogenic. Thus, adjuvants are required to boost the immune response toward the desired antigen. Alum, which is composed of aluminum hydroxide and aluminum phosphate, and Freund's adjuvant, a water in oil emulsion containing heat-killed *Mycobacterium tuberculosis*, were the first two adjuvants used in vaccines.[21,24] However, unwanted inflammation and side effects have been observed with these adjuvants. Alum and Freund's adjuvant also bias toward eliciting strong antibody responses and weak cellular responses. These effects are unfavorable as targeted inflammation is preferred over systemic inflammation in order to elicit an effective immune response. In addition, both antibody and cellular responses are required to eliminate many pathogens successfully.

TLR agonists are at the forefront of adjuvant discovery because their administration tends to elicit a strong cellular T_H1 response in addition to antibody responses.[22,23] As previously mentioned, successful vaccines elicit both cellular and antibody responses to target specific diseases and provide effective immune responses. Additionally, in terms of structure and composition, TLR agonists are defined molecular entities, providing more homogeneous vaccine formulations. As a result, researchers can parse out information about their role as vaccine adjuvants and their effect on immune signaling pathways, as opposed to the entire pathogen, which is more heterogeneous. Some TLR agonists, such as MPLA (TLR4 agonist), CpG-DNA (TLR9 agonist), imidazoquinolines (TLR7 agonist), and flagellin (TLR5 agonist), are being used in clinical studies to treat diseases ranging from Hepatitis B to melanoma.[21,26,27] Thus far, the success with TLR agonists as adjuvants demonstrates promise for new adjuvant discovery and formulation.

1.4 Immune Synergies: Administration of Multiple TLR Agonists

Unfortunately, individual TLR agonists are not always as effective as whole pathogens at eliciting an effective immune response and at high doses can cause unwanted inflammation and systemic toxicity. Recently, administering multiple TLR agonists together to study TLR immune synergies has resulted in enhanced immune responses, more efficacious protection, and dose sparing.[11,28–30] For example, Pulendran, *et al*.[31] reported studies on the yellow fever virus vaccine, one of the most successful vaccines due to the prolonged and targeted immune response elicited. Only after the empirical discovery of the vaccine did they discover that the vaccine activated four different TLRs (TLR2, 7, 8, and 9), which contributed to the success of the vaccine.[32] Furthermore, Napolitani, *et al*.[33] introduced a temporal component to study immune synergies by adding two different TLR agonists at specific time intervals. By spacing out the agonist incubation times, they found that the order of addition of certain agonist combinations resulted in enhanced cytokine and gene production, where as other combinations did not.

Presently, chemistry and engineering methods are being used to address immunological questions that cannot be solved solely by biological methods. For example, Hubbell, *et al*.[34] fabricated a microfluidic chip that probed a wide array of cytokine responses from 10 different TLR adjuvants. Using this device, they determined which pairs of agonists produced a synergistic increase as well as inhibitory decrease in specific cytokines. Not only were changes in cytokine responses observed, but also increases in antibody breadth and depth. Research performed by Fox, *et al*.[35] demonstrated that delivery of TLR4 and TLR7 agonists in a nanoliposome formulation impacted antibody and cytokine responses. As a result, they developed a manufacturable adjuvant formulation for clinical trials. Each of these studies

showcases how immune agonist synergies modulates the immune response and will be significant for improved adjuvant development and new vaccine discovery.

Despite enhanced immune responses when administering multiple TLR agonists, little is still known about mechanism behind these enhanced responses. Currently, there are several proposed mechanisms.[28,36] One main hypothesis involves cooperative signaling between the two adaptor proteins Myeloid Differentiation Primary Response 88 (MyD88) and TIR-domain-containing adapter-inducing interferon-β (TRIF).[37,38] MyD88 and TRIF adaptor proteins are recruited to the TIR domains of the dimeric TLRs after TLRs are activated. This recruitment then initiates MyD88 and TRIF signaling pathways. Studies have shown that activation of both pathways is required for synergistic immune activation, providing a strong case for this proposed mechanism of action. The cooperation between the two adaptor proteins MyD88 and TRIF may only be a contributing factor, and there are other potential immune signaling components that may cause immune synergy. Investigating the mechanism of action is an ongoing and debated field of research.

1.5 Application of Synthetic Chemistry to Synergistic Adjuvant Discovery

Many different TLR agonist combinations influence immune signaling pathways in both spatially and temporally dependent manners. Until recently, understanding how the spatial organization of multiple TLR agonists affects TLR activation and the overall immune response has been difficult, as probing synergies has been limited to combining mixtures of TLR agonists in solution. However, the mixture of unconjugated agonists does not recreate the defined spatial arrangement of native agonists present in a pathogen. To probe and elucidate the mechanism of action behind immune synergies, synthetic chemistry is being applied to covalently conjugate immune agonists together.[39–41] As a result of covalent linkage, the immunostimulatory molecules

are localized and delivered as one entity to the immune system, as opposed to unconjugated agonists that suffer from diffusion in solution. This spatial confinement allows researchers to study how multiple immunostimulatory agonists affect the immune response, like in a native pathogen, and looking at the role of each specific molecule. Determining the optimal immune response from a given molecule will enable adjuvant discovery and provide knowledge to direct the immune response to a specific target.

Figure 1.3 Chemical Modifications of Whole Tumor Cell Antigens with TLR Agonists[a] and Synthesis of Di- and Tri-TLR Agonist Conjugates[b,c]

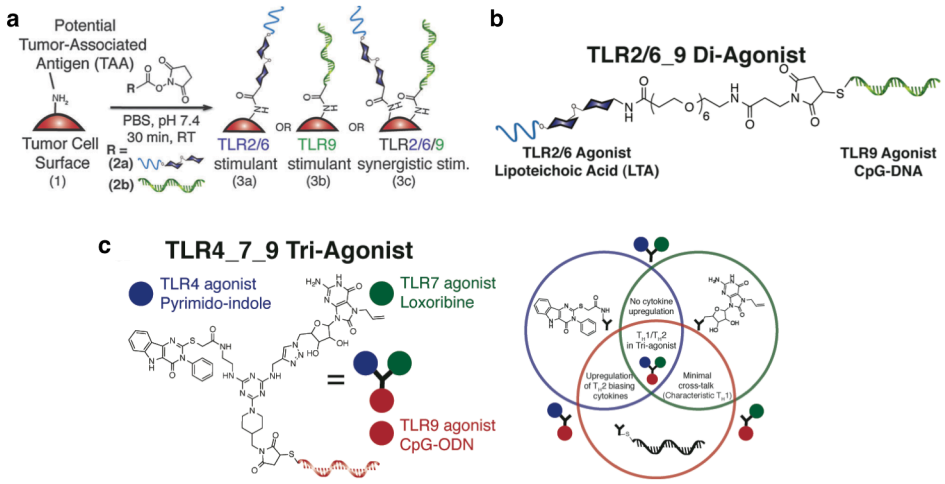

[a] Synthetic modification of whole tumor cell antigens with either one or two different TLR agonist(s) used to enhance immunogenicity. [b] Chemical structure of a TLR2/6_9 di-agonist used to study how linking two different TLR agonists with a defined linker length affects immune activation. [c] Chemical structure of a TLR4_7_9 tri-agonist and how each TLR agonist contributed to immune activation.

The main method used to study TLR synergy was to administer two agonists unconjugated in solution, neglecting the spatial organization of native pathogens detected by the immune system. Therefore, we sought to study the spatial arrangement of distinct TLR agonists using two different methods. Chapters 2 and 3 of this dissertation discuss the study of immune synergies with two different TLR agonists. The first approach involves covalently modifying non-immunogenic whole tumor cell antigens with two different agonists compared to the use of a

single agonist. In the second method, we covalently linked two TLR agonists together to observe how spatial confinement affected immune responses. We observed in both cases an increase in NF-κB activation, dendritic cell surface markers, and cytokines produced by dendritic cells, all components necessary for an effective adaptive immune response. Thus, these adjuvant approaches show promise for cancer immunotherapies and novel adjuvant discovery.

Chapters 4 and 5 discuss our work to expand the immune synergy studies to treatment with three different agonists, since the components of many successful vaccines activate three to five TLRs. Thus, to gain a better understanding of TLR synergies, we covalently linked three agonists together allowing spatially defined activation of three distinct TLRs. We observed that treatment with the tri-agonist compound produced a distinct array of cytokines and immune-related gene expression *in vitro*. This activity also translated *in vivo* to generate a wider set of antibodies against a model vaccinia vaccine. Currently, we are synthesizing a library of tri-agonist compounds to determine how different agonist combinations affect the immune response *in vitro* and in an *in vivo* vaccination model. Our progress thus far is discussed. These studies demonstrate how activation of multiple TLRs through chemically and spatially defined organization assists in guiding immune responses, providing the potential to use chemical tools to design and develop more effective vaccines.

1.6 Conclusion

Immune synergies are becoming an area of research with significant impact on vaccine design and development. Here, we report and discuss our work using synthetic chemistry to modify whole cell antigens with a synergistic combination of TLR agonists and to conjugate TLR agonists together. Treatment with either type of conjugate resulted in immune response modulation, *via* cellular and antibody responses, which is promising for applications in adjuvant

discovery. Our compounds are currently being used as vaccine adjuvants in vaccination model studies with the aim of developing more effective vaccines toward target pathogens.

1.7 References

(1) Roush, S. W. Historical Comparisons of Morbidity and Mortality for Vaccine-Preventable Diseases in the United States. *JAMA* **2007**, *298* (18), 2155.
(2) De Gregorio, E.; Rappuoli, R. From Empiricism to Rational Design: A Personal Perspective of the Evolution of Vaccine Development. *Nat. Rev. Immunol.* **2014**, *14* (7), 505–514.
(3) Plotkin, S. History of Vaccination. *Proc. Natl. Acad. Sci.* **2014**, *111* (34), 12283–12287.
(4) Hoebe, K.; Janssen, E.; Beutler, B. The Interface between Innate and Adaptive Immunity. *Nat. Immunol.* **2004**, *5* (10), 971–974.
(5) Jr, C. A. J.; Travers, P.; Walport, M.; Shlomchik, M. J.; Jr, C. A. J.; Travers, P.; Walport, M.; Shlomchik, M. J. *Immunobiology*, 5th ed.; Garland Science, 2001.
(6) Janeway, C. A.; Medzhitov, R. Innate Immune Recognition. *Annu. Rev. Immunol.* **2002**, *20* (1), 197–216.
(7) Medzhitov, R.; Janeway Jr, C. A. Innate Immunity: Impact on the Adaptive Immune Response. *Curr. Opin. Immunol.* **1997**, *9* (1), 4–9.
(8) Iwasaki, A.; Medzhitov, R. Control of Adaptive Immunity by the Innate Immune System. *Nat. Immunol.* **2015**, *16* (4), 343–353.
(9) Mogensen, T. H. Pathogen Recognition and Inflammatory Signaling in Innate Immune Defenses. *Clin. Microbiol. Rev.* **2009**, *22* (2), 240–273.
(10) Takeuchi, O.; Akira, S. Pattern Recognition Receptors and Inflammation. *Cell* **2010**, *140* (6), 805–820.
(11) Cao, X. Self-Regulation and Cross-Regulation of Pattern-Recognition Receptor Signalling in Health and Disease. *Nat. Rev. Immunol.* **2016**, *16* (1), 35–50.
(12) Akira, S.; Takeda, K. Toll-like Receptor Signalling. *Nat. Rev. Immunol.* **2004**, *4* (7), 499–511.
(13) Takeda, K.; Kaisho, T.; Akira, S. Toll-like Receptors. *Annu. Rev. Immunol.* **2003**, *21*, 335–376.
(14) Beutler, B. A. TLRs and Innate Immunity. *Blood* **2009**, *113* (7), 1399–1407.
(15) Akira, S.; Takeda, K.; Kaisho, T. Toll-like Receptors: Critical Proteins Linking Innate and Acquired Immunity. *Nat. Immunol.* **2001**, *2* (8), 675–680.
(16) Barton, G. M.; Kagan, J. C. A Cell Biological View of Toll-like Receptor Function: Regulation through Compartmentalization. *Nat Rev Immunol* **2009**, *9* (8), 535–542.
(17) Barton, G. M.; Medzhitov, R. Control of Adaptive Immune Responses by Toll-like Receptors. *Curr. Opin. Immunol.* **2002**, *14* (3), 380–383.
(18) Botos, I.; Segal, D. M.; Davies, D. R. The Structural Biology of Toll-like Receptors. *Structure* **2011**, *19* (4), 447–459.
(19) Gay, N. J.; Symmons, M. F.; Gangloff, M.; Bryant, C. E. Assembly and Localization of Toll-like Receptor Signalling Complexes. *Nat. Rev. Immunol.* **2014**, *14* (8), 546–558.
(20) Coffman, R. L.; Sher, A.; Seder, R. A. Vaccine Adjuvants: Putting Innate Immunity to Work. *Immunity* **2010**, *33* (4), 492–503.

(21) Reed, S. G.; Bertholet, S.; Coler, R. N.; Friede, M. New Horizons in Adjuvants for Vaccine Development. *Trends Immunol.* **2009**, *30* (1), 23–32.
(22) Reed, S. G.; Orr, M. T.; Fox, C. B. Key Roles of Adjuvants in Modern Vaccines. *Nat. Med.* **2013**, *19* (12), 1597–1608.
(23) Kanzler, H.; Barrat, F. J.; Hessel, E. M.; Coffman, R. L. Therapeutic Targeting of Innate Immunity with Toll-like Receptor Agonists and Antagonists. *Nat. Med.* **2007**, *13* (5), 552–559.
(24) Petrovsky, N.; Aguilar, J. C. Vaccine Adjuvants: Current State and Future Trends. *Immunol. Cell Biol.* **2004**, *82* (5), 488–496.
(25) Steinhagen, F.; Kinjo, T.; Bode, C.; Klinman, D. M. TLR-Based Immune Adjuvants. *Vaccine* **2011**, *29* (17), 3341–3355.
(26) Guy, B. The Perfect Mix: Recent Progress in Adjuvant Research. *Nat. Rev. Microbiol.* **2007**, *5* (7), 505–517.
(27) Engel, A. L.; Holt, G. E.; Lu, H. The Pharmacokinetics of Toll-like Receptor Agonists and the Impact on the Immune System. *Expert Rev. Clin. Pharmacol.* **2011**, *4* (2), 275–289.
(28) Tan, R. S. T.; Ho, B.; Leung, B. P.; Ding, J. L. TLR Cross-Talk Confers Specificity to Innate Immunity. *Int. Rev. Immunol.* **2014**, *33* (6), 443–453.
(29) Trinchieri, G.; Sher, A. Cooperation of Toll-like Receptor Signals in Innate Immune Defence. *Nat. Rev. Immunol.* **2007**, *7* (3), 179–190.
(30) Zhu, Q.; Egelston, C.; Vivekanandhan, A.; Uematsu, S.; Akira, S.; Klinman, D. M.; Belyakov, I. M.; Berzofsky, J. A. Toll-like Receptor Ligands Synergize through Distinct Dendritic Cell Pathways to Induce T Cell Responses: Implications for Vaccines. *Proc. Natl. Acad. Sci.* **2008**, *105* (42), 16260–16265.
(31) Pulendran, B. Learning Immunology from the Yellow Fever Vaccine: Innate Immunity to Systems Vaccinology. *Nat. Rev. Immunol.* **2009**, *9* (10), 741–747.
(32) Querec, T.; Bennouna, S.; Alkan, S.; Laouar, Y.; Gorden, K.; Flavell, R.; Akira, S.; Ahmed, R.; Pulendran, B. Yellow Fever Vaccine YF-17D Activates Multiple Dendritic Cell Subsets via TLR2, 7, 8, and 9 to Stimulate Polyvalent Immunity. *J. Exp. Med.* **2006**, *203* (2), 413–424.
(33) Napolitani, G.; Rinaldi, A.; Bertoni, F.; Sallusto, F.; Lanzavecchia, A. Selected Toll-like Receptor Agonist Combinations Synergistically Trigger a T Helper Type 1-Polarizing Program in Dendritic Cells. *Nat. Immunol.* **2005**, *6* (8), 769–776.
(34) Garcia-Cordero, J. L.; Nembrini, C.; Stano, A.; Hubbell, J. A.; Maerkl, S. J. A High-Throughput Nanoimmunoassay Chip Applied to Large-Scale Vaccine Adjuvant Screening. *Integr. Biol. Quant. Biosci. Nano Macro* **2013**, *5* (4), 650–658.
(35) Fox, C. B.; Sivananthan, S. J.; Duthie, M. S.; Vergara, J.; Guderian, J. A.; Moon, E.; Coblentz, D.; Reed, S. G.; Carter, D. A Nanoliposome Delivery System to Synergistically Trigger TLR4 AND TLR7. *J. Nanobiotechnology* **2014**, *12* (1), 17.
(36) Liu, Q.; Ding, J. L. The Molecular Mechanisms of TLR-Signaling Cooperation in Cytokine Regulation. *Immunol. Cell Biol.* **2016**, *94* (6), 538–542.
(37) Ting Tan, R. S.; Lin, B.; Liu, Q.; Tucker-Kellogg, L.; Ho, B.; Leung, B. P.; Ding, J. L. The Synergy in Cytokine Production through MyD88-TRIF Pathways Is Co-Ordinated with ERK Phosphorylation in Macrophages. *Immunol. Cell Biol.* **2013**, *91* (5), 377–387.
(38) Bagchi, A.; Herrup, E. A.; Warren, H. S.; Trigilio, J.; Shin, H.-S.; Valentine, C.; Hellman, J. MyD88-Dependent and MyD88-Independent Pathways in Synergy, Priming, and

Tolerance between TLR Agonists. *J. Immunol. Baltim. Md 1950* **2007**, *178* (2), 1164–1171.
(39) Mancini, R. J.; Tom, J. K.; Esser-Kahn, A. P. Covalently Coupled Immunostimulant Heterodimers. *Angew. Chem. Int. Ed Engl.* **2014**, *53* (1), 189–192.
(40) Modulation of Innate Immune Responses via Covalently Linked TLR Agonists - ACS Central Science (ACS Publications) http://pubs.acs.org/doi/full/10.1021/acscentsci.5b00274 (accessed Oct 16, 2016).
(41) Pavot, V.; Rochereau, N.; Rességuier, J.; Gutjahr, A.; Genin, C.; Tiraby, G.; Perouzel, E.; Lioux, T.; Vernejoul, F.; Verrier, B.; et al. Cutting Edge: New Chimeric NOD2/TLR2 Adjuvant Drastically Increases Vaccine Immunogenicity. *J. Immunol.* **2014**, *193* (12), 5781–5785.

CHAPTER 2

Covalently Modifying Whole Cell Antigen Surfaces with Multiple Toll-Like Receptor (TLR) Agonists

2.1 Introduction

Cell-based therapies are gaining widespread use in the vaccination field, where immune cells are redirected or programmed to fight and eliminate targeted pathogens. This method has been highly utilized for targeting tumors and treating different types of cancer.[1–3] Since antigen-presenting cells (APCs), such as dendritic cells, are the body's first line of defense, there has been a major push to create dendritic cell-based cancer therapies or modified tumor cells that activate the innate immune system.[4,5] These therapies tend to contain one kind of immune agonist that stimulates and signals only one type of PRR on an immune cell, resulting in a partial immune response. In contrast, many effective vaccines, such as the yellow fever vaccine,[6] are comprised of several molecular signals that interact with multiple PRRs to elicit a robust immune response.[7–11] Our efforts to study the effect of administering multiple immune signals with a whole tumor cell antigen are described here.

Targeting antigens with immune agonists is an important aspect of effective vaccines.[12,13] The chemical identity of a stimulating signal and its proximity to target antigens enhance the efficacy of a therapy by eliciting a specific immune response that is both directed and prolonged. Spatially constraining immune agonists, such as TLR agonists, to an antigenic peptide or whole cell antigen aids in localized delivery of the antigen and stimulatory signal. Several methods used to localize antigens and agonists for cancer immunotherapies include lipid anchoring and physical entrapment of a single molecular signal on tumor cells and are known to enhance the immune response.[4,5,14] By spatial confinement and close proximity of the agonist and antigen, an

increase in tumor targeting and decrease in tumor growth were observed. However, the covalent attachment of multiple, synergistic agonist combinations to whole cell antigens has not been attempted.

Figure 2.1 Diagram Illustrating Synthesis of TLR Agonist Modified Lewis Lung Carcinoma[a]

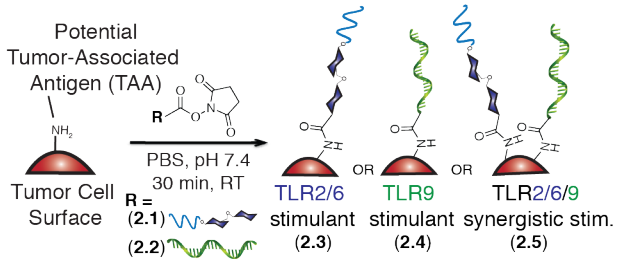

[a] Conjugation of NHS-LTA (2.1), NHS-CpG-DNA (2.2), and both NHS-LTA and NHS-CpG-DNA to Lewis Lung Carcinoma (LLC) cell surfaces *via* a polyethylene glycol $(PEG)_6$ linker in phosphate buffer (pH 7.4) for 30 min at RT.

Here, we report the use of a polymeric linker to covalently modify Lewis Lung Carcinoma (LLC) with lipoteichoic acid (LTA – TLR2/6 agonist) and CpG-DNA (CpG – TLR9 agonist) (**Fig. 2.1**).[15–19] We were interested if direct, chemical modification of cell surface proteins would enhance stimulation and if the synergistic combination of agonists would increase immune activation or direct the immune response. In these studies, we found that TLR agonist-labeled LLCs upregulated cell surface marker expression, critical for T cell activation. The multi-TLR agonist-labeled constructs also modulated cytokine production, allowing for the potential to design targeted vaccines. We also observed the macrophagocytosis of our TLR agonist-labeled cells, indicating a potential mechanism by which the immune-stimulating constructs are presented to an endosomal TLR9. The direct, covalent attachment of LTA and CpG to cell surface proteins on tumor cells enhanced dendritic cell activation compared to the non-immunogenic tumor cells alone. Our approach demonstrates the significance of directly and

chemically conjugating TLR agonist signals to target cell antigens as well as the use of multiple TLR agonists in developing more effective vaccines.

2.2 Synthesis of TLR Agonists Conjugated to a Bi-Functional PEG_6 Linker

To modify cell surfaces with immune agonists, we aimed to synthesize TLR agonist–polymer conjugates that react with free amines on cell surfaces (**Scheme 2.1**). TLR agonists were used due to their potency and use in vaccination studies. LTA and CpG-DNA were chosen as the initial TLR agonists. CpG-DNA is a 20 base pair sequence of single stranded DNA (ssDNA) containing cytosine-guanosine repeats.[17] The cytosine-guanosine repeats are the stimulatory portion of the molecule that target TLR9 in the endosome. On the other hand, LTA is located on the cell surface of Gram-positive bacteria and targets TLR2 and TLR6.[15,16] LTA is a biopolymer with a phosphate backbone, varying units of alanine and *N*-acetylglucosamine (GlcNAc), and two lipid chains. The two lipid chains, common to most TLR2 agonists, are the stimulatory component of the molecule.[20] These two TLR agonists were used, since they are potent TLR agonists and often exhibit a synergistic effect when used in combination.[7,21,22]

Scheme 2.1 Bioconjugation of TLR Agonists to NHS-PEG_6-Maleimide Linker

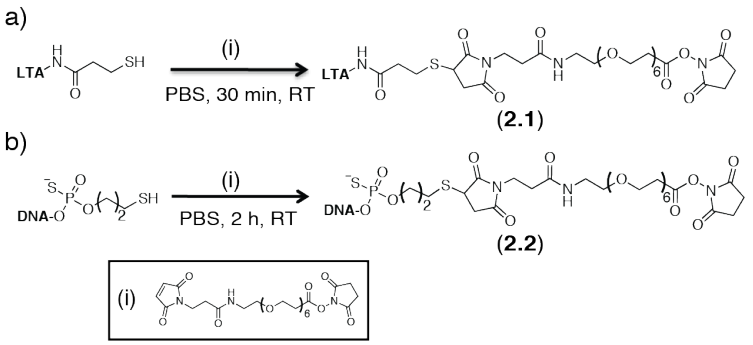

a) Conjugation of thiolated-LTA to the PEG_6 linker to provide NHS-LTA (**2.1**) and b) conjugation of 3'-end thiol-CpG to the PEG_6 linker to provide NHS-CpG-DNA (**2.2**) by treating each thiolated agonist with a NHS-PEG_6-maleimide linker in phosphate buffer (pH 7.4) for 30 min and 2 h, respectively, at RT.

Hsiao, *et al*.[23] demonstrated the chemical attachment of ssDNA to cell surfaces *via* a commercially available, bi-functional NHS-PEG_6-maleimide linker. The maleimide end of the linker was reacted with the free thiol on each TLR agonist. CpG-ODN 1826 (CpG),[24] a CpG-DNA sequence that activates murine immune cell lines, was purchased containing a disulfide modification at the 3'-end for conjugation and 6-carboxyfluorescein (6-FAM) tag at the 5'-end for quantification and compound tracking. The disulfide on the 3'-end of CpG (0.10 mL, 0.40 mM) was reduced using tris(2-carboxyethyl)phosphine (TCEP) providing a free thiol. Then, the 3'-end thiol of CpG was conjugated to the maleimide end of the NHS-PEG_6-maleimide linker in phosphate buffer (pH 7.4) after 2 hours at room temperature. For LTA attachment, the lipid-tails of LTA are responsible for stimulation, so primary amines along the backbone were thiolated by treating LTA (0.20 mL, 1.0 mM) with N-succinimidyl-S-acetylthiopropionate (SATP) in phosphate buffer (pH 7.4 with 1.0 mM EDTA) for 1 hour at room temperature (see Appendix A, **Fig. S2.6**). The acetylated thiol was then deprotected using 0.5 M hydroxylamine in PBS, pH 7.4, with 25 mM EDTA at 4 °C for 16 hours to provide the free thiol. Subsequently, the thiolated LTA was reacted with the maleimide end of the linker in phosphate buffer (pH 7.4) for 30 minutes at room temperature. The resulting TLR agonist_PEG_6-NHS conjugate **2.1** was confirmed *via* ^{1}H NMR and thin-layer chromatography (TLC) (see Appendix A, **Figs. S2.5–S2.9**) and conjugate **2.2** was confirmed *via* MALDI-TOF (see Appendix A, **Fig. S2.10**).

2.3 Synthetic Modification of Lewis Lung Carcinoma (LLC) Cells with TLR Agonists

We then conjugated the TLR agonist_PEG_6-NHS conjugates to Lewis Lung Carcinoma (LLC) cells. LLC is a model lung cancer cell line often employed in C57BL/6 mice studies. The NHS ester end of each TLR agonist_PEG_6–NHS conjugate (36 μM, 0.10 mL) was reacted with free amines on LLC surface proteins in phosphate buffer (pH 7.4) for 30 minutes at room

temperature. To quantify the modification, CpG_LLCs (**2.4**) were detected by incubating **2.4** with the 6-FAM tagged anti-sense strand of CpG-ODN1826 (10 μL, 100 μM) in phosphate buffer (pH 7.4) for 30 minutes at 0 °C (see footnote in Appendix A, **Fig. S2.15).** A similar method was used to detect LTA_LLCs (**2.3**). Instead of a 6-FAM tag, Rhodamine B isothiocyanate was conjugated to amines on the LTA backbone before modifying LLC cell surfaces (see Appendix A, **Figs. S2.2–S2.4**). To synthesize CpG_LTA_LLCs (**2.5**), **2.1** and **2.2** (in a 1:1 molar ratio) were incubated with LLCs to provide the same total concentration of the two TLR agonists as that used for the single TLR agonist modifications **(2.3 or 2.4**).

2.4 Characterization of TLR Agonist Modified Lewis Lung Carcinoma

We confirmed covalent attachment of the TLR agonist_PEG_6-NHS conjugates to LLCs using flow cytometry and confocal microscopy (**Fig. 2.2**). For all LTA and CpG LLC modifications, we observed a shift in the median fluorescence intensity (MFI) of the 6-FAM or RITC labeled LLCs using flow cytometry compared to unlabeled LLCs, confirming the cell surface modifications (**Figs. 2.2a-c**). Minor non-specific sticking of the fluorescently tagged TLR agonists to the LLCs was observed, but distinct cell populations were observed for all TLR agonist_LLCs (see Appendix A, **Fig. S2.11**). Using confocal microscopy, we also observed fluorescence for each single TLR agonist modified LLC as well as co-localized fluorescence for the CpG_LTA_LLCs (**Fig. 2.2d**, and see footnote in Appendix A, **Fig. S2.11**).

Figure 2.2 Characterization and Analysis of Fluorescently Labeled TLR Agonist Modified LLCs by Flow Cytometry

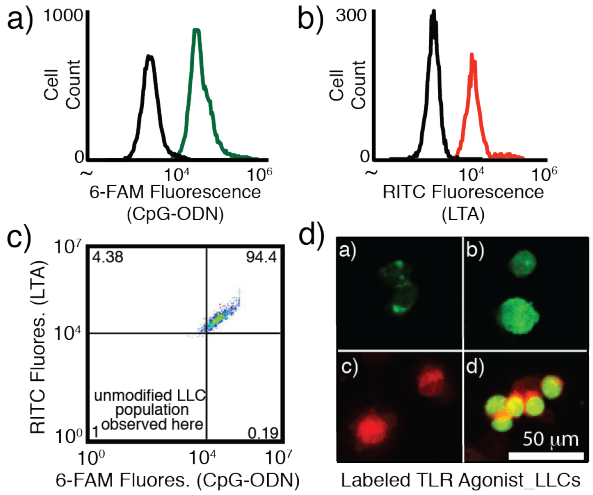

a) CpG-ODN1826_LLCs incubated with 6-FAM CpG-ODN1826 anti-sense strand in Tris-EDTA (TE) buffer for 30 min at 0 °C (unmodified LLCs-black, CpG_LLCs-green), b) RITC LTA_LLCs (unmodified LLCs-black, LTA_LLCs-red), and c) CpG_LTA_LLCs (upper right quadrant). d) Confocal microscopy images (at 488 nm for 6-FAM & 555 nm for RITC) of (a) unmodified LLCs incubated with 6-FAM CpG-ODN1826 anti-sense strand exhibiting non-specific sticking, (b) CpG_LLCs incubated with 6-FAM CpG1826 anti-sense strand, (c) RITC LTA_LLCs, and (d) CpG_LTA_LLCs with 6-FAM and RITC fluorescent tags.

2.5 Testing *In Vitro* Activity of TLR Agonist_LLC Constructs

2.5.1 NF-κB Activity in RAW-Blue Macrophages

Next, we determined the effect of the TLR agonist modifications on the stimulation of immune signaling pathways in RAW-Blue cells, a murine macrophage reporter cell line derived from RAW264.7 cells (**Fig. 2.3**). RAW-Blue cells are engineered to produce secreted embryonic alkaline phosphatase (SEAP) when the transcription factor NF-κB, downstream of TLR activation, is activated. The SEAP is then reacted with a colorimetric reagent to measure relative NF-κB stimulation. In all experiments involving unmodified LLCs, we observed little stimulation of the RAW-Blue cells. Incubating the RAW-Blue cells with single agonist labeled **2.3** or **2.4** for 18 hours at 37 °C displayed a five-fold increase in NF-κB activation from the

unmodified LLCs. Interestingly, both **2.3** and **2.4** stimulated the RAW-Blue cells to a similar degree despite interacting with a cell surface and an endosomal TLR, respectively. Multi-agonist labeled **2.5** evoked the greatest NF-κB signaling. Approximately a two-fold increase in stimulation was observed compared to a single TLR agonist modification despite that **2.5** contained only half the total cell-surface concentration of each TLR agonist. This result suggests that covalently conjugating multiple TLR agonists to a whole cell antigen increases immune activation, which can lower loading levels compared to the use of a single immune agonist.

Figure 2.3 NF-κB Activation of RAW-Blue 264.7 Macrophage Cell Line Treated with TLR Agonist Modified LLCs[a]

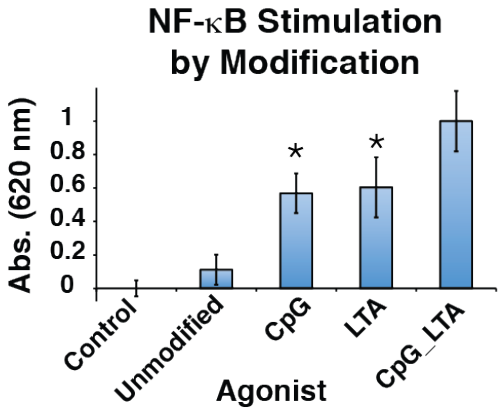

[a] RAW-Blue cells were incubated with TLR Agonist_LLC constructs for 18 h at 37 °C. Each bar is the result of n=6, where *p < 0.05, where the asterisk is compared to CpG_LTA_LLC (**2.5**). Results are expressed as the mean ± SD.

2.5.2 Cell Surface Marker Activation and Cytokine Production in Bone Marrow-Derived Dendritic Cells (BMDCs)

To further examine the potential synergistic effects of covalently conjugated TLR agonists, we tested TLR agonist_LLCs against bone marrow-derived dendritic cells (BMDCs). BMDCs are a primary cell line harvested from the murine femur bones to provide monocytes that are differentiated into dendritic cells using a cocktail of growth factors and signaling molecules. After differentiation to the dendritic cell pathway, the BMDCs are then treated with

the TLR agonist modified LLC constructs and analyzed for biomarkers downstream of the NF-κB pathway to examine other aspects of immune activation.

Activation of BMDCs was confirmed *via* the upregulation of cell surface markers by cell surface staining and analysis by flow cytometry. Cell-surface markers CD86, CD40, MHCII, and CD80 are proteins on dendritic cells that bind to and present antigenic peptides to T cells. As a result, the proteins act as costimulatory signals to help elicit T cell mediated immune responses. The upregulation of these cell surface markers signifies the potential for robust T cell activation, resulting in an adaptive immune response. To determine cell surface marker expression, BMDCs were incubated with each construct for 18 hours at 37 °C, stained, and analyzed by flow cytometry. Upon treatment with unmodified LLCs, minor upregulation of cell surface markers CD86, CD40, and MHCII was observed. Expression of CD80 was also quantified, but the basal level observed was high, resulting in minor upregulation of CD80 (see Appendix A, **Fig. S2.15**). All of the TLR agonist_LLCs resulted in enhanced activation of BMDC cell surface markers. The percentage of CD86 expressing BMDCs was 20% greater for cells treated with **2.4** and 30% greater with **2.5** than cells treated with unmodified LLCs. **2.3** displayed greater activation relative to the unmodified LLCs. However, **2.3** showed modest activation compared to the other modified constructs. The discrepancy in activation could be explained by localization of the CpG modified constructs inside and throughout the cell, resulting in more effective TLR9 stimulation within the endosome. (see footnote in Appendix A, **Fig. S2.20**). The potency of each ligand may also contribute to the difference in activation levels.[25,26] LLCs modified with both CpG and LTA (**2.5**) enhanced BMDC activation, which demonstrated the potential for using multiple TLR agonists to increase dendritic cell activation. All TLR agonist_LLCs provided increased activation over BMDCs incubated with the unconjugated components (see Appendix A, **Fig.**

S2.16). The TLR agonist_LLCs demonstrated that the covalent conjugation of multiple TLR agonists to potential tumor-associated antigens (TAAs) can enhance immune activation, indicative of T cell priming.

Figure 2.4 Analysis of BMDC Activation *via* Cell Surface Marker Expression and Intracellular Cytokine Production using Flow Cytometry

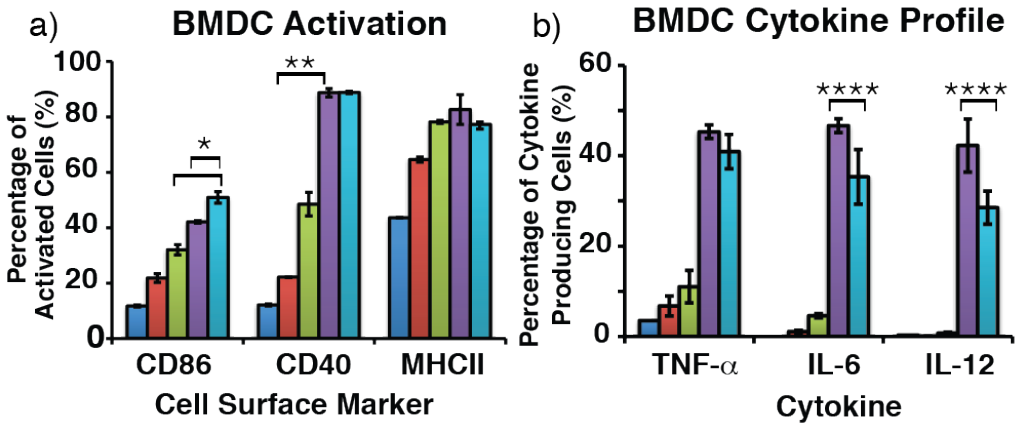

a) BMDC activation *via* cell surface marker expression when incubated with TLR agonist_LLC constructs for 18 h at 37 °C. b) BMDC cytokine profile measured by intracellular cytokine production when incubated with TLR agonist_LLC constructs for 8 h at 37 °C. IFN-γ and IL-10 secretion were not observed for any TLR agonist_LLC constructs (see Appendix A, **Fig. S2.18**). Sample legend: control (dark blue), unmodified LLCs (red), LTA_LLCs (green), CpG_LLCs (purple), CpG_LTA_LLCs (light blue). Each result is from n=3, where *$p < 0.05$, **$p < 0.01$, and ****$p < 0.1$. Results are expressed as the mean ± SD.

To determine the cytokine profile elicited by the TLR agonist_LLC constructs, intracellular cytokine flow cytometry was used to analyze cytokine production (**Fig. 2.4**). TLR agonist_LLCs were incubated with BMDCs for 8 hours at 37 °C. GolgiPlug (BD Biosciences), containing Brefeldin A – a transport inhibitor, was added to cell cultures for the final 4 hours of incubation to prevent cytokine release and build up produced cytokines inside the cells. The cells can then be permeablized, stained for specific cytokines, and analyzed by flow cytometry. **2.4** elicited the greatest production of IL-6, IL-12, and TNF-α, all pro-inflammatory cytokines, which are cell-signaling molecules that alert immune cells of infection as well as contribute to T cell differentiation. **2.4** exhibited a 45% increase of IL-6, IL-12, and TNF-α production

compared to unmodified LLCs. **2.5** produced the second greatest amount of IL-6, IL-12, and TNF-α, approximately a 35% increase compared to unmodified LLCs. The production of pro-inflammatory cytokines may lead to the activation of a cytotoxic T cell response toward the LLC target antigen, resulting in the recruitment of APCs to the whole tumor cells. It also appeared that the LTA modulated cytokine production, since **2.5** resulted in approximately a 5–10% decrease in IL-6 and IL-12 compared to **2.4**, while TNF-α cytokine production remained the same. **2.3** induced minor IL-6, IL-12, and TNF-α production, a 1–5% increase from unmodified LLCs. Our data suggests that the TLR2/6 and TLR9 combination resulted in limited inflammation and a muted T_H1 response while still activating T cells *via* CD86 and CD40. This approach will allow us to simultaneously activate the immune system and modify cytokine production. A combination of T_H1/T_H2 responses may also be present, which is similar to an effective broad-based vaccine, where both cellular (T_H1) and antibody responses (T_H2) are produced. The potential to modulate cytokine production may allow us to direct APC immune responses toward a target antigen (see footnote in Appendix A, **Fig. S2.18**).

2.6 Probing the Mechanism of Action using Confocal Microscopy

To determine possible mechanisms by which our TLR agonist_LLCs stimulated APCs, we examined dendritic cells using confocal microscopy. An immortalized dendritic cell line, JAWS II, was employed as a model owing to its ease of use. APCs were labeled with DiO (green) and our LLC constructs with DiI (red), lipophilic fluorescent dyes that integrate into the cell membrane.[27] CpG_LLCs were internalized by the APC cell line, confirming that macrophagocytosis is one possible mechanism by which stimulation proceeds (**Fig. 2.5**, and see Appendix A, **Fig. S2.20**).

Figure 2.5 Confocal Microscopy Analysis of DiI-labeled CpG_LLCs (red) Macrophagocytosed by DiO-labeled dendritic cells (green)

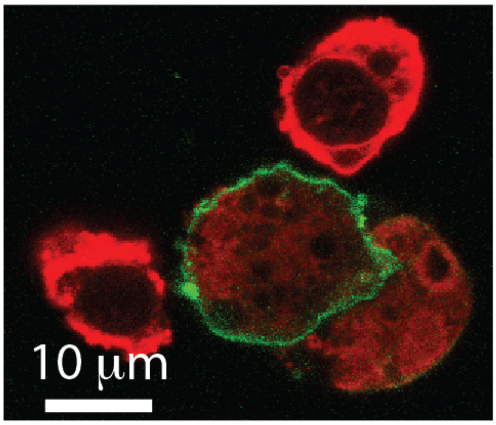

2.7 Conclusion

In this work, we presented the first covalent conjugation of multiple TLR agonists to antigens on whole cells. A general, modular bioconjugation approach was employed, so different combinations of immune agonists, antigens, and target cell types can be tested. Our studies confirmed that directly and chemically modifying target cell antigens using multiple different TLR agonists elicited greater stimulation of APC lines. Future immunotherapies can use these techniques to enable a lower therapeutic dose and greater activation of dendritic cells in *in vivo* immunotherapeutic applications as well as modify TAAs in biopsied tumor samples. The use of these chemical tools can potentially enhance cell-mediated immunity and create more potent, directed cancer immunotherapies.

2.8 Experimental Procedures

TLR Agonist-PEG$_6$-NHS Conjugate Synthetic Procedures.

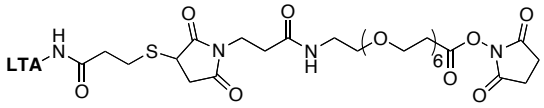

Lipoteichoic Acid-PEG$_6$-NHS Conjugate Synthesis (2.1).

Lipoteichoic acid (LTA) was fluorescently labeled by reacting amines in the alanine residues of LTA (2 mg, 0.2 μmol) with rhodamine B isothiocyanate (RITC) (10.7 μL of 10 mg/mL solution in DMF, 0.2 μmol) in phosphate buffered saline (PBS) buffer (pH 7.4 with 1 mM EDTA) for 15 min at RT. Subsequently, the remaining amines were thiolated by incubating the RITC-LTA solution with N-succinimidyl-S-acetylthiopropionate (SATP) (0.16 mg per 1.0 mg LTA) in DMF for 1 h at RT. The LTA solution was filtered using a Centriprep Centrifugal Filter Device (3K device). The thiol was deprotected by incubating the filtered LTA solution with hydroxylamine in PBS buffer (100 μL, pH 7.4, with 25 mM EDTA and 0.5 M hydroxylamine) at 4 °C overnight (~16 h). The thiolated LTA was filtered using a Centriprep Centrifugal Filter Device (3K device). The extent of RITC conjugation was quantified *via* UV-Vis to provide one RITC molecule for every five LTA molecules (1:5 RITC:LTA). Thiolation of LTA was confirmed *via* Ellman's Assay. Thiols per LTA molecule were determined relative to a cysteine standard curve, which resulted in a mixture where 60% of the LTA contained a thiol. (This indicated that one LTA potentially contained more than one thiol.) The thiolated LTA (150 μL) was then reacted with the NHS-PEG$_6$-maleimide linker (60 μL of 20 mg/mL solution in DMSO) for 30 min at RT. The resulting conjugate was passed through a NAP-5 Column pre-equilibrated with PBS buffer (pH 7.4). The conjugate was quantified *via* UV-Vis and confirmed using proton nuclear

magnetic resonance (^{1}H NMR) and thin-layer chromatography (TLC). ^{1}H NMR spectra were taken in D_2O. The TLC was run in 65:25:4 $CHCl_3$:MeOH:H_2O.

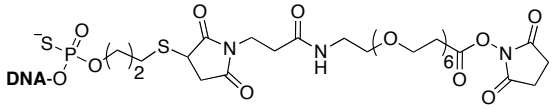

CpG-PEG$_6$-NHS Conjugate Synthesis (2.2).

Single stranded CpG-ODN1826 (5'-TCCATGACGTTCCTGACGTT-3') was obtained with a 3'-disulfide modification. The 3'-disulfide modification was reduced to the free thiol using 3% tris(2-carboxyethyl)phosphine hydrochloride (TCEP) in water (400 μL). The reduced CpG-ODN1826 was precipitated in EtOH (1.5 mL) and 3 M NaOAc (50 μL) and placed in an -80 °C freezer for 30 min. The precipitated CpG-ODN1826 was centrifuged at 13,000 RPM and 4 °C for 20 min. The supernatant was removed and the precipitated CpG-ODN1826 was rinsed with EtOH (200 μL). The CpG-ODN1826 was placed in a speed-vacuum to remove excess solvent and dry the reduced CpG-ODN1826. The reduced CpG-ODN1826 (2.0 mM) was resuspended in Tris-EDTA (TE) buffer (1x) and passed through a NAP-5 Column, which was pre-equilibrated with TE buffer (1x). Subsequently, the NHS-PEG$_6$-maleimide linker (120 μL of 20 mg/mL solution in DMSO) was added to the eluted DNA (0.40 mM, 100 μL). The reaction mixture was incubated at RT for 2 h. The pH of the reaction was monitored to ensure a constant pH ~8. If slightly acidic, PBS buffer (40 μL) was added to the reaction mixture. Maintaining a slightly basic pH facilitated deprotonation of the thiol to increase the rate of conjugate addition. The reaction mixture was passed through a NAP-5 Column pre-equilibrated with PBS buffer (pH 7.4). The conjugate was quantified *via* UV-Vis and confirmed using MALDI-TOF.

TLR Agonist Cell Surface Modification of LLCs with LTA-PEG$_6$-NHS (2.1) and/or CpG-PEG$_6$-NHS (2.2) to Provide TLR Agonist_LLC Constructs (2.3, 2.4, or 2.5).

A solution of conjugate **2.1** or **2.2** or **2.1** and **2.2** (36 μM, 100 μL) in PBS buffer was incubated with Lewis Lung Carcinoma (LLC) cells ($2x10^6$ cells) for 30 min at RT. The solution was mixed thoroughly using a vortexer. The cell solution was centrifuged at 2500 RPM and RT for 10 min, and the supernatant was removed. The modified cells were rinsed with PBS buffer (1 x 200 μL), then cell media (2 x 200 μL) and finally incubated with dendritic cells.

The cell surface modification was quantified using flow cytometry and fluorescent microscopy. To confirm the modification of CpG_LLCs, the 6-FAM-labeled CpG-ODN1826 anti-sense strand (10 μL, 100 μM) was incubated with the modified CpG_LLCs. The solution was incubated for 30 min at 0 °C removed from light. The cells were rinsed using PBS buffer (2 x 200 μL) and resuspended in PBS buffer (100 μL) to be analyzed.

To confirm the LTA_LLC modification, the LTA was labeled with rhodamine B as mentioned in the synthesis of **2.1**.

Cell Culture and Flow Cytometry Procedures.

Bone Marrow-Derived Dendritic Cell Harvest and Culture.

Femur bones were removed from 6-week-old C57BL/6 mice according to Matheu, *et al*.,[28] and the bone marrow was extracted into PBS buffer. The cell suspension was made into a homogeneous solution using a pipette and subsequently filtered through a 70 μm cell strainer (Fisher Scientific). The cell solution was centrifuged at 300 RCF for 10 min at RT. The supernatant was removed, and ACK Lysing Buffer (Lonza) (3 mL) was added to the cell pellet and incubated for 2 min at RT. PBS buffer (13 mL) was then added to the cell suspension, and the cell solution was centrifuged at 300 RCF for 10 min at RT. The cell pellet was resuspended in RPMI 1640 (Fisher Scientific Hyclone), and centrifuged at 300 RCF for 10 min at RT. The

cell pellet was resuspended in BMDC primary media: RPMI 1640 (Life Technologies), 10% heat inactivated fetal bovine serum (FBS), 20 ng/mL granulocyte-macrophage colony-stimulating factor (GM-CSF) (Cahalan Lab), 2 mM L-glutamine (Life Technologies), antibiotic-antimycotic (1x) (Life Technologies), and 50 μM beta-mercaptoethanol (all components were sterile filtered (0.22 μm) together before use). Harvested cells were then counted and plated at 1 million cells/mL density in 100 mm petri dishes (10 mL total media) and incubated at 37 °C in a CO_2 incubator (day 0 of cell culture). On day 3, 10 mL of BMDC primary media was added to each petri dish. Day 5 BMDCs were released using a pipette, centrifuged at 300 RCF for 10 min at RT, and replated in 24-well plates at 1.2 x 10^6 cells/mL density for cell surface marker activation and cytokine profile flow cytometry experiments.

General Procedure for Flow Cytometry for Cell Surface Marker Upregulation.

BMDCs were incubated individually with each TLR Agonist_LLC (**2.3**, **2.4**, or **2.5**) (9:1 BMDCs:TLR Agonist_LLCs in 0.5 mL culture media) for 18 h at 37 °C in a CO_2 incubator. Stimulated BMDCs were released from the plate and transferred to 1 mL eppendorf tubes. The cells were centrifuged at 2500 RPM and 4 °C for 10 min and the supernatant was removed. The cell pellet was resuspended in cold FACS buffer (100 μL) and incubated with CD16/32 FcR blocking antibodies (1.0 μg/1*10^6 cells) (BioLegend) on ice for 10 min. The cell suspension was centrifuged at 2500 RPM for 10 min at 4 °C and the supernatant removed. The cell pellet was resuspended in cold FACS buffer (100 μL) and incubated with FITC-CD11c (1.0 μg/1*10^6 cells) and PE-CD86 (1.0 μg/1*10^6 cells), -CD40 (1.0 μg/1*10^6 cells), -MHCII (0.25 μg/1*10^6 cells), or -CD80 (0.5 μg/1*10^6 cells)) on ice and removed from light for 30 min. Cold FACS buffer (300 μL) was added to each sample. The cell suspension was centrifuged at 2500 RPM and 4 °C for 10 min, and the supernatant was removed. The cells were then rinsed with cold FACS buffer

(300 μL) one final time, and the supernatant was removed. The dendritic cells were resuspended in cold FACS buffer (200 μL) and kept on ice until being analyzed on the flow cytometer.

General Procedure for Intracellular Cytokine Flow Cytometry Staining.

BMDCs were incubated individually with a solution of TLR Agonist_LLC (**2.3**, **2.4**, or **2.5**) (9:1 BMDCs:TLR Agonist_LLCs in 0.5 mL culture media) for 8 h at 37 °C in a CO_2 incubator. GolgiPlug (BD Biosciences), containing Brefeldin A, was added to cell culture (according to BD Biosciences Protocol) for the final 4 h of culture. After 8 h, stimulated BMDCs were released from the plate and transferred to 1 mL eppendorf tubes. The cells were centrifuged at 2500 RPM and 4 °C for 10 min, and the supernatant was removed. The cell pellet was resuspended in cold FACS buffer (100 μL) and incubated with CD16/32 FcR blocking antibodies (1.0 μg/1*10^6 cells) on ice for 10 min. The cell suspension was centrifuged at 2500 RPM and 4 °C for 10 min, and the supernatant was removed. The cell pellet was resuspended in cold FACS buffer (100 μL) and incubated with FITC-CD11c (0.25 μg/1*10^6 cells) on ice and removed from light for 30 min. Cold FACS buffer (300 μL) was added to each sample. The cell suspension was centrifuged at 2500 RPM for 10 min at 4 °C, and the supernatant was removed. The cells were rinsed with cold FACS buffer (300 μL) one more time, and the supernatant was removed. The cell pellet was resuspended in 100 μL BD Cytofix/Cytoperm solution and incubated on ice and removed from light for 20 min. The cell suspension was centrifuged at 2500 RPM and 4 °C for 10 min and the supernatant removed. BMDCs were washed in BD Perm/Wash solution (2 x 300 μL) and the supernatant removed. The cell pellet was resuspended in cold FACS buffer (100 μL) and incubated with APC-IFN-γ (1.0 μg/1*10^6 cells), -TNF-α (0.25 μg/1*10^6 cells), -IL-6 (0.25 μg/1*10^6 cells), -IL-10 (0.25 μg/1*10^6 cells), or -IL-12 (0.25 μg/1*10^6 cells)) on ice and removed from light for 30 min. Cold FACS buffer (300 μL) was added to each sample. The cell

suspension was centrifuged at 2500 RPM and 4 °C for 10 min, and the supernatant was removed. The cells were rinsed with cold FACS buffer (300 μL) one more time. BMDCs were resuspended in cold FACS buffer (200 μL) and kept on ice until analysis *via* flow cytometer.

General Procedure for RAW264.7 Macrophage (RAW-Blue) NF-κB assay.

RAW-Blue cells were plated at $10*10^4$ cells/mL density (180 μL) in 96-well plates using D-MEM High Glucose media (LifeTechnologies), 10% FBS, 2 mM L-glutamine, and antibiotic-antimycotic (1x) and experiments were run in D-MEM High Glucose media (LifeTechnologies), 10% heat inactivated FBS, 2 mM L-glutamine, and antibiotic-antimycotic (1x). RAW-Blue cells were incubated individually with 20 μL of each TLR Agonist_LLC (**2.3**, **2.4**, or **2.5**) (9:1 RAW-Blue:TLR Agonist_LLCs in 200 μL total cell media volume) for 18 h at 37 °C in a CO_2 incubator. Cell media (50 μL) from the stimulated RAW-Blue cells was removed, placed into a 96-well plate, and incubated with QUANTI-Blue solution (Invivogen) (150 μL) for 1 h at 37 °C in a CO_2 incubator. The absorbance (620 nm) was measured using a Bio-Tek μQuant microplate spectrophotometer.

MALDI-MS.

CpG-PEG$_6$-NHS Conjugate (2.2).

The reaction mixture was passed through ZipTip$_{C18}$ (Millipore) according to Millipore protocol: A ZipTip$_{C18}$ was equilibrated with 50% acetonitrile/water (2 x 10 μL) and subsequently 0.1 M triethylammonium acetate (TEAA) (3 x 10 μL). The reaction mixture was passed through the ZipTip$_{C18}$ (10 x 10 μL). The ZipTip$_{C18}$ was washed with 0.1 M TEAA buffer (3 x 10 μL) followed by nanopure water (3 x 10 μL). Conjugate **2.2** was eluted using 50% acetonitrile/water (3 x 10 μL). Purified conjugate **2.2** was dried using a speed-vacuum and resuspended in 0.36 M 3-hydroxypicolinic acid matrix (1:1 acetonitrile:300 mM ammonium citrate solution in 50%

acetonitrile/water) (2.0 μL). The sample was spotted on a MALDI plate and analyzed in negative ion mode.

Confocal Microscopy.

Fluorescent Cell Labeling with DiO and DiI and Confocal Microscopy Colocalization Experiments.

Stock solutions of DiI and DiO dye (1 mg/mL) were prepared in DMSO. Working solutions of DiI and DiO (100 μg/mL) were prepared by diluting the stock solutions with glucose labeling buffer (300 mM glucose and 10 mM HEPES in nanopure water).[27] The cells were plated one day prior in 6-well plates at $2*10^5$ cells/mL. Before labeling the cells, the media was removed. JAWS II and LLC cell lines were suspended in DiO or DiI solutions (0.5 mL of 100 μg/mL), respectively, and incubated at 37 °C in a CO_2 incubator for 2 h. The DiI or DiO solution was then removed. The cells were washed with glucose buffer (2 x 1 mL) and resuspended in cell media. The LLCs were labeled with **2.1**, **2.2**, or **2.1** and **2.2** as described in the synthetic procedures. The TLR Agonist_LLCs were incubated with the dendritic cell line overnight (~ 14-18 h) at 37 °C. The cell media was removed. The cells were then resuspended in PBS buffer, and analyzed *via* confocal microscopy.

Statistics.

Data was analyzed using a two-tailed t test. All values were reported as mean ± SD, unless stated otherwise.

***See Appendix A for Additional Figures.**

2.9 References

(1) Banchereau, J.; Palucka, A. K. Dendritic Cells as Therapeutic Vaccines against Cancer. *Nat. Rev. Immunol.* **2005**, *5* (4), 296–306.

(2) Banchereau, J.; Steinman, R. M. Dendritic Cells and the Control of Immunity. *Nature* **1998**, *392* (6673), 245–252.

(3) Leen, A. M.; Rooney, C. M.; Foster, A. E. Improving T Cell Therapy for Cancer. *Annu. Rev. Immunol.* **2007**, *25* (1), 243–265.

(4) Shirota, H.; Klinman, D. M. CpG-Conjugated Apoptotic Tumor Cells Elicit Potent Tumor-Specific Immunity. *Cancer Immunol. Immunother. CII* **2011**, *60* (5), 659–669.

(5) Liu, H.; Kwong, B.; Irvine, D. J. Membrane Anchored Immunostimulatory Oligonucleotides for In Vivo Cell Modification and Localized Immunotherapy. *Angew. Chem. Int. Ed Engl.* **2011**, *50* (31), 7052–7055.

(6) Pulendran, B. Learning Immunology from the Yellow Fever Vaccine: Innate Immunity to Systems Vaccinology. *Nat. Rev. Immunol.* **2009**, *9* (10), 741–747.

(7) Duggan, J. M.; You, D.; Cleaver, J. O.; Larson, D. T.; Garza, R. J.; Pruneda, F. A. G.; Tuvim, M. J.; Zhang, J.; Dickey, B. F.; Evans, S. E. Synergistic Interactions of TLR2/6 and TLR9 Induce a High Level of Resistance to Lung Infection in Mice. *J. Immunol.* **2011**, *186* (10), 5916–5926.

(8) Shukla, N. M.; Mutz, C. A.; Malladi, S. S.; Warshakoon, H. J.; Balakrishna, R.; David, S. A. Toll-Like Receptor (TLR)-7 and -8 Modulatory Activities of Dimeric Imidazoquinolines. *J. Med. Chem.* **2012**, *55* (3), 1106–1116.

(9) Garcia-Cordero, J. L.; Nembrini, C.; Stano, A.; Hubbell, J. A.; Maerkl, S. J. A High-Throughput Nanoimmunoassay Chip Applied to Large-Scale Vaccine Adjuvant Screening. *Integr. Biol. Quant. Biosci. Nano Macro* **2013**, *5* (4), 650–658.

(10) Timmermans, K.; Plantinga, T. S.; Kox, M.; Vaneker, M.; Scheffer, G. J.; Adema, G. J.; Joosten, L. A. B.; Netea, M. G. Blueprints of Signaling Interactions between Pattern Recognition Receptors: Implications for the Design of Vaccine Adjuvants. *Clin. Vaccine Immunol.* **2013**, *20* (3), 427–432.

(11) Kasturi, S. P.; Skountzou, I.; Albrecht, R. A.; Koutsonanos, D.; Hua, T.; Nakaya, H. I.; Ravindran, R.; Stewart, S.; Alam, M.; Kwissa, M.; et al. Programming the Magnitude and Persistence of Antibody Responses with Innate Immunity. *Nature* **2011**, *470* (7335), 543–547.

(12) Coffman, R. L.; Sher, A.; Seder, R. A. Vaccine Adjuvants: Putting Innate Immunity to Work. *Immunity* **2010**, *33* (4), 492–503.

(13) Levitz, S. M.; Golenbock, D. T. Beyond Empiricism: Informing Vaccine Development through Innate Immunity Research. *Cell* **2012**, *148* (6), 1284–1292.

(14) Goldstein, M. J.; Varghese, B.; Brody, J. D.; Rajapaksa, R.; Kohrt, H.; Czerwinski, D. K.; Levy, S.; Levy, R. A CpG-Loaded Tumor Cell Vaccine Induces Antitumor CD4+ T Cells That Are Effective in Adoptive Therapy for Large and Established Tumors. *Blood* **2011**, *117* (1), 118–127.

(15) Cleveland, M. G.; Gorham, J. D.; Murphy, T. L.; Tuomanen, E.; Murphy, K. M. Lipoteichoic Acid Preparations of Gram-Positive Bacteria Induce Interleukin-12 through a CD14-Dependent Pathway. *Infect. Immun.* **1996**, *64* (6), 1906–1912.

(16) Schwandner, R.; Dziarski, R.; Wesche, H.; Rothe, M.; Kirschning, C. J. Peptidoglycan- and Lipoteichoic Acid-Induced Cell Activation Is Mediated by Toll-like Receptor 2. *J. Biol. Chem.* **1999**, *274* (25), 17406–17409.
(17) Krieg, A. M. Cpg Motifs in Bacterial Dna and Their Immune Effects*. *Annu. Rev. Immunol.* **2002**, *20* (1), 709–760.
(18) Krieg, A. M. The Role of CpG Motifs in Innate Immunity. *Curr. Opin. Immunol.* **2000**, *12* (1), 35–43.
(19) Kuramoto, E.; Yano, O.; Kimura, Y.; Baba, M.; Makino, T.; Yamamoto, S.; Yamamoto, T.; Kataoka, T.; Tokunaga, T. Oligonucleotide Sequences Required for Natural Killer Cell Activation. *Cancer Sci.* **1992**, *83* (11), 1128–1131.
(20) Ginsburg, I. Role of Lipoteichoic Acid in Infection and Inflammation. *Lancet Infect. Dis.* **2002**, *2* (3), 171–179.
(21) Tuvim, M. J.; Gilbert, B. E.; Dickey, B. F.; Evans, S. E. Synergistic TLR2/6 and TLR9 Activation Protects Mice against Lethal Influenza Pneumonia. *PLoS ONE* **2012**, *7* (1), e30596.
(22) Deininger, S.; Stadelmaier, A.; Aulock, S. von; Morath, S.; Schmidt, R. R.; Hartung, T. Definition of Structural Prerequisites for Lipoteichoic Acid-Inducible Cytokine Induction by Synthetic Derivatives http://www.jimmunol.org (accessed May 23, 2013).
(23) Hsiao, S. C.; Shum, B. J.; Onoe, H.; Douglas, E. S.; Gartner, Z. J.; Mathies, R. A.; Bertozzi, C. R.; Francis, M. B. Direct Cell Surface Modification with DNA for the Capture of Primary Cells and the Investigation of Myotube Formation on Defined Patterns. *Langmuir* **2009**, *25* (12), 6985–6991.
(24) Chu, R. S.; Targoni, O. S.; Krieg, A. M.; Lehmann, P. V.; Harding, C. V. CpG Oligodeoxynucleotides Act as Adjuvants That Switch on T Helper 1 (Th1) Immunity. *J. Exp. Med.* **1997**, *186* (10), 1623–1631.
(25) Liu, J.; Xu, C.; Liu, Y.-L.; Matsuo, H.; Hsieh, R. P.; Lo, J.-F.; Tseng, P.-H.; Yuan, C.-J.; Luo, Y.; Xiang, R.; et al. Activation of Rabbit TLR9 by Different CpG-ODN Optimized for Mouse and Human TLR9. *Comp. Immunol. Microbiol. Infect. Dis.* **2012**, *35* (5), 443–451.
(26) Irvine, K. L.; Hopkins, L. J.; Gangloff, M.; Bryant, C. E. The Molecular Basis for Recognition of Bacterial Ligands at Equine TLR2, TLR1 and TLR6. *Vet. Res.* **2013**, *44* (1), 50.
(27) Underhill, D. M.; Bassetti, M.; Rudensky, A.; Aderem, A. Dynamic Interactions of Macrophages with T Cells during Antigen Presentation. *J. Exp. Med.* **1999**, *190* (12), 1909–1914.
(28) Matheu, M. P.; Sen, D.; Cahalan, M. D.; Parker, I. Generation of Bone Marrow Derived Murine Dendritic Cells for Use in 2-Photon Imaging. *J. Vis. Exp. JoVE* **2008**, No. 17.

CHAPTER 3

Covalent Linkage of Two TLR Agonists to Study Spatial Effects on Immune Activation

3.1 Introduction

Since the molecular basis for TLR activation relies on the formation of higher-order complexes,[1–4] we sought to study the spatial component of immune activation by covalently linking two TLR agonists together. TLRs cluster when activated suggesting that signaling is increased by spatial organization and receptor proximity, but spatially confining TLR agonists by covalent linkage has not been directly tested on activation of multiple, unique TLRs. In addition, pathogens, like a virus, have a defined spatial distance between native agonists, such as that between the viral capsid and the genetic information (DNA/RNA) within a virus. As a result, native agonists are presented to the immune system in a distinct spatial organization, resulting in activation of different signaling pathways in a cell.

We hypothesized that the spatial confinement of two different TLR agonists would mimic the spatial proximity of agonists in a pathogen. Therefore, linking two TLR agonists with a defined spatial distance would present the agonists to immune cells in a similar manner as that in a pathogen, providing increased immune activation compared to a mixture of the same agonists in solution (**Fig. 3.1**). This could potentially occur through the confined association of multiple receptors, thereby promoting TLR dimerization and subsequent immune activation. Simultaneous activation of multiple TLRs results in increased stimulatory effects broadly called synergies that result from activation of different combinations of pathways and direct the polarization of the immune response.[5–8] Several approaches, including the use of virus, nanoparticle, and dendrimer motifs, have combined multiple agonists to localize delivery and

mimic natural pathogens.[9–12] Additionally, in other immune cell systems, multivalent ligands enhance activation.[13,14] Increased synergistic activity appears to be correlated with proximity or multivalency, but this concept has not been shown with TLRs. Our operating hypothesis is that multivalent TLR agonists might stimulate higher-order TLR structures. In this study, we found that the coupling of TLR agonists results in increased stimulation, but we cannot yet conclude that this behavior is due exclusively to TLR ordering.

Figure 3.1 Probing the Immune Response with TLR Agonists Conjugated at a Discrete Molecular Distance

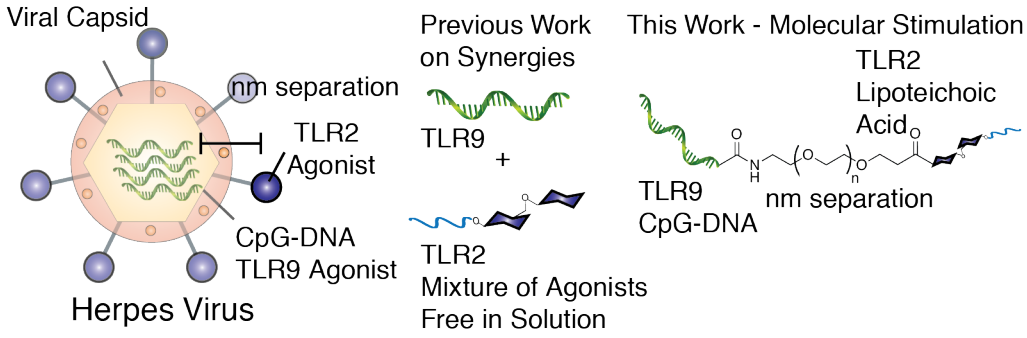

Others have studied TLR homodimers, where well-defined and short inter-agonist spacings of imidazoquinoline homodimers resulted in synergistic or antagonistic modulation of immunostimulation through TLR7 and TLR8.[15] Similar to approaches used to investigate other biological heterodimers,[16–20] we sought to explore the effect of inter-agonist proximity on the activation of two different TLRs. We used a bi-functional polyethylene glycol (PEG) linker to synthesize a TLR di-agonist consisting of TLR2/6 and 9 immunostimulants that activate two TLRs, known to have a mild synergy,[21,22] from two different signaling pathways. These TLR agonists activate the corresponding TLRs, which are expressed in two different cellular locations, on the cell surface and in endosomal compartments. The resulting conjugate provided a synergistic enhancement of the innate immune response compared to the same agonists unconjugated in solution. The increased potency resulted from the defined distance between the

two agonists. Thus, the linked conjugate provided a more potent immunostimulant for vaccine development and a defined molecular tool to explore the mechanism of action of this immune synergy.

3.2 Synthesis and Characterization of the LTA_CpG (TLR2/6_9) Di-Agonist

The initial di-agonist synthesized was inspired by the Herpes Simplex Virus, which activates TLRs 2 and 9.[21,22] We covalently conjugated CpG-DNA (CpG, TLR9) to lipoteichoic acid (LTA, TLR2/6) using a bi-functional PEG_6 linker bearing N-hydroxysuccinimide (NHS) and maleimide end groups (**Figure 3.2**). LTA (2 mg from 10 mg/mL solution in PBS, pH 7.4) from *Bacillus subtilis* was first coupled to the bi-functional PEG_6 linker (12 μL from 100 mg/mL solution in DMSO) through the alanine side chain to the NHS ester end-group of the PEG_6 linker in approximately 1:1 molar ratio maintained at pH 7.4 for 1 hour, as LTA is susceptible to hydrolysis under acidic or basic conditions (see 3.6 Experimental Procedures for conjugation procedures). The LTA_PEG_6-maleimide was purified by spin dialysis. ^{1}H NMR spectroscopy was used to quantify the ratio of PEG_6 linker to LTA (1:2), using the maleimide protons from the linker and the methyl protons from the LTA lipid chains. We further elaborated the LTA_PEG_6-maleimide conjugate (approximately 2 mg in 200 μL PBS, pH 7.4) to synthesize the LTA_CpG (TLR2/6_9) di-agonist by treatment with CpG (50 μL from 1 mM solution in PBS, pH 7.4) for 15 hours at room temperature.

Figure 3.2 Synthesis of the LTA_CpG (TLR2/6_9) Di-Agonist

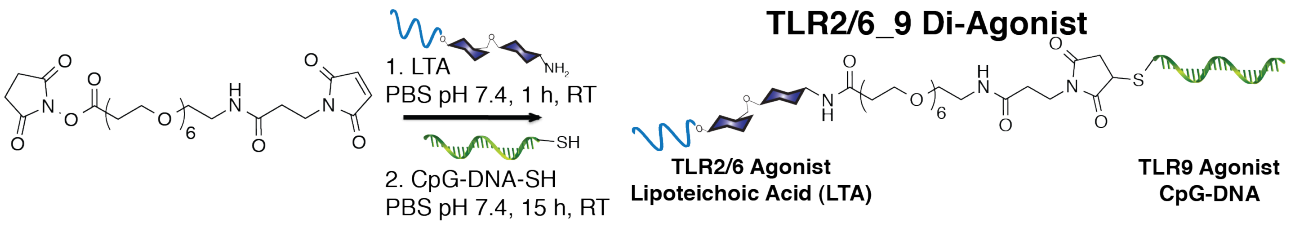

Initially, SDS-PAGE was used to detect the TLR2/6_9 conjugate. There appeared to be a diffuse high molecular weight band, which was potentially the product since LTA is a biopolymer (**Fig. 3.3**). To further confirm and characterize the desired bioconjugate, ^{1}H NMR spectroscopy, fast protein liquid chromatography, and UV/Vis spectroscopy were used for analysis (see Appendix B, **Figs. S3.2-S3.4**). The LTA_CpG di-agonist was purified by FPLC (Superdex G75, PBS pH 7.4, 0.2 mL/min) (**Fig. 3.4**) and quantified by UV/Vis spectroscopy at 495 nm by the 6-FAM tag on the 5'-end of the CpG (see Appendix B, **Figs. S3.4-S3.5**). Dynamic light scattering (see Appendix B, **Fig. S3.6**) was performed to determine if the TLR2/6_9 conjugate formed particles in solution. Stable particles were not observed by DLS. However, the LTA_CpG di-agonist was found to agglomerate over time; this is similar to LTA alone.

Figure 3.3 SDS-PAGE Analysis of the LTA_CpG Di-Agonist[a]

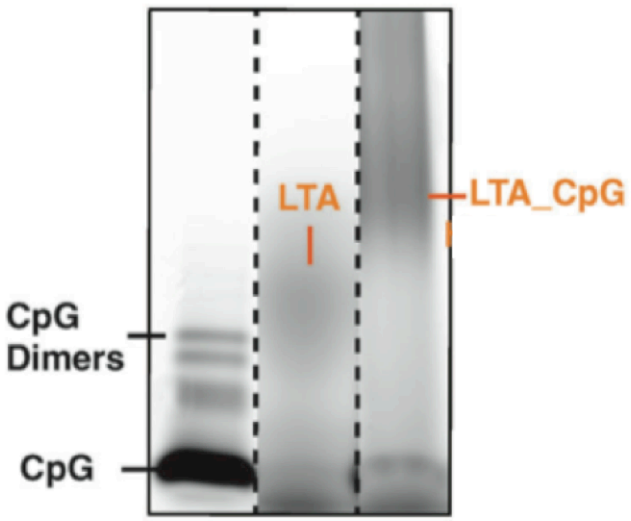

[a] SDS-PAGE of CpG (left), LTA (middle), and the crude reaction mixture containing LTA_CpG (right).

Figure 3.4 FPLC Analysis of the LTA_CpG Di-Agonist[a]

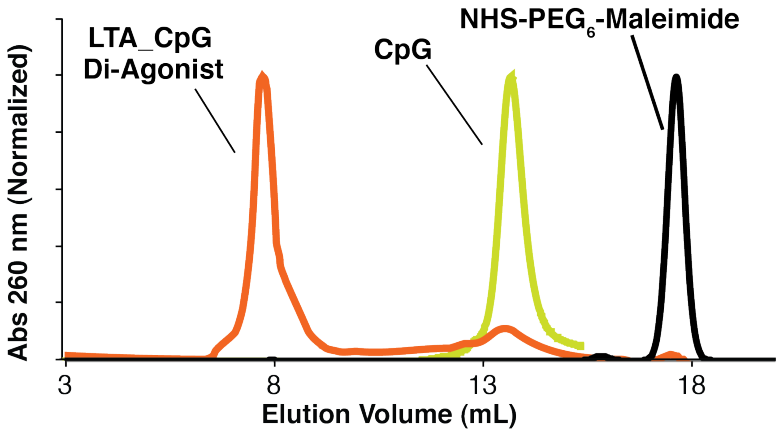

[a] FPLC traces of LTA_CpG (orange), CpG (green), and NHS-PEG_6-maleimide (black) using a Superdex G75 column, PBS pH 7.4, 0.2 mL/min.

3.3 Testing *In Vitro* Activity of the LTA_CpG Di-Agonist

3.3.1 NF-κB Activity in RAW-Blue Macrophages

The LTA_CpG di-agonist was tested with two different murine cell lines, macrophage RAW-Blue cells and bone marrow-derived dendritic cells (BMDCs). The RAW-Blue reporter cell line was used to measure general immune cell stimulation *via* NF-κB activation (**Fig. 3.5**). RAW-Blue cells were stimulated with LTA, CpG, an unconjugated mixture of LTA and CpG, or the LTA_CpG di-agonist (see Appendix B, **Fig. S3.7**). Concentrations ranging from 10 to 100 ng per mL were tested. In the case of the LTA_CpG di-agonist, the concentration was quantified with respect to the 6-FAM tag on CpG. The LTA_CpG di-agonist activated the RAW-Blue cell line to a greater extent than the unconjugated mixture of CpG and LTA.

Figure 3.5 NF-κB Activation of RAW-Blue 264.7 Macrophage Cell Line Treated with the LTA_CpG Di-Agonist[a]

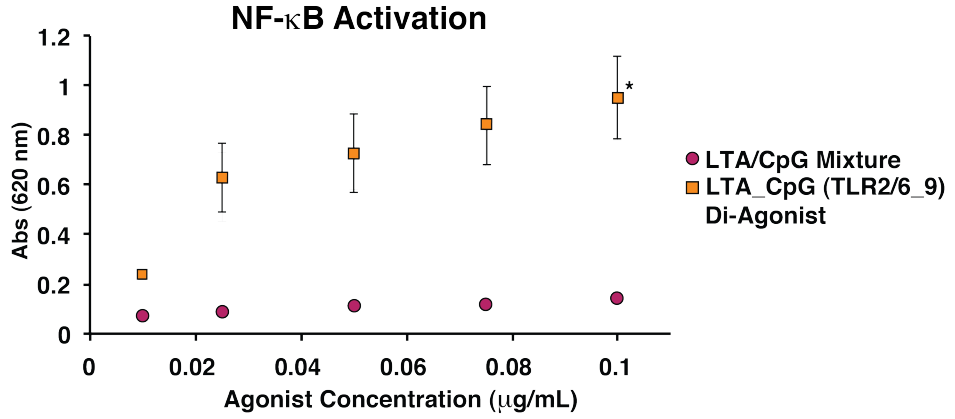

[a] RAW-Blue cells were incubated with TLR2/6_9 di-agonist or a mixture of LTA and CpG unconjugated for 18 h at 37 °C. Each bar is the result of n=6, where *p < 0.001. Results are expressed as the mean ± SD.

3.3.2 Cell Surface Marker Activation and Cytokine Production in Bone Marrow-Derived Dendritic Cells (BMDCs)

The magnitude and polarization of the increased immune response was further examined in BMDCs to better understand the effect of the LTA_CpG di-agonist on the stimulation of primary APCs. The LTA_CpG di-agonist (100 ng/mL) provided greater upregulation of cell surface markers and cytokine production, associated with the activation of the innate immune response and necessary for T cell activation, compared to the two agonists unconjugated (100 ng/mL of each agonist). Exposure to the LTA_CpG di-agonist increased the expression of CD40, CD80, CD86, and MHCII. This increase was most evident with CD40, in which case there was over a 40% increase in cell surface expression for the LTA_CpG di-agonist relative to the unconjugated mixture of the two agonists (**Fig. 3.6a**). The stimulation profile we observed indicates a potential for an increase in T cell activation and antigen presentation based on increases in T cell adhesion proteins and MHCII. These results suggest that the LTA_CpG di-agonists may perform as a superior immunostimulant relative to either agonist alone or an unconjugated mixture. The high

potency of the LTA_CpG conjugate may provide dose sparing *in vivo*, which allows administration of a lower dose of the adjuvant, and is favorable in vaccine applications.

Figure 3.6 Analysis of BMDC Activation *via* Cell Surface Marker Expression and Intracellular Cytokine Production using Flow Cytometry[a]

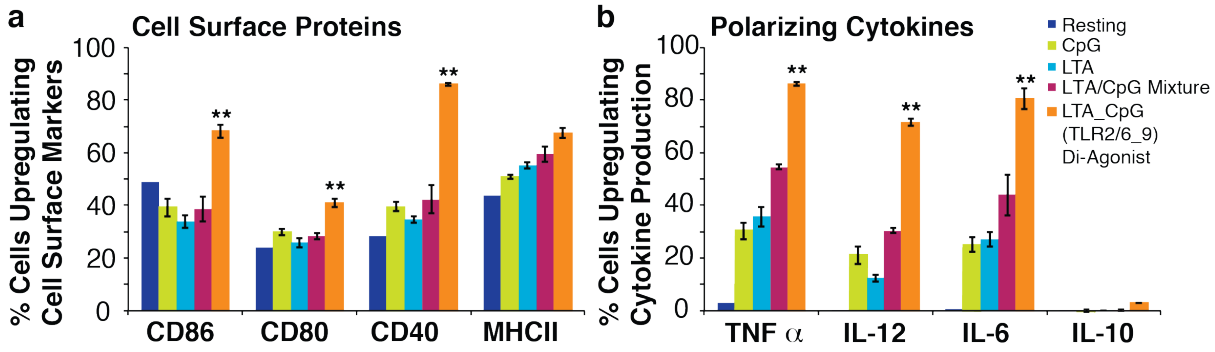

a) BMDC activation *via* cell surface marker expression when incubated with TLR2/6_9 di-agonist, a mixture of LTA and CpG unconjugated, and the individual agonists for 18 h at 37 °C. b) BMDC cytokine profile measured by intracellular cytokine production when incubated with TLR2/6_9 di-agonist, a mixture of LTA and CpG unconjugated, and the individual agonists for 6 h at 37 °C. Resting/media control (dark blue), CpG (green), LTA (light blue), LTA/CpG mixture (magenta), LTA_CpG (orange). Each bar is the result of n=3, where **$p < 0.01$ comparing LTA_CpG to the Resting – media control. Results are expressed as the mean ± SD.

To screen the types of cytokines produced, we measured the expression of five cytokines, TNF-α, IL-6, IL-10, and IL-12, (**Fig. 3.6b**), and IFN-γ (see Appendix B, **Fig. S3.8**). CpG, LTA, and the mixture of CpG and LTA all induced the production of cytokines associated with a pro-inflammatory response, typical of TLR agonists (TNF-α, IL-6, IL-12). The LTA_CpG di-agonist induced greater than a 30% increase in the production of each of these cytokines and also induced the production of the anti-inflammatory cytokine IL-10 at low (3% of $CD11c^+$ dendritic cells expressed IL-10), but significant levels ($p < 0.001$, for LTA_CpG as compared to the media control).

3.4 Examining the Mechanism of Action using TLR Signaling Inhibitors

Mechanistic studies were performed with TLR2 and TLR9 antagonists (OxPAPC, TLR2

and CpG-ODN2088, TLR9), an endosomal-protease inhibitor to block TLR9 activation (chloroquine), and LTA conjugated to CpG-ODN2088 (**Fig. 3.7**). First, we used OxPAPC (Invivogen, CA) to competitively inhibit the TLR2 pathway. The resulting decrease in stimulation confirmed that LTA_CpG acts partially through TLR2. The addition of either CpG-ODN2088 or chloroquine with OxPAPC further decreased stimulation, confirming that the activity was dependent on both TLR2 and TLR9. Stimulation also decreased upon the addition of CpG-ODN2088 or chloroquine alone, showing that activation was partially dependent on the TLR9 pathway. A combination of CpG-ODN2088 and chloroquine produced an additive effect in decreasing stimulation (see Appendix B, **Fig. S3.7**). Cumulatively, these results indicate that stimulation by LTA_CpG proceeds through traditional TLR2/6 and TLR9 pathways. To test whether the increased activity of LTA_CpG was due to activation of both TLRs, LTA was conjugated to the antagonist CpG-ODN2088. This sequence competitively binds TLR9, thereby inhibiting activity while retaining TLR9 binding. Stimulation with the antagonist construct was less than that observed with the LTA_CpG di-agonist but greater than that observed with a mixture of the two TLR agonists. Taken together, these results suggest that although the ability of the LTA_CpG di-agonist to access the TLR2/6 and TLR9 pathways is partially responsible for the synergies, there may be a second mechanism at work, as inhibitor and antagonist treatment did not completely return immune activity to baseline levels.

Figure 3.7 NF-κB Activation of RAW-Blue 264.7 Macrophage Cell Line Treated with the LTA_CpG (TLR2/6_9) Di-Agonist and TLR2 or 9 Inhibitors and Antagonists[a]

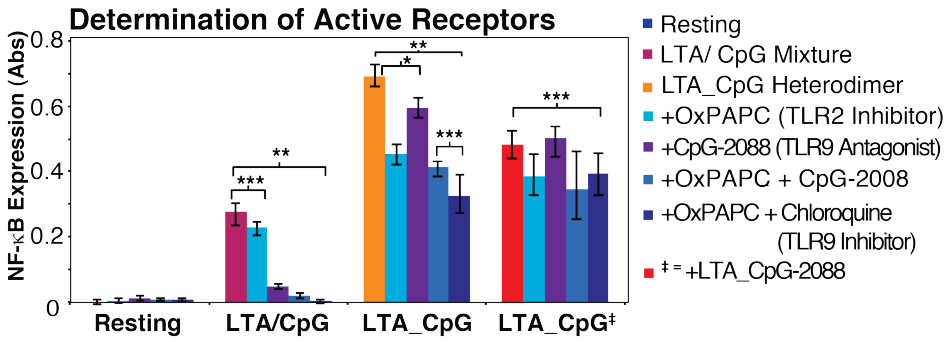

[a] RAW-Blue cells were incubated with a mixture of LTA and CpG unconjugated, LTA_CpG di-agonist, or LTA_CpG‡ antagonist for 18 h at 37 °C. Each bar is the result of n=6, where *p < 0.1, **p < 0.001, and ***NS is non-significant. Results are expressed as the mean ± SD.

Our current operating hypothesis is that a molecular-level synergy between TLR2 and TLR9 is enhanced by tethering the TLR2/6 agonist LTA to the TLR9 agonist CpG. This hypothesis is supported by synergies found in the herpes virus, which successively activates TLR2 and then TLR9, and by the decreased activity when the respective inhibitors were added.[21] We are not yet sure of the mechanism of this synergy. One possibility is that the LTA_CpG di-agonist creates an avidity effect for each TLR. Thereby, promoting formation of dimeric signaling complexes and recruitment of adaptor proteins, which results in increased stimulation. Although we have shown that the LTA_CpG di-agonist is sensitive to both TLR2 and TLR9 antagonists, we have not fully characterized the mechanism of increased stimulation. Therefore, this rationalization remains only one possible explanation. We also observed the RAW-Blue cell line stimulated with CpG or the LTA_CpG di-agonist by confocal microscopy. Cell binding and entry differed in time and location for CpG compared to the LTA_CpG di-agonist. CpG localized more rapidly, and LTA_CpG showed a greater, but more diffuse presence (see Appendix B, **Fig. S3.9**). This evidence in conjunction with the antagonist/inhibitor assay

provides support for the presence of a molecular-level synergy.

3.5 Conclusion

In summary, we synthesized a covalently coupled LTA_CpG di-agonist and observed increases in immune cell stimulation with the LTA_CpG di-agonist relative to a mixture of LTA and CpG. This increased stimulation was conserved across two different cell types and among T cell adhesion proteins as well as polarizing cytokines. Enhancement of the formation of higher-order signaling structures is a possible effect of covalent conjugation, but an effect that operates outside of TLRs cannot be ruled out. Increases in cell adhesion proteins and antigen presentation proteins were observed for the LTA_CpG di-agonist relative to a mixture of the two agonists. The corresponding cytokine profile was also greater in magnitude for the LTA_CpG di-agonist and suggested a pro-inflammatory, T_H1 response, similar to many individual TLR agonists. These results indicate that controlling the spatial presentation of agonists to dendritic cell receptors alters the stimulation of dendritic cells. We plan to further probe this amplification in T cell expansion assays. In addition, we are currently exploring different linker lengths and alternative di-agonist combinations to confirm a molecular level effect as well as using confocal microscopy to explore the mechanism of action.

3.6 Experimental Procedures

Lipoteichoic Acid_CpG-ODN1826 Di-Agonist (LTA_CpG) Synthesis.

Synthesis of Lipoteichoic Acid Conjugate (LTA_PEG$_6$-maleimide)

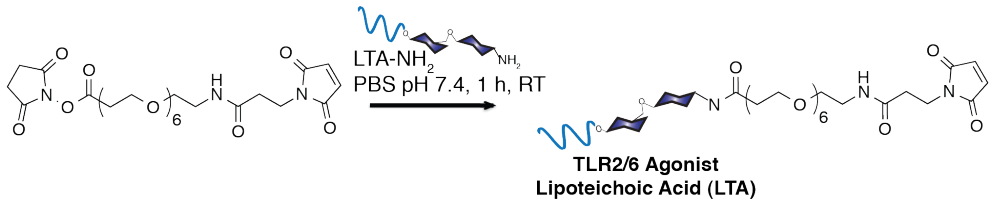

A stock solution of lipoteichoic acid (LTA) was prepared by dissolving 5 mg of solid LTA in 500 µL of PBS (pH 7.4). In a typical reaction, the PEG linker (12 µL of 100 mg/mL in DMSO) was added to LTA (2 mg of 10 mg/mL in PBS), and the solution was incubated at RT with constant shaking for 1 h. The crude reaction mixture was subjected to centriprep purification (3 kDa MWCO, PBS pH 7.4). Removal of excess PEG linker was confirmed by monitoring the UV/Vis absorbance of the filtrate at 260 nm (typically, 3 mL of buffer was required). The resulting LTA_PEG$_6$-maleimide conjugate was diluted to a final volume of 200 µL PBS (pH 7.4) before analysis by FPLC and UV/Vis (Abs_{max} = 260 nm).

For analysis of LTA by SDS-PAGE: The free amines of LTA and LTA_PEG$_6$-maleimide were reacted with fluorescein isothiocyanate (FITC). A stock solution of FITC (10 mg/mL in DMF) was diluted to a working concentration or 0.1 mg/mL in PBS. Aliquots (3 µL) of LTA (10 mg/mL in PBS) and the purified LTA_PEG$_6$-maleimide conjugate (10 mg/mL in PBS) were incubated with 1 µL each of the FITC stock solution at 40 °C for 15 min. Samples were immediately analyzed by SDS-PAGE without further purification. For confocal microscopy FITC (10 µL of 1 mg/mL in DMF) was added to a larger LTA aliquot (0.1 mL of 10 mg/mL in PBS), and the reaction mixture was incubated at 40 °C for 24 h. Excess FITC was removed from the LTA_FITC conjugate *via* centriprep purification (3 kDa MWCO, PBS). Removal of excess

FITC was confirmed by monitoring UV/Vis absorbance of the filtrate at 495 nm (see Appendix B, **Fig. S1**).

Disulfide Reduction of 5'-FAM-tccatgacgttcctgacgtt-3'-SH (CpG)

The DNA sequence 5'-FAM-tccatgacgttcctgacgtt-3'-SS-Et was obtained from Eurofins MWG Operon and diluted to a concentration of 1 mM in endotoxin free water. The 5'-FAM-tccatgacgttcctgacgtt-3'-SS-Et (100 μL of 1 mM in H_2O) was added to 300 μL of a 3% aqueous TCEP solution, and the reaction was incubated at RT for 1 h with constant shaking. Next, 50 μL of 3 M sodium acetate and 1.5 mL of EtOH were added to the reaction mixture. The solution was cooled at -78°C for 30 min. The frozen solution was centrifuged for 20 min at 4 °C, the supernatant was removed, and the pellet was dissolved in 400 μL of endotoxin free water. This procedure was repeated 3 times and the resulting CpG pellet was dried *in vacuo* before dilution to 1 mM PBS (pH 7.4) as measured by UV/Vis at 260 nm (ε = 196184 $M^{-1}cm^{-1}$). In a typical reaction, the extent of reduction was 70-80% as measured by Ellman's Assay. The reduced CpG was then used without further purification from the unreduced starting material.

Synthesis of Lipoteichoic Acid_CpG-ODN1826 Di-Agonist (LTA_CpG Di-Agonist)

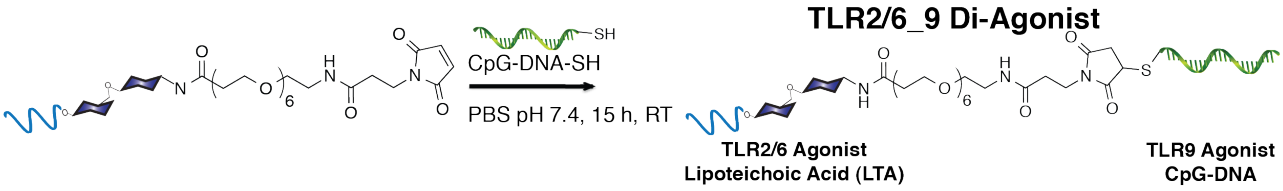

In a typical conjugation reaction, reduced CpG (50 μL of 1 mM in PBS) was added to LTA_PEG_6-maleimide (approximately 2 mg) diluted from the previous step to 200 μL in PBS (pH 7.4). The reaction mixture was incubated at RT overnight (15 h) with constant shaking. The

crude reaction mixture was passed through a 0.2 μm filter and directly purified by fast protein liquid chromatography (Superdex G75, PBS, 0.2 mL/min). Elution of the LTA_CpG di-agonist was confirmed by monitoring the elution absorbance at 260 nm (see Appendix B, **Fig. S3.3**). The LTA_CpG di-agonist was analyzed by UV/Vis and quantified via the local Abs_{max} at 495 nm (ε = 8.6 mL mg^{-1} cm^{-1}) as CpG by mass relative to known standards at 10 μg/mL (Di-agonist Abs 495/260 = 4.4, CpG Abs 495/260 = 3.2, see Appendix B, **Fig. S3.4**). The LTA_CpG di-agonist was further characterized *via* SDS-PAGE (see Appendix B, **Fig. S3.5**) and dynamic light scattering. Stable particles were not found by DLS (see Appendix B, **Fig. S3.6**) for CpG, LTA, a CpG/LTA mixture, or the CpG_LTA di-agonist when tested at a concentration of 10 μg/mL. Over time, agglomeration/sedimentation was detected for the LTA_CpG di-agonist and this was consistent with the sedimentation observed with LTA alone or in a mixture with CpG (LTA_CpG di-agonist ζ = -11.9 mV). Significant particle formation was also not observed by confocal microscopy (see Appendix B, **Fig. S3.9**).

Statistics.

Data was analyzed using a two-tailed t test. All values were reported as mean ± SD, unless stated otherwise.

***See Appendix B for Additional Figures.**

3.7 References

(1) Botos, I.; Segal, D. M.; Davies, D. R. The Structural Biology of Toll-like Receptors. *Structure* **2011**, *19* (4), 447–459.

(2) Yoon, S.; Kurnasov, O.; Natarajan, V.; Hong, M.; Gudkov, A. V.; Osterman, A. L.; Wilson, I. A. Structural Basis of TLR5-Flagellin Recognition and Signaling. *Science* **2012**, *335* (6070), 859–864.

(3) Tanji, H.; Ohto, U.; Shibata, T.; Miyake, K.; Shimizu, T. Structural Reorganization of the Toll-Like Receptor 8 Dimer Induced by Agonistic Ligands. *Science* **2013**, *339* (6126), 1426–1429.

(4) Chan, M.; Hayashi, T.; Kuy, C. S.; Gray, C. S.; Wu, C. C. N.; Corr, M.; Wrasidlo, W.; Cottam, H. B.; Carson, D. A. Synthesis and Immunological Characterization of Toll-Like Receptor 7 Agonistic Conjugates. *Bioconjug. Chem.* **2009**, *20* (6), 1194–1200.

(5) Napolitani, G.; Rinaldi, A.; Bertoni, F.; Sallusto, F.; Lanzavecchia, A. Selected Toll-like Receptor Agonist Combinations Synergistically Trigger a T Helper Type 1-Polarizing Program in Dendritic Cells. *Nat. Immunol.* **2005**, *6* (8), 769–776.

(6) Raman, V. S.; Bhatia, A.; Picone, A.; Whittle, J.; Bailor, H. R.; O'Donnell, J.; Pattabhi, S.; Guderian, J. A.; Mohamath, R.; Duthie, M. S.; et al. Applying TLR Synergy in Immunotherapy: Implications in Cutaneous Leishmaniasis. *J. Immunol.* **2010**, *185* (3), 1701–1710.

(7) Cao, X. Self-Regulation and Cross-Regulation of Pattern-Recognition Receptor Signalling in Health and Disease. *Nat. Rev. Immunol.* **2016**, *16* (1), 35–50.

(8) Trinchieri, G.; Sher, A. Cooperation of Toll-like Receptor Signals in Innate Immune Defence. *Nat. Rev. Immunol.* **2007**, *7* (3), 179–190.

(9) Reddy, S. T.; Swartz, M. A.; Hubbell, J. A. Targeting Dendritic Cells with Biomaterials: Developing the next Generation of Vaccines. *Trends Immunol.* **2006**, *27* (12), 573–579.

(10) Kasturi, S. P.; Skountzou, I.; Albrecht, R. A.; Koutsonanos, D.; Hua, T.; Nakaya, H. I.; Ravindran, R.; Stewart, S.; Alam, M.; Kwissa, M.; et al. Programming the Magnitude and Persistence of Antibody Responses with Innate Immunity. *Nature* **2011**, *470* (7335), 543–547.

(11) Shukla, N. M.; Salunke, D. B.; Balakrishna, R.; Mutz, C. A.; Malladi, S. S.; David, S. A. Potent Adjuvanticity of a Pure TLR7-Agonistic Imidazoquinoline Dendrimer. *PLoS ONE* **2012**, *7* (8), e43612.

(12) Fox, C. B.; Sivananthan, S. J.; Duthie, M. S.; Vergara, J.; Guderian, J. A.; Moon, E.; Coblentz, D.; Reed, S. G.; Carter, D. A Nanoliposome Delivery System to Synergistically Trigger TLR4 AND TLR7. *J. Nanobiotechnology* **2014**, *12* (1), 17.

(13) Kiessling, L. L.; Gestwicki, J. E.; Strong, L. E. Synthetic Multivalent Ligands as Probes of Signal Transduction. *Angew. Chem. Int. Ed.* **2006**, *45* (15), 2348–2368.

(14) Puffer, E. B.; Pontrello, J. K.; Hollenbeck, J. J.; Kink, J. A.; Kiessling, L. L. Activating B Cell Signaling with Defined Multivalent Ligands. *ACS Chem. Biol.* **2007**, *2* (4), 252–262.

(15) Shukla, N. M.; Mutz, C. A.; Malladi, S. S.; Warshakoon, H. J.; Balakrishna, R.; David, S. A. Toll-Like Receptor (TLR)-7 and -8 Modulatory Activities of Dimeric Imidazoquinolines. *J. Med. Chem.* **2012**, *55* (3), 1106–1116.

(16) Farrar, M. A.; Alberol-Ila, J.; Perlmutter, R. M. Activation of the Raf-1 Kinase Cascade by Coumermycin-Induced Dimerization. *Nature* **1996**, *383* (6596), 178–181.

(17) Fegan, A.; White, B.; Carlson, J. C. T.; Wagner, C. R. Chemically Controlled Protein Assembly: Techniques and Applications. *Chem. Rev.* **2010**, *110* (6), 3315–3336.
(18) Belshaw, P. J.; Ho, S. N.; Crabtree, G. R.; Schreiber, S. L. Controlling Protein Association and Subcellular Localization with a Synthetic Ligand That Induces Heterodimerization of Proteins. *Proc. Natl. Acad. Sci. U. S. A.* **1996**, *93* (10), 4604–4607.
(19) Lin, H.; Abida, W. M.; Sauer, R. T.; Cornish, V. W. Dexamethasone−Methotrexate: An Efficient Chemical Inducer of Protein Dimerization In Vivo. *J. Am. Chem. Soc.* **2000**, *122* (17), 4247–4248.
(20) Miyamoto, T.; DeRose, R.; Suarez, A.; Ueno, T.; Chen, M.; Sun, T.; Wolfgang, M. J.; Mukherjee, C.; Meyers, D. J.; Inoue, T. Rapid and Orthogonal Logic Gating with a Gibberellin-Induced Dimerization System. *Nat. Chem. Biol.* **2012**, *8* (5), 465–470.
(21) Sato, A.; Linehan, M. M.; Iwasaki, A. Dual Recognition of Herpes Simplex Viruses by TLR2 and TLR9 in Dendritic Cells. *Proc. Natl. Acad. Sci.* **2006**, *103* (46), 17343–17348.
(22) Sørensen, L. N.; Reinert, L. S.; Malmgaard, L.; Bartholdy, C.; Thomsen, A. R.; Paludan, S. R. TLR2 and TLR9 Synergistically Control Herpes Simplex Virus Infection in the Brain. *J. Immunol. Baltim. Md 1950* **2008**, *181* (12), 8604–8612.

CHAPTER 4

Synthesis of a TLR4_7_9 Tri-Agonist and *In Vitro* and *In Vivo* Biological Testing Thereof

4.1 Introduction

Since many effective, whole pathogen vaccines activate the innate immune system through synergistic interactions of multiple immune cell receptors, where Toll-like receptor (TLR) synergies are the most established, we sought to expand our immune synergy studies to covalently conjugating three TLR agonists together.[1–4] To determine how the spatial arrangement of three agonists affects immune synergies and to eliminate diffusion issues, a single molecular entity that activates multiple receptors is needed. Here, we covalently conjugated three TLR agonists *via* a tri-functional, small molecule core and correlated how the specific spatial arrangement directly controlled innate immune cell activation. We observed that treatment with the tri-agonist compound produced a distinct array of cytokines *in vitro*, and this activity translated *in vivo* to generate a wider set of antibodies against a model vaccinia virus vaccine.

In recent years, the conjugation of up to two TLR agonists has been explored, where treatment with covalently conjugated TLR agonists can generate immune responses that are synergistic or repressive.[5–8] However, the components of many vaccines activate three to five TLRs. A prime example is the Yellow Fever Vaccine, one of the most successful vaccines, which activates four different TLRs (2, 7, 8, and 9).[1,9,10] Some of these enhanced synergies are postulated to result from cooperation between MyD88 and TRIF adaptor proteins that are downstream from TLR activation and modulate changes in transcription.[11–16] As a result, our working hypothesis was that stimulating a specific set of TLRs on one cell *via* covalent linkage of three TLR agonists would activate a distinct pattern of cell-signaling molecules as measured

by transcription. If each molecular combination yields a distinct immune response profile, then the synthetic, spatial manipulation of TLR agonists could guide a particular immune response. To gain a better understanding of TLR synergies, we covalently attached three agonists together allowing spatially defined activation of three distinct TLRs.

In this chapter, we present the conjugation of pyrimido[5,4-b]indole, loxoribine, and CpG-ODN1826, TLR4, 7, and 9 agonists, respectively, into a single tri-agonist compound. TLR7 and 9 are endosomal receptors, while TLR4 is located on the cell surface and in the endosome. Once stimulated, each TLR activates a specific immune signaling pathway.[17,18] TLR4, 7, and 9 agonists were chosen on the basis of these agonists' previously reported synergistic effects on the immune response.[19–22] Using these agonists, the tri-agonist would activate multiple signaling pathways from the endosome or from both the endosome and cell surface, instead of a single pathway, which could result in a modulated cytokine and chemokine immune response. Immune activation with our tri-agonist was determined by measurement of NF-κB activation in RAW264.7 macrophage cells (RAW-Blue) and cytokine transcription levels in bone marrow-derived dendritic cells (BMDCs). Immune cells incubated with the covalently conjugated TLR4, 7, and 9 agonists exhibited an increase in NF-κB activation and changes in cytokine expression profiles relative to a mixture of the three unconjugated agonists. Additionally, using gene expression profiling, we observed that the covalent tri-agonist displayed a shift from a characteristic T_H1 biased response (cellular response) toward a balanced response with upregulation of genes linked to a T_H2 type response (humoral/antibody response), B cell activation, and innate and adaptive immune cell recruitment. Subsequently, we used the corresponding TLR signaling inhibitors to confirm contribution from TLR4 and TLR9 activation pathways. Additional studies comparing the effect of the tri-agonist on wild-type, MyD88, and

TRIF knockout mice verified activation of MyD88 and TRIF pathways, thus contributing to a synergistic increase in the immune response. Taking our studies into an *in vivo* vaccination model demonstrated that covalent conjugation of TLR agonists changes antibody production in terms of antibody breadth and depth, showing how synthetic chemical tools can shape the immune response. By chemically linking the three agonists in close proximity, we can begin to decipher how spatial arrangement contributes to immune agonist synergies at the molecular, cytokine, and gene expression levels.

4.2 Synthesis, Purification, and Characterization of a TLR4_7_9 Tri-Agonist

To covalently probe TLR synergies, we first synthesized a tri-agonist compound using three agonists exhibiting synergistic activity through specific TLRs (**Scheme 4.1**, and for additional synthetic details see Appendix C, **Schemes S4.1-S4.5**). The agonists were linked using orthogonal coupling chemistries on a tri-functional small molecule core. The triazine based molecule was synthesized by treating cyanuric chloride with amines containing alkyne, amine, and maleimide functional handles.[23] Increasing the reaction temperature with the addition of each moiety resulted in a modular asymmetric core. This approach allows many three-TLR agonist combinations to be synthesized and tested in future studies.

Scheme 4.1 Synthesis of the Tri-Functional Core and TLR4_7_9 Tri-Agonist

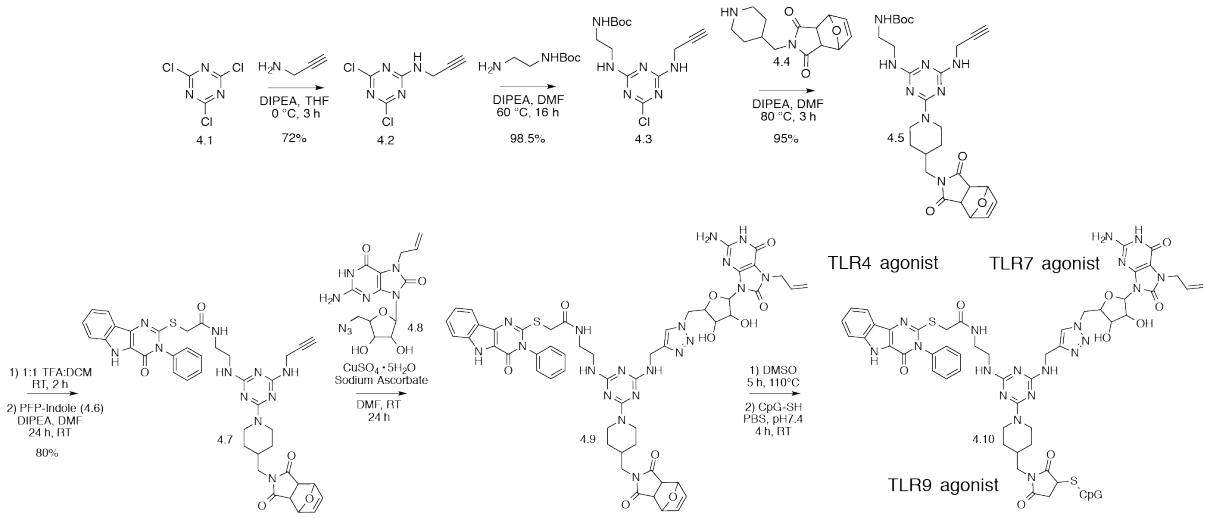

With a core that could be conjugated to three different bioactive molecules, we attached three TLR agonists, a pyrimido[5,4-b]indole (Indole, TLR4 agonist), loxoribine (Lox, TLR7 agonist), and CpG-ODN1826 (CpG, TLR9 agonist) to our core.[24–27] As mentioned, we chose these TLR agonists based on previous immune synergy studies activating two of the three TLRs together.[19–22] A pyrimido[5,4-b]indole compound was used to activate TLR4.[24] The carboxylic acid precursor of the pyrimido[5,4-b]indole compound was conjugated to the primary amine functionality on the core. Next, to activate TLR7, we attached an azide-modified loxoribine to the alkyne handle using copper-catalyzed Huisgen cycloaddition chemistry. Finally, to conjugate the TLR9 agonist CpG, the protected maleimide was revealed *via* a retro-Diels-Alder reaction and conjugated to a 5'-C6 linked thiol modified CpG-ODN1826 providing the tri-agonist conjugate, Indole_Lox_CpG (TLR4_7_9). 89.5% conversion was achieved when treating CpG with the TLR4_7 di-agonist (**4.9**) to provide the tri-agonist (**4.10**), as determined by gel electrophoresis using ImageJ software. The tri-agonist was extracted from the gel and isolated as the purified tri-agonist before analysis and use. Synthesis of the tri-agonist was confirmed by

MALDI-TOF and quantified *via* UV/Vis spectroscopy using the fluorescent 6-FAM tag on CpG (**Fig. 4.1a-c**, and see Appendix C, **Fig. S4.1**). In parallel reactions, the corresponding di-agonist compounds, Indole_Lox (TLR4_7), Lox_CpG (TLR7_9), and Indole_CpG (TLR4_9), were also synthesized to determine how each agonist contributed to immune activation (see Appendix C, **Schemes S4-S5**).

Figure 4.1 Structure and Characterization of the TLR4_7_9 Tri-Agonist (Indole_Lox_CpG)

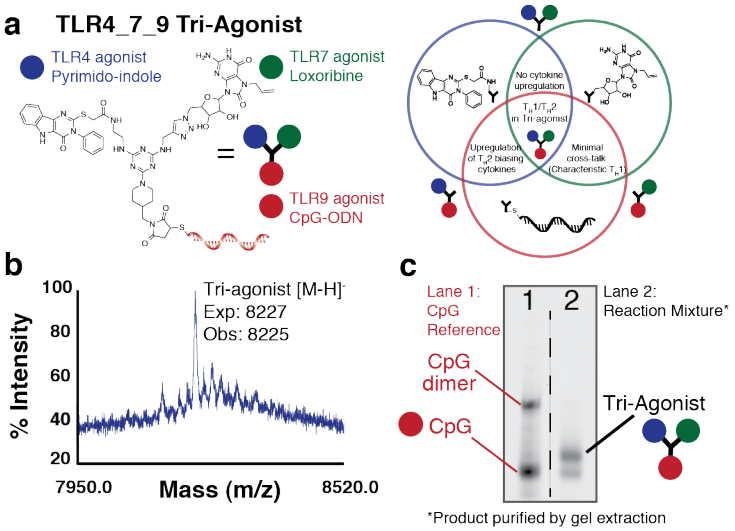

a) Chemical structure of the covalently conjugated tri- agonist compound (Indole_Lox_CpG) (left). Diagram illustrating how each TLR agonist (pyrimido-indole, loxoribine, or CpG-ODN) and the corresponding combinations (Indole_Lox, Lox_CpG, or Indole_CpG) contributed to innate immune activation (right). (b) Confirmation of synthesized Indole_Lox_CpG *via* MALDI-TOF. (c) Analysis of Indole_Lox_CpG *via* gel electrophoresis: CpG-ODN1826 reference (lane 1) and Indole_Lox_CpG reaction mixture (lane 2). Tri-agonist was extracted from the gel and isolated as purified Indole_Lox_CpG.

4.3 Testing *In Vitro* Biological Activity of TLR4, 7, 9 Di- and Tri-Agonists

4.3.1 NF-κB Activity in RAW-Blue Macrophages

First, to determine how covalent attachment of the three agonists affected synergistic activity, we measured NF-κB activation, one of the main transcription pathways involved in immune-related cytokine transcription, using the colorimetric macrophage reporter cell line,

RAW-Blue. The tri- and di- agonist compounds were incubated with RAW-Blue cells for 18 h, where Indole_Lox_CpG activity (0.5 μM) was compared to the same three TLR agonists in solution (0.5 μM Indole/0.5 μM Lox/0.5 μM CpG) as well as the related di-agonists (0.5 μM) (see Appendix C, **Fig. S4.4** for dose response curves). For all further experiments, we used our compounds exclusively at 0.5 μM, which was the concentration at which we observed the most distinct differences in NF-κB activation (with RAW-Blue cells) and cytokine production (with bone marrow-derived dendritic cells) between tri- and di-agonist compounds.

Figure 4.2 NF-κB Activation of RAW-Blue 264.7 Macrophage Cell Line Treated with the TLR4_7_9 Tri-Agonist[a]

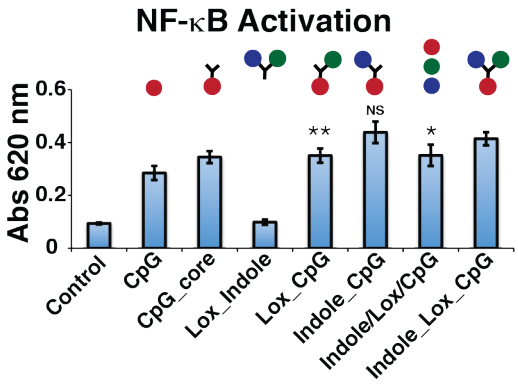

[a] RAW-Blue macrophage cells were treated with each compound at 0.5 μM for 18 h at 37 °C. Each bar is the result of n=6, where *p < 0.05 and **p < 0.01. All statistics represent the asterisked compound compared to Indole_Lox_CpG. Results are expressed as the mean ± SD.

We evaluated the differences in NF-κB activity between tri- and di-agonist constructs. Interestingly, comparing the dose response curves of Indole_Lox_CpG and Indole/Lox/CpG in RAW-Blue cells demonstrated that the linked tri-agonist and the individual agonists in solution were equipotent, but different levels of NF-κB activity were observed at 0.5 μM (**Fig. 4.2** and see Appendix C, **Fig. S4.4**). RAW-Blue cells treated with our tri-agonist compound, Indole_Lox_CpG, exhibited a 15% increase in NF-κB activation compared to the addition of the mixture of individual agonists (**Fig. 4.2**, *p < 0.05). This increase in NF-κB activation was

attributed to the covalent attachment between multiple TLR agonists. We hypothesized that the chemically linked agonists were presented to cells in a local manner that provided enhanced activation. Incubation with either the di-agonist compound, Lox_CpG, or CpG_core (only CpG attached to the small molecule center) resulted in a 15% decrease in NF-κB activation compared to the tri-agonist compound (**$p < 0.01$ and ***$p < 0.001$, respectively). These results demonstrated how Lox (TLR7) had no effect on immune activation when conjugated to only CpG (TLR9). This observation was likely due to CpG (EC_{50}: 0.15 μM) being a more potent agonist relative to Lox (see Appendix C, **Fig. S4.7** for loxoribine dose response curve).[25,28] In addition, we incubated RAW-Blue cells with the TLR4_9 di-agonist, while increasing the concentration of soluble Lox. We observed that at least 50 μM of soluble Lox was required to increase NF-κB activity over that elicited by just the TLR4_9 di-agonist (see Appendix C, **Fig. S4.5**, *$p < 0.05$), supporting that Lox is a weaker agonist. Therefore, Lox in the mixture of three agonists should contribute little to the overall immune activation at 0.5 μM. There was also no significant difference in NF-κB activity between Indole_ Lox_CpG and the di-agonist compound Indole_CpG. This result was also likely due to the lower potency of Lox. However, Indole_CpG exhibited 27% higher NF-κB activity than CpG_core (**$p < 0.01$), showing that Indole (TLR4) contributed to an increase in CpG (TLR9) activation. These results demonstrated that treatment with covalently linked Indole_Lox_CpG activated immune cells more than the mixture of three TLR agonists at equimolar concentrations, suggesting that agonist proximity has an effect on immune activation.

4.3.2 Cytokine Production in Bone Marrow-Derived Dendritic Cells (BMDCs)

We then analyzed how our molecules affected cytokine levels by testing our compounds on primary murine bone marrow-derived dendritic cells (BMDCs). BMDCs were incubated with

each compound (0.5 μM) for 6 h, and then analyzed by intracellular cytokine staining (ICS) to quantify changes in IL- 12 production, a pro-inflammatory cytokine signature of TLR activation (**Fig. 4.3**, and see Appendix C, **Fig. S4.8** for flow cytometry histograms).[14,29] These studies defined more subtle changes in immune activation. We observed that cells incubated with Indole_Lox_CpG exhibited a two-fold increase in the median fluorescent intensity (MFI) of IL-12 expressing cells compared to cells treated with Indole/Lox/CpG (**p < 0.01). These results correlated with our RAW-Blue studies that Indole_Lox_CpG resulted in increased immune activation compared to Indole/Lox/CpG. By placing the agonists in closer proximity due to covalent conjugation, Indole_Lox_CpG possibly achieves more effective stimulation of multiple TLRs, resulting in the observed synergy. In contrast, when the three agonists are in solution, the molecules freely diffuse through the cellular environment. This diffusion could prevent localization of the TLR agonists and subsequent activation of TLR4, 7, and 9 in a spatial manner.

Figure 4.3 Analysis of BMDC IL-12 Cytokine Profile[a]

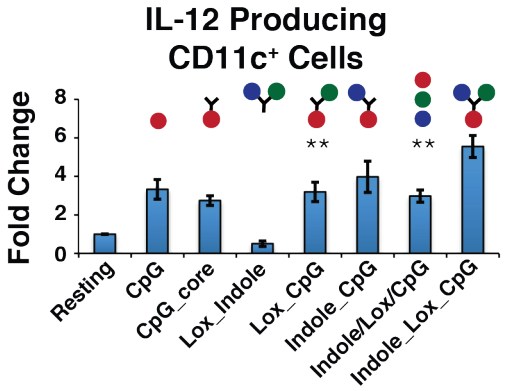

[a] BMDC activation *via* IL-12 cytokine profile as measured by intracellular cytokine staining flow cytometry, represented as the fold change of median fluorescent intensity (MFI) of IL-12 expressing cells compared to the no agonist control (Resting). BMDCs were incubated with each compound at 0.5 μM for 6 h at 37 °C, where Brefeldin A was added for the last 4 h of incubation. Each bar is the result of n=3, where **p < 0.01. All statistics represent the asterisked compound compared to Indole_Lox_CpG. Results are expressed as the mean ± SD.

To further examine how each agonist contributed to immune activation, we also compared

covalently conjugated di-agonist combinations that activated only two TLRs. IL-12 production of Indole_CpG, Lox_CpG, and CpG_core treated cells was comparable to that of Indole/Lox/CpG. On the other hand, Indole_Lox_CpG displayed nearly 1.5-fold higher IL-12 production than Indole_CpG, and Indole_CpG exhibited nearly 1.5-fold higher IL-12 production relative to CpG_core. Although both results were not significant, this data alluded to Lox's contribution to the upregulation of TLR activation in the tri-agonist and Indole's (TLR4) contribution to the upregulation of TLR activation when presented to immune cells with CpG (TLR9). These observations were confirmed with significant results in the gene expression profile experiments. In contrast, the activity of Lox_CpG was similar to that of CpG_core, demonstrating that Lox (TLR7) did not affect CpG (TLR9) activity and thus resulted in no change in IL-12 production. These results suggest how each agonist added to the overall activity of Indole_Lox_CpG, implying that particular agonist combinations give distinct responses.

4.3.3 Gene Expression Profiling of BMDCs

Since these covalent synergies were suggestive of specific changes in the cytokine levels based on the covalent conjugation and agonist combinations, we examined the global influence of these two parameters on dendritic cell gene expression profiles. Using microarray gene expression profiling, we measured changes in the transcription level of 561 genes associated with an immune response using a NanoString Immunology Assay (**Fig. 4.4a**). BMDCs were incubated with tri- and di-agonist constructs at 0.5 μM for 18 h. Then, total RNA was extracted (Qiagen RNeasy kit) and subsequently analyzed in triplicate using the microarray technology (UC Irvine Genomics High Throughput Facility). We mapped the activity of our compounds to gene expression for specific immune-related functions, such as T_H1 and T_H2 linked responses (**Fig. 4.4b**), to observe if activating specific agonist combinations in close proximity upregulated

a response and to what extent. We validated that the gene expression of *Il12* agreed with our intracellular flow cytometry experiments (**Fig. 4.4c**).

Figure 4.4 BMDC Gene Expression Profile

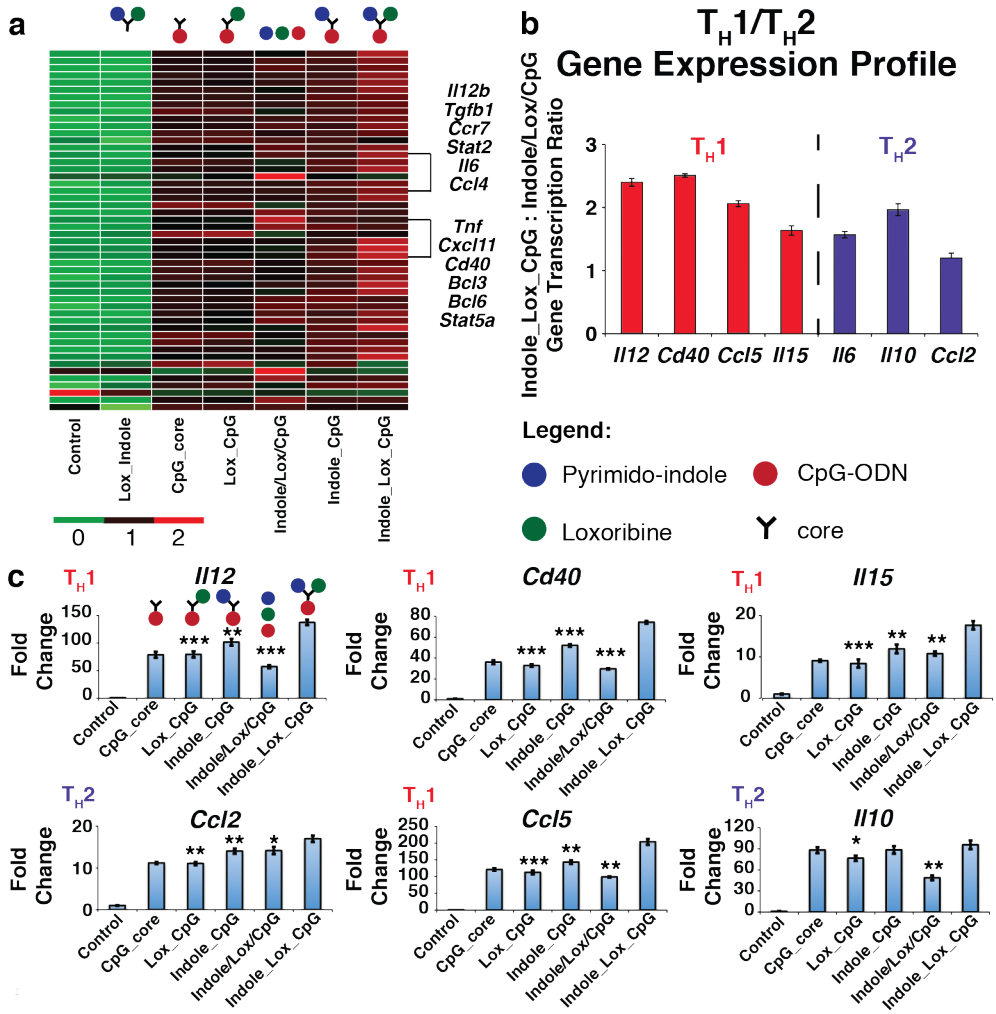

a) Heat map of immune function related genes. Each bar represents n=3. BMDCs were incubated with each compound for 18 h at 37 °C. Total RNA was then isolated using RNeasy kit (Qiagen) and analyzed using NanoString Technology. b) Graph illustrating T_H1/T_H2 gene expression profile comparing the gene transcription level of Indole_Lox_CpG to Indole/Lox/CpG. c) BMDC gene profile illustrating the main trend: Indole_Lox_CpG treated cells elicited the most upregulation in a subset of gene expression. Each figure illustrates the fold change of the specified agonist compared to the no agonist, media control and is the result of n=3, where *$p < 0.05$, **$p < 0.01$, and ***$p < 0.001$. All statistics represent the asterisked compound compared to Indole_Lox_CpG. Results are expressed as the mean ± SD.

Additionally, we observed two main trends in the gene profile data: one in which a subset

of gene expression related to T_H2 and T and B cell development was upregulated and a second in which a subset of gene expression related to inflammation and chemotaxis was upregulated, but to a lesser extent. The first trend corresponded to what we observed for *Il12* gene expression where Indole_Lox_CpG expressed the highest gene count, followed by Indole_CpG and last, Lox_CpG, CpG_core, and Indole/Lox/CpG, which were typically comparable (**Fig. 4.4b-c**). This major trend of upregulation was observed not only with *Il12* expression, which is associated with a T_H1 polarized response, but also with a subset of gene expression related to T_H2 responses and activation of innate and adaptive immunity, which included *Il6*, *Il10*, *Il15*, *Cd40*, *Ccl2*, and *Ccl5* (**Fig. 4.4c**).[30,31]

Comparing CpG_core to the di-agonists, Indole_CpG and Lox_CpG, showed that Indole (TLR4) upregulated CpG (TLR9) activity as exemplified by the 1.3-fold increase in *Il12* gene expression of Indole_CpG compared to CpG_core (**Fig. 4.4c**, $^{**}p < 0.01$). Lox (TLR7), on the other hand, did not change CpG (TLR9) activity in Lox_CpG, and Indole_Lox still did not activate immune cells. However, the addition of Lox (TLR7) to the TLR4_9 combination in Indole_Lox_CpG was associated with upregulation of the immune response gene expression profile. This upregulation correlated with our previous observations, signifying the importance of activating specific TLR agonist combinations in close proximity and the effect of synergistic interactions on innate immune cells.

Interestingly, Indole_Lox_CpG activity also exhibited a lower level of gene upregulation with a subset of genes compared to the agonists in solution (**Fig. 4.5**). Regulatory genes and those in the TNF ligand family were upregulated to a lower degree by our covalent compound Indole_Lox_CpG compared to Indole/Lox/CpG ($^{**}p < 0.01$). This subset of genes included *Tnfsf14*, *Tgfbi*, and *Tnfsf13b*.[32,33] In other cases, when compared to Lox_CpG, the tri-agonist

compound exhibited a decrease in gene upregulation, with genes such as *Tnf* and *Ccl4* (***p < 0.001 and *p < 0.05, respectively), related to inflammation and immune cell chemoattraction. In general, this repressive trend showed that Indole_CpG and Indole_Lox_CpG exhibited lower gene expression compared to Lox_CpG and CpG_core. This result suggested that Indole (TLR4) caused less upregulation of a subset of genes related to the TNF ligand family and inflammation, which contributed to the lower fold change in gene expression observed with Indole_Lox_CpG treated cells. Comparing the tri- and di- agonist compounds demonstrated how each TLR agonist affected specific families of genes. Thus, particular agonist combinations upregulated defined subsets of gene expression to different extents, possibly affecting downstream signaling and adaptive immune responses.

Figure 4.5 BMDC Gene Expression Profile Data

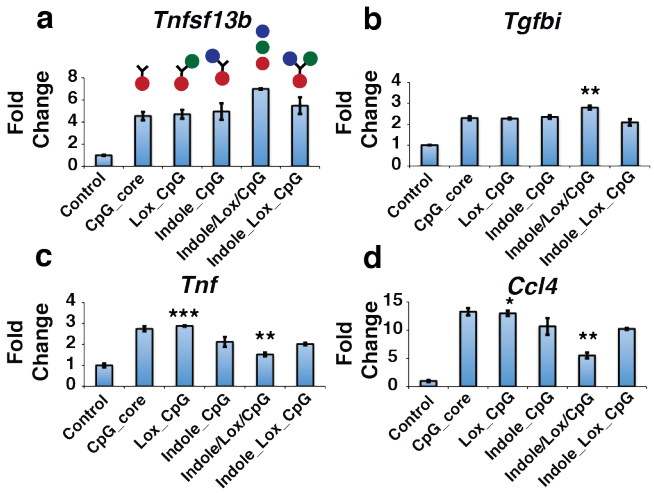

a-d) BMDC gene expression profile illustrating second main trend observed, where Indole contributed to a decrease in CpG immune activity exhibited by Indole_Lox_CpG. BMDCs were incubated with each compound for 18 h at 37 °C. Total RNA was then isolated using RNeasy kit (Qiagen) and analyzed using NanoString Technology. Each figure illustrates the fold change of the specified agonist compared to the no agonist control and is the result of n=3, where *p < 0.05, **p < 0.01, and ***p < 0.001. All statistics represent the asterisked compound compared to Indole_Lox_CpG. Results are expressed as the mean ± SD.

4.4 Mechanism of Action: TLR Inhibitor and Knockout Studies

To understand what signaling pathways were involved in Indole_Lox_CpG activation, we used BMDCs harvested from MyD88 knockout ($MyD88^{-/-}$) and TRIF knockout ($TRIF^{-/-}$) mice. MyD88 and TRIF are adaptor proteins downstream of TLR activation and control transcription of immune-signaling molecules. Research has shown that MyD88 and TRIF work together to synergistically activate cytokine production and enhance the immune response.[11,12] We treated each group of BMDCs with Indole_Lox_CpG for 6 h and then assessed IL-12 production using ICS. When treated with the tri-agonist, both $TRIF^{-/-}$ and $MyD88^{-/-}$ BMDCs showed decreases in IL-12 production compared to treated wild-type (WT) BMDCs, nearly two-fold and seven-fold decreases ($*p < 0.05$ and $**p < 0.01$), respectively (**Fig. 4.6a**). These results demonstrated that Indole_Lox_CpG activated the TRIF pathway, probably originating from Indole, since TLR4 agonists can signal *via* both MyD88 and TRIF pathways.[12,17,34] Activation was heavily dependent on MyD88 activation, as shown by the seven-fold decrease in IL-12 production, which was likely due to CpG (TLR9) being a strong MyD88 activator.[35] The difference in TRIF and MyD88 activation levels may also be due to a temporal component of immune pathway activation that will require further investigation.[36] With the ability to change MyD88 and TRIF activation levels using tri-agonist constructs, we can synthesize other multi-agonist adjuvants that potentially provide tailored immune responses.

Figure 4.6 BMDC Cytokine and Gene Expression Profile of Mechanistic Studies using TRIF and MyD88 Knockout Mice or TLR Signaling Inhibitors

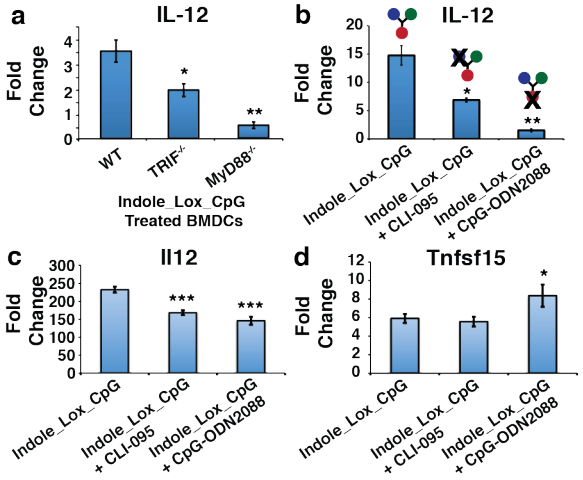

a) IL-12 cytokine profile of wild-type (WT), TRIF knockout (TRIF$^{-/-}$), and MyD88 knockout (MyD88$^{-/-}$) BMDCs treated with Indole_Lox_CpG, represented as the fold change of median fluorescent intensity (MFI) of IL-12 expressing cells compared to the no agonist, media control. BMDCs were incubated with Indole_Lox_CpG for 6 h at 37 °C, where Brefeldin A was added for the last 4 h of incubation. Each figure is the result of n=3, where *$p < 0.05$ and **$p < 0.01$. b) BMDC IL-12 cytokine profile with TLR signaling inhibitors, represented as the fold change of median fluorescent intensity (MFI) of IL-12 expressing cells compared to the no agonist, media control. BMDCs were incubated with the designated inhibitor for 1 h at 37 °C and then each compound for 6 h at 37 °C. Brefeldin A was added for the last 4 h of incubation. Each figure is the result of n=3, where *$p < 0.05$ and **$p < 0.01$. c-d) Gene expression profile representative of the two main trends observed when BMDCs were treated with TLR signaling inhibitors: c) *Il12* expression of Indole_Lox_CpG treated cells incubated with CLI-095 (TLR4 inhibitor) and CpG-ODN2088 (TLR9 antagonist), showing contributions from TLR4 and TLR9 pathways, and d) upregulation of gene expression profile when TLR9 signaling was inhibited. Each figure illustrates the fold change of the specified agonist compared to the no agonist, media control and is the result of n=3, where *$p < 0.05$ and ***$p < 0.001$. All statistics represent the asterisked compound compared to Indole_Lox_CpG. Results are expressed as the mean ± SD.

In order to identify the precise role of each agonist/receptor set in directing BMDCs, we used a TLR inhibitor and antagonist to perform mechanistic studies. Our hypothesis was that inhibiting activation of a single type of TLR would lead to a subsequent change in cytokine levels and gene expression, confirming that receptor's role in the response elicited from Indole_Lox_CpG. A TLR4 intracellular domain inhibitor, CLI-095,[37,38] and a TLR9 antagonist oligonucleotide, CpG-ODN2088,[39] were used to selectively inhibit TLR signaling or block TLR

agonist binding, respectively. The inhibitor or the antagonist was used along with the tri-agonist compound, Indole_Lox_CpG. Resulting cytokine production allowed us to determine the contribution of each agonist and TLR activation pathway.

First, we examined whether each signaling inhibitor reduced IL-12 production. BMDCs were incubated with a designated inhibitor for 1 h before adding in Indole_Lox_CpG. The cells were then incubated for an additional 6 h, and ICS was performed to assess IL-12 production. Using CLI-095 (100 nM), a minimal, but significant, decrease in IL-12 (20% decrease of Indole_Lox_CpG IL-12 production with CLI-095 compared to Indole_Lox_CpG, *$p < 0.05$) was observed (**Fig. 4.6b**, and see Appendix C, **Fig. S4.9** for flow cytometry histograms). When incubating with CpG-ODN 2088 (100 nM), greater inhibition of IL-12 production (80% decrease of Indole_Lox_CpG IL-12 production with CpG-ODN2088 compared to Indole_Lox_CpG, **$p < 0.01$) was observed, confirming that TLR9 was the main contributor of IL-12 production when treating cells with Indole_Lox_CpG. The TLR9 antagonist, CpG-ODN2088, was used to synthesize an antagonist version of the tri-agonist compound (Indole_Lox_CpG2088). Incubating Indole_Lox_CpG2088 with BMDCs reduced IL-12 production to near resting state (see Appendix C, **Fig. S4.10**, **$p < 0.01$). The low amount of cytokine production without CpG was attributed to the potency of CpG, also showing that the incorporation of CpG was necessary to observe synergistic activity between TLR4, 7, and 9.

Expanding our studies to a broader range of cytokines and proteins *via* the NanoString assay, we analyzed gene expression of BMDCs after exposure to CLI-095 or CpG-ODN2088 and Indole_Lox_CpG (**Fig. 4.6c-d**). We observed two main trends that correlated to the two trends observed in the previous tri- and di-agonist comparisons: first, that activation of all three receptors is important for the upregulation of genes to elicit a more balanced response, and

second, that defined agonist combinations control the specific direction of the activity. The ICS experiment matched the main trend observed in the gene studies. *Il12* gene expression was reduced by CLI-095 (28% decrease of Indole_Lox_CpG *Il12* expression with CLI-095 compared to Indole_Lox_CpG, ***p < 0.001) and further by CpG-ODN2088 (38% decrease of Indole_Lox_CpG *Il12* expression with CpG-ODN2088 compared to Indole_Lox_CpG, ***p < 0.001), confirming contribution from TLR4 and TLR9 signaling pathways. This trend applied to the majority of genes, including pro-inflammatory genes *Il6* and *Il15* as well as adaptive immune-related genes *Ccl2* and *Ccl5*. The second trend observed resulted in gene upregulation relative to Indole_Lox_CpG when TLR9 inhibition occurred and minimal to no decrease in gene expression with TLR4 inhibition. This was observed for genes related to $CD4^+$ cell chemotaxis and development as well as the TNF ligand family. This confirmed how close agonist proximity through covalent modifications resulted in contribution from multiple TLR activation pathways, which altered and directed innate immune responses.

4.5 Testing *In Vivo* Activity for Antibody Depth and Breadth with a Vaccinia Virus Vaccination Model

After studying how our compounds changed the immune response *in vitro*, we wanted to observe how Indole_Lox_CpG performed *in vivo* using a model vaccination system, vaccinia virus (small pox). C57BL/6 mice were immunized *via* intramuscular (i.m.) injection with heat-inactivated vaccinia virus (2.5 × 107 pfu/ mL) and adjuvanted with either phosphate buffered saline (PBS) as the vehicle, Indole/Lox/CpG (0.05 nmol of each agonist), or Indole_Lox_CpG (0.05 nmol). Mice were boosted on day 14 with the designated vaccine. Serum was drawn from the mice on day 0, 7, 14, 21, and 28, and analyzed using a vaccinia protein microarray[40] to determine antibody depth and breadth. Looking at the immunodominant vaccinia antigen

(WR148), Indole_Lox_CpG displayed the greatest depth in IgG1 antibody response (**Fig. 4.7a**). Additionally, Indole_Lox_CpG elicited the broadest breadth in antigen-specific antibody response compared to the no adjuvant vehicle or Indole/Lox/CpG (**Fig. 4.7b**, **p < 0.01). In contrast, Indole/ Lox/CpG did not significantly change antibody depth or breadth compared to the vehicle. These results demonstrated that delivering a single, spatially defined tri-agonist compound *in vivo* can control antibody responses. The difference in antibody response between the tri-agonist, Indole_Lox_CpG, and Indole/Lox/CpG may be attributed to the different immune signaling pathways that are activated and the order in which the TLRs are stimulated, as a result of the covalent linkage and spatial arrangement of the TLR agonists. We are currently working on performing more *in vivo* studies to understand the mechanism and effect of different agonist combinations. These experiments show the utility and influence covalently linked multi-agonists might have on immunotherapy development.

Figure 4.7 Vaccinia Virus Vaccination Model with Indole_Lox_CpG as the Adjuvant

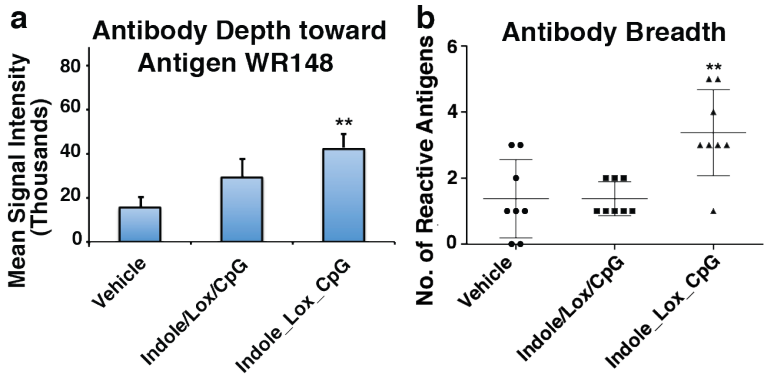

a-b) Effect of Indole_Lox_CpG on IgG1 immune response in heat-inactivated vaccinia virus immunized mice. Mice were vaccinated *via* i.m. injection on day 0 with heat inactivated vaccinia virus (2.5 × 107 pfu/mL) adjuvanted with PBS (Vehicle), Indole/Lox/CpG, or Indole_Lox_CpG with a total injection volume of 50 μL. Mice were boosted on day 14. At day 28, the experiment end point, serum was collected from mice and probed on a vaccinia protein microarray. a) Mean signal intensities of sera toward vaccinia immunodominant antigen WR148 at day 28, where **p < 0.01. b) Number of reactive antigens in sera of immunized mice at day 28, where **p < 0.01. Results are expressed as the mean ± SEM; n = 8/group; unpaired, two-tailed t test. All statistics represent the asterisked compound compared to the no adjuvant vehicle.

4.6 Conclusion

Here, we present evidence that the spatial arrangement of TLR agonists and the specific combinations of stimulated receptors resulted in defined activation patterns of dendritic cells. We detailed the synthesis of a tri-agonist construct, expanding recent two agonist synergistic studies to the use of three agonists. Through conjugation of a third agonist and in close proximity, we created a distinctive, more balanced response, shifting the immune response from T_H1 polarization to a more balanced T_H1/T_H2 response and activation of innate and adaptive immunity. By comparing the tri-agonist compound to di-agonist constructs, we observed how each agonist shaped the innate immune response. Mechanistic studies were performed with adaptor protein knockout mice and the corresponding TLR inhibitor and antagonist to show the specific receptors and pathways through which the tri-agonist compound proceeded. We also observed that Indole_Lox_CpG increased antibody breadth and signal intensity toward a specific antigen when compared to the mixture of three agonists. In future studies, we plan to synthesize other TLR agonist combinations. These molecules will aid in determining how covalent synergies direct antigen presentation and the types of cell populations that become activated. The covalently linked Indole_Lox_CpG aided in elucidating how TLR4, 7, and 9 synergies contributed to the observed changes in innate immune responses. Chemically controlling the spatial organization of innate immune agonists and specific agonist combinations can be used as a tool to direct immune responses and further understand how the immune system responds to pathogens. From this, researchers can potentially start to develop more effective immunotherapies using adjuvants designed to elicit targeted responses.

4.7 Experimental Procedures

RAW264.7 Macrophage (RAW-Blue) NF-κB Assay.

RAW-Blue cells were plated at 10 x 10^4 cells/mL density (180 μL) in 96-well plates using testing media: D-MEM High Glucose medium (Life Technologies), 10% heat inactivated FBS, 2 mM L-glutamine, and antibiotic-antimycotic (1x). RAW-Blue cells were incubated with 20 μL of each agonist for 18 h at 37 °C in a CO_2 incubator. Cell medium (50 μL) from the stimulated RAW-Blue cells was removed, placed into a 96-well plate, and incubated with QUANTI-Blue solution (InvivoGen) (150 μL) for 1.5 h at 37 °C in a CO_2 incubator. The absorbance (620 nm) was measured using a Fisher Scientific MultiSkan FC.

In Vitro Bone Marrow-Derived Dendritic Cell Culture and Intracellular Cytokine Staining.

Monocytes were harvested from 6-week-old C57BL/6, B6.129P2(SJL)-Myd88$^{tm1.1Defr}$/J(MyD88$^{-/-}$), or C57BL/6J-*Ticam1*^{Lps2}/J (TRIF$^{-/-}$) mice.[41] Monocytes were differentiated into dendritic cells (BMDCs) using supplemented culture medium: RPMI 1640 (Life Technologies), 10% heat inactivated fetal bovine serum (Sigma), 20 ng/mL granulocyte-macrophage colony-stimulating factor (produced using "66" cell line), 2 mM L-glutamine (Life Technologies), antibiotic-antimycotic (1x) (Life Technologies), and 50 μM beta-mercaptoethanol (Sigma). After 5 days of culture, BMDCs were incubated with each agonist (0.5 μM) in culture medium for 6 h at 37 °C in a CO_2 incubator. GolgiPlug (BD Biosciences), containing Brefeldin A, was added to cell culture for the final 4 h of culture. Cells were stained for intracellular IL-12 cytokine production and analyzed using BD Accuri C6.

Immunization.

C57BL/6 mice were vaccinated intramuscularly (i.m.) at day 0 with heat-inactivated vaccinia virus Western Reserve (VVWR) strain (2.5 × 107 pfu/mL) adjuvanted with specified multi-

agonist compound(s) (0.05 nmol) or PBS as a control in a total injection volume of 50 μL. Mice received vaccine boost at day 14. Serum samples were collected from mice *via* saphenous vein at day 0, 7, 14, 21, and 28 post vaccination.

Viruses.

VVWR stocks were grown on HeLa cells in T175 flasks, infecting at a multiplicity of infection of 0.5. Cells were harvested at 60 h, and virus was isolated by rapidly freeze-thawing the cell pellet three times in a volume of 2.3 mL of RPMI plus 1% fetal calf serum (FCS). Cell debris was removed by centrifugation. Clarified supernatant was frozen at -80 °C as virus stock. VVWR stocks were titered on Vero cells (2 × 108 pfu/mL). Heat-inactivated VVWR stock was prepared by incubating virus on a water bath at 65 °C for 1 h.

Gel Electrophoresis.

CpG-ODN containing compounds were purified using Mini-PROTEAN TBE-Urea Precast Gels (BIO-RAD) and Mini-PROTEAN Tetra Cell system. Compounds were loaded into gels in TBE urea buffer (7:20 compound:loading buffer). Gels were run in TBE buffer at 100 V for 1 h. The resulting gels were imaged using a GE Typhoon gel scanner. The desired band was excised, crushed, and eluted into HPLC grade water overnight at 37 °C. The resulting solution was concentrated using 3k Amicon Centrifugal Filter Units (EMD Millipore) and filtered using 0.2 μM cellulose acetate syringe filter (Restek). The resulting product was desalted using $ZipTip_{C18}$, analyzed by MALDI-TOF using 3-hydroxypicolinic acid matrix, and quantified using a NanoDrop spectrophotometer.

MALDI-TOF.

The reaction mixture was passed through $ZipTip_{C18}$ (Millipore) according to Millipore protocol: $ZipTip_{C18}$ was equilibrated with 50% acetonitrile/water (2 x 10 μL) and subsequently 0.1 M

triethylammonium acetate (TEAA) (3 x 10 μL). The oligonucleotide-containing compound was passed through the $ZipTip_{C18}$ (10 x 10 μL). The $ZipTip_{C18}$ was washed with 0.1 M TEAA buffer (3 x 10 μL) followed by nanopure water (3 x 10 μL). The desired product was eluted using 50% acetonitrile/water (3 x 10 μL). The eluted product was concentrated using a speed-vacuum and mixed with 0.36 M 3-hydroxypicolinic acid matrix (1:1 acetonitrile:300 mM ammonium citrate solution in 50% acetonitrile/water) (2 μL). The sample was spotted directly onto the MALDI plate and analyzed in negative ion mode. For small molecules, the sample was spotted with α-cyano-4-hydroxycinnamic acid matrix (in 1:1 acetonitrile:water with 0.1% TFA) and analyzed in positive ion mode.

Production and Probing of Vaccinia Protein Microarray.

The cloning and expression platform is described in detail previously.[40] Briefly, custom PCR primers comprising 20 bp of gene-specific sequence with 33 bp of "adapter" sequences were used in PCRs with vaccinia virus WR strain genomic DNA as a template. The adapter sequences, which become incorporated into the termini flanking the amplified gene, were homologous to the cloning site of the T7 expression vector pNHisCHA (Gene Therapy Systems, San Diego, CA) and allowed the PCR products to be cloned by homologous recombination in competent DH5α cells. The adapters also incorporated a 5'-polyhistidine epitope, an ATG translation start codon, and a 3'-hemagglutinin epitope and T7 terminator. Sequence-confirmed plasmids were expressed in 5 h *in vitro* transcription-translation reactions (RTS 100 kits from Roche) according to the manufacturer's instructions. Protein expression was monitored either by dot blot or by microarray using both monoclonal anti-polyhistidine (clone His-1 from Sigma) and monoclonal anti-hemagglutinin (clone 3F10 from Roche) antibodies, followed by appropriate secondary antibodies. Microarrays were printed onto nitrocellulose coated glass slides (FAST from

Schleicher & Schuell Bioscience) using an Omni Grid 100 microarray printer (Gene Machines). Prior to array staining, the sera were diluted to 1/100 in Protein Array Blocking Buffer (Schleicher & Schuell Bioscience) containing *Escherichia coli* lysate at a final concentration of 10% and incubated at room temperature for 1 h with constant mixing. The arrays were rehydrated in blocking buffer for 30 min and probed with the pretreated sera for 2 h at room temperature with constant agitation. The slides were then washed 3 times in Tris buffer containing 0.05% Tween-20 and incubated with biotin conjugated anti-mouse IgG1 secondary antibodies at 1:200 in blocking buffer for 1 h. The slides were then washed 3 times with Tris buffer containing 0.05% Tween-20 followed by incubation with streptavidin-Surelight P-3 conjugated at 1:200 in blocking buffer for 45 min. After washing, the slides were air-dried under brief centrifugation and stored in a desiccator at room temperature. The microarrays were scanned using a Gene Pix 4100A scanner (Molecular Devices, Sunnyvale, CA), and image analysis was performed with Genepix Pro 5.0 software (Molecular Devices). The spot intensity was calculated as the median spot value minus local spot background. A secondary correction for background binding to *E. coli* proteins in the reaction mixture was done by subtracting an average of the no-DNA spots from the background-corrected spot value.

Synthetic Procedures

Compounds **4.2** and **4.3** (synthetic scheme provided in **Scheme 4.1** in the main text) were synthesized according to Banerjee, R. *et* al.[23] Pyrimido-indole carboxylic acid derivative (see Appendix C, **Scheme S4.1**) was synthesized according to Chan, M. *et al*.[24]

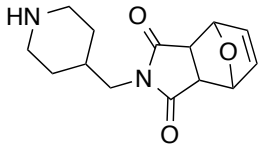

2-(piperidin-4-ylmethyl)-3a,4,7,7a-tetrahydro-1*H*-4,7-epoxyisoindole-1,3(2*H*)-dione (4.4). Exo-7-oxabicyclo[2.2.1]hept-5-ene-2,3-dicarboxylic anhydride (3.6 mL, 0.030 mol) was dissolved in ethanol (30.1 mL). 4-(Aminomethyl) piperidine (3.6 mL, 0.030 mol) was subsequently added to the solution. The reaction mixture was heated at reflux for 3 h. The mixture was concentrated and dissolved in deionized water. The aqueous layer was washed with dichloromethane (5x). The organic layer was dried with sodium sulfate, filtered, and concentrated. The desired product was a white solid (3.2 g, 40% yield). ^{1}H NMR (500 MHz, CD_3OD) δ 6.55 (s, 2H), 5.15 (s, 2H), 3.34 (d, *J* = 5, 2H), 2.99 (br td, *J* = 12.5, 3**,** 2H), 2.92 (s, 2H), 2.49 (td, *J* **=** 12.5, 3, 2H), 1.84-1.76 (m, 1H), 1.60 (app. br d, *J* = 12.5, 2H), 1.05 (qd, *J* = 25, 12.5, 4, 2H). ^{13}C NMR (500 MHz, CD_3OD)

δ 178.7, 137.6, 82.3, 48.3, 46.3, 45.1, 35.7, 30.8. HRMS: *m/z* calcd for $C_{14}H_{18}N_2O_3$ $[M+H]^+$ 263.1396, observed 263.1393.

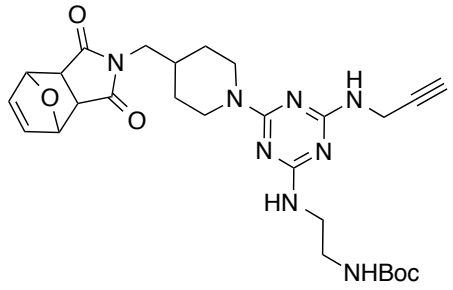

***Tert*-butyl (2-((4-(4-((1,3-dioxo-1,3,3a,4,7,7a-hexahydro-2*H*-4,7-epoxyisoindol-2-yl)methyl)piperidin-1-yl)-6-(prop-2-yn-1-ylamino)-1,3,5-triazin-2-yl)amino)ethyl)carbamate (4.5).** Compound **4.3** (0.10 g, 0.31 mmol) was dissolved in anhydrous DMF (1.0 mL). DIPEA (59 μL) and **4.4** (0.090 g, 0.34 mmol) were subsequently added to the solution. The reaction

mixture was heated at 80 °C for 3 h. The mixture was concentrated and purified by column chromatography (100% EtOAc). The product was a light yellow shiny solid (0.16 g, 95% yield). ^{1}H NMR (500 MHz, $CDCl_3$) δ 6.52 (s, 2H), 5.27 (s, 2H), 4.70 (br s, 2H), 4.15 (br s, 1H), 3.48 (br s, 2H), 3.38 (d, *J* = 7.5, 2H), 3.30 (br d, *J* = 4, 2H), 2.85 (s, 2H), 2.75 (app. br t, *J* = 10.5, 2H), 2.21 (t, *J* = 2.5, 1H), 1.98 (br m, 1H), 1.65 (app. br d, *J* = 12.5, 2H), 1.42 (s, 9H), 1.16 (app. br q, *J* = 11, 2H). ^{13}C NMR (500 MHz, $CDCl_3$) δ 176.5, 166.2, 165.3, 164.4, 156.2, 136.5, 80.9, 79.1, 70.8, 56.0, 47.3, 44.1, 42.8, 41.5, 40.5, 34.9, 30.3, 29.5, 28.3. HRMS: *m/z* calcd for $C_{27}H_{36}N_8O_5$ $[M+Na]^+$ 575.2706, observed 575.2717.

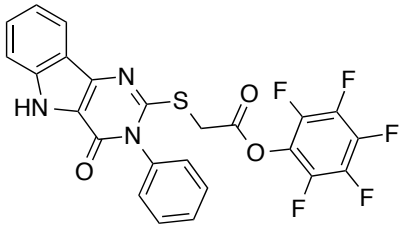

Perfluorophenyl 2-((4-oxo-3-phenyl-4,5-dihydro-3*H*-pyrimido[5,4-*b*]indol-2-yl)thio)acetate (PFP-pyrimido-indole, 4.6). The carboxylic acid derivative[24] (0.50 g, 1.4 mmol) was dissolved in anhydrous DMF (2.8 mL). DIPEA (0.49 mL, 2.8 mmol) and pentafluorophenyl triflouroacetate (PFP-TFA) (0.37 mL, 2.1 mmol) were then added. The reaction stirred for 18 h at room temperature and the solution turned dark brown black color. The reaction mixture was concentrated and recrystallized using ethyl acetate to obtain brown, green crystals. The product was confirmed by ^{1}H NMR, ^{19}F NMR, and ESI-MS and submitted crude. ^{1}H NMR (500 MHz, DMSO-d_6) δ 13.4 (s, 1H), 9.03 (d, *J* = 9.5, 1H), 7.78 (br t, *J* = 7, 3H), 7.71 (app. br dd, *J* = 7.5, 2H), 7.68 (app. br d, *J* = 10, 1H), 7.60 (t, *J* = 8, 1H), 7.39 (t, *J* = 8, 1H), 3.57 (br s, 1H), 3.09 (br s, 1H). ^{19}F NMR (400 MHz, DMSO-d_6) δ -164.1, -167.3. ESI-MS: *m/z* calcd for $C_{24}H_{12}F_5N_3O_3S$ $[M+H]^+$ 540.0, observed 540.0.

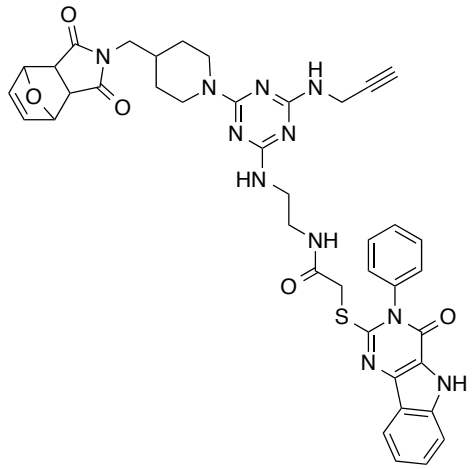

***N*-(2-((4-(4-((1,3-dioxo-1,3,3a,4,7,7a-hexahydro-2*H*-4,7-epoxyisoindol-2-yl)methyl)piperidin-1-yl)-6-(prop-2-yn-1-ylamino)-1,3,5-triazin-2-yl)amino)ethyl)-2-((4-oxo-3-phenyl-4,5-dihydro-3*H*-pyrimido[5,4-*b*]indol-2-yl)thio)acetamide (Indole_core, 4.7).** Compound **4.5** (0.20 g, 0.36 mmol) was dissolved in dichloromethane (0.90 mL). Trifluoroacetic acid (0.90 mL) was then added. The reaction was allowed to stir for 2 h at RT. The solution was concentrated. The crude residue was dissolved in a dilute sodium bicarbonate solution. The aqueous layer was washed with dichloromethane (3x). The organic layer was dried with sodium sulfate, filtered, and concentrated to provide a sticky white solid (150 mg, 91% crude yield). The product was confirmed by ^{1}H NMR and ESI-MS and submitted crude. ^{1}H NMR (500 MHz, $CDCl_3$) δ 6.54 (s, 2H), 5.28 (s, 2H), 4.79 (d, *J* = 12, 1H), 4.65 (br s, 1H), 4.17 (br s, 2H), 3.81 (br s, 2H), 3.42 (d, *J* = 6.5, 2H), 3.38 (br s, 2H), 2.91 (s, 2H), 2.91 (br s, 2H), 2.27 (br s, 1H), 2.06 (br m, 1H), 1.74 (app. br t, *J* = 13, 2H), 1.22 (app. br q, *J* = 11, 2H). ESI-MS: *m/z* calcd for $C_{22}H_{28}N_8O_3$ $[M+H]^+$ 453.2, observed 453.4.

Boc-deprotected core (0.20 g, 0.45 mmol) and **4.6** (0.25 g, 0.49 mmol) were dissolved in anhydrous DMF, followed by the addition of DIPEA (0.16 mL, 0.90 mmol). The solution was stirred at RT for 24 h and then concentrated. The crude mixture was purified by column chromatography (100% EtOAc). The desired product was a yellow, brown solid (0.28 g, 80%

yield). ^{1}H NMR (500 MHz, DMSO-d_6) δ 7.69-7.66 (br m, 3H), 7.39 (t, J = 7.5, 4H), 7.15 (t, J = 7, 2H), 6.57 (s, 2H), 5.16 (s, 2H), 4.65 (br s, 2H), 3.96 (br s, 2H), 3.71 (br s, 1H), 3.48 (br s, 2H), 3.35 (br s, 3H), 3.25 (br s, 2H), 3.01 (br s, 1H), 2.95 (br d, J = 8, 2H), 2.70 (br s, 2H), 1.84 (br m, 1H), 1.55 (app. br d, J = 13, 2H), 0.99 (br s, 2H). ^{13}C NMR (500 MHz, $CDCl_3$) δ 176.7, 165.7, 164.3, 138.3, 136.4, 134.3, 129.0, 124.0, 119.7, 112.7, 82.5, 80.4, 71.9, 47.1, 43.2, 42.1, 40.1, 34.5, 29.4, 29.0. HRMS: m/z calcd for $C_{40}H_{39}N_{11}O_5S$ $[M+H]^+$ 786.2935, observed 786.2941.

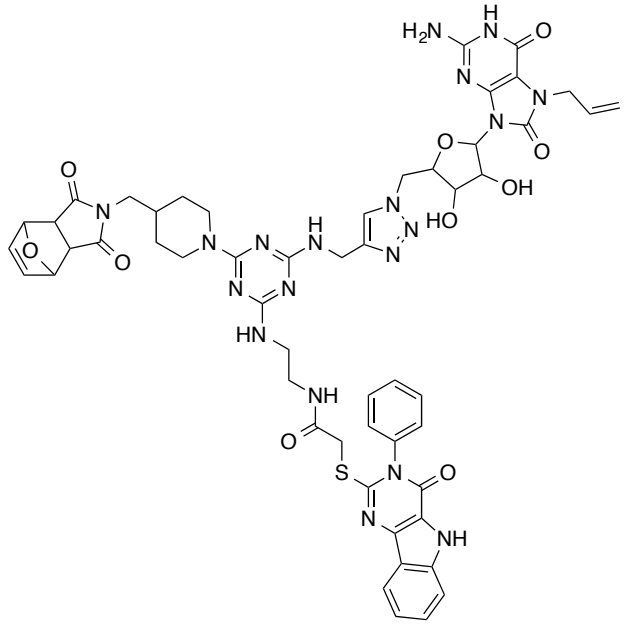

***N*-(2-((4-(((1-((5-(7-allyl-2-amino-6,8-dioxo-1,6,7,8-tetrahydro-9*H*-purin-9-yl)-3,4-dihydroxytetrahydrofuran-2-yl)methyl)-1*H*-1,2,3-triazol-4-yl)methyl)amino)-6-(4-((1,3-dioxo-1,3,3a,4,7,7a-hexahydro-2*H*-4,7-epoxyisoindol-2-yl)methyl)piperidin-1-yl)-1,3,5-triazin-2-yl)amino)ethyl)-2-((4-oxo-3-phenyl-4,5-dihydro-3*H*-pyrimido[5,4-*b*]indol-2-yl)thio)acetamide (Indole_Lox core, 4.9).** Compounds **4.7** (30 mg, 40 μmol) and **4.8** (17 mg, 46 μmol) were dissolved in anhydrous DMF (0.50 mL). Copper sulfate pentahydrate (9.5 mg, 38 μmol) and sodium ascorbate (8.3 mg, 42 μmol) were then added to the mixture and the reaction

was allowed to stir at RT for 22 h. The reaction mixture was concentrated and purified by semi-prep HPLC to provide 15 mg of product as a lyophilized white powder. Analysis for purity checked by analytical HPLC C8, A: water + 0.1% TFA, B: acetonitrile + 0.1% TFA (10-90% acetonitrile/water + 0.1% TFA gradient, 0-11 minutes), where t_R: 8.78 min. MALDI-TOF: *m/z* calcd for $C_{53}H_{55}N_{19}O_{10}S$ $[M+H]^+$ 1150.4, observed 1150.4.

General Procedure to Conjugate CpG-ODN.

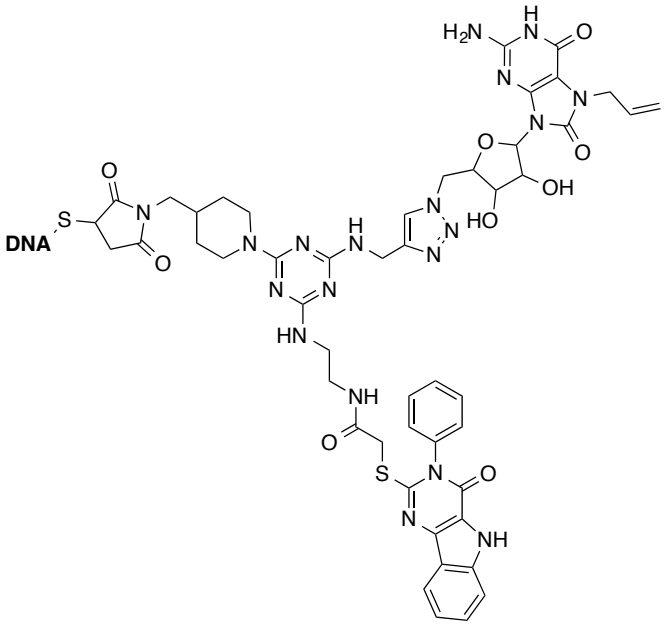

Tri-agonist (4.10). Compound **4.9** (0.80 mg, 0.70 μmol) was dissolved in anhydrous DMSO (0.050 mL). The solution was heated at 110 °C for 5 h in a sealed vial. The solution was concentrated and submitted crude. MALDI-TOF: *m/z* calcd for $C_{49}H_{51}N_{19}O_9S$ $[M+H]^+$ 1082.4, observed 1082.2.

Maleimide-deprotected Indole_Lox (0.040 mg, 56 nmol) was dissolved in anhydrous DMSO (0.040 mL) and treated with CpG-ODN1826 (0.10 mg, 14 nmol) in PBS (14 μL). The reagents were allowed to react at RT on a shaker for 4 h. The solution was purified by gel electrophoresis.

The product band was excised and eluted into HPLC grade water overnight at 37 °C. The solution was concentrated using a 3k centrifugal filter unit (EMD Millipore). The product was confirmed using MALDI-TOF and quantified using UV-Vis at 495 nm. MALDI-TOF: *m/z* calcd $[M-H]^-$ 8227.1, observed 8224.6.

Modified Loxoribine Procedures.

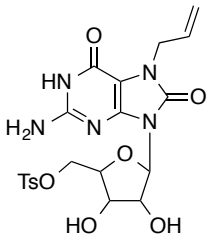

(5-(7-allyl-2-amino-6,8-dioxo-1,6,7,8-tetrahydro-9*H*-purin-9-yl)-3,4-dihydroxytetrahydrofuran-2-yl)methyl 4-methylbenzenesulfonate (4.11). To a cooled solution (0 °C) of loxoribine (1.0 g, 2.9 mmol) in dry pyridine (9.7 mL), a solution of 4-toluenesulfonyl chloride (0.72 g, 3.8 mmol) in dry pyridine (2.5 mL) was added dropwise. The reaction was stirred at 0 °C and was allowed to warm to room temperature for 24 h. The reaction was quenched with methanol (4 mL) and concentrated. The crude mixture was purified using column chromatography (3:5 MeOH: DCM) to provide the product (770 mg, 54% yield). ^{1}H NMR (500 MHz, CD_3OD) δ 7.71 (d, *J* = 8.5, 2H), 7.29 (t, *J* = 8.5, 2H), 5.99-5.93 (m, 1H), 5.74 (app. d, *J* = 4, 1H), 5.17 (app. dt, *J* = 1.5, 2H), 4.77 (qd, *J* = 4, 1.5, 1H), 4.52 (dd, *J* = 5, 1, 2H), 4.46 (td, *J* = 6,2, 1H), 4.33 (dd, *J* = 11, 3.5, 1H), 4.26 (dd, *J* = 11, 7, 1H), 4.04-4.01 (m, 1H), 2.39 (s, 3H). ^{13}C NMR (500 MHz, CD_3OD) δ 154.8, 153.8, 152.8, 150.0, 148.8, 146.3, 134.1, 130.7, 129.1, 117.6, 100.8, 88.6, 82.7, 73.0, 71.7, 71.6, 45.1, 21.6. HRMS: *m/z* calcd for $C_{20}H_{23}N_5O_8S$ $[M+Na]^+$ 516.1165, observed 516.1153.

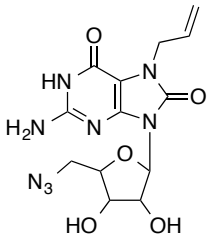

7-allyl-2-amino-9-(5-(azidomethyl)-3,4-dihydroxytetrahydrofuran-2-yl)-7,9-dihydro-1*H*-purine-6,8-dione (4.8). Compound **4.11** (140 mg, 0.28 mmol), sodium azide (24 mg, 0.37 mmol), and dry DMF (1.4 mL) were added to a round bottom flask. The solution was heated at 80 °C for 24 h. Then, the mixture was concentrated and purified by column chromatography (4:5 MeOH:DCM) to provide the desired product (56 mg, 55% yield). ^{1}H NMR (500 MHz, CD_3OD) δ 5.99-5.91 (m, 1H), 5.84 (d, *J* = 4.5, 1H), 5.15 (br s, 1H), 5.12 (d, *J* = 7.5, 1H), 5.00 (t, *J* = 5, 1H), 4.53 (d, *J* = 5, 2H), 4.47 (t, *J* = 5, 1H), 4.02 (q, *J* = 6.5, 1H), 3.57 (dd, *J* = 13, 7, 1H), 3.47 (dd, *J* = 13, 3.5, 1H). ^{13}C NMR (500 MHz, CD_3OD) **δ** 155.0, 153.9, 153.0, 149.2, 134.2, 117.3, 100.9, 88.4, 84.3, 72.6, 72.5, 52.9, 45.0. HRMS: *m/z* calcd for $C_{13}H_{16}N_8O_5$ $[M+Na]^+$ 387.1141, observed 387.1139.

Synthesis of Di-agonists Compounds.

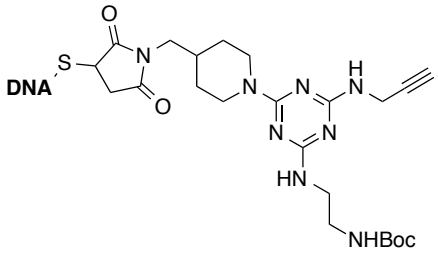

CpG_core (4.12). Followed general procedure for CpG-ODN conjugation. Compound **4.5** (7.5 mg, 14 μmol) was dissolved in anhydrous DMSO (0.20 mL). The solution was heated at 110 °C for 5 h in a sealed vial. The solution was concentrated and submitted crude. Maleimide-deprotected tricore (27 μg, 56 nmol) was dissolved in anhydrous DMSO (0.040 mL) and treated with CpG-ODN1826 (0.10 mg, 14 nmol) in PBS (14 μL). The reagents were allowed to react at

RT on a shaker for 4 h. The solution was purified by gel electrophoresis. The product band was excised and eluted into HPLC grade water overnight at 37 °C. The solution was concentrated using a 3k centrifugal filter unit (EMD Millipore). The product was confirmed using MALDI-TOF and quantified using UV-Vis at 495 nm. MALDI-TOF: *m/z* calcd $[M-H]^-$ 7629.7, observed 7628.4.

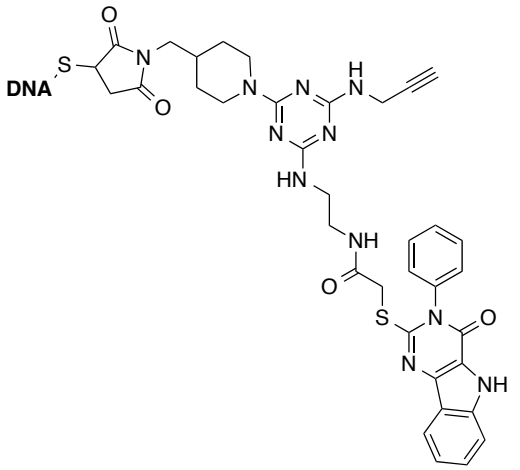

Indole_CpG (4.13). Followed general procedure for CpG-ODN conjugation. Compound **4.7** (6.3 mg, 8.0 μmol) was dissolved in anhydrous DMSO (0.15 mL). The solution was heated at 110 °C for 5 h in a sealed vial. The solution was concentrated and submitted crude. Maleimide-deprotected tricore (0.040 mg, 56 nmol) was dissolved in anhydrous DMSO (0.040 mL) and treated with CpG-ODN1826 (0.10 mg, 14 nmol) in PBS (14 μL). The reagents were allowed to react at RT on a shaker for 4 h. The solution was purified by gel electrophoresis. The product band was excised and eluted into HPLC grade water overnight at 37 °C. The solution was concentrated using a 3k centrifugal filter unit (EMD Millipore). The product was confirmed using MALDI-TOF and quantified using UV-Vis at 495 nm. MALDI-TOF: *m/z* calcd $[M-H]^-$ 7862.9, observed 7864.5.

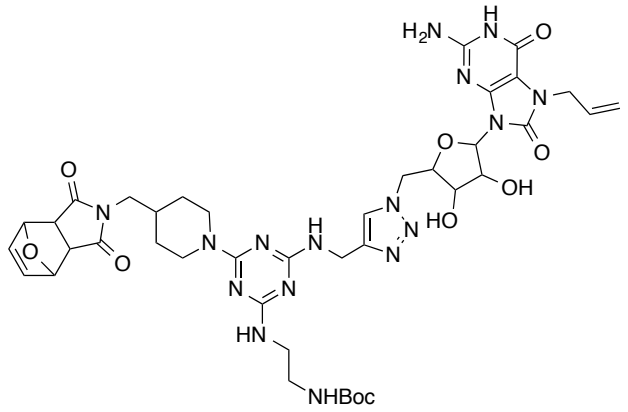

Lox_core (4.14). Compounds **4.5** (41 mg, 75 μmol) and **4.8** (0.030 g, 82 μmol) were dissolved in anhydrous DMSO:MeOH:degassed H_2O (2:7:1) (1.5 mL). Copper sulfate pentahydrate (19 mg, 75 μmol) and sodium ascorbate (16 mg, 82 μmol) were then added to the mixture and the reaction was allowed to stir at RT for 23 h. The reaction mixture was filtered and the solid was purified by semi-prep HPLC to provide the product as a lyophilized white powder in quantitative yield. MALDI-TOF: *m/z* calcd for $C_{40}H_{52}N_{16}O_{10}$ $[M+H]^+$ 917.4, observed 917.4.

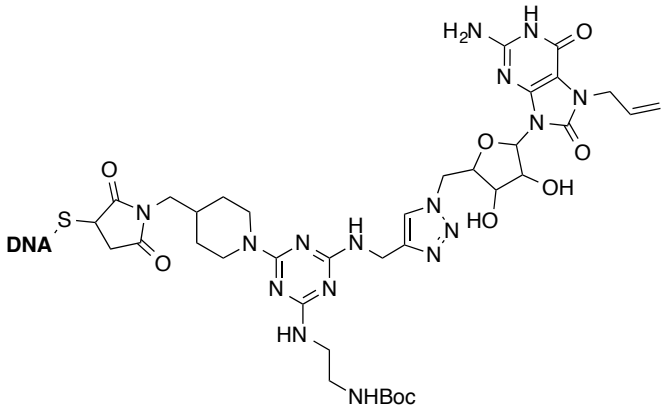

Lox_CpG (4.15). Followed general procedure for CpG-ODN conjugation. Compound **4.14** (11 mg, 12 μmol) was dissolved in anhydrous DMSO (0.70 mL). The solution was heated at 110 °C for 5 h in a sealed vial. The solution was concentrated and submitted crude. Maleimide-deprotected tricore (24 μg, 28 nmol) was dissolved in anhydrous DMSO (0.040 mL) and treated with CpG-ODN1826 (0.10 mg, 14 nmol) in PBS (14 μL). The reagents were allowed to react at

RT on a shaker for 4 h. The solution was purified by gel electrophoresis. The product band was excised and eluted into HPLC grade water overnight at 37 °C. The solution was concentrated using a 3k centrifugal filter unit (EMD Millipore). The product was confirmed using MALDI-TOF and quantified using UV-Vis at 495 nm. MALDI-TOF: *m/z* calcd $[M-H]^-$ 7994.0, observed 7995.3.

Statistics.

Data was analyzed using a two-tailed t test. All values were reported as mean ± SD, unless stated otherwise.

***See Appendix C for Additional Figures and Characterization Data: NMR spectra and HPLC traces.**

4.8 References

(1) Schreibelt, G.; Benitez-Ribas, D.; Schuurhuis, D.; Lambeck, A. J. A.; Hout-Kuijer, M. van; Schaft, N.; Punt, C. J. A.; Figdor, C. G.; Adema, G. J.; Vries, I. J. M. de. Commonly Used Prophylactic Vaccines as an Alternative for Synthetically Produced TLR Ligands to Mature Monocyte-Derived Dendritic Cells. *Blood* **2010**, *116* (4), 564–574.

(2) Taub, D. D.; Ershler, W. B.; Janowski, M.; Artz, A.; Key, M. L.; McKelvey, J.; Muller, D.; Moss, B.; Ferrucci, L.; Duffey, P. L.; et al. Immunity from Smallpox Vaccine Persists for Decades: A Longitudinal Study. *Am. J. Med.* **2008**, *121* (12), 1058–1064.

(3) Garcia-Cordero, J. L.; Nembrini, C.; Stano, A.; Hubbell, J. A.; Maerkl, S. J. A High-Throughput Nanoimmunoassay Chip Applied to Large-Scale Vaccine Adjuvant Screening. *Integr. Biol. Quant. Biosci. Nano Macro* **2013**, *5* (4), 650–658.

(4) Trinchieri, G.; Sher, A. Cooperation of Toll-like Receptor Signals in Innate Immune Defence. *Nat Rev Immunol* **2007**, *7* (3), 179–190.

(5) Mancini, R. J.; Tom, J. K.; Esser-Kahn, A. P. Covalently Coupled Immunostimulant Heterodimers. *Angew. Chem. Int. Ed Engl.* **2014**, *53* (1), 189–192.

(6) Pavot, V.; Rochereau, N.; Rességuier, J.; Gutjahr, A.; Genin, C.; Tiraby, G.; Perouzel, E.; Lioux, T.; Vernejoul, F.; Verrier, B.; et al. Cutting Edge: New Chimeric NOD2/TLR2 Adjuvant Drastically Increases Vaccine Immunogenicity. *J. Immunol.* **2014**, 1402184.

(7) Shukla, N. M.; Mutz, C. A.; Malladi, S. S.; Warshakoon, H. J.; Balakrishna, R.; David, S. A. Toll-Like Receptor (TLR)-7 and -8 Modulatory Activities of Dimeric Imidazoquinolines. *J. Med. Chem.* **2012**, *55* (3), 1106–1116.

(8) Shukla, N. M.; Salunke, D. B.; Balakrishna, R.; Mutz, C. A.; Malladi, S. S.; David, S. A. Potent Adjuvanticity of a Pure TLR7-Agonistic Imidazoquinoline Dendrimer. *PLoS ONE* **2012**, *7* (8), e43612.

(9) Pulendran, B. Learning Immunology from the Yellow Fever Vaccine: Innate Immunity to Systems Vaccinology. *Nat. Rev. Immunol.* **2009**, *9* (10), 741–747.

(10) Querec, T.; Bennouna, S.; Alkan, S. K.; Laouar, Y.; Gorden, K.; Flavell, R.; Akira, S.; Ahmed, R.; Pulendran, B. Yellow Fever Vaccine YF-17D Activates Multiple Dendritic Cell Subsets via TLR2, 7, 8, and 9 to Stimulate Polyvalent Immunity. *J. Exp. Med.* **2006**, *203* (2), 413–424.

(11) Bagchi, A.; Herrup, E. A.; Warren, H. S.; Trigilio, J.; Shin, H.-S.; Valentine, C.; Hellman, J. MyD88-Dependent and MyD88-Independent Pathways in Synergy, Priming, and Tolerance between TLR Agonists. *J. Immunol. Baltim. Md 1950* **2007**, *178* (2), 1164–1171.

(12) Ouyang, X.; Negishi, H.; Takeda, R.; Fujita, Y.; Taniguchi, T.; Honda, K. Cooperation between MyD88 and TRIF Pathways in TLR Synergy via IRF5 Activation. *Biochem. Biophys. Res. Commun.* **2007**, *354* (4), 1045–1051.

(13) Ting Tan, R. S.; Lin, B.; Liu, Q.; Tucker-Kellogg, L.; Ho, B.; Leung, B. P.; Ding, J. L. The Synergy in Cytokine Production through MyD88-TRIF Pathways Is Co-Ordinated with ERK Phosphorylation in Macrophages. *Immunol. Cell Biol.* **2013**, *91* (5), 377–387.

(14) Krummen, M.; Balkow, S.; Shen, L.; Heinz, S.; Loquai, C.; Probst, H.-C.; Grabbe, S. Release of IL-12 by Dendritic Cells Activated by TLR Ligation Is Dependent on MyD88 Signaling, Whereas TRIF Signaling Is Indispensable for TLR Synergy. *J. Leukoc. Biol.* **2010**, *88* (1), 189–199.

(15) Kwissa, M.; Nakaya, H. I.; Oluoch, H.; Pulendran, B. Distinct TLR Adjuvants Differentially Stimulate Systemic and Local Innate Immune Responses in Nonhuman Primates. *Blood* **2012**, *119* (9), 2044–2055.
(16) Pulendran, B. Modulating Vaccine Responses with Dendritic Cells and Toll-like Receptors. *Immunol. Rev.* **2004**, *199* (1), 227–250.
(17) O'Neill, L. A. J.; Golenbock, D.; Bowie, A. G. The History of Toll-like Receptors — Redefining Innate Immunity. *Nat. Rev. Immunol.* **2013**, *13* (6), 453–460.
(18) Kagan, J. C.; Su, T.; Horng, T.; Chow, A.; Akira, S.; Medzhitov, R. TRAM Couples Endocytosis of Toll-like Receptor 4 to the Induction of Interferon-β. *Nat. Immunol.* **2008**, *9* (4), 361–368.
(19) Kasturi, S. P.; Skountzou, I.; Albrecht, R. A.; Koutsonanos, D.; Hua, T.; Nakaya, H. I.; Ravindran, R.; Stewart, S.; Alam, M.; Kwissa, M.; et al. Programming the Magnitude and Persistence of Antibody Responses with Innate Immunity. *Nature* **2011**, *470* (7335), 543–547.
(20) De Nardo, D.; De Nardo, C. M.; Nguyen, T.; Hamilton, J. A.; Scholz, G. M. Signaling Crosstalk during Sequential TLR4 and TLR9 Activation Amplifies the Inflammatory Response of Mouse Macrophages. *J. Immunol. Baltim. Md 1950* **2009**, *183* (12), 8110–8118.
(21) Moody, M. A.; Santra, S.; Vandergrift, N. A.; Sutherland, L. L.; Gurley, T. C.; Drinker, M. S.; Allen, A. A.; Xia, S.-M.; Meyerhoff, R. R.; Parks, R.; et al. Toll-like Receptor 7/8 (TLR7/8) and TLR9 Agonists Cooperate to Enhance HIV-1 Envelope Antibody Responses in Rhesus Macaques. *J. Virol.* **2014**, *88* (6), 3329–3339.
(22) Theiner, G.; Rössner, S.; Dalpke, A.; Bode, K.; Berger, T.; Gessner, A.; Lutz, M. B. TLR9 Cooperates with TLR4 to Increase IL-12 Release by Murine Dendritic Cells. *Mol. Immunol.* **2008**, *45* (1), 244–252.
(23) Chan, M.; Hayashi, T.; Mathewson, R. D.; Nour, A.; Hayashi, Y.; Yao, S.; Tawatao, R. I.; Crain, B.; Tsigelny, I. F.; Kouznetsova, V. L.; et al. Identification of Substituted Pyrimido[5,4-B]indoles as Selective Toll-Like Receptor 4 Ligands. *J. Med. Chem.* **2013**, *56* (11), 4206–4223.
(24) Heil, F.; Ahmad-Nejad, P.; Hemmi, H.; Hochrein, H.; Ampenberger, F.; Gellert, T.; Dietrich, H.; Lipford, G.; Takeda, K.; Akira, S.; et al. The Toll-like Receptor 7 (TLR7)-Specific Stimulus Loxoribine Uncovers a Strong Relationship within the TLR7, 8 and 9 Subfamily. *Eur. J. Immunol.* **2003**, *33* (11), 2987–2997.
(25) Krieg, A. M. The Role of CpG Motifs in Innate Immunity. *Curr. Opin. Immunol.* **2000**, *12* (1), 35–43.
(26) Vollmer, J.; Krieg, A. M. Immunotherapeutic Applications of CpG Oligodeoxynucleotide TLR9 Agonists. *Adv. Drug Deliv. Rev.* **2009**, *61* (3), 195–204.
(27) Liu, J.; Xu, C.; Liu, Y.-L.; Matsuo, H.; Hsieh, R. P.; Lo, J.-F.; Tseng, P.-H.; Yuan, C.-J.; Luo, Y.; Xiang, R.; et al. Activation of Rabbit TLR9 by Different CpG-ODN Optimized for Mouse and Human TLR9. *Comp. Immunol. Microbiol. Infect. Dis.* **2012**, *35* (5), 443–451.
(28) Mitchell, D.; Yong, M.; Raju, J.; Willemsen, N.; Black, M.; Trent, A.; Tirrell, M.; Olive, C. Toll-like Receptor-Mediated Adjuvanticity and Immunomodulation in Dendritic Cells: Implications for Peptide Vaccines. *Hum. Vaccin.* **2011**, *7* (0), 85–93.

(29) Gu, L.; Tseng, S.; Horner, R. M.; Tam, C.; Loda, M.; Rollins, B. J. Control of TH2 Polarization by the Chemokine Monocyte Chemoattractant Protein-1. *Nature* **2000**, *404* (6776), 407–411.
(30) Ouyang, W.; Rutz, S.; Crellin, N. K.; Valdez, P. A.; Hymowitz, S. G. Regulation and Functions of the IL-10 Family of Cytokines in Inflammation and Disease. *Annu. Rev. Immunol.* **2011**, *29* (1), 71–109.
(31) Menten, P.; Wuyts, A.; Van Damme, J. Macrophage Inflammatory Protein-1. *Cytokine Growth Factor Rev.* **2002**, *13* (6), 455–481.
(32) Collette, Y.; Gilles, A.; Pontarotti, P.; Olive, D. A Co-Evolution Perspective of the TNFSF and TNFRSF Families in the Immune System. *Trends Immunol.* **2003**, *24* (7), 387–394.
(33) Orr, M. T.; Duthie, M. S.; Windish, H. P.; Lucas, E. A.; Guderian, J. A.; Hudson, T. E.; Shaverdian, N.; O'Donnell, J.; Desbien, A. L.; Reed, S. G.; et al. MyD88 and TRIF Synergistic Interaction Is Required for TH1-Cell Polarization with a Synthetic TLR4 Agonist Adjuvant. *Eur. J. Immunol.* **2013**, *43* (9), 2398–2408.
(34) Hacker, G.; Redecke, V.; Hacker, H. Activation of the Immune System by Bacterial CpG-DNA. *Immunology* **2002**, *105* (3), 245–251.
(35) Napolitani, G.; Rinaldi, A.; Bertoni, F.; Sallusto, F.; Lanzavecchia, A. Selected Toll-like Receptor Agonist Combinations Synergistically Trigger a T Helper Type 1-Polarizing Program in Dendritic Cells. *Nat. Immunol.* **2005**, *6* (8), 769–776.
(36) Kawamoto, T.; Ii, M.; Kitazaki, T.; Iizawa, Y.; Kimura, H. TAK-242 Selectively Suppresses Toll-like Receptor 4-Signaling Mediated by the Intracellular Domain. *Eur. J. Pharmacol.* **2008**, *584* (1), 40–48.
(37) Takashima, K.; Matsunaga, N.; Yoshimatsu, M.; Hazeki, K.; Kaisho, T.; Uekata, M.; Hazeki, O.; Akira, S.; Iizawa, Y.; Ii, M. Analysis of Binding Site for the Novel Small-Molecule TLR4 Signal Transduction Inhibitor TAK-242 and Its Therapeutic Effect on Mouse Sepsis Model. *Br. J. Pharmacol.* **2009**, *157* (7), 1250–1262.
(38) Lenert, P.; Stunz, L.; Yi, A.-K.; Krieg, A. M.; Ashman, R. F. CpG Stimulation of Primary Mouse B Cells Is Blocked by Inhibitory Oligodeoxyribonucleotides at a Site Proximal to NF-ϰB Activation. *Antisense Nucleic Acid Drug Dev.* **2001**, *11* (4), 247–256.
(39) Davies, D. H.; Liang, X.; Hernandez, J. E.; Randall, A.; Hirst, S.; Mu, Y.; Romero, K. M.; Nguyen, T. T.; Kalantari-Dehaghi, M.; Crotty, S.; et al. Profiling the Humoral Immune Response to Infection by Using Proteome Microarrays: High-Throughput Vaccine and Diagnostic Antigen Discovery. *Proc. Natl. Acad. Sci. U. S. A.* **2005**, *102* (3), 547–552.
(40) Matheu, M. P.; Sen, D.; Cahalan, M. D.; Parker, I. Generation of Bone Marrow Derived Murine Dendritic Cells for Use in 2-Photon Imaging. *J. Vis. Exp. JoVE* **2008**, No. 17.
(41) Banerjee, R.; Pace, N. J.; Brown, D. R.; Weerapana, E. 1,3,5-Triazine as a Modular Scaffold for Covalent Inhibitors with Streamlined Target Identification. *J. Am. Chem. Soc.* **2013**, *135* (7), 2497–2500.

CHAPTER 5

Synthesis of a Tri-Agonist Library and *In Vitro* and *In Vivo* Biological Testing Thereof

5.1 Introduction

With the increase in antibody depth and breadth observed with the first tri-agonist, we sought to synthesize a library of covalently conjugated tri-agonists and determine the effects of different agonist combinations on the immune response. Since our group and others have reported that specific agonist combinations elicit defined responses,[1,2] we aimed to perform a comparative study of the immune response produced by different tri-agonist combinations. Characterization of the immune response from distinct tri-agonists would allow us to determine a trend or "code" for immune activation. If we could methodically determine the molecular code of agonists to produce a specific cellular and/or antibody response desired for a disease of interest, then that specific agonist combination could be used as the optimal adjuvant in a vaccine targeting that disease.

Our aim was to compare the immune response elicited by compounds in our tri-agonist library and use the tri-agonist compounds as adjuvants in a vaccination model. First, we synthesized new tri-agonist combinations, by introducing three other TLR agonists into the set of agonists used for conjugation. Five new agonist combinations have been synthesized to date, and the syntheses of additional combinations that include the TLR5 agonist flagellin are in progress. Immunological activity of each tri-agonist was evaluated *in vitro* using the NF-κB RAW-Blue macrophage reporter cell line. In addition, cell surface marker upregulation and cytokine production were assessed in a BMDC primary cell line to observe changes in the immune response downstream of NF-κB. Subsequent administration of our compounds *in vivo* allowed us

to study the effects in a vaccination model. We chose Q fever as our vaccination model due to its prevalence and lack of a safe and effective vaccine.[3,4] Q fever is caused by the infectious agent *C. burnetii* and is a current bioterrorism threat. The only licensed vaccine is available in Australia, but safety concerns make approval unlikely in the U.S. We are using the tri-agonist compounds to adjuvant Q fever antigens and determine which tri-agonist adjuvants prove optimal against Q fever, with the main objective of formulating a better Q fever vaccine.

Here, we report modulation of the immune response *in vitro* with three new tri-agonists, TLR4_7_9 (second generation), TLR2/6_4_7, and TLR1/2_4_7, and their corresponding di-agonists. Differences in immune activation and potency were observed with each combination when compared to the corresponding three agonists unconjugated as well as the respective di-agonists. *In vitro* studies with the other two tri-agonists are currently ongoing. Using the TLR2/6_4_7 tri-agonist as an adjuvant, we performed *in vivo* toxicity and vaccination studies with a Q fever mouse model. From the vaccination model study, we observed the linked and unlinked tri-agonist combinations increased antibody production against specific Q fever antigens as compared to the antigen only control. The ability to elicit targeted antibody production with the tri-agonist adjuvant is a promising result because directed antibody responses largely contribute to the efficacy of the immune response against *C. burnetii*. *In vivo* studies are still ongoing with the TLR2/6_4_7 tri-agonist and the remaining agonist combinations to fully understand the properties of the adjuvant and vaccine as a whole. Once murine vaccination studies are complete, we will be taking the best candidates onto murine challenge studies as well as non-human primate studies to determine the best formulation for a Q fever vaccine.

5.2 The Second Generation TLR4_7_9 Tri-Agonist

5.2.1 Synthesis of a Second Generation TLR4_7_9 Tri-Agonist

Even though our first TLR4_7_9 tri-agonist (Indole_Lox_CpG) proved to be a promising adjuvant in a vaccinia virus model, we sought to improve the scaffold and agonists used. Polyethylene glycol (PEG) linkers were incorporated between the agonist and scaffold to improve solubility and flexibility. PEG_{12} length (46.5 Å) was chosen because the TLR crystal structures showed that the optimal distance from the TLR binding site to the edge of the TLR itself ranges from 10-30 Å, depending on the TLR.[5,6] Having the longer linker length may also help avoid any steric interactions between the different agonists as well as provide more degrees of freedom for the TLR agonist to bind their respective TLRs. In addition, an imidazoquinoline derivative was used as the TLR7 agonist instead of loxoribine due to the increased potency and success of imidazoquinolines in therapeutic studies.[7–9] The Indole and CpG-ODN1826 were kept as the TLR4 and TLR9 agonists, respectively.

Scheme 5.1. Derivatization of Tri-Functional Core Scaffold to Provide a Carboxylic Acid Functional Handle

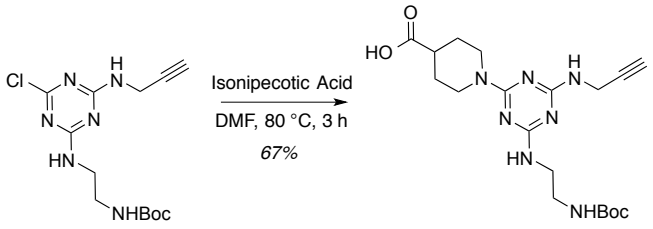

4.3 **5.1**

To synthesize the second-generation TLR4_7_9 tri-agonist, a derivative of the core scaffold was synthesized to accommodate the amine functional handle on the imidazoquinoline. The precursor to the original triazine scaffold, with alkyne and Boc-protected amine conjugation

handles, (**4.3**) was treated with isonipecotic acid to provide a carboxylic acid functional handle on the core (**5.1**) (**Scheme 5.1**). With the new small molecule scaffold, the imidazoquinoline[8,10] (TLR7, **5.2**) could be functionalized with a PEG_{12} linker and conjugated to the core (**Scheme 5.2**). A pegylated (PEG_{12}) imidazoquinoline (**5.3**) was synthesized by coupling the benzyl amine conjugation handle to a bi-functional NHS-PEG_{12}-NH-Fmoc. Subsequent Fmoc deprotection and HATU coupling to the carboxylic acid functionalized core (**5.1**) yielded the TLR7_PEG_{12}_Core (**5.4**) in 57% yield. To install the TLR4 agonist, **5.4** was Boc-deprotected and coupled to the NHS functional group on another bi-functional NHS-PEG_{12}-NH-Fmoc. **5.5** was then Fmoc deprotected and coupled with the Indole-COOH (TLR4) using HATU to provide the desired product (**5.6**) in 27% yield. Several coupling agents were screened, including HBTU/HOBt, PyBOP, NHS esters, and PFP esters. However, 27% remained the highest yield achieved. The low yield may be due to the potential side reactivity of the TLR4 Indole agonist or the additional reactivity of the amidine nitrogen on the imidazoquinoline. Lastly, CpG (TLR9) was conjugated *via* copper-catalyzed azide-alkyne click chemistry (CuAAC). The crude reaction mixture was analyzed and purified by TBE-urea gel electrophoresis. The isolated product was confirmed by MALDI-TOF (see Appendix D, **Fig. S5.1**) to provide the second generation TLR4_7_9 tri-agonist (**5.7**) with 92% conversion. The corresponding di-agonists were also synthesized and used as comparison in cellular studies.

Scheme 5.2. Synthetic Route Toward the Second Generation TLR4_7_9 Tri-Agonist.

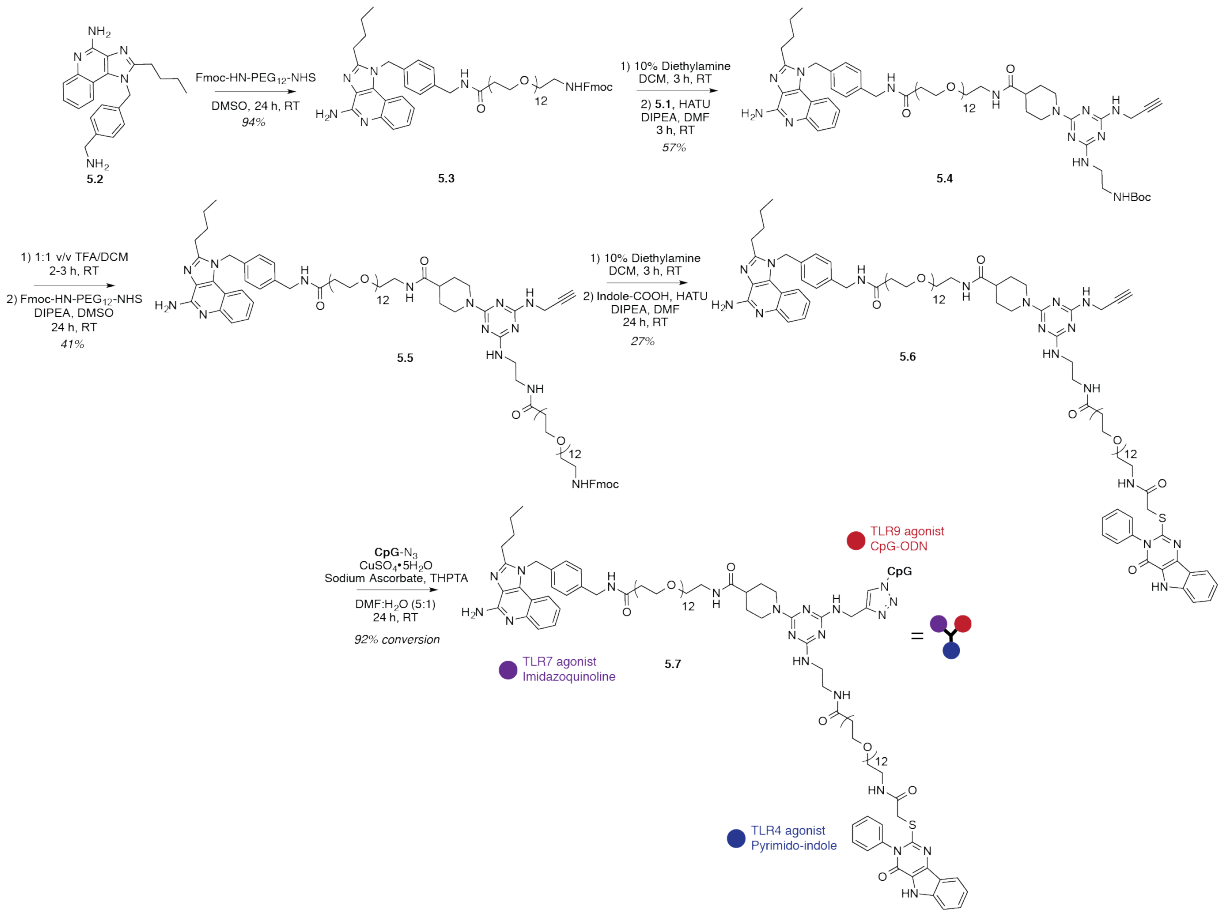

5.2.2 *In Vitro* Biological Studies of the Second Generation TLR4_7_9 Tri-Agonist

With the second generation TLR4_7_9 tri-agonist in hand, we proceeded with *in vitro* biological studies, assaying for NF-κB activity, cell surface marker upregulation, and cytokine production. First, we tested our tri- and di-agonist compounds on RAW-Blue macrophages to compare relative immune activation *via* NF-κB activity (**Fig. 5.1**). The TLR4_9 and TLR7_9 di-agonists, the three individual TLR4, 7, and 9 agonists unconjugated in solution, and the linked TLR4_7_9 tri-agonist were all tested on the macrophage cell line at a range of concentrations (0.1 nM - 1 μM). The TLR4_7 di-agonist was also tested, but as previously observed there was little to no activity above the media control (data not shown).

All of the covalently linked di- and tri-agonists exhibited similar levels of NF-κB activity compared to CpG (TLR9) alone, suggesting that the origin of most of the NF-κB activity is from CpG (TLR9). This result may be due to the decreased activity of the imidazoquinoline (TLR7) after conjugation (see Appendix D, **Fig. S5.3**) or the high potency of CpG (TLR9) compared to the TLR4 and TLR7 agonists. CpG (TLR9) conjugation does not alter its immunological activity, as previously shown in Chapter 4 (see Appendix C, **Fig. S4.3**). Immune cells treated with the three agonists free in solution elicited 27% higher NF-κB activity than the chemically conjugated TLR4_7_9 (***$p < 0.001$). This was not surprising as conjugating the imidazoquinoline (TLR7) decreases activity compared to the native agonist (see Appendix D, **Fig. S5.3**), and the Indole (TLR4) is not a potent agonist. In addition, a MTT assay and an endotoxin test were performed to assay for cell cytotoxicity and endotoxin levels resulting from our compounds, respectively. The MTT assay showed good cell viability (75-100%) for all compounds (see Appendix D, **Fig. S5.2**). Endotoxin levels of our compounds were below 0.1 EU/mL (standard conditions – data not shown), confirming no additional immune activity from endotoxin contamination.

Figure 5.1. NF-κB Activation of RAW-Blue 264.7 Macrophage Cell Line Treated with the Second Generation TLR4_7_9 Tri-Agonist[a]

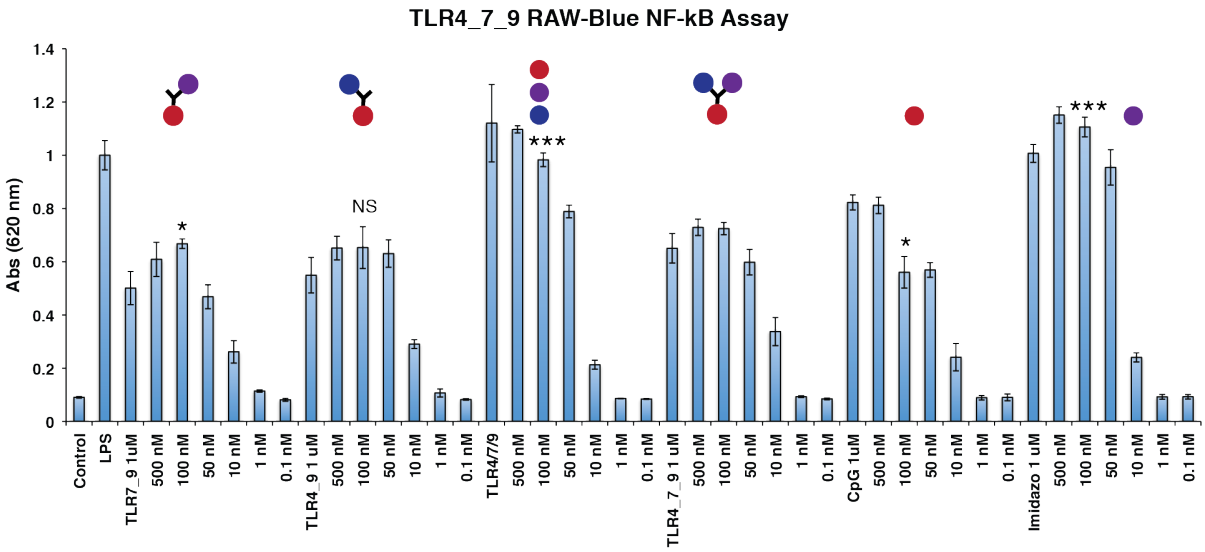

[a] RAW-Blue macrophage cells were treated with each compound at concentrations ranging from 1 μM to 0.1 nM for 18 h at 37 °C. Each bar is the result of n=3, where *p < 0.05, ***p < 0.001, and NS is non-significant. All statistics represent the asterisked compound compared to the second generation TLR4_7_9 tri-agonist. Results are expressed as the mean ± SD.

To further understand how the second generation TLR4_7_9 tri-agonist affected immune cells, BMDCs were used to examine cell surface marker upregulation and cytokine production. Cell surface markers CD86, CD40, and MHCII were all upregulated by the three agonists unconjugated, the conjugated TLR4_7_9, and TLR4_9 and TLR7_9 di-agonists compared to the media control (**Fig. 5.2**). Interestingly, all of the chemically linked tri- and di-agonists upregulated T cell adhesion proteins, CD86 and CD40, and antigen presentation protein, MHCII, expression compared to the TLR4, 7, and 9 agonists in solution. This protein upregulation may support our aforementioned hypothesis because the covalently linked tri-agonist localizes the three agonists, thereby activating distinct pathways in a single cell, leading to the observed increase in immune activation *via* cell surface protein expression. In comparison, the three agonists unconjugated can diffuse through the solution and may not activate the same signaling

pathways in one cell, resulting in a lower amount of immune activation. Similar to the results from the NF-κB activity assay, the covalently linked tri- and di-agonists exhibited similar expression levels. The TLR7_9 di-agonist treated BMDCs expressed significantly higher levels of CD86 and lower levels of CD40 compared to the TLR4_7_9 tri-agonist, but not MHCII. On the other hand, there were no significant differences between TLR4_9 di-agonist and the second generation TLR4_7_9 tri-agonist. The subtle differences in activation demonstrate how specific TLR agonist combinations contribute to distinct immune activation, which may translate *in vivo*.

Figure 5.2. Analysis of Cell Surface Marker Expression of the Second Generation TLR4_7_9 Treated BMDCs[a]

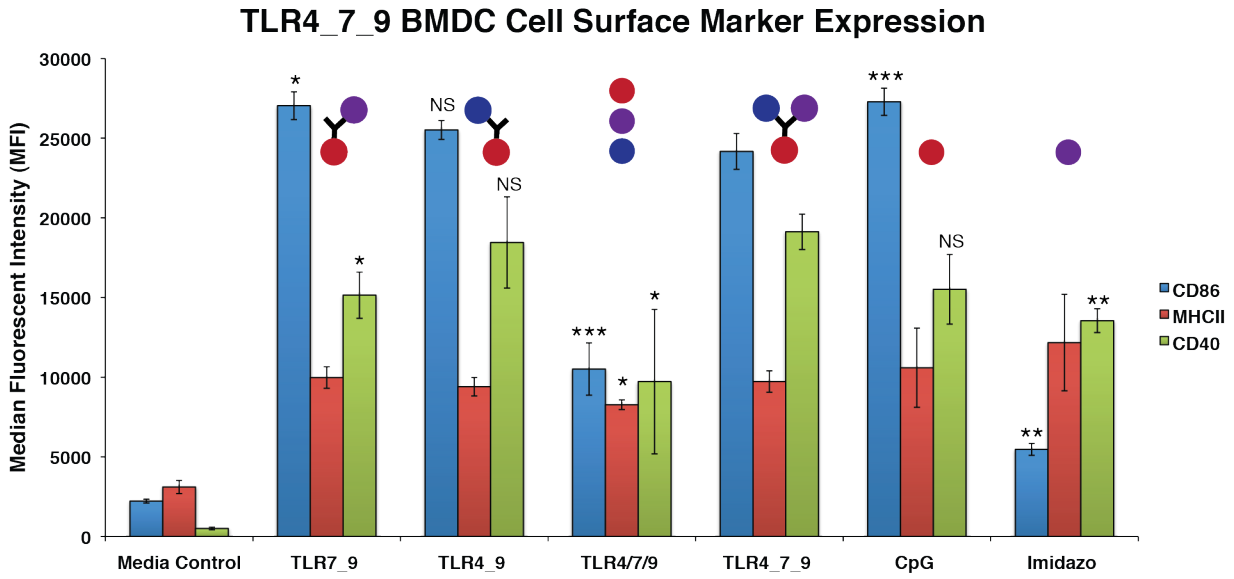

[a] BMDC activation *via* cell surface marker expression as measured by flow cytometry, represented as the median fluorescent intensity (MFI) of $CD11c^+$ dendritic cells. BMDCs were incubated with each compound at 100 nM for 18 h at 37 °C. Each bar is the result of n=3, where *p < 0.05, ***p < 0.001, and NS is non-significant. All statistics represent the asterisked compound compared to the second generation TLR4_7_9 tri-agonist. Results are expressed as the mean ± SD.

Next, we examined cytokine signatures further downstream in immune activation to see if the immune response was polarized. TNF-α, MCP-1, IL-12p70, IL-6, IL-10, and IFN-γ, pro-inflammatory, anti-inflammatory, and innate immune cell recruitment cytokines, produced by

BMDCs treated with the designated compounds were measured by cytokine bead array (flow cytometry) (**Figs. 5.3 & 5.4**). TNF-α, MCP-1, and IL-12p70, inflammatory and immune cell recruitment cytokines, were produced at significantly higher levels with the linked TLR4, 7, and 9 tri- and di-agonists compared to their unconjugated counterparts. This result could have important implications *in vivo* for innate cell recruitment and alerting the immune system to the immunized pathogen. There were no significant differences in cytokine production between the tri- and di-agonists as observed with the aforementioned NF-κB and BMDC assays. The small molecule agonists (TLR4 or TLR7) may be contributing to different extents compared to what we previously observed with the first TLR4_7_9 tri-agonist (Indole_Lox_CpG). Further studies are required to understand the mechanism behind this result. IL-6 and IL-10, pro- and anti-inflammatory cytokines, respectively were also produced, but there was no distinction between sample treatments. *In vivo* studies are currently being performed to see how these *in vitro* results translate to a murine vaccination model.

Figure 5.3. The Second Generation TLR4_7_9 BMDC Cytokine Profile: Part I[a]

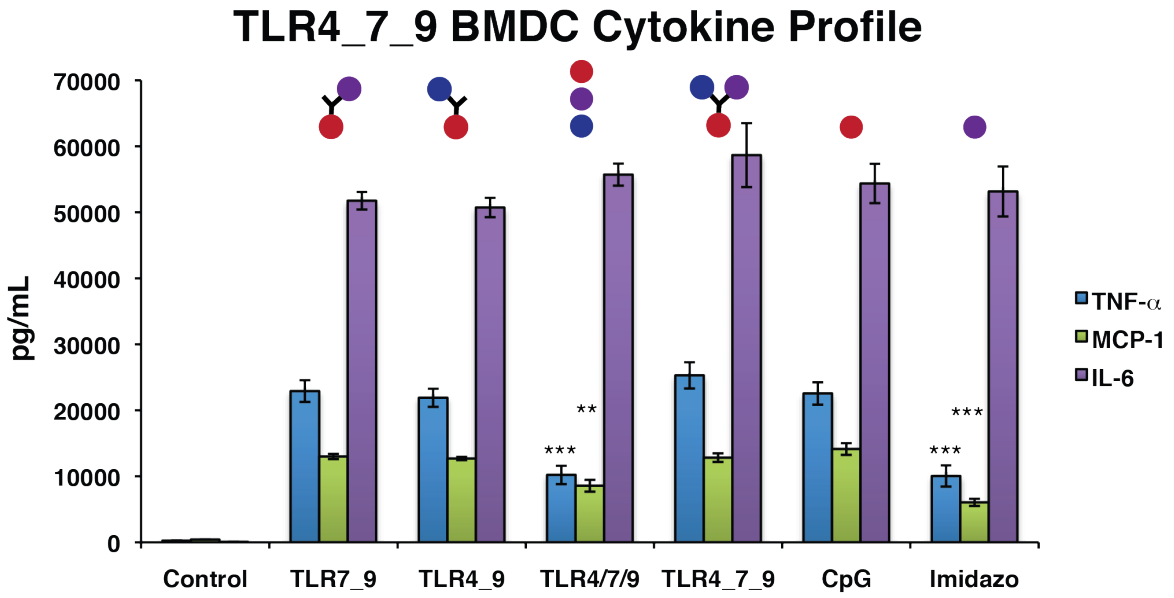

[a] BMDC TNF-alpha, MCP-1, and IL-6 cytokine production *via* cytokine bead array as measured by flow cytometry, represented in pg/mL. BMDCs were incubated with each compound at 100 nM for 18 h at 37 °C and supernatant was analyzed as a 1:5 dilution. Each bar is result of n=3, where **p < 0.01 and ***p < 0.001. All statistics represent the asterisked compound compared to the second generation TLR4_7_9 tri-agonist. Results are expressed as the mean ± SD.

Figure 5.4. The Second Generation TLR4_7_9 BMDC Cytokine Profile: Part II[a]

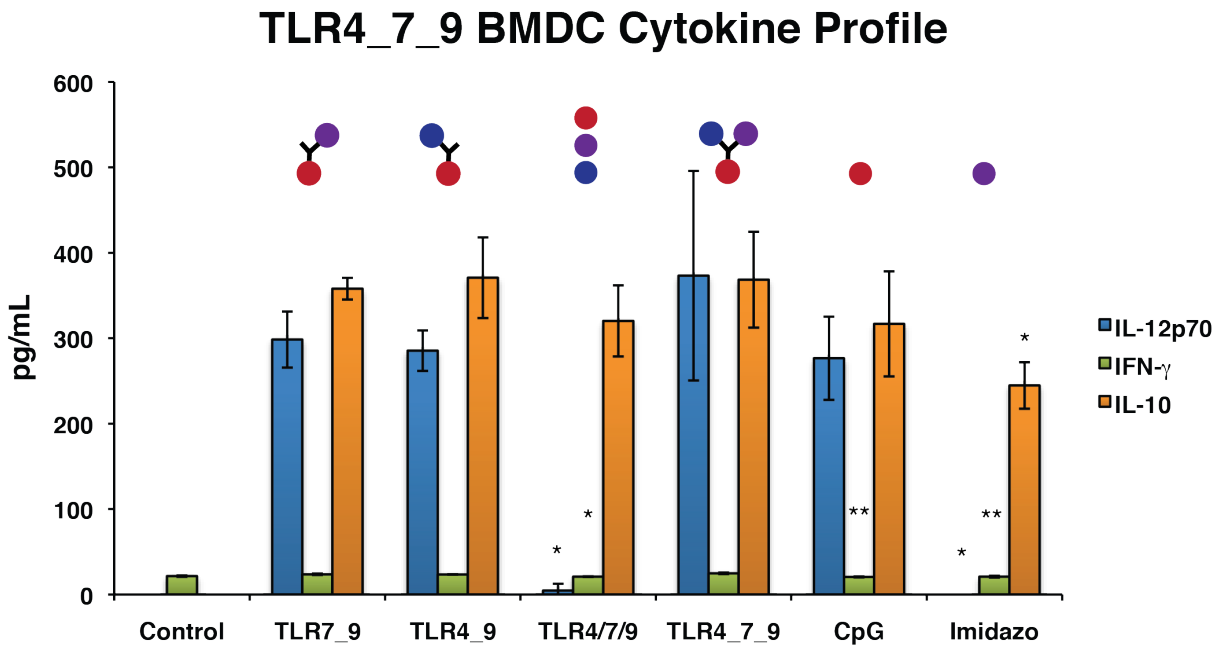

[a] BMDC IL-12p70, IFN-gamma, IL-10 cytokine production *via* cytokine bead array as measured by flow cytometry, represented in pg/mL. BMDCs were incubated with each compound at 100 nM for 18 h at 37 °C and supernatant was analyzed as a 1:5 dilution. Each bar is the result of n=3, where *p < 0.05 and **p < 0.01. All statistics represent the asterisked compound compared to the second generation TLR4_7_9 tri-agonist. Results are expressed as the mean ± SD.

5.3 TLR2/6_4_7 Tri-Agonist

5.3.1 Synthesis of a TLR2/6_4_7 Tri-Agonist

In addition to the TLR4_7_9 tri-agonist, we wanted to synthesize tri-agonists that incorporated the agonists PAM_2CSK_4 (TLR2/6 agonist) and PAM_3CSK_4 (TLR1/2 agonist) due to their potency and use in clinical trials to elicit strong antibody responses.[11–14] PAM_2CSK_4 and

PAM_3CSK_4 are synthetic acylated lipopeptide TLR agonists that activate TLR2 and dimerize with either TLR6 or TLR1, respectively.[15,16] They contain a pentapeptide (CSK_4) and two or three palmitoyl lipid tails, depending on the TLR agonist, where the lipid tails are the stimulatory portions of the molecules.

Scheme 5.3. Synthetic Route Toward the TLR2/6_4_7 Tri-Agonist

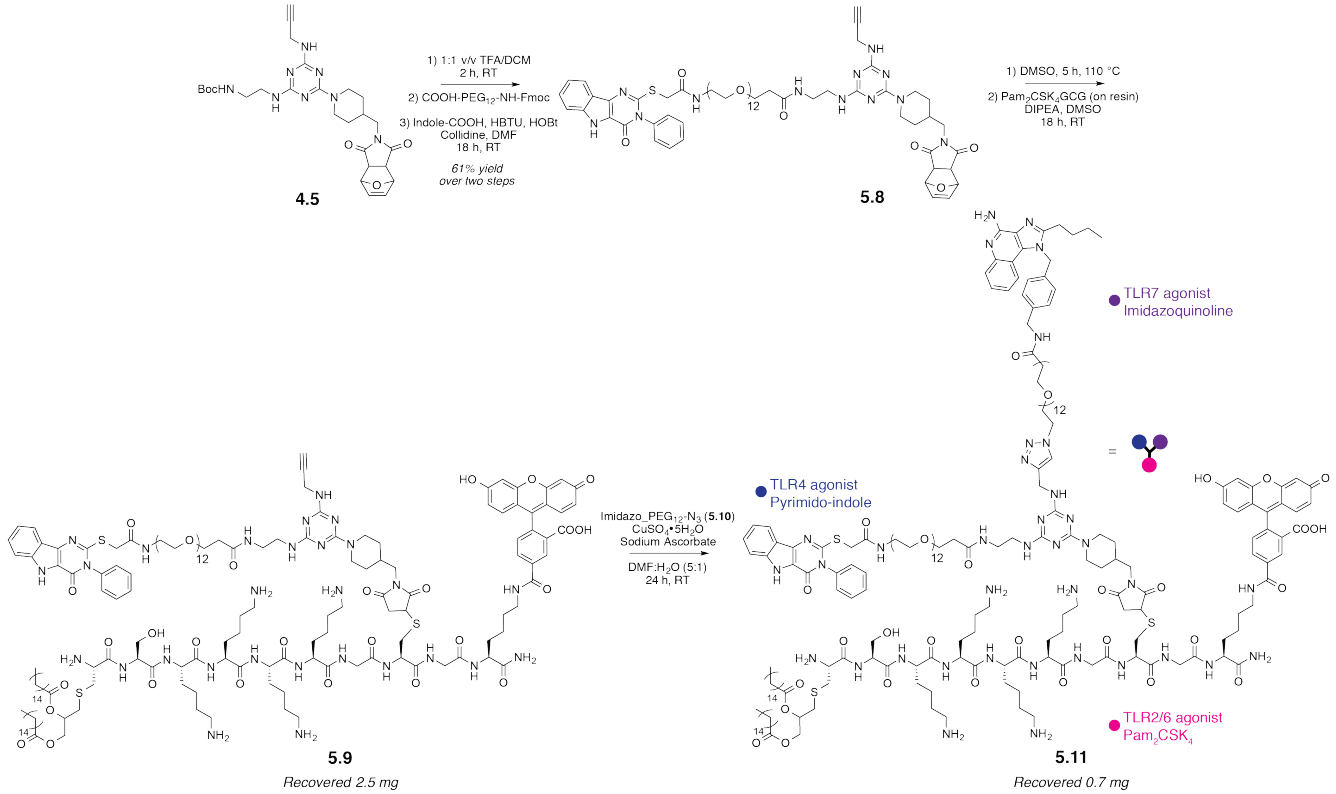

Two new tri-agonists we sought to synthesize were the TLR2/6_4_7 (**5.11**) (**Scheme 5.3**) and the TLR1/2_4_7 tri-agonists due to known synergies in natural pathogens.[17,18] We first synthesized the TLR2/6_4_7 tri-agonist, since the TLR1/2_4_7 tri-agonist was synthetically accessible by replacing PAM_2CSK_4 with PAM_3CSK_4 in a one step derivatization. To conjugate the TLR2 agonist, a PAM_2CSK_4 derivative, PAM_2CSK_4GCG, was synthesized by solid phase synthesis using Rink amide resin. Conjugation of the TLR2 agonist was attempted in solution, but proved difficult due to solubility challenges. The synthesized TLR2/6 agonist contained a

free thiol *via* a cysteine residue, which could also be reacted to install a carboxylic acid functional handle using bromoacetic acid, in case alternative conjugation routes were necessary. Before conjugating the TLR2/6 agonist to the core, Indole_PEG_{12}_Core (**5.8**) was synthesized, and the protected maleimide was deprotected *via* a retro-Diels-Alder reaction. The maleimide was then reacted with the PAM_2CSK_4 derivative on resin for 18 hours at room temperature. The crude product was then cleaved from the resin, HPLC purified, and lyophilized to obtain the TLR2/6_4 di-agonist (**5.9**). To conjugate the last agonist (TLR7 agonist), an azide conjugation handle was required to react with the alkyne on the core. The amine functional handle on the imidazoquinoline (TLR7) was reacted with the bi-functional NHS-PEG_{12}-N_3 to provide an azide functional handle on the TLR7 agonist (**5.10**). The azide-functionalized imidazoquinoline was then reacted with the free alkyne on the TLR2/6_4 di-agonist *via* CuAAC to provide the target TLR2/6_4_7 tri-agonist (**5.11**). The identity of the product was confirmed by MALDI-TOF, and the purity was assessed by HPLC (see Appendix D).

5.3.2 *In Vitro* Biological Studies of the TLR2/6_4_7 Tri-Agonist

The TLR2/6_4_7 tri-agonist was tested on RAW-Blue macrophages and BMDCs for *in vitro* immunological activity. In RAW-Blue macrophages, all of the tested compounds showed activity above the media control (**Fig. 5.5**). However, no significant differences in activation between the di-agonists (TLR2/6_4 and TLR2/6_7), the three individual agonists unconjugated, and the covalently linked TLR2/6_4_7 tri-agonist were observed when comparing NF-κB activity (0.1 nM – 1 μM). There were also normal levels of cell viability, which was detected using a MTT assay (data not shown).

Figure 5.5. NF-κB Activation of RAW-Blue 264.7 Macrophage Cell Line Treated with the TLR2/6_4_7 Tri-Agonist[a]

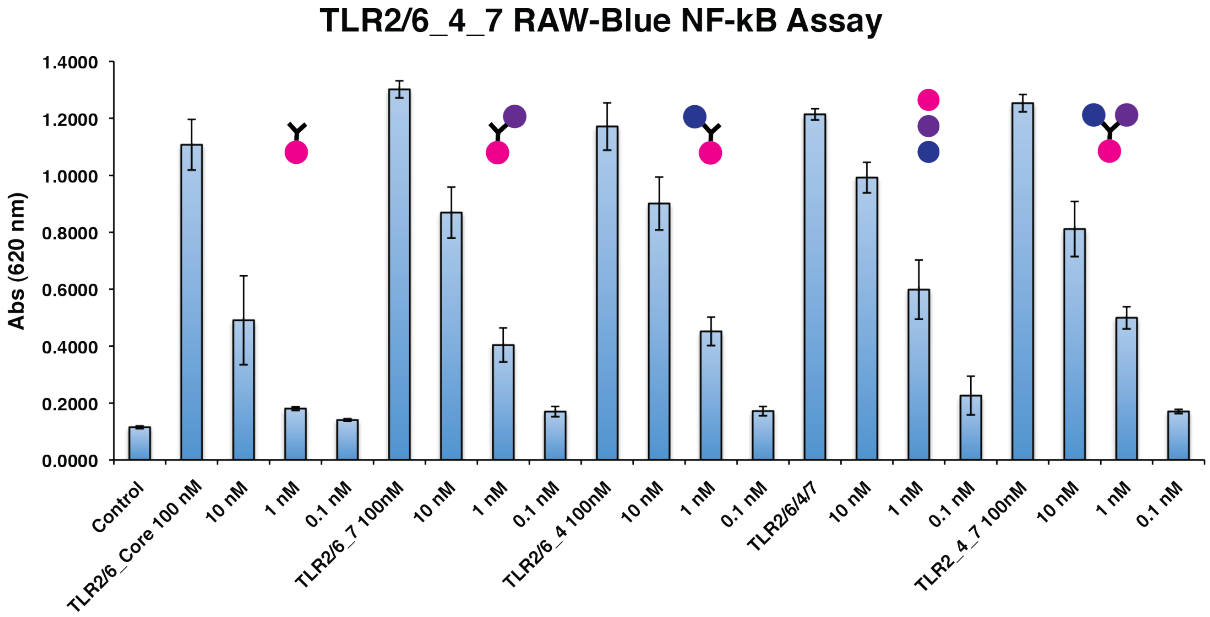

[a] RAW-Blue macrophage cells were treated with each compound at concentrations ranging from 100 nM to 0.1 nM for 18 h at 37 °C. Each bar is the result of n=3, where comparisons to the TLR2/6_4_7 were non-significant at 100 nM. Results are expressed as the mean ± SD.

Even though distinct differences in activation were not observed with NF-κB activation, BMDCs were treated with the TLR2/6, 4, and 7 di- and tri-agonists to determine if there were changes downstream of NF-κB activity (**Fig. 5.6**). At 100 nM, the conjugated TLR2/6_4_7 tri-agonist displayed significant increases in cell surface protein expression for MHCII and CD40, necessary for T cell activation and antigen presentation, compared to the three agonists in solution. However, significant differences were not observed for CD86 expression between the linked tri-agonist and the same agonists unlinked. The TLR2/6_7 di-agonist treated BMDCs also showed a noticeable increase in cell surface marker expression. This result might be due to the high potency of the TLR2/6 and TLR7 agonists, PAM_2CSK_4 and imidazoquinoline, respectively. The three agonists free in solution, the TLR2/6_4 di-agonist, and individual agonists alone displayed little to no increase in cell surface proteins compared to the media control. The lack of activity was probably a result of the low concentration (100 nM) at which each compound was

used in the study. At higher concentrations, immune activity would be observed with these compounds.

Figure 5.6. Analysis of Cell Surface Marker Expression of TLR2/6_4_7 Treated BMDCs[a]

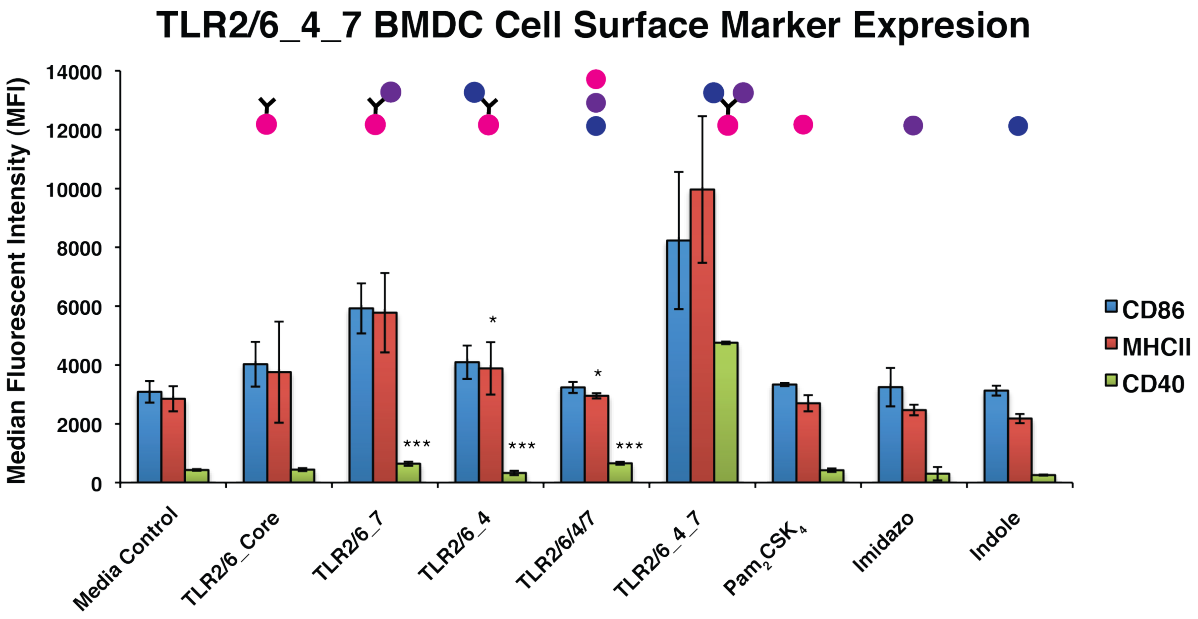

[a] BMDC activation *via* cell surface marker expression as measured by flow cytometry, represented as the median fluorescent intensity (MFI) of $CD11c^+$ dendritic cells. BMDCs were incubated with each compound at 100 nM for 18 h at 37 °C. Each bar is the result of n=3, where *$p < 0.05$ and ***$p < 0.001$. All statistics represent the asterisked compound compared to the TLR2/6_4_7 tri-agonist. Results are expressed as the mean ± SD.

Since we observed more defined changes in immune activation, we analyzed the supernatant from BDMCs treated with the tri- and di-agonist compounds to detect polarizing cytokines that guide the adaptive immune response. We observed distinctly higher levels of TNF-α and MCP-1 from cells treated with the TLR2/6_4_7 tri-agonist compared to the unconjugated agonists in solution (**Fig. 5.7**). TNF-α and MCP-1 are cytokines responsible for inflammation and innate cell recruitment, respectively. Similar to that observed with the TLR4_7_9 tri-agonist, IL-6 and IL-10, pro- and anti-inflammatory cytokines, were also observed, but with little distinction between compounds (data not shown). Since the TLR2/6_4_7

elicited high cell surface protein expression and cytokine output necessary to alert the immune system, this tri-agonist may be a promising candidate for *in vivo* vaccination studies.

Figure 5.7. TLR2/6_4_7 BMDC Cytokine Profile[a]

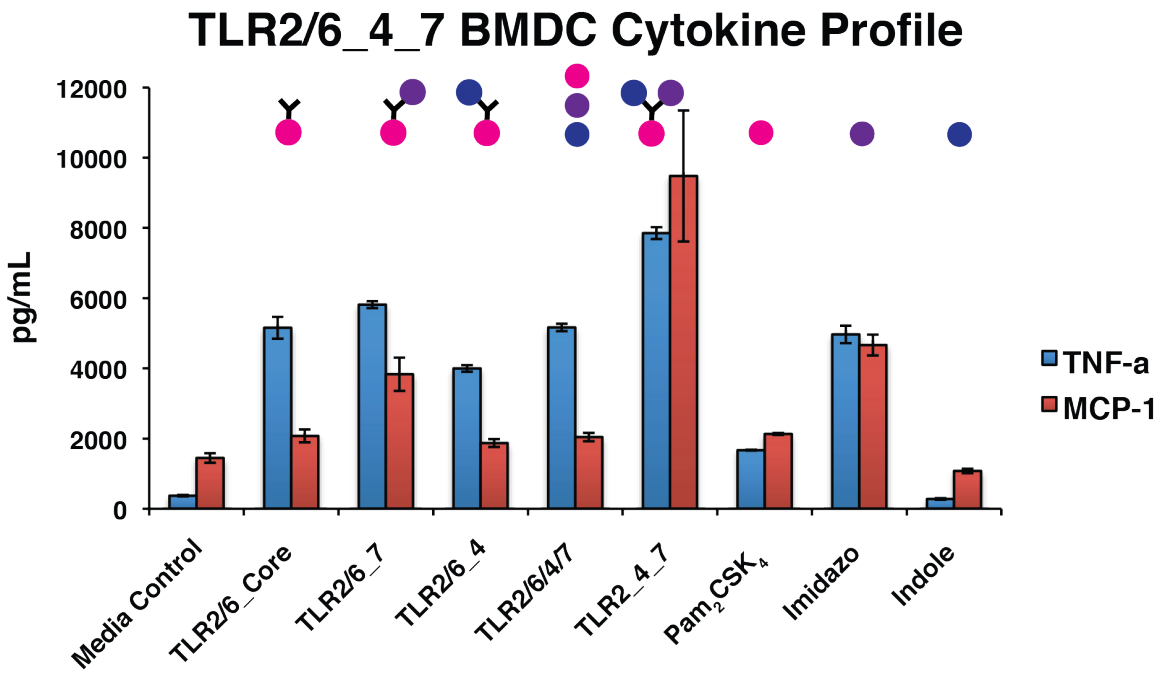

[a] BMDC TNF-alpha and MCP-1 cytokine production *via* cytokine bead array as measured by flow cytometry, represented in pg/mL. BMDCs were incubated with each compound at 100 nM for 18 h at 37 °C and supernatant was analyzed without dilution. Each bar is the result of n=3, where all sample treatments compared to that with TLR2/6_4_7 were ***$p < 0.001$ for TNF-alpha and **$p < 0.01$ for MCP-1. Results are expressed as the mean ± SD.

5.4 TLR1/2_4_7 Tri-Agonist

5.4.1 Synthesis of a TLR1/2_4_7 Tri-Agonist

The next tri-agonist we aimed to synthesize was the TLR1/2_4_7 tri-agonist, as a comparison to the TLR2/6_4_7 tri-agonist and due to the ease of synthesis from the TLR2 agonist on the resin. PAM_3CSK_4 was synthesized on resin by deprotecting the Fmoc group on the N-terminus of PAM_2CSK_4 and subsequently coupling the amine with palmitic acid using HBTU to provide the PAM_3CSK_4 derivative on resin. The PAM_3CSK_4GCG was then carried through the

same synthetic scheme as with the TLR2/6_4_7 tri-agonist to obtain the TLR1/2_4_7 tri-agonist (**Scheme 5.4**), which was purified using HPLC and confirmed by MALDI-TOF (see Appendix D).

Scheme 5.4. Synthetic Route Toward the TLR1/2_4_7 Tri-Agonist

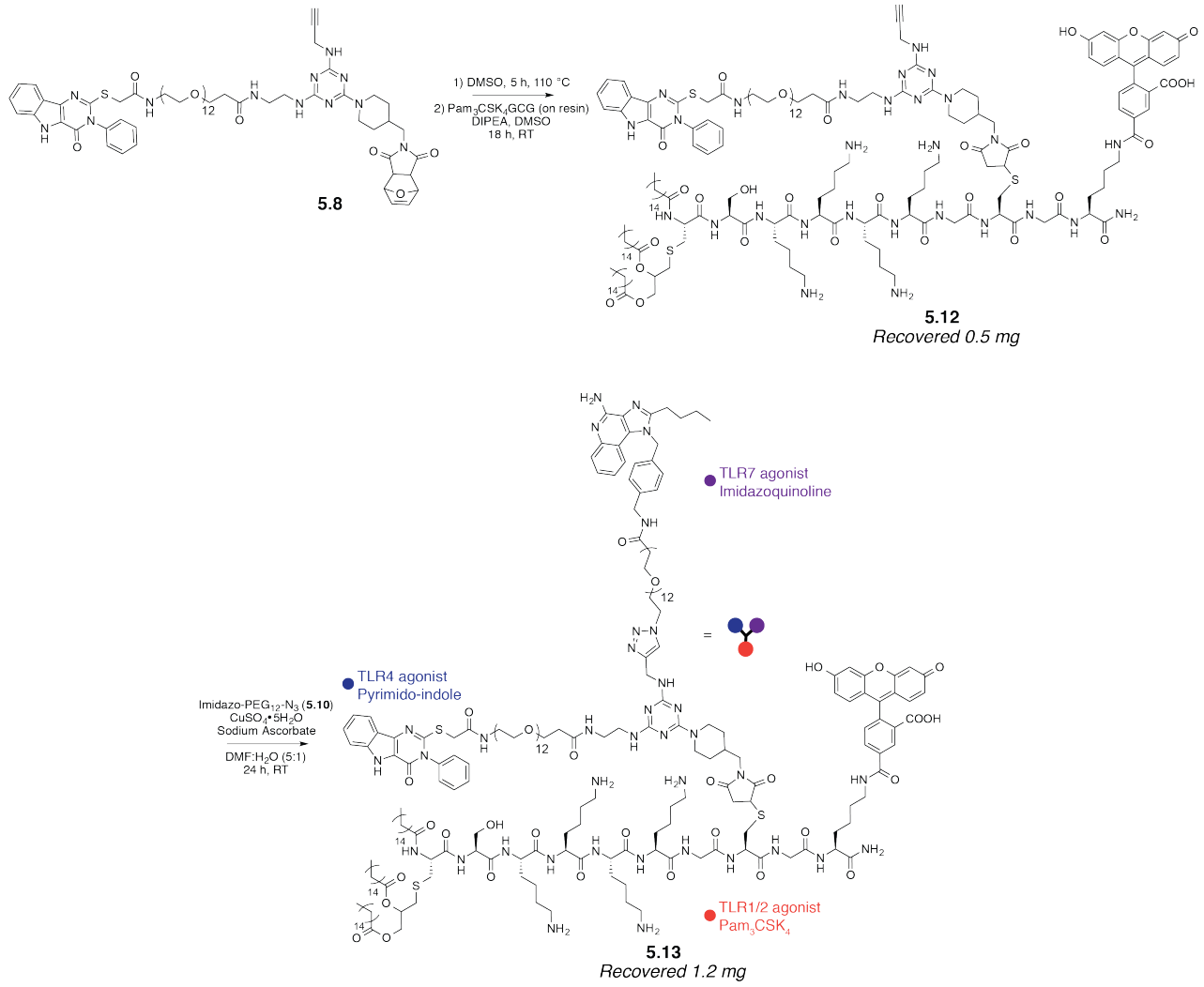

5.4.2 *In Vitro* Biological Studies of the TLR1/2_4_7 Tri-Agonist

In preliminary RAW-Blue NF-κB activity studies, we observed distinct differences between the tri- and di-agonists (**Fig. 5.8**). At 10 nM, the TLR1/2_4_7 tri-agonist treated RAW-Blue cells elicited 18%, 70%, 43%, 45%, and 225% higher NF-κB activity compared to

TLR1/2_7, TLR1/2_4, TLR1/2/4/7 (unconjugated), PAM_3CSK_4, and imidazoquinoline, respectively. The PAM_3CSK_4 (TLR1/2) alone was potent at low concentrations. Conjugating the TLR1/2 agonist with the TLR7 agonist increased immune activation, whereas the TLR1/2_4 di-agonist exhibited a decrease in activation compared to PAM_3CSK_4 alone. This result suggests that the imidazoquinoline (TLR7) upregulated immune activation, which was previously observed with the TLR2/6_7 di-agonist. In contrast, the indole inhibited immune activation.

Figure 5.8. NF-κB Activation of RAW-Blue 264.7 Macrophage Cell Line Treated with the TLR1/2_4_7 Tri-Agonist[a]

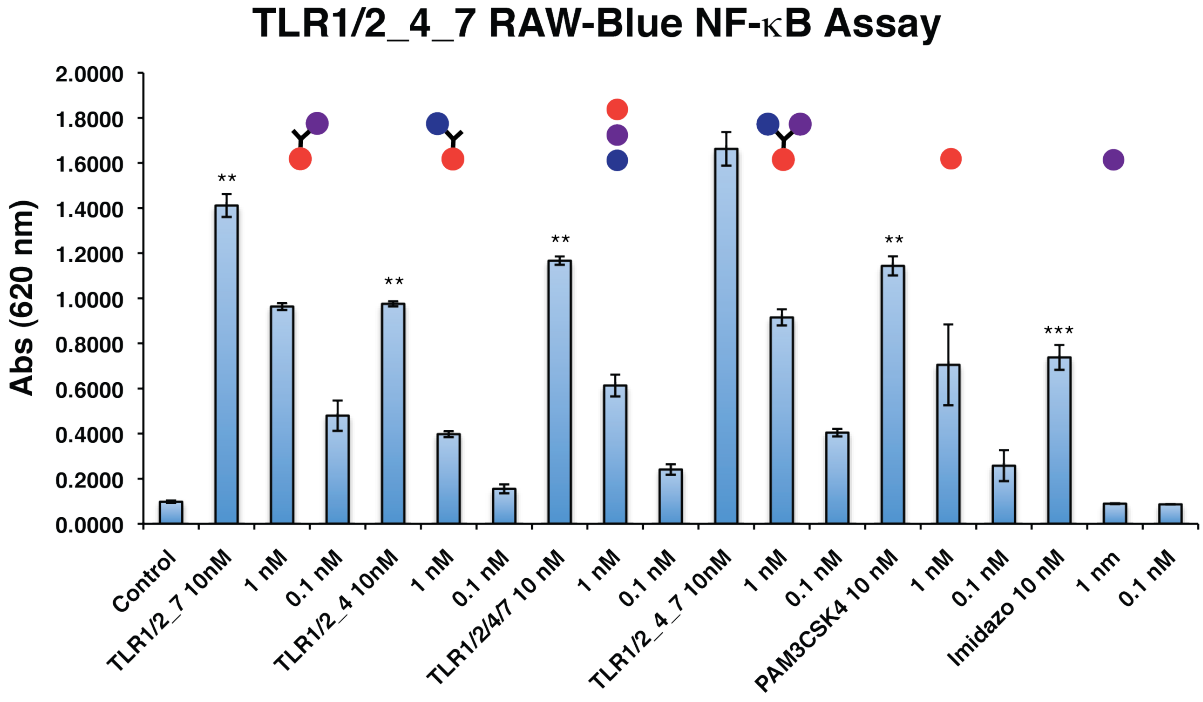

[a] RAW-Blue macrophage cells were treated with each compound at concentrations ranging from 10 nM to 0.1 nM for 18 h at 37 °C. Each bar is the result of n=3, where **$p < 0.01$ and ***$p < 0.001$. All statistics represent the asterisked compound compared to the TLR1/2_4_7 tri-agonist. Results are expressed as the mean ± SD.

To further understand the results from the NF-κB activity assay, we looked at cell surface marker expression on BMDCs (**Fig. 5.9**). Interestingly, the TLR1/2_7 di-agonist elicited the highest CD86 and MHCII expression, with the TLR1/2_4_7 tri-agonist having the second

highest expression. The three agonists unconjugated and TLR1/2_4 di-agonist treated cells expressed cell surface proteins slightly above the media control or at basal level. From this data, both the TLR1/2_4_7 tri-agonist and the TLR1/2_7 di-agonist may perform well as adjuvants *in vivo*. *In vivo* vaccination studies are in progress.

Figure 5.9. Analysis of Cell Surface Marker Expression of TLR1/2_4_7 Treated BMDCs

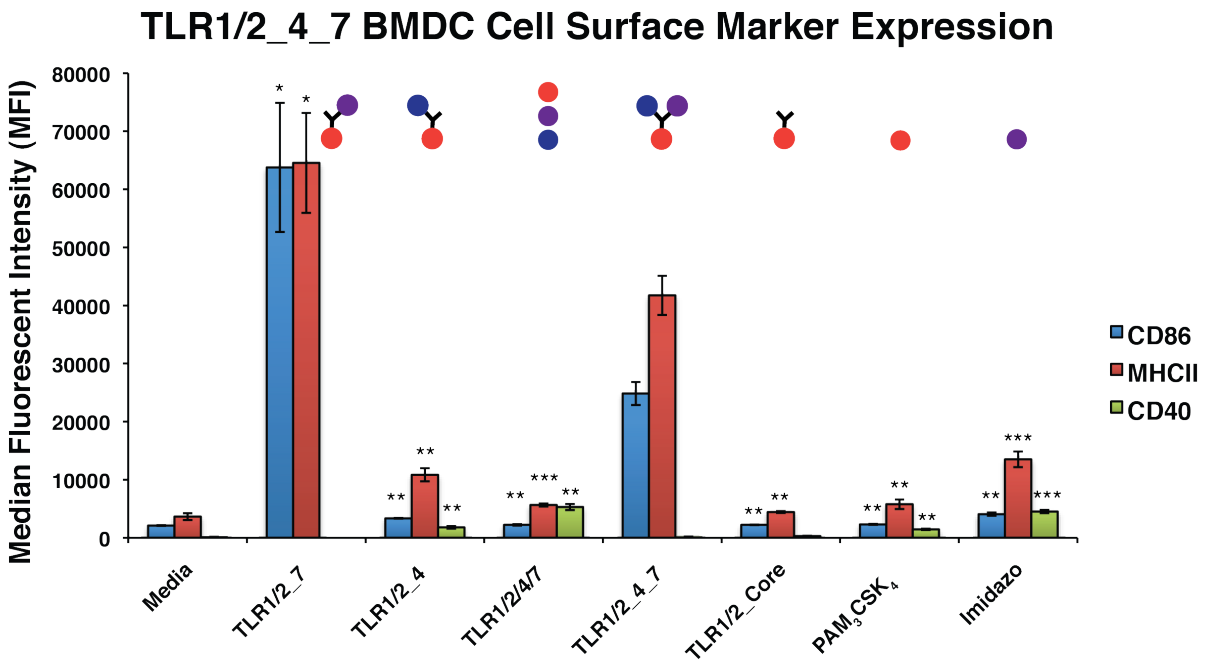

[a] BMDC activation *via* cell surface marker expression as measured by flow cytometry, represented as the median fluorescent intensity (MFI) of $CD11c^+$ dendritic cells. BMDCs were incubated with each compound at 10 nM for 18 h at 37 °C. Each bar is the result of n=3, where *p < 0.05, **P < 0.01, and ***p < 0.001. All statistics represent the asterisked compound compared to the TLR1/2_4_7 tri-agonist. Results are expressed as the mean ± SD.

5.5 TLR2/6_4_9 Tri-Agonist

5.5.1 Synthesis of a TLR2/6_4_9 Tri-Agonist

Due to known synergies between two of the three agonists and ease of synthesis, the next tri-agonist combination we sought to synthesize was the TLR2/6_4_9 tri-agonist (**Scheme 5.5**). With our modular system, the alkyne functional handle on the TLR2/6_4 di-agonist could be

conjugated to any azide-functionalized agonist. Using the 5'-end azide modified CpG (TLR9), we conjugated CpG (TLR9) to the TLR2/6_4 di-agonist using CuAAC. The TLR2/6_4_9 tri-agonist was analyzed and purified by SDS-PAGE (see Appendix D, **Fig. S5.4**). Due to the high lipophilic character of the molecule, HPLC purification proved to be challenging, and the product did not ionize *via* MALDI-TOF using a wide range of conditions. In addition, extensive CuAAC conditions were screened, with 45% as the highest observed percent conversion. The modest yield may be due to the solubility of the TLR agonists or the TLR agonists reacting with the copper in an unfavorable way. Scale up of this tri-agonist is in progress for *in vitro* and *in vivo* studies.

Scheme 5.5. Synthesis Toward the TLR2/6_4_9 Tri-Agonist

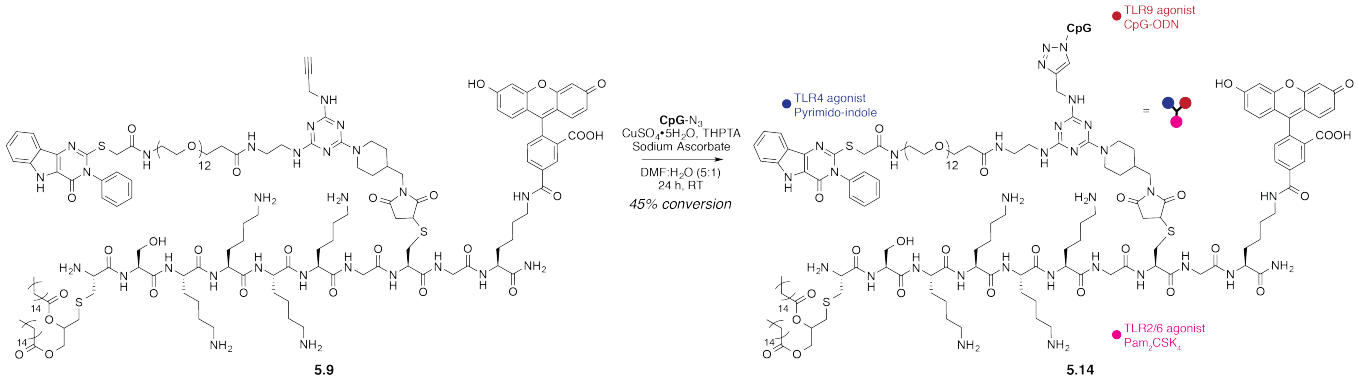

5.6 TLR2/6_7_9 Tri-Agonist

5.6.1 Synthesis of a TLR2/6_7_9 Tri-Agonist

To synthesize the TLR2/6_7_9 tri-agonist (**Scheme 5.6**), TLR7_PEG_{12}_Core (**5.4**) was Boc-deprotected and reacted with the PAM_2CSK_4 derivative with the carboxylic acid functional handle on resin. The resulting TLR2/6_7 di-agonist was then reacted with the 5'-end azide modified CpG (TLR9) *via* CuAAC. The product was analyzed and purified by SDS-PAGE (see Appendix D, **Fig. S5.5**). Similar to the TLR2/6_4_9 tri-agonist, due to the high lipophilic

character of the molecule, HPLC purification proved to be challenging, and the product did not ionize *via* MALDI-TOF using a wide range of conditions. As observed with the TLR2/6_4_9 tri-agonist, modest yield was obtained and may be due to the solubility of the TLR agonists or the TLR agonists reacting with the copper in an unfavorable way. Scale up of this tri-agonist is in progress for *in vitro* and *in vivo* studies.

Scheme 5.6. Synthetic Route Toward the TLR2/6_7_9 Tri-Agonist

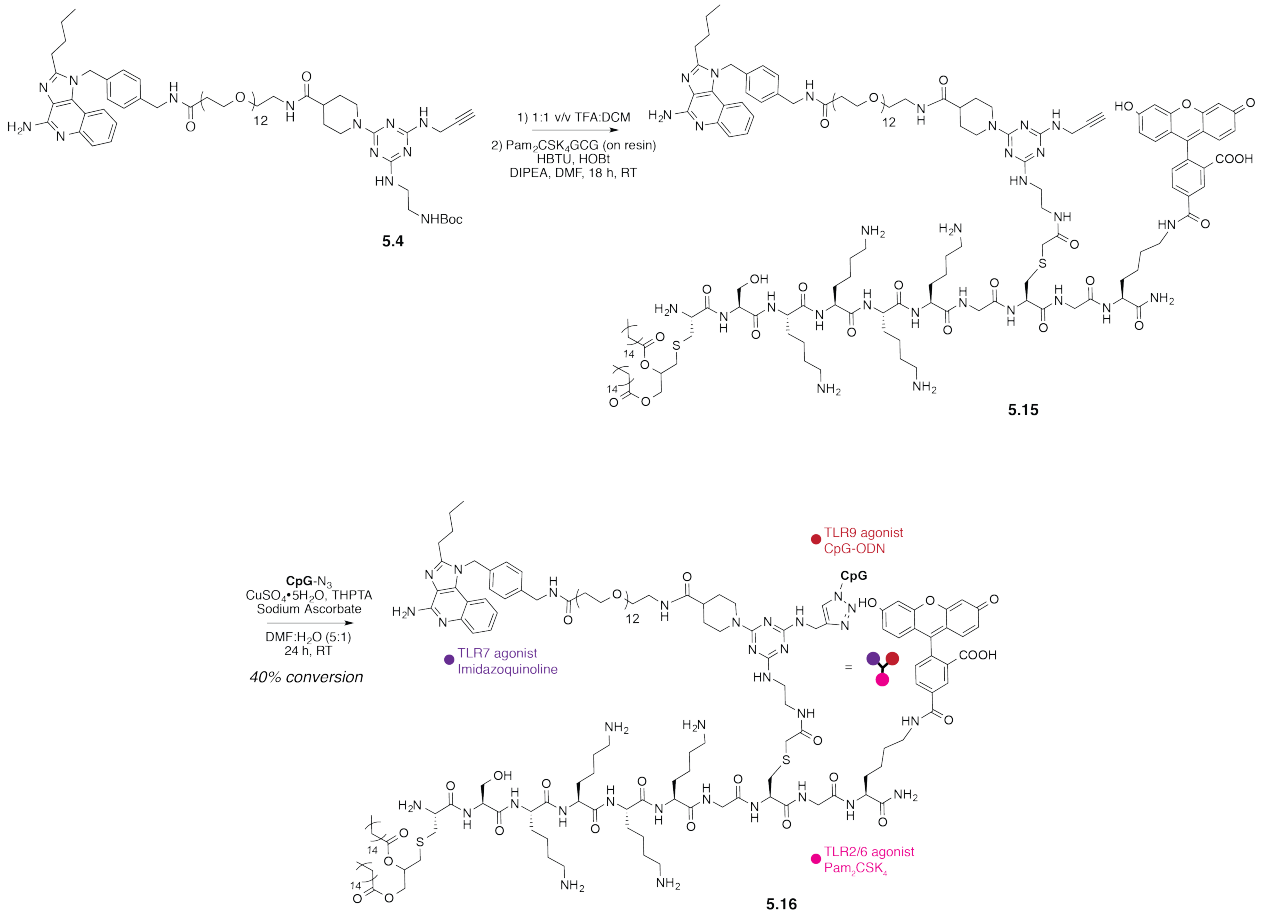

5.7 *In Vivo* Toxicity Studies with the TLR2/6_4_7 Tri-Agonist

Since we observed promising results *in vitro*, we wanted to investigate how our results would translate *in vivo*. Thus far, all of the *in vivo* studies have been performed with the TLR2/6_4_7 tri-agonist, but the other tri-agonist combinations will be subsequently tested. We

performed a short term *in vivo* toxicity study, where we injected our tri-agonist without an antigen, to see if there were any adverse effects on behavior or function of mice. In this study, there were three groups of C57/BL6 mice: the control (injected with PBS), the unconjugated TLR2/6, 4, and 7 agonist (1 nmol of each agonist), and the conjugated TLR2/6_4_7 tri-agonist (1 nmol). The mice were injected with their respective treatment intramuscularly (i.m.), and their behavior was monitored. After five days, the mice were bled, sacrificed, and their organs harvested (lymph node and spleen). Immune cell populations from the lymph nodes were analyzed by flow cytometry for cell surface markers indicative of immune activation and an adaptive immune response. We observed significant differences in $CD86^+$ and $CD4^+$ expressing lymphocytes in the inguinal lymph node (**Fig. 5.10**). The conjugated TLR2/6_4_7 promoted an increase in the percentage of cells expressing either $CD86^+$ or $CD4^+$, which are cell surface markers necessary for T cell activation and on activated T cells, respectively. This result along with no observed toxicity or abnormal behavior proved promising as we moved forward with our vaccination model studies.

Figure 5.10. *In Vivo* Toxicity Study: Analysis of Lymphocytes from the Inguinal Lymph Node at Day 5 Termination[a]

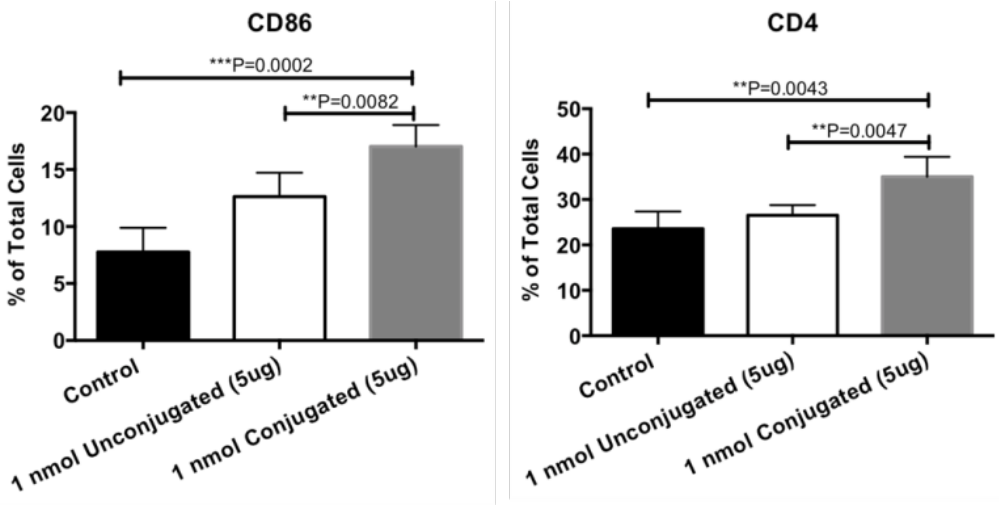

[a] $CD86^+$ (left) and $CD4^+$ (right) lymphocyte populations in the inguinal lymph node as

measured by flow cytometry, reported as percentage of total lymphocytes. Lymphocytes were harvested from C57/BL6 mice vaccinated with PBS (Control), unconjugated TLR2/6/4/7 (1 nmol of each agonists unconjugated), or conjugated TLR2/6_4_7 (1 nmol of conjugated agonists). Each bar is the result of n=5. Results are expressed as the mean ± SD.

5.8 *In Vivo* Vaccination Studies

With the increase in $C86^+$ and $CD4^+$ cells resulting from injection with the TLR2/6_4_7 tri-agonist, we aimed to study the effects of our compounds with the addition of an antigen in a vaccination model study. Working with the Felgner Lab in the UC Irvine School of Medicine, we sought to vaccinate mice with the TLR2/6_4_7 tri-agonist as the adjuvant and a Q fever antigen and compare its effects to the unconjugated agonists as an adjuvant and a control group with just the antigen alone. This study allowed us to determine the types of immune responses elicited *in vivo* toward the target pathogen as a result of the adjuvant and antigen formulation.

The Felgner Lab previously identified five Q fever antigens from sera that was obtained from human cohorts immunized with the only available Q fever vaccine (Q-Vax) and cohorts that had Q fever.[3] Mice were immunized with each of the five antigens combined with the TLR2/6_4_7 tri-agonist or a mixture of the unconjugated TLR2/6, 4, and 7 agonists as the adjuvant to boost immune activation toward the target antigen. On day 0, mice were bled and vaccinated with one of the Q fever antigens of interest and corresponding adjuvant. The mice were monitored and bled on day 1, with the sera kept for analysis. After two weeks, on day 14, the mice were boosted with the same vaccine formula and bled on day 15. The experiment was terminated on day 21, where the mice were bled and spleen and lymph nodes were harvested. Immune cell populations isolated from the lymph node and spleen as well as the sera were analyzed for specific immune cell populations, cytokines, and antibodies.

Sera was probed using a microarray chip platform developed by the Felgner Lab.[3,19] The Q fever antigens were printed on microarray chips, and the chips were incubated with serum

from each mouse. Any Q fever antigen specific antibodies in the sera would bind to the corresponding antigen printed on the chip. The antigen specific antibodies were then detected using fluorescently tagged IgG, IgM, IgG1, or IgG2c antibodies. Two of the antigens (CBU_1910-COM1 and CBU_0307-OmpA, protein antigens from *C. burnetii*) were good vaccine candidates, as specific antibodies were produced toward each of the antigens using the linked TLR2/6_4_7 tri-agonist as well as with the unconjugated agonist mixture. The production of specific IgG antibodies against the target Q fever antigens is required for an efficacious immune response against Q fever bacteria and has important implications for future challenge studies. Unfortunately, there was no distinction in IgG antibodies titers elicited by the linked TLR2/6_4_7 tri-agonist and the mixture of unlinked agonists (**Fig. 5.11**, and see Appendix D, **Figs. S5.6-5.7**). Examining IgG1 and IgG2c antibody subtypes, which are subtypes associated with T_H2 and T_H1 responses, respectively, we observed differences in the CBU_1910 specific antibody titers, with higher antibody titers produced with the unlinked agonists as the adjuvant (**Fig. 5.12**). Cellular and antibody probing are ongoing to elucidate why these differences in the antibody response were observed and what the results suggest for a protective immune response.

Figure 5.11. CBU_1910 Specific IgG Antibodies Probed by Microarray Chip Technology[a]

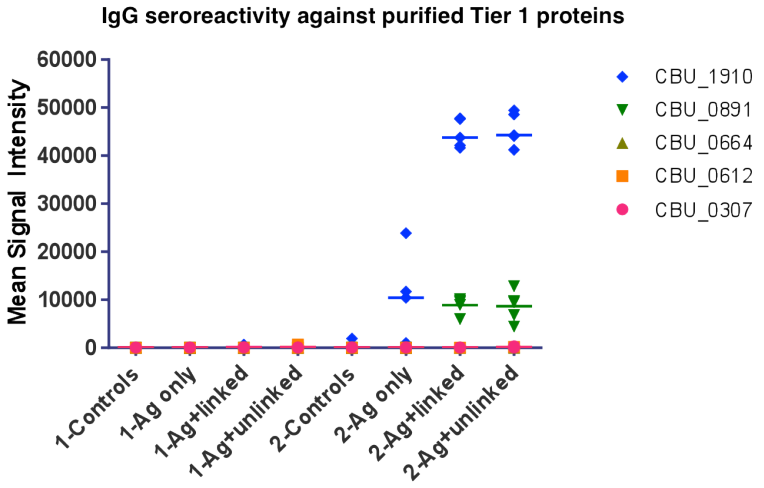

[a] Detection of IgG antibodies specific to CBU_1910 expressed as mean signal intensity. Sera were drawn from C57/BL6 mice vaccinated with PBS (Control), CBU_1910 (Ag only), CBU_1910 plus unlinked TLR2/6/4/7 (1 nmol of each agonists unconjugated), or CBU_1910 plus linked TLR2/6_4_7 (1 nmol of conjugated agonists). Each bar is the result of n=5. Results are expressed as the mean ± SD.

Figure 5.12. CBU_1910 Specific IgG1 and IgG2c Antibodies Probed by Microarray Chip Technology[a]

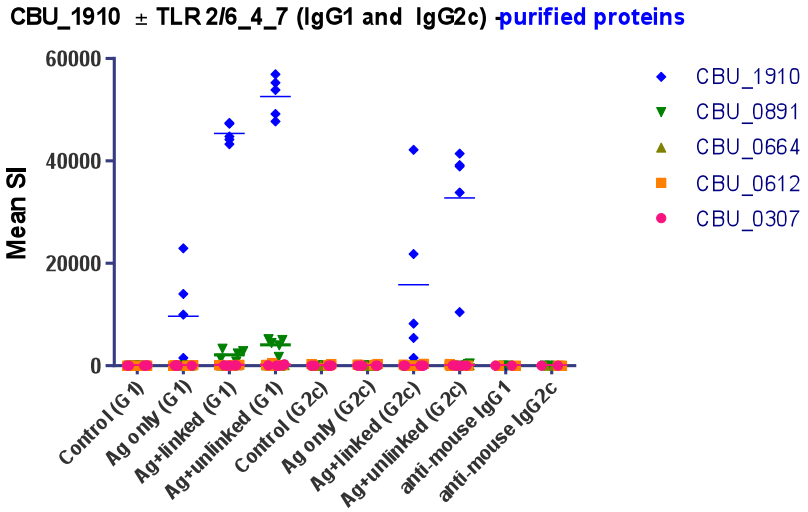

[a] Detection of IgG1 or IgG2c antibodies specific to CBU_1910 expressed as mean signal intensity. Sera were drawn from C57/BL6 mice vaccinated with PBS (Control), CBU_1910 (Ag only), CBU_1910 plus unlinked TLR2/6/4/7 (1 nmol of each agonists unconjugated), or CBU_1910 plus linked TLR2/6_4_7 (1 nmol of conjugated agonists). Each bar is the result of n=5. Results are expressed as the mean ± SD.

5.9 Conclusion

We described here the synthesis of five new TLR tri-agonists, the second generation TLR4_7_9, TLR2/6_4_7, TLR1/2_4_7, TLR2/6_4_9, and TLR2/6_7_9. *In vitro* cell studies were performed with three out of the five combinations, as optimization and scale up are being conducted on the remaining two combinations. With RAW-Blue macrophages and BMDCs, distinct differences were observed between the covalent tri-agonist and the three agonists in solution with each combination. Depending on the agonist combination used, changes in immune activation were also observed between linked tri- and di-agonists. From these cell studies, each tri-agonist candidate exhibited promising immune activation for *in vivo* studies. *In vivo* toxicity and vaccination studies were reported for the TLR2/6_4_7 tri-agonist, with differences in IgG1 and IgG2c antibody titers, and further studies are ongoing to understand our observations. As a result of these and future challenge studies, we aim to determine the optimal formula of adjuvant and antigen for a safer and more effective Q fever vaccine.

5.10 Experimental Procedures

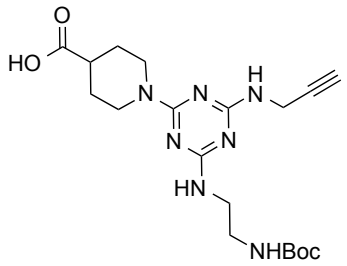

Carboxylic Acid Derivatized Core (5.1).

Compound 4.3 (0.20 g, 0.61 mmol) was dissolved in DMF (2.0 mL). DIPEA (0.12 mL) and isonipecotic acid (87 mg, 0.67 mmol) were subsequently added. The reaction was heated at 80 °C and stirred for 3 h. The reaction was then concentrated and purified by column chromatography (1% MeOH/EtOAc with 1% NH_4OH). The product was a white powder (170 mg, 67%). ^{1}H NMR (600 MHz, DMSO-d_6) δ 12.24 (br s, 1H), 7.04-6.44 (br m, 3 H), 4.50 (br s, 2H), 3.96 (s, 2H), 3.22 (br s, 2H), 3.04 (br s, 2H), 2.99 (s, 1H), 2.89 (br s, 2H), 2.48 (br s, 1H), 1.80 (br s, 2H), 1.40 (br s, 2H), 1.36 (s, 9H). ^{13}C NMR (600 MHz, DMSO-d_6) δ 175.84, 165.80, 165.79, 164.42, 159.60, 82.52, 77.55, 71.99, 41.95, 40.57, 40.00, 29.38, 28.24, 27.73. HRMS: *m/z* calcd for $C_{19}H_{29}N_7O_4$ $[M+Na]^+$ 442.2179, observed 442.2162. Analysis for purity checked by analytical HPLC C8, A: water + 0.1% TFA, B: acetonitrile + 0.1% TFA (10-90% acetonitrile/water + 0.1% TFA gradient, 0-11 minutes), where t_R: 8.26 min.

Imidazoquinoline Synthesis (5.2).

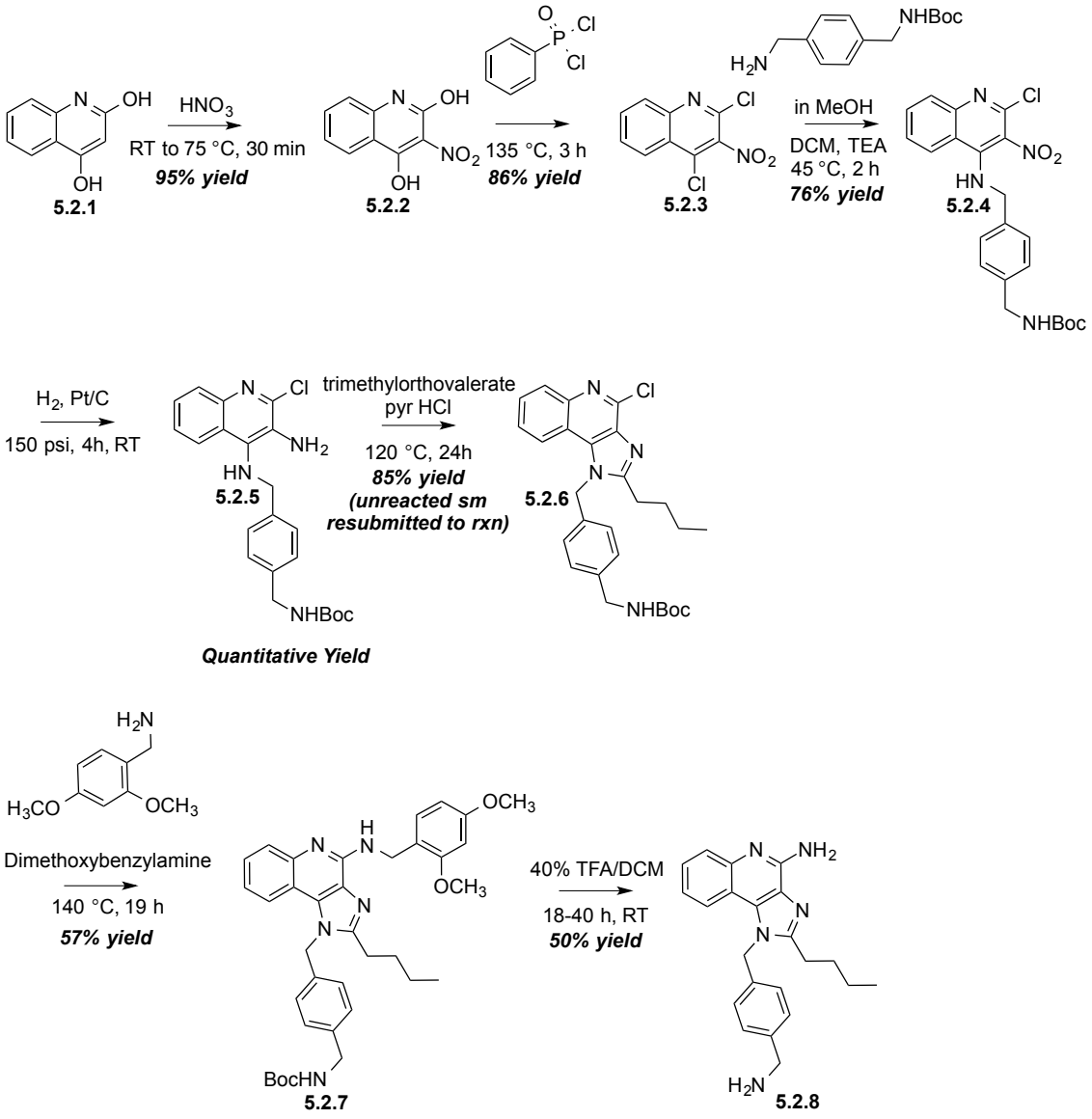

Compounds 5.2.1-5.2.4 were synthesized according to literature procedures reported by Shukla, *et al*.[10,20] Compounds 5.2.5-5.2.8 were synthesized according to the modified procedures[8] below to increase yield for scale up purposes.

Compound 5.2.5:

The nitro-substrate (**5.2.4**) (5.0 g, 11 mmol) and sodium sulfate (0.050 g) were dissolved in ethyl acetate (0.040 L) that was purged with argon in a Parr Reactor (Parr Instrument Company). 10%

Pt/C (0.050 g) was added to the reaction mixture and the reactor was filled with hydrogen gas at 350 psi. The reaction was allowed to stir at room temperature until hydrogen gas was consumed and the pressure remained constaint (overnight, ~ 24 hours). The reaction was filtered through Celite and concentrated by rotary evaporation. A yellow solid was obtained (4.5 g, 98% yield).

^{1}H NMR (500 MHz, DMSO-d_6) δ7.98 (d, J = 6.5 Hz, 1H), 7.65 (d, J = 7.5 Hz, 1H), 7.40-7.35 (m, 2H), 7.30 (d, J = 6.5 Hz, 3H), 7.13 (d, J =6.5 Hz, 2H), 5.81 (s, 1H), 5.07 (s, 2H), 4.42 (d, J = 6 Hz, 2H), 4.06 (d, J =5.5 Hz, 2H), 1.38 (s, 9H). HRMS: m/z calcd for $C_{22}H_{25}ClN_4O_2$ $[M+Na]^+$ 435.17, observed 435.1566.

Compound 5.2.6:

The reduced substrate (**5.2.5**) (0.15 g, 0.36 mmol) was suspended in toluene (2.0 mL). Trimethylorthovalerate (0.13 mL, 0.73 mmol) and pyridine hydrochloride (5.0 mg, 36 μmol) were added to the solution. The reaction was allowed to stir and heated at 120 ºC for 20 h. The crude reaction was then concentrated and purified by column chromatography (50% EtOAc/Hex) to obtain the product as a white solid (70 mg, 41%).

The uncyclized intermediate was resubmitted to the reaction according to the following procedure. The uncyclized substrate (0.11 g, 0.22 mmol) was dissolved in xylenes (2.0 mL). Pyridine hydrochloride (5.1 mg, 44 μmol) was added to the reaction mixture, which was heated at 130 ºC for 24 h. The reaction was allowed to cool, was concentrated, and purified by column chromatography (50% EtOAc/Hex) to obtain the product (77 mg, 73%).

Combined total yield (147 mg, 85% yield).

^{1}H NMR (500 MHz, CD_3OD) δ8.08–8.04 (dd, J = 14, 7.3 Hz, 2H), 7.65 (t, J = 5.8 Hz, 1H), 7.48 (t, J = 7 Hz, 1H), 7.25 (d, J = 7 Hz, 2H), 7.02 (d, 2H), 5.98 (s, 1H), 4.18 (s, 2H), 3.06 (t, J = 6.3

Hz, 2H), 1.79-1.74 (m, 2H), 1.41 (s, 9H), 1.29 (br s, 2H), 0.92 (t, *J* = 6 Hz, 3H). HRMS: *m/z* calcd for $C_{27}H_{31}ClN_4O_2$ $[M+Na]^+$ 501.21, observed 501.2023.

Compound 5.2.7:

Cyclized compound **5.2.6** (44 mg, 0.090 mmol) was suspended in dimethoxybenzylamine (1.6 mL, 0.010 mol). The reaction was run neat and heated at 140 ºC for 19 h. The crude reaction mixture was poured into methylene chloride (0.10 L) and washed with 1 M HCl (4 x 100 mL). The organic layer was dried with sodium sulfate, filtered, and concentrated. The crude product was purified by column chromatography (5% MeOH/methylene chloride) to provide the product as a white powder (31 mg, 57%).

^{1}H NMR (500 MHz, CD_3OD) δ7.86 (t, *J* = 6.5 Hz, 2H), 7.50 (t, *J* = 6.5 Hz, 1H), 7.33 (d, *J* = 7.3 Hz, 1H), 7.25 (d, *J* = 6.5 Hz, 2H), 7.20 (br s, 1H), 7.03 (d, *J* = 6.5 Hz, 2H), 6.61 (s, 1H), 6.53-6.52 (dd, *J* = 6.5, 2 Hz, 1H), 5.87 (s, 2H), 4.18 (br s, 2H), 3.87 (s, 3H), 3.80 (s, 3H), 2.94 (t, *J* = 6.3 Hz, 2H), 1.79-1.74 (m, 2H), 1.42 (s, 9H), 1.29 (br s, 2H), 0.91 (t, *J* = 6.3 Hz, 3H). HRMS: *m/z* calcd for $C_{36}H_{43}N_5O_4$ $[M+H]^+$ 610.34, observed 610.3387.

Compound 5.2.8:

Protected imidazoquinoline **5.2.7** (0.20 g, 0.50 mmol) was dissolved in methylene chloride (15 mL). Trifluoroacetic acid (0.010 L) was added to the solution to provide a 40% TFA/methylene chloride solution. The reaction was allowed to stir at RT for 38 h. The reaction mixture was concentrated and 1 M HCl (100 mL) was added to the crude solid. The solid was filtered off and the filtrate was adjusted to pH 10 using 10 M NaOH. The aqueous solution was extracted with methylene chloride (6 x 200 mL). The organic layer was then dried with sodium sulfate, filtered, and concentrated to provide the product as a white solid (180 mg, 50% yield).

^{1}H NMR (500 MHz, DMSO-d_6) δ7.79 (d, J = 7.5 Hz, 1H), 7.56 (t, J = 8.5 Hz, 1H), 7.32 (t, J = 7 Hz, 1H), 7.26 (d, J = 8.5 Hz, 2H), 7.02 (t, J = 7 Hz, 1H), 6.95 (d, J = 8 Hz, 2H), 6.53 (s, 1H), 5.82 (s, 2H), 3.64 (s, 2H), 2.90 (t, J = 7.5 Hz, 2H), 1.74-1.68 (m, 2H), 1.42-1.34 (m, 2H), 0.87 (t, J = 7.5 Hz, 3H). HRMS: m/z calcd for $C_{22}H_{25}N_5$ $[M+H]^+$ 360.22, observed 360.2183.

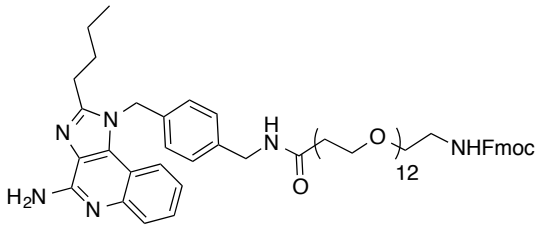

TLR7_PEG$_{12}$-NH-Fmoc (5.3).

Imidazoquinoline (75 mg, 0.21 mmol) and NHS-PEG$_{12}$-NH-Fmoc (0.20 g, 0.21 mmol) were dissolved in DMSO (2.1 mL). The reaction was allowed to stir at RT overnight (18 h). The crude solution was purified by reverse phase HPLC using a C8 preparatory column (Luna 5 μm C18(2) 100 Å, LC Column 250 x 21.2 mm, AXIA, Phenomenex), where the solvent system was A: water + 0.1% TFA, B: acetonitrile + 0.1% TFA (10-90% acetonitrile/water + 0.1% TFA gradient, 0-19 minutes). The HPLC fractions were lyophilized to afford the desired product as a clear gel (230 mg, 94% yield). ^{1}H NMR (600 MHz, $CDCl_3$) δ 10.1 (br s, 1H), 7.90 (d, J = 9.6 Hz, 1H), 7.75 (d, J = 9 Hz, 2H), 7.70 (d, J = 10.2 Hz, 1H), 7.59 (d, J = 8.4 Hz, 2H), 7.56-7.51 (br m, 3H), 7.39 (t, J = 9 Hz, 2H), 7.30 (t, J = 8.4 Hz, 2H), 7.28 (d, J = 9.6 Hz, 3H), 6.97 (d, J = 9.6 Hz, 2H), 5.73 (s, 2H), 5.52 (br s, 1H), 4.43 (d, J = 7.2 Hz, 2H), 4.39 (d, J = 8.4 Hz, 2H), 4.22 (t, J = 8.1 Hz, 1H), 3.73 (t, J = 6.6 Hz, 2H), 3.63-3.55 (br m, 38H), 3.53-3.51 (br m, 4H), 3.48 (br d, J = 4.8 Hz, 4H), 3.39 (br s, 2H), 2.90 (t, J = 9.3 Hz, 2H), 2.56 (t, J = 6.9 Hz, 2H), 1.80 (quintet, J = 9.6 Hz, 2H), 1.44 (sextet, J = 9 Hz, 2H), 0.934 (t, J = 8.7 Hz, 3H). ^{13}C NMR (600 MHz, $CDCl_3$) δ 173.6,157.2, 149.4, 144.1, 141.4, 139.2, 135.8, 134.6, 132.7, 130.1, 128.8, 127.8, 127.2, 125.6,

125.2, 120.8, 120.1, 119.9, 112.5, 70.6, 70.5, 70.4, 70.2, 67.0, 66.8, 49.2, 47.4, 43.0, 41.0, 36.4, 2 9.6, 26.9, 22.5, 13.8. MALDI-TOF: *m/z* calcd for $C_{64}H_{88}N_6O_{15}$ $[M+H]^+$ 1181.6, observed 1181.4.

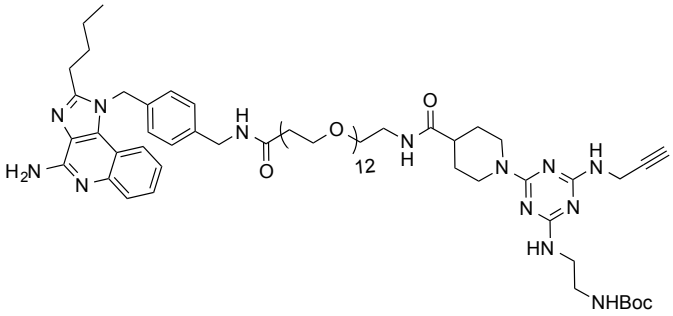

TLR7_PEG$_{12}$_Core (5.4).

Compound **5.3** (230 mg, 0.19 mmol) was dissolved in anhydrous methylene chloride (1.8 mL). Diethylamine (10% v/v, 0.19 mL) was then added to the solution. The reaction was allowed to stir at RT for 10 h. The reaction mixture was concentrated and re-dissolved in minimal methylene chloride, which was then precipitated in diethyl ether (2x). The product was spun down, removed of diethyl ether, and dried on high-vacuum. The resulting free amine was used in the following procedure to synthesize **5.4**. MALDI-TOF: *m/z* calcd for $C_{49}H_{78}N_6O_{13}$ $[M+H]^+$ 959.6, observed 959.3.

Carboxylic acid core (**5.1**) (88 mg, 0.21 mmol) was suspended in DMF (1.8 mL). DIPEA (66 μL, 0.38 mmol) and subsequently HATU (0.080 g, 0.21 mmol) were added to the carboxylic acid. The cloudy solution was allowed to stir for 15 min until cleared. In another round bottom flask, the free amine substrate (180 mg, 0.19 mmol) was dissolved in DMF (2.1 mL). The activated carboxylic acid was slowly added to the reaction mixture (over 1 h). The reaction was allowed to stir at RT for 3 h. The reaction mixture was concentrated, re-dissolved in DMSO, and purified by reverse phase HPLC using a C8 preparatory column, where the solvent system was A: water + 0.1% TFA, B: acetonitrile + 0.1% TFA (10-90% acetonitrile/water + 0.1% TFA gradient, 0-19

minutes). The HPLC fractions were lyophilized to afford the desired product as a clear gel (150 mg, 57% yield). ^{1}H NMR (500 MHz, $CDCl_3$) δ 10.6 (br s, 1H), 7.87 (br s, 1H), 7.82 (d, *J* = 8.5 Hz, 1H), 7.77 (br t, *J* = 4.8 Hz, 1H), 7.67 (d, *J* = 8.5 Hz, 1H), 7.46 (t, *J* = 7.8 Hz, 1H), 7.29-7.23 (m, 3H), 6.94 (d, *J* = 8, 2H), 6.88 (br s, 1H), 6.51 (br s, 1H), 5.71 (s, 2H), 5.19 (br s, 1H), 4.73 (br t, *J* = 12.5 Hz, 2H), 4.39 (d, *J* = 6 Hz, 2H), 4.11 (br s, 2H), 3.70 (t, *J* = 5.8 Hz, 2H), 3.63-3.57 (m, 32H), 3.54-3.50 (m, 10H), 3.47 (br d, *J* = 2.5, 6H), 3.42 (br q, *J* = 5 Hz, 2H), 3.32-3.29 (br m, 2H), 3.19 (d, *J* = 8.5 Hz, 1H), 3.04-2.98 (m, 2H), 2.86 (t, *J* = 7.8 Hz, 2H), 2.50 (t, *J* = 5.5 Hz, 2H), 2.43 (br t, *J* = 11 Hz, 1H), 2.22 (s, 1H), 1.89 (br d, *J* = 13 Hz, 2H), 1.78 (quintet, *J* = 8 Hz, 2H), 1.70 (br q, *J* = 11.5 Hz, 2H), 1.43-1.39 (m, 2H), 1.39 (s, 9H), 0.91 (t, *J* = 7 Hz, 3H). ^{13}C NMR (500 MHz, $CDCl_3$) δ 174.3, 172.4, 162.6, 161.4, 157.0, 156.0, 155.5, 149.7, 139.4, 135.6, 134.6, 132.7, 129.6, 128.6, 125.5, 125.2, 124.7, 120.7, 119.6, 117.3, 115.0, 112.5, 79.6, 78.5, 77.4, 71.9, 70.3, 70.2, 70.1, 69.8, 67.1, 49.0, 43.8, 42.7, 41.2, 39.7, 39.3, 36.6, 30.3, 29.4, 28.4, 27.0, 22.4, 13.8. MALDI-TOF: *m/z* calcd for $C_{68}H_{105}N_{13}O_{16}$ $[M+H]^+$ 1360.8, observed 1360.7.

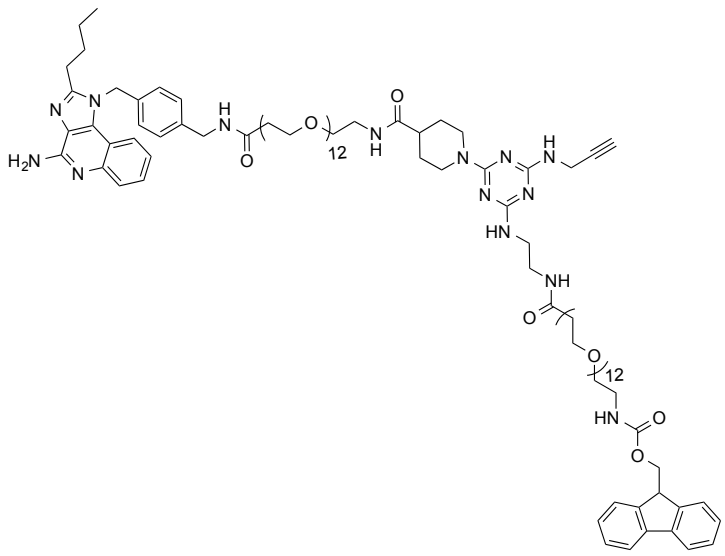

TLR7_PEG$_{12}$_Core_PEG$_{12}$-NH-Fmoc (5.5).

Compound **5.4** (0.080 g, 59 μmol) was dissolved in TFA/methylene chloride (1:1 v/v) (0.60 mL). The reaction was allowed to stir at RT for 3 h. The solution was concentrated and re-dissolved in minimal methylene chloride, which was then precipitated in diethyl ether (2x). The product was spun down, removed of diethyl ether, and dried on high-vacuum. The resulting free amine was used in the following procedure to synthesize **5.5**.

The free amine substrate (74 mg, 59 μmol) and NHS-PEG$_{12}$-NH-Fmoc (58 mg, 62 μmol) were dissolved in DMSO (0.60 mL). DIPEA (21 μL, 120 μmol) was then added to the reaction mixture, which was allowed to stir at RT for 16 h. The reaction mixture was purified by reverse phase HPLC using a C8 preparatory column, where the solvent system is A: water + 0.1% TFA, B: acetonitrile + 0.1% TFA (40-60% acetonitrile/water + 0.1% TFA gradient, 0-15 minutes). The HPLC fractions were lyophilized to afford the desired product as a light brown gel (51 mg, 41% yield). ^{1}H NMR (500 MHz, $CDCl_3$) δ 10.63 (br s, 1H), 8.16 (br s, 1H), 7.87 (d, *J* = 7.8 Hz, 2H), 7.73 (d, *J* = 7.8 Hz, 2H), 7.68 (d, *J* = 8.4 Hz, 1H), 7.58 (d, *J* = 7.2 Hz, 2H), 7.49 (t, *J* = 7.5 Hz, 1H), 7.37 (t, *J* = 7.2 Hz, 2H), 7.30-7.24 (m, 6H), 6.94 (d, *J* = 7.8 Hz, 2H), 6.85 (br s, 1H), 6.57

(br s, 1H), 5.70 (s, 2H), 5.52 (br s, 1H), 4.74 (br t, *J* = 12.6 Hz, 2H), 4.39 (d, *J* = 6 Hz, 2H), 4.37 (d, *J* = 6.6 Hz, 2H), 4.19 (t, *J* = 6.9 Hz, 1H), 4.12 (br d, *J* = 3 Hz, 2H), 3.71 (t, *J* = 5.7 Hz, 2H), 3.69-3.66 (m, 1H), 3.63-3.59 (m, 72H), 3.57-3.51 (m, 18H), 3.48 (br d, *J* = 3 Hz, 6H), 3.43-3.41 (br m, 4H), 3.38-3.36 (br m, 2H), 3.00 (br q, *J* = 10.8 Hz, 2H), 2.86 (t, *J* = 7.8 Hz, 2H), 2.50 (t, *J* = 5.7 Hz, 2H), 2.46 (br t, *J* = 5.1 Hz, 2H), 2.44 (br s, 1H), 2.22 (t, *J* = 2.4 Hz, 1H), 1.89 (br d, *J* = 12 Hz, 2H), 1.79 (quintet, *J* = 7.8 Hz, 2H), 1.70 (br t, *J* = 10.5 Hz, 2H), 1.42 (sextet, *J* = 7.2 Hz, 2H), 0.92 (t, *J* = 7.5 Hz, 3H). ^{13}C NMR (600 MHz, $CDCl_3$) δ 174.4, 172.9, 172.2, 162.3, 162.0, 161.4, 156.9, 156.7, 155.9, 155.6, 149.8, 144.1, 141.5, 139.5, 135.6, 134.7, 132.7, 129.7, 128.6, 127.7, 127.1, 125.5, 125.1, 124.9, 120.7, 120.0, 119.8, 117.2, 115.2, 112.6, 78.7, 71.8, 70.5, 70.4, 70.3, 70.2, 70.1, 69.9, 67.2, 67.0, 66.6, 49.0, 47.3, 43.8, 42.7, 41.0, 40.4, 39.3, 38.5, 36.7, 36.5, 30.3, 29.4, 28.6, 27.0, 22.4, 13.8. MALDI-TOF: *m/z* calcd for $C_{105}H_{160}N_{14}O_{29}$ $[M+H]^+$ 2082.2, observed 2082.2.

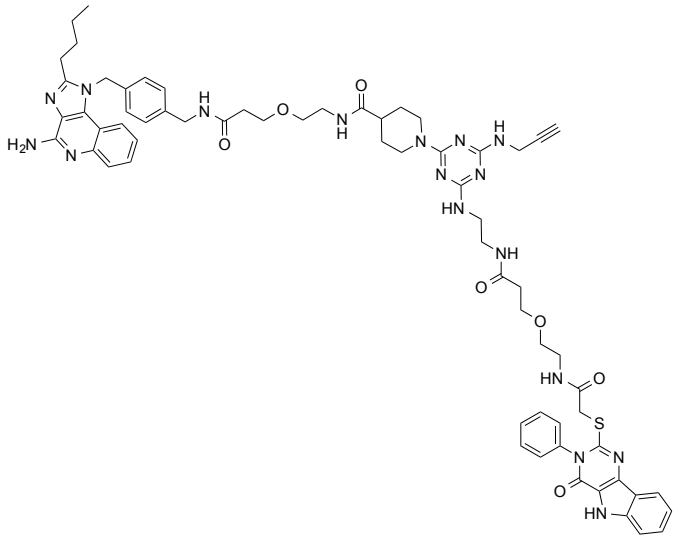

TLR4_7 (5.6).

Compound **5.5** (0.050 g, 24 μmol) was dissolved in anhydrous methylene chloride (0.90 mL). Diethylamine (10% v/v, 0.10 mL) was then added to the solution. The reaction was allowed to stir at RT for 3 h. The reaction mixture was concentrated and re-dissolved in minimal methylene

chloride, which was then precipitated in diethyl ether (2x). The product was spun down, removed of diethyl ether, and dried on high-vacuum. The resulting free amine was used in the following procedure to synthesize **5.6**.

Indole-COOH (2.4 mg, 6.9 μmol) was dissolved in DMF (0.25 mL). DIPEA (3.3 μL, 19 μmol) and HATU (2.6 mg, 6.9 μmol) were then added to the solution in this order to give a blue colored solution. The free amine substrate (12 mg, 6.3 μmol) was dissolved in DMF in a separate vial. The preactivated indole carboxylic acid solution was slowly added to the solution of free amine and the reaction was allowed to stir at RT for 22 h. The reaction mixture was concentrated, re-dissolved in DMSO, and purified by reverse phase HPLC using a C8 preparatory column, where the solvent system was A: water + 0.1% TFA, B: acetonitrile + 0.1% TFA (10-90% acetonitrile/water + 0.1% TFA gradient, 0-19 minutes, $t_{retention}$: 12.25 min). The HPLC fractions were lyophilized to afford the desired product as a clear gel (3.7 mg, 27% yield). ^{1}H NMR (600 MHz, $CDCl_3$) δ 10.16 (br s, 1H), 8.22 (br s, 1H), 8.11 (d, *J* = 9.6 Hz, 1H), 7.96 (d, *J* = 10.2 Hz, 2H), 7.72 (d, *J* = 11.4 Hz, 1H), 7.58-7.44 (m, 7H), 7.38-7.36 (m, 2H), 7.29 (br d, *J* = 9.6 Hz, 3H), 6.97 (d, *J* = 9 Hz, 2H), 6.78 (br s, 1H), 5.73 (s, 2H), 4.74 (br m, 2H), 4.42 (d, *J* = 6.6 Hz, 2H), 4.09 (br s, 2H), 3.90 (s, 2H), 3.73 (t, *J* =6.6 Hz, 2H), 3.69-3.53 (m, 84H), 3.49-3.45 (m, 16H), 3.40-3.38 (m, 2H), 3.32-3.30 (br m, 2H), 3.21-3.19 (br m, 2H), 2.99 (br s, 2H), 2.87 (t, *J* = 9.3 Hz, 3H), 2.53 (t, *J* = 6.9 Hz, 2H), 2.49 (br s, 3H), 2.23 (br s, 1H), 1.91 (br d, *J* = 13.2 Hz, 2H), 1.82 (quintet, *J* = 9 Hz, 2H), 1.74-1.69 (br s, 2H), 1.44 (sextet, *J* = 9 Hz, 2H), 0.94 (t, *J* = 8.7 Hz, 3H). Analysis for purity checked by analytical HPLC C8, A: water + 0.1% TFA, B: acetonitrile + 0.1% TFA (10-90% acetonitrile/water + 0.1% TFA gradient, 0-11 minutes, $t_{retention}$: 8.46 min). MALDI-TOF: *m/z* calcd for $C_{108}H_{161}N_{17}O_{29}S$ $[M+H]^+$ 2193.2, observed 2193.0.

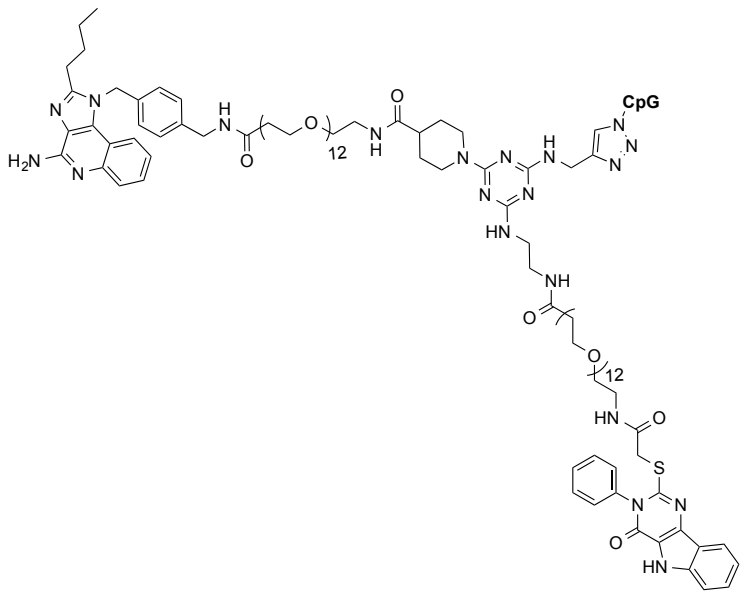

TLR4_7_9 (5.7).

Compound **5.6** (0.14 mg, 66 nmol) in anhydrous DMF (73 μL) and CpG (0.080 mg, 11 nmol) in degassed water (11 μL) were mixed in a vial. Copper sulfate pentahydrate (55 μg, 220 nmol) pre-dissolved in degassed water (4.0 μL) and tris(3-hydroxypropyltriazolylmethyl)amine (THPTA) (0.14 mg, 330 nmol) in degassed water (4.8 μL) were mixed and then added to the reaction vial. Lastly, sodium ascorbate (65 μg, 330 nmol) in degassed water (2.7 μL) was added to the reaction mixture to give a final volume (DMF: H2O 5:1). The reaction mixture was placed on a shaker at RT for 24 h. The crude reaction was purified *via* TBE-urea gel electrophoresis (Fig. S5.1) and gel extraction. The product band was excised and eluted into endotoxin free water overnight at RT. The solution was concentrated and desalted using a 3k centrifugal filter unit (EMD Millipore) to provide the desired product (92% conversion). MALDI-TOF in negative reflector mode: *m/z* calcd $[M-H]^-$ 9460.6, observed 9460.8.

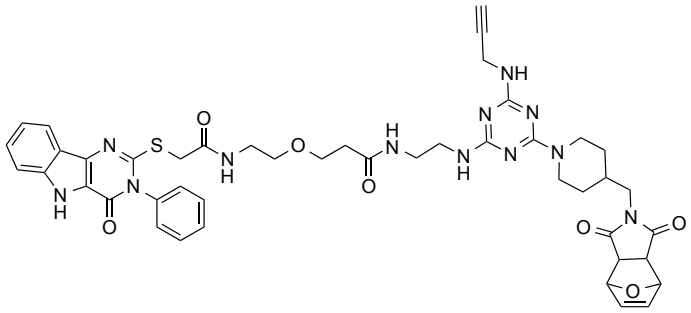

Indole_PEG$_{12}$_Core (5.8). (*provided by Tyler Albin*)

Tri-agonist Core **4.5** (160 mg, 0.29 mmol) was dissolved in 50% TFA/methylene chloride (5.0 mL) and allowed to stir for 2 h. The solvent was removed by rotary evaporation.

Fmoc-HN-PEG$_{12}$-COOH coupling: Fmoc-HN-PEG$_{12}$-COOH (0.20 g, 0.24 mmol), Boc-deprotected tri-agonist core (described above), HBTU (0.11 g, 0.29 mmol), and HOBt (44 mg, 0.29 mmol) were dissolved in 25% 2,4,6-collidine/DMF (0.50 mL) and allowed to stir at RT for 18 h. The reaction mixture was diluted with methylene chloride (0.20 L) and the organic layer washed with 0.1 M HCl (3 x 200 mL), 10% saturated $NaHCO_3$ (aq.) in water (3 x 200mL), and DI water (3 x 200 mL). The organic layer was dried with sodium sulfate, filtered, and evaporated to dryness. The crude product was purified by flash chromatography to obtain the final product as a viscous, tan oil (250 mg, 81% yield). The product (**5.8.1**) was characterized by ^{1}H NMR, ^{13}C NMR, and ESI-MS. R_f 0.44 (10% MeOH/methylene chloride); ^{1}H NMR (500 MHz, $CDCl_3$) δ 7.75 (d, J = 7.6 Hz, 2H), 7.60 (d, J = 7.5 Hz, 2H), 7.39 (t, J = 7.3 Hz, 2H), 7.30 (td, J = 7.5, 1.1 Hz, 2H), 6.51 (s, 2H), 5.27 (s, 2H), 4.70 (s, 2H), 4.39 (d, J = 6.9 Hz, 2H), 4.21 (t, J = 6.7 Hz, 2H), 4.14 (s, 2H), 3.69 (t, J = 5.7 Hz, 2H), 3.62 (m, 42H), 3.56 (t, J = 5.0, 2H), 3.48 (s, 2H), 3.43 – 3.33 (m, 6H), 2.84 (s, 2H), 2.69 (t, J = 11.7 Hz, 2H), 2.42 (t, J = 5.8 Hz, 2H), 2.19 (s, 1H), 2.09 (s, 1H), 1.95 (s, 1H), 1.61 (d, J = 11.8 Hz, 2H), 1.13 (m, 2H). ^{13}C NMR (126 MHz, $CDCl_3$) δ 176.49, 171.97, 144.06, 141.35, 136.58, 127.71, 127.09, 125.14, 120.00, 81.10, 81.10, 77.30, 70.78, 70.55, 70.49, 70.37, 70.35, 70.25, 70.12, 67.32, 66.59, 47.39, 47.32, 44.21, 42.81, 40.98,

40.24, 37.09, 34.98, 30.40, 29.57. ESI-MS m/z calcd for $C_{64}H_{91}N_9O_{18}$ $[M+H]^+$: 1274.66, observed 1274.46.

Fmoc Deprotection: Fmoc-HN-PEG_{12}-Core (**5.8.1**) (250 mg, 0.19 mmol) was dissolved in 20% diethylamine/methylene chloride and allowed to stir at RT for 2 h. The solution was evaporated to dryness by rotary evaporation. The product was precipitated in diethyl ether (10 mL), centrifuged, and decanted. This process was repeated 2x. The product was dried under high vacuum and obtained as a white solid.

Indole, TLR4 agonist coupling: Indole-COOH (82 mg, 0.23 mmol) and H_2N-PEG_{12}-Core (0.19 mmol) were dissolved in 25% 2,4,6-collidine (2.0 mL). HBTU (88 mg, 0.23 mmol) and HOBt (36 mg, 0.23 mmol) were then added to the reaction solution, which was allowed to stir at RT for 18 h. The reaction was concentrated by rotary evaporation and the crude product purified by flash chromatography. The product was further purified with a silica plug by washing with ethyl acetate and subsequently eluted with 10% MeOH/methylene chloride to afford the pure product. The solvent was evaporated, the solid lyophilized, and the product obtained as a white powder (110 mg, 41% yield). The product was characterized by ^{1}H NMR, ^{13}C NMR, HPLC, and ESI-MS. R_f 0.37 (10% MeOH/methylene chloride); ^{1}H NMR (500 MHz, CD_3OD) δ 8.14 (d, J = 7.9 Hz, 1H), 7.63-7.58 (m, 3H), 7.56 (m, 1H), 7.50 (ddd, J = 8.4, 7.0, 1.2 Hz, 1H), 7.47 – 7.40 (m, 2H), 7.28 (ddd, J = 8.0, 7.0, 1.0 Hz, 1H), 6.53 (s, 2H), 5.15 (s, 2H), 4.72 (s, 1H), 4.13 (s, 2H), 3.94 (s, 2H), 3.68 (t, J = 5.9 Hz, 2H), 3.62 – 3.32 (m, 52H), 2.90 (s, 2H), 2.77 (m, 2H), 2.61 (s, 1H), 2.41 (t, J = 5.9 Hz, 2H), 1.95 (s, 1H), 1.66 (s, 2H), 1.11 (s, 2H). ^{13}C NMR (126 MHz, CD_3OD) δ 177.3, 173.1, 169.6, 155.9, 152.5, 139.6, 138.5, 136.2, 135.9, 130.0, 129.5, 129.3, 127.7, 120.8, 120.6, 120.5, 119.1, 112.4, 80.9, 70.12, 70.06, 70.02, 69.9, 69.1, 66.8, 43.3, 39.6,

36.4, 35.8, 34.8, 29.6, 29.3. ESI-MS m/z calcd for $C_{64}H_{91}N_9O_{18}$ $[M+Na]^+$: 1407.60, observed 1407.56.

Pam_2CSK_4 and TLR2/6 _Core Syntheses. (*provided by Tyler Albin*)

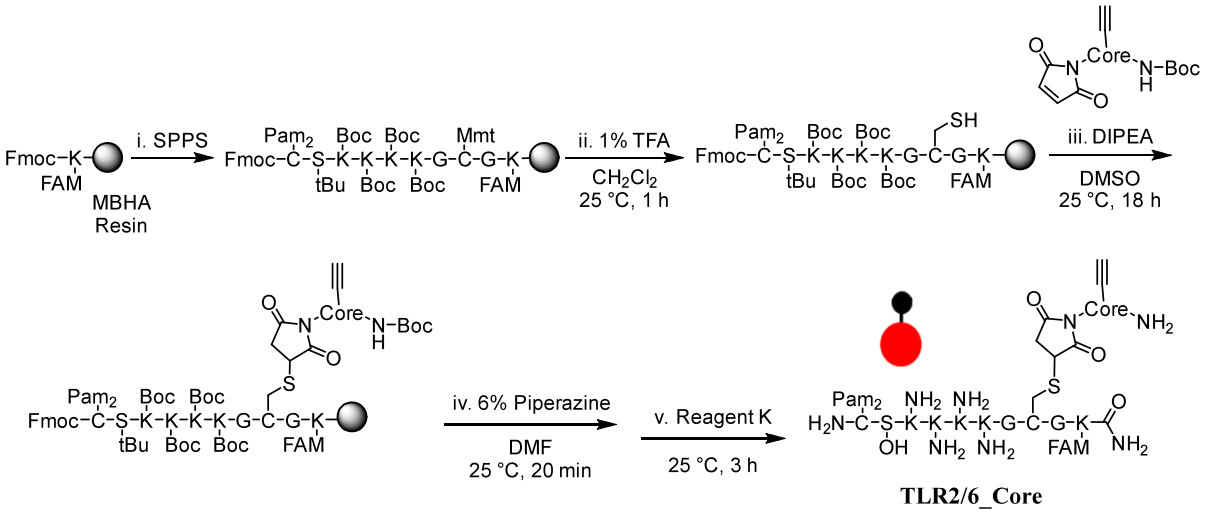

Synthetic scheme of TLR2/6_Core by modified SPPS. (i.) Fmoc-based SPPS. (ii.) Mmt deprotection. (iii.) Michael addition to tri-agonist core. (iv.) Fmoc deprotection (v.) Resin cleavage.

Resin Loading: MBHA rink amide resin (0.30 g, 0.78 mmol/g) was added to a Bio-Rad Poly Prep column. The resin was suspended in methylene chloride (10 mL) and agitated for 30 min. The resin was drained of the solution and suspended in DMF (10 mL) for 10 min. Fmoc deprotection was performed by suspending the resin in 6% piperazine/DMF (10 mL) for 10 min (2x). The resin was then washed with DMF (3 x 10 mL). The DMF was drained and the resin suspended in a solution of Fmoc-Lys(5/6 FAM)-OH (0.19 g, 0.26 mmol) and HATU (0.10 g, 0.26 mmol) in 25% 2,4,6-collidine/DMF (3 mL) for 1 h. The resin was drained of the solution, washed with DMF (3 x 10 mL), and capped by suspending in a solution of acetic anhydride (0.48 g, 4.7 mmol) in 25% DIPEA/DMF (3 mL) for 20 min. The solution was drained and the resin washed with DMF (3 x 10 mL).

Solid Phase Peptide Synthesis: The following steps were followed to synthesize the sequence Fmoc-S(OtBu)-K(Boc)$_4$-G-C(Mmt)-G-K(5,6 FAM)-Resin: i. Fmoc deprotection with 6% piperazine/DMF (10 mL) for 10 min (2x) ii. DMF wash (3 x 10 mL) iii. Coupling of the amino acid (0.94 mmol) in the presence of HBTU (360 mg, 0.94 mmol) dissolved in 25% 2,4,6-collidine/DMF (3 mL) for 30 min, and iv. DMF wash (3 x 10 mL). The same four steps were followed for Fmoc-C(Pam$_2$)-OH (320 mg, 0.35 mmol) coupling, but the amino acid was coupled to the resin in a solution of 25% 2,4,6-collidine/DMF (3 mL), HBTU (180 mg, 0.47 mmol), and HOBt (190 mg, 0.47 mmol) and shaken for 18 h.

Fmoc-Pam$_2$CS(OtBu)K(Boc)$_4$GC(Mmt)G-Resin cysteine SN$_2$ with bromoacetic acid. (*provided by Tyler Albin*)

Fmoc-Pam$_2$CS(OtBu)K(Boc)$_4$GC(Mmt)G-Resin (0.30 g) was added to a Biorad poly prep column. The resin was swollen in methylene chloride (10 mL) for 30 minutes and the methylene chloride drained. The Cys(Mmt) was deprotected by washing the resin several times with 1% TFA/methylene chloride over 1 h. The resin was washed 3x with methylene chloride and 3x with DMF. The resin was suspended in bromoacetic acid (98 mg, 0.70 mmol), tetrabutylammonium iodide (87 mg, 0.23 mmol), and DIPEA (250 μL, 1.4 mmol) dissolved in DMF (3 mL) and agitated for 3 h. The solution was drained, the resin washed 3x with DMF (10 mL), and 3x with methylene chloride (10 mL). A portion of the resin was cleaved in Reagent K (TFA/phenol/water/EDT/thioanisole 34:2:2:2:1, 0.5 mL) for 2 h and the peptide was precipitated in cold diethyl ether (2 mL), and centrifuged. The peptide pellet was washed 2x with cold diethyl ether (2 mL). The resulting product was dried by blowing with nitrogen gas. The product was

analyzed by HPLC and MALDI-TOF. MALDI-TOF m/z calcd for $C_{89}H_{150}N_{14}O_{18}S_2$ [M+Na] 1790.1, observed 1789.8.

Pam_2CSK_4 _ Indole (TLR2/6_4 Di-agonist) (5.9). (*provided by Tyler Albin*)

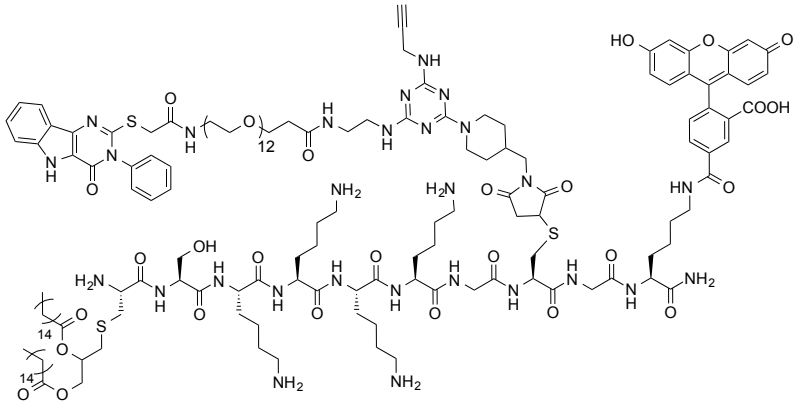

Coupling of TLR4_Core to resin bound TLR2/6 agonist. Furan protected TLR4_Core (54 mg, 0.039 mmol) was conjugated to the resin bound peptide and the product obtained analogously as TLR2/6_Core described above. The crude reaction mixture was analyzed and purified by reverse phase HPLC using a C8 column. Analysis for purity checked by analytical HPLC C8 column, using a solvent system of A: water + 0.1% TFA, B: acetonitrile + 0.1% TFA (50-90% acetonitrile/water + 0.1% TFA gradient, 0-10 minutes, $t_{retention}$: 8.6 min). The isolated product was analyzed by MALDI-TOF (2.5 mg recovered). MALDI-TOF: m/z calcd for $C_{162}H_{248}N_{28}O_{38}S_3$ $[M+H]^+$: 3290.8, observed 3289.0.

Pam_2CSK_4GC(Core)GK(5/6 FAM) (TLR2/6 _Core) Synthesis (5.9.1).

(*provided by Tyler Albin*)

Coupling of Triazine Core to Resin bound TLR2/6 agonist. Furan protected tri-agonist Core (65 mg, 1.2 mmol) was dissolved in DMSO (3 mL) and stirred for 5 h at 110 °C to expose the maleimide. The Fmoc-Pam_2CS(OtBu)K(Boc)$_4$GC(Mmt)GK(5/6 FAM)-Resin ($1/6^{th}$ of batch,

0.039 mmol peptide) described above was swollen in methylene chloride (10 mL) for 30 min and then the methylene chloride drained. Cys(Mmt) was deprotected by washing the resin several times with 1% TFA/methylene chloride (5 mL each wash) over 1 h. The resin was washed with methylene chloride (3 x 10 mL) and with DMF (3 x 10 mL). The furan deprotected triagonist core solution and DIPEA (1 mL) was then added to the peptide bound resin and the reaction mixture shaken for 18 h. The solution was drained from the resin and the resin washed with DMF (3 x 10 mL) and with methylene chloride (3 x 10 mL). The peptide was Fmoc deprotected with 6% piperazine/DMF (2 x 10mL, 10 min) washed with DMF (3 x 10 mL) and methylene chloride (3 x 10 mL). The peptide was cleaved from the resin with Reagent K (TFA/phenol/water/EDT/thioanisole 34:2:2:2:1, 2 mL) for 4 h, and the resin washed with Reagent K (2 x 2 mL). The cleavage solutions were combined and the peptide was precipitated in ice cold diethyl ether (20 mL), and centrifuged (2,400 x g, 10 min, 4 °C). The peptide pellet was washed with ice cold diethyl ether (2 x 20 mL). The resulting crude product was dried and purified by HPLC. Analysis for purity checked by analytical HPLC C8 column, using a solvent system of A: water + 0.1% TFA, B: acetonitrile + 0.1% TFA (50-90% acetonitrile/water + 0.1% TFA gradient, 0-10 minutes, $t_{retention}$: 7.9 min). The pure isolated product was analyzed by MALDI-TOF (0.80 mg recovered, TLR2/6_Core). MALDI-TOF: m/z calcd for $C_{117}H_{184}N_{24}O_{23}S_2$ $[M+H]^+$ 2358.3, observed 2357.5.

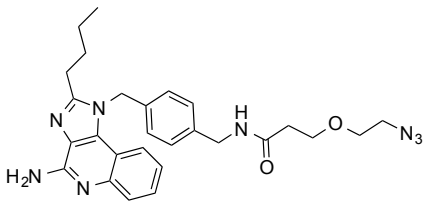

Imidazoquinoline-N_3 (5.10).

Imidazoquinoline (49 mg, 0.13 mmol) and NHS-PEG_{12}-N_3 (0.10 g, 0.13 mmol) were dissolved in DMSO (1.3 mL). The reaction was allowed to stir at RT for 17 h. The reaction was poured into ethyl acetate and washed with slightly basic water (pH 8). The organic layer was dried with Na_2SO_4, filtered, and concentrated. The resulting product was obtained as a yellow gel (130 mg, 91% yield). ^{1}H NMR (600 MHz, $CDCl_3$) δ 7.92 (d, *J* = 8.4 Hz, 1H), 7.72 (d, *J* = 8.4 Hz, 1H), 7.54-7.51 (m, 1H), 7.30-7.23 (m, 2H), 7.10 (br s, 1H), 6.96 (d, *J* = 8.4 Hz, 2H), 5.74 (s, 2H), 4.41 (d, *J* = 6 Hz, 2H), 3.72 (t, *J* = 5.7 Hz, 2H), 3.65-3.62 (m, 34H), 3.60-3.59 (m, 2H), 3.57-3.56 (m, 2H), 3.54-3.53 (m, 4H), 3.51-3.48 (m, 4H), 3.38 (t, *J* = 4.8 Hz, 2H), 2.87 (t, *J* = 7.8 Hz, 2H), 2.50 (t, *J* = 5.7 Hz, 2H), 1.82 (quintet, *J* = 7.8 Hz, 2H), 1.44 (sextet, *J* = 7.8 Hz, 2H), 0.94 (t, *J* = 7.5 Hz, 3H). ^{13}C NMR (600 MHz, $CDCl_3$)

δ 171.93, 157.13, 149.3, 139.8, 136.0, 133.9, 132.6, 129.8, 128.7, 125.6, 125.5, 124.8, 120.8, 120 .1, 112.6, 70.8, 70.7, 70.6, 70.5, 70.3, 70.2, 67.3, 50.8, 49.2, 42.7, 37.0, 29.4, 27.1, 25.5, 22.5, 13. 9. HRMS: *m/z* calcd for $C_{49}H_{76}N_8O_{13}$ $[M+Na]^+$ 1007.5430, observed 1007.5413.

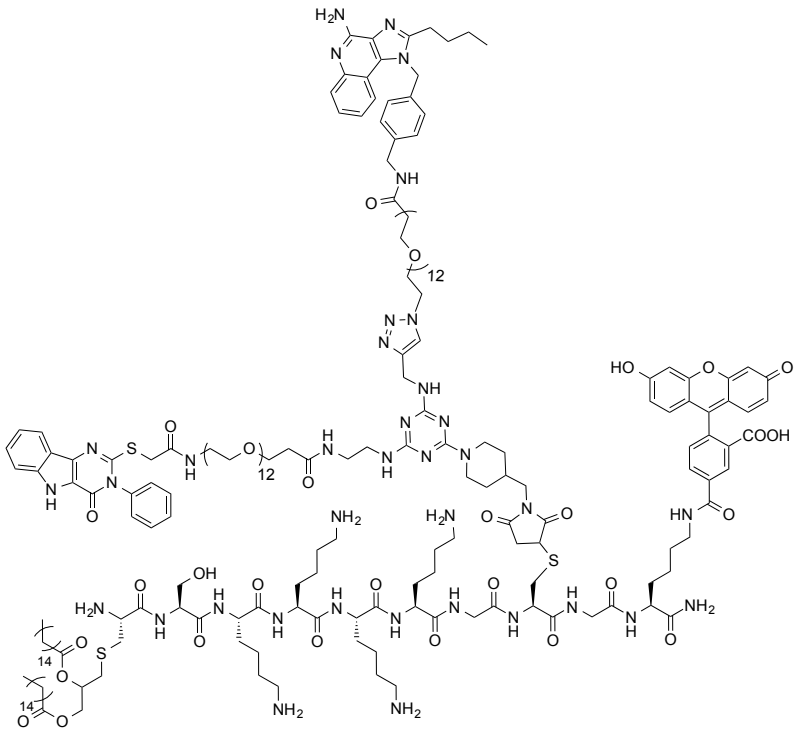

TLR2/6_4_7 (5.11).

The TLR2/6_4 di-agonist (1.3 mg, 0.38 μmol) pre-dissolved in water (150 μL) and imidazoquinoline-PEG_{12}-N_3 (**5.10**) (3.1 mg, 3.2 μmol) in DMF (0.85 mL) were mixed. A solution of copper sulfate pentahydrate (2.5 mg, 0.010 mmol) in degassed water (23 μL) and sodium ascorbate (3.0 mg, 15 μmol) in degassed water (21 μL) were added to the reaction mixture in that order. The solution was allowed placed on a shaker at RT for 24 h.

The crude solution was centrifuged at 8,000 g for 10 minutes at 4 °C. The supernatant was removed and the fluorescent pellet was washed with 0.1 M EDTA (2 x 200 μL) to remove excess copper. The pellet was then re-dissolved in DMSO and purified by reverse phase HPLC using a C8 preparatory column, where the solvent system was A: water + 0.1% TFA, B: acetonitrile + 0.1% TFA (50-90% acetonitrile/water + 0.1% TFA gradient, 0-29 minutes, $t_{retention}$: 12.9 min). The HPLC fractions were lyophilized to afford the desired product as a fluorescent yellow powder (0.60 mg, 40% yield). MALDI-TOF: *m/z* calcd $[M+H]^+$ 4275.3, observed 4275.8.

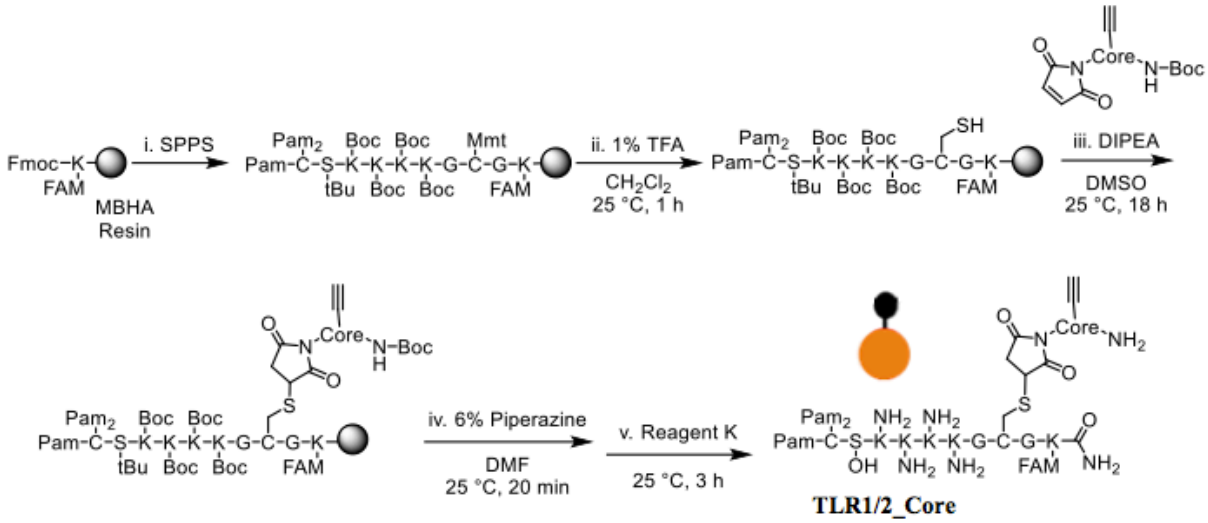

Pam_3CSK_4 and TLR1/2_Core Syntheses (5.11). (*provided by Tyler Albin*)

Fmoc-Pam_2CSK_4GC(Mmt)GK(5/6 FAM)-Resin was synthesized as described above. The resin was suspended in methylene chloride (10 mL) and agitated for 30 min. The resin was drained of the solution and suspended in DMF (10 mL) for 10 min. Fmoc deprotection was performed by suspending the resin in 6% piperazine/DMF (2 x 10 mL) for 10 min. The resin was then washed with DMF (3 x 10 mL). The DMF was drained and the resin suspended in a solution of palmitic acid (41 mg, 0.16 mmol) and HBTU (61 mg, 0.16 mmol) in 25% 2,4,6-collidine/DMF (3 mL) for 3 h. The solution was drained from the resin, the resin washed with DMF (3 x 10 mL), and with methylene chloride (3 x 10 mL). The peptide was then conjugated to furan deprotected tri-agonist core analogously as described above. The resin-bound peptide was cleaved in Reagent K (TFA/phenol/water/EDT/thioanisole 34:2:2:2:1, 2 mL) for 2 h, and the resin washed with Reagent K (2 x 2 mL). The cleavage solutions were combined and the peptide was precipitated in ice 1:1 cold hexanes/diethyl ether (20 mL), and centrifuged (2,400 x g, 10 min, 4 °C). The peptide pellet was washed with ice cold diethyl ether (2 x 20 mL). The resulting crude product was dried and purified by HPLC C8 reverse phase chromatography. Analysis for purity checked

by analytical HPLC C8 column, using a solvent system of A: water + 0.1% TFA, B: acetonitrile + 0.1% TFA (50-90% acetonitrile/water + 0.1% TFA gradient, 0-10 minutes, then hold at 90% B, 10-19 minutes, $t_{retention}$: 14 min). The pure isolated product was analyzed by MALDI-TOF (1.1 mg recovered, TLR1/2_ Core). MALDI-TOF: m/z calcd for $C_{133}H_{214}N_{24}O_{24}S_2$ $[M+H]^+$ 2596.6, observed 2596.6.

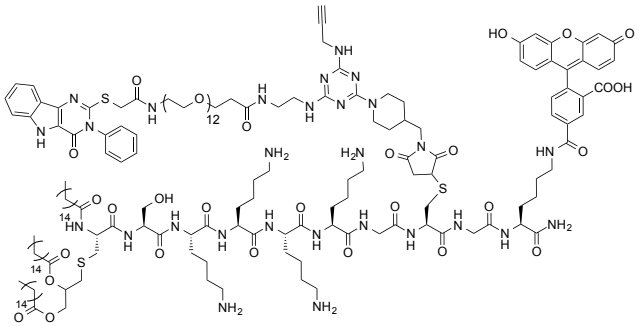

TLR1/2_4 (5.12). (*provided by Tyler Albin*)

$Pam_3CSK_4GC(Mmt)GK(5,6\ FAM)$-Resin was prepared as described above. TLR4_Core was then conjugated by Michael addition, analogously to that of Fmoc-$Pam_2CS(OtBu)K(Boc)_4GC(Mmt)GK(5/6\ FAM)$-Resin described above. The pure isolated product was analyzed by MALDI-TOF and HPLC (0.50 mg recovered). Analysis for purity checked by analytical HPLC C8 column, using a solvent system of A: water + 0.1% TFA, B: acetonitrile + 0.1% TFA (50-90% acetonitrile/water + 0.1% TFA gradient, 0-10 minutes, then hold at 90% acetonitrile/water + 0.1% TFA 10-19 minutes, $t_{retention}$: 14.1 min). MALDI-TOF: m/z calcd for $C_{178}H_{278}N_{28}O_{39}S_3$ $[M+H]^+$: 3529.0, observed 3527.4.

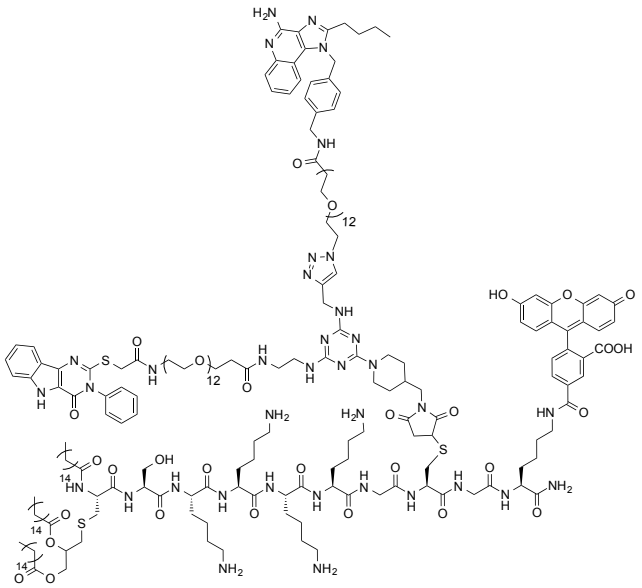

TLR1/2_4_7 (5.13).

The TLR1/2_4 di-agonist (1.0 mg, 0.28 μmol) and imidazoquinoline-PEG_{12}-N_3 (**5.10**) (1.4 mg, 1.4 μmol) in DMF (0.75 mL) were mixed. A solution of copper sulfate pentahydrate (1.4 mg, 5.7 μmol) in degassed water (0.070 mL) and sodium ascorbate (1.7 mg, 8.5 μmol) in degassed water (92 μL) were added to the reaction mixture in that order. The solution was allowed placed on a shaker at RT for 24 h.

The crude solution was centrifuged at 8,000 g for 10 minutes at 4 °C. The supernatant was removed and the fluorescent pellet was washed with 0.1 M EDTA (2 x 200 μL) to remove excess copper. The pellet was then re-dissolved in DMSO and purified by reverse phase HPLC using a C8 preparatory column, where the solvent system was A: water + 0.1% TFA, B: acetonitrile + 0.1% TFA (70-90% acetonitrile/water + 0.1% TFA gradient, 0-32 minutes, $t_{retention}$: 17.3 min). The HPLC fractions were lyophilized to afford the desired product as a fluorescent yellow powder (1.2 mg recovered). MALDI-TOF: *m/z* calcd $[M+H]^+$ 4535.5, observed 4535.6.

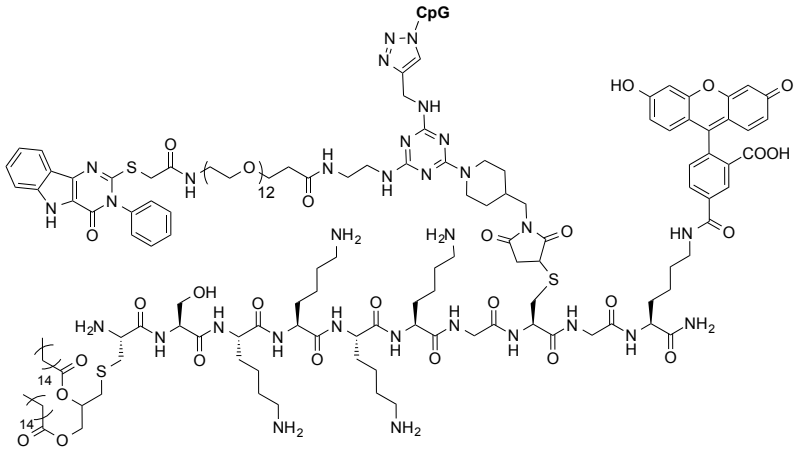

TLR2/6_4_9 (5.14).

The TLR2/6_4 di-agonist (0.040 mg, 12 nmol) in water (4.5 μL) and CpG-ODN1826-N_3 (16 μg, 2.4 nmol) in water (2.4 μL) were mixed with DMF (0.080 mL). Copper sulfate pentahydrate (12 μg, 48 nmol) pre-dissolved in degassed water (2.0 μL) and THPTA (31 μg, 72 nmol) in degassed water (2.2 μL) were mixed and then added to the reaction vial. Lastly, sodium ascorbate (14 μg, 72 nmol) was added to the reaction mixture to give a final ratio of DMF: H2O (5:1). The reaction mixture was placed on a shaker at RT for 24 h. The crude reaction was purified *via* SDS-PAGE and gel extraction (45% conversion). The product band was excised and eluted into endotoxin free water overnight at RT. The solution was concentrated and desalted using a 3k centrifugal filter unit (EMD Millipore) to provide the desired product. MALDI-TOF and LC-MS were attempted using various conditions; however, the product did not ionize well under any attempts.

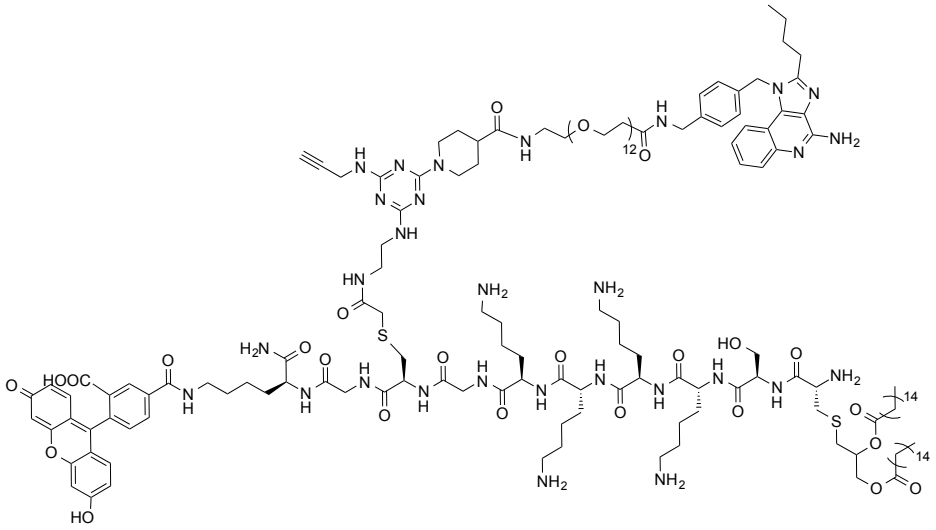

TLR2/6_7 Di-Agonist (5.15). (*provided by Tyler Albin*)

Compound **5.4** (43 mg, 32 μmol) was dissolved in 50% TFA/methylene chloride (2 mL) and stirred for 2 h. The methylene chloride/TFA was removed by rotary evaporation and the Boc-deprotected core was dissolved in 25% collidine/DMF (3 mL). Fmoc-$PAM_2CS(OtBu)K(Boc)_4GC(COOH)G$-Resin (≈100 mg, 78 mmol) was swollen in methylene chloride (10 mL) for 30 minutes and the methylene chloride drained. The resin was swollen in DMF (10 mL) for 30 min and then drained. The resin was then suspended in a solution of 25% collidine/DMF (3 mL) containing HBTU (36 mg, 94 μmol) for 5 minutes. The Boc-deprotected core/DIPEA/DMF solution was added to the HBTU activated peptide solution and agitated overnight. The solution was drained from the resin, the resin washed with DMF (3 x 10 mL), and with methylene chloride (3 x 10 mL). The resin was fmoc deprotected with 20% piperidine/DMF, washed with DMF and methylene chloride. The peptide was cleaved in Reagent K (TFA/phenol/water/EDT/thioanisole 34:2:2:2:1, 2 mL) for 2 h, and the resin washed with Reagent K (2 x 2 mL). The TFA solutions were combined and the peptide was precipitated in cold diethyl ether (20 mL), and centrifuged. The peptide pellet was washed with cold diethyl ether (2 x 20 mL). The crude reaction was dried and analyzed by HPLC, MALDI-TOF, and UV-

Vis. The product was purified by reverse phase HPLC using a C8 preparatory column, where the solvent system was A: water + 0.1% TFA, B: acetonitrile + 0.1% TFA (40-90% acetonitrile/water + 0.1% TFA gradient, 0-10 minutes, $t_{retention}$: 9.2 min). The HPLC fractions were lyophilized to afford the desired product as a fluorescent yellow powder (0.10 mg recovered). MALDI-TOF: *m/z* calcd $[M+H]^+$ 3273.7, observed 3273.9.

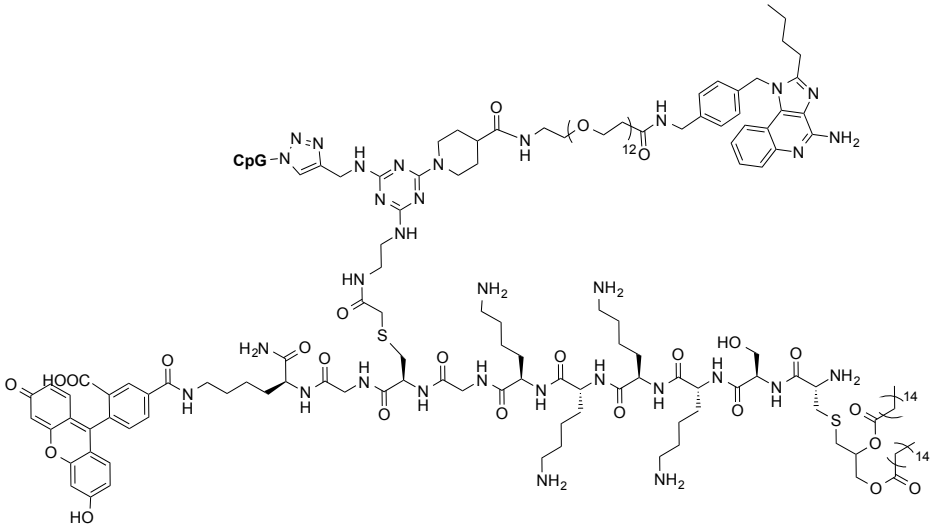

TLR2/6_7_9 (5.16).

The TLR2/6_7 di-agonist (150 μg, 46 nmol) in water (51 μL) and CpG-ODN1826-N_3 (610 μg, 92 nmol) in water (92 μL) were mixed with DMF (0.34 mL). Copper sulfate pentahydrate (0.23 mg, 0.92 μmol) pre-dissolved in degassed water (4.0 μL) and THPTA (0.61 mg, 1.4 μmol) in degassed water (4.3 μL) were mixed and then added to the reaction vial. Lastly, sodium ascorbate (0.28 mg, 1.4 μmol) was added to the reaction mixture to give a final ratio of DMF: H2O (5:1). The reaction mixture was placed on a shaker at RT for 24 h. The crude reaction was purified *via* SDS-PAGE and gel extraction (40% conversion). The product band was excised and eluted into endotoxin free water overnight at RT. The solution was concentrated and desalted using a 3k centrifugal filter unit (EMD Millipore) to provide the desired product. MALDI-TOF

and LC-MS were attempted using various conditions; however, the product did not ionize well under any attempts.

Di-Agonist Syntheses:

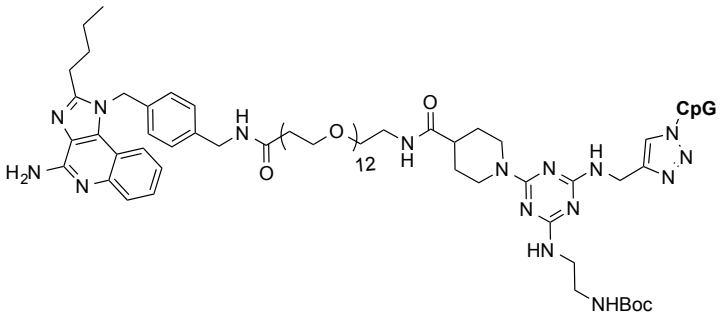

TLR7_9 (5.17).

Compound **5.4** (52 μg, 39 nmol) in anhydrous DMF (69 μL) and CpG (0.070 mg, 9.6 nmol) in degassed water (9.6 μL) were mixed in a vial. Copper sulfate pentahydrate (48 μg, 190 nmol) pre-dissolved in degassed water (3.4 μL) and THPTA (0.13 mg, 290 nmol) in degassed water (4.2 μL) were mixed and then added to the reaction vial. Lastly, sodium ascorbate (57 μg, 290 nmol) in degassed water (2.4 μL) was added to the reaction mixture to give a final volume (DMF: H2O 5:1). The reaction mixture was placed on a shaker at RT for 24 h. The crude reaction was purified *via* TBE-urea gel electrophoresis and gel extraction. The product band was excised and eluted into endotoxin free water overnight at RT. The solution was concentrated and desalted using a 3k centrifugal filter unit (EMD Millipore) to provide the desired product. MALDI-TOF: *m/z* calcd $[M-H]^-$ 8627.7, observed 8627.1.

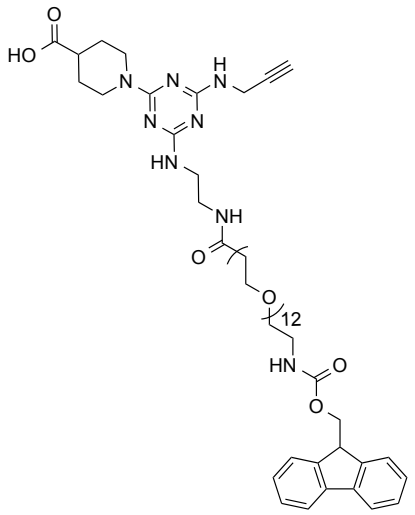

Acid Core_PEG$_{12}$-NH-Fmoc (5.18).

Compound **5.1** (38 mg, 0.12 mmol) and NHS-PEG$_{12}$-NH-Fmoc (0.12 g, 0.13 mmol) were dissolved in DMSO (1.2 mL). DIPEA (42 μL, 0.24 mmol) was then added and the reaction was allowed to stir at RT for 19 h. The crude reaction mixture was purified by reverse phase HPLC using a C8 preparatory column, where the solvent system was A: water + 0.1% TFA, B: acetonitrile + 0.1% TFA (10-90% acetonitrile/water + 0.1% TFA gradient, 0-19 minutes, $t_{retention}$: 13.25 min). The HPLC fractions were lyophilized to afford the desired product as a clear gel (80 mg, 58% yield). ^{1}H NMR (600 MHz, $CDCl_3$) δ 8.21 (br s, 1H), 7.89 (br s, 1H), 7.82 (br s, 1H), 7.75 (d, *J* = 9 Hz, 2H), 7.59 (d, *J* =8.4 Hz, 2H), 7.48 (br s, 1H), 7.38 (t, *J* = 9 Hz, 2H), 7.30 (t, *J* = 9 Hz, 2H), 5.62 (br s, 1H), 4.57 (br s, 2H), 4.38 (d, *J* = 8.4 Hz, 2H), 4.20 (t, *J* = 8.1 Hz, 1H), 4.14 (br s, 2H), 3.76-3.28 (m, 50H), 3.21-3.15 (br m, 2H), 2.65-2.59 (m, 1H), 2.51 (t, *J* = 6.6 Hz, 2H), 2.23 (t, *J* = 2.7 Hz, 1H), 2.05-2.00 (br m, 2H), 1.75-1.69 (br m, 2H). ^{13}C NMR (600 MHz, $CDCl_3$) δ 176.9, 173.9, 161.2, 156.8, 155.8, 144.1, 141.4, 127.8, 127.1, 125.2, 120.0, 116.6, 114.7, 78.6, 71.8, 70.5, 70.4, 70.3, 70.2, 70.0, 66.8, 66.8, 47.3, 43.6, 41.0, 40.5, 40.2, 38.7, 36.3, 30.4, 27.9. MALDI-TOF: *m/z* calcd for $C_{56}H_{84}N_8O_{17}$ $[M+H]^+$ 1141.6, observed 1141.5.

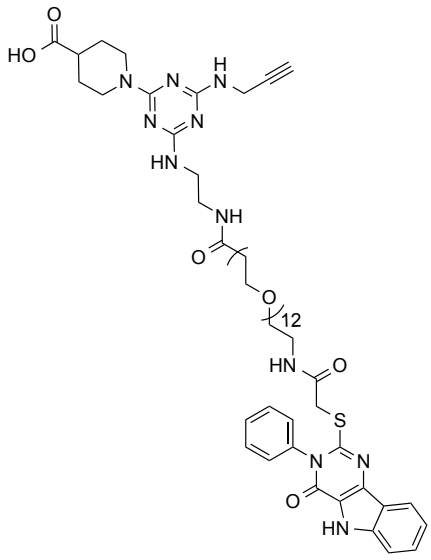

TLR4_acid core (5.19).

Compound **5.18** (75 mg, 0.070 mmol) was dissolved in anhydrous methylene chloride (0.54 mL). Diethylamine (10% v/v, 60 μL) was then added to the solution. The reaction was allowed to stir at RT for 6 h. The reaction mixture was concentrated and re-dissolved in minimal methylene chloride, which was then precipitated in diethyl ether (2x). The product was spun down, removed of diethyl ether, and dried on high-vacuum. The resulting free amine was used in the following procedure to synthesize **5.19**.

Indole-COOH (25 mg, 0.070 mmol) was dissolved in DMF (0.3 mL). DIPEA (37 μL, 0.21 mmol) and HATU (27 mg, 0.070 mmol) were then added to the solution in this order to give a blue colored solution. The free amine substrate (0.060 g, 0.070 mmol) was dissolved in DMF in a separate vial. The preactivated indole-COOH solution was added to the free amine substrate solution and the reaction was allowed to stir at RT for 24 h. The reaction mixture was concentrated, re-dissolved in DMSO, and purified by reverse phase HPLC using a C8 preparatory column, where the solvent system is A: water + 0.1% TFA, B: acetonitrile + 0.1% TFA (10-90% acetonitrile/water + 0.1% TFA gradient, 0-19 minutes, $t_{retention}$: 13.4 min). The

HPLC fractions were lyophilized to afford the desired product as a clear gel (6.0 mg, 7% yield). ^{1}H NMR (500 MHz, $CDCl_3$) δ 10.63 (br s, 1H), 8.29 (br s, 1H), 8.12 (d, *J* = 8.5 Hz, 1H), 7.82 (br s, 1H), 7.77 (br s, 1H), 7.59-7.57 (m, 4H), 7.51 (t, *J* = 7.2 Hz, 1H), 7.44 (br s, 1H), 7.38-7.37 (m, 2H), 7.30 (t, *J* = 7.5 Hz, 1H), 4.57 (br s, 2H), 4.13 (br s, 3H), 3.91 (s, 2H), 3.63-3.47 (m, 52H), 3.20-3.19 (m, 4H), 2.64 (br s, 1H), 2.50 (br s, 2H), 2.23 (s, 1H), 2.01 (br s, 2H), 1.73 (br s, 2H). Analysis for purity checked by analytical HPLC C8 column, A: water + 0.1% TFA, B: acetonitrile + 0.1% TFA, 10-90% acetonitrile/water + 0.1% TFA gradient, 0-11 minutes, where $t_{retention}$: 8.50 min. MALDI-TOF: *m/z* calcd for $C_{59}H_{85}N_{11}O_{17}S$ $[M+H]^+$ 1252.6, observed 1252.6.

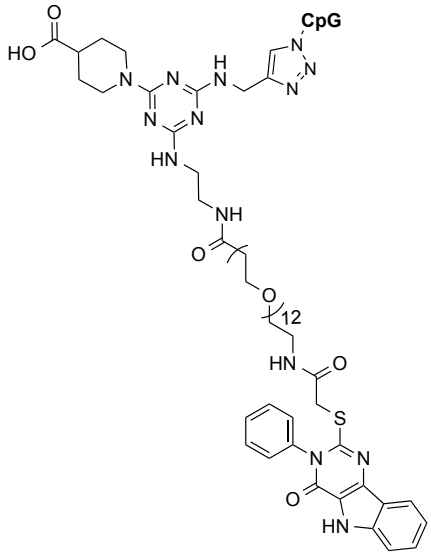

TLR4_9 (5.20).

Compound **5.19** (72 μg, 58 nmol) in anhydrous DMF (80 μL) and CpG (70 μg, 10 nmol) in degassed water (9.6 μL) were added to a vial and mixed. Copper sulfate pentahydrate (48 μg, 190 nmol) pre-dissolved in degassed water (3.4 μL) and THPTA (130 μg, 290 nmol) in degassed water (4.2 μL) were mixed and then added to the reaction vial. Lastly, sodium ascorbate (57 μg, 290 nmol) in degassed water (2.4 μL) was added to the reaction mixture to give a final volume

(DMF: H2O 5:1). The reaction mixture was placed on a shaker at RT for 24 h. The crude reaction was purified *via* TBE-urea gel electrophoresis and gel extraction. The product band was excised and eluted into endotoxin free water overnight at RT. The solution was concentrated and desalted using a 3k centrifugal filter unit (EMD Millipore) to provide the desired product. MALDI-TOF: *m/z* calcd $[M-H]^-$ 8519.4, observed 8520.7.

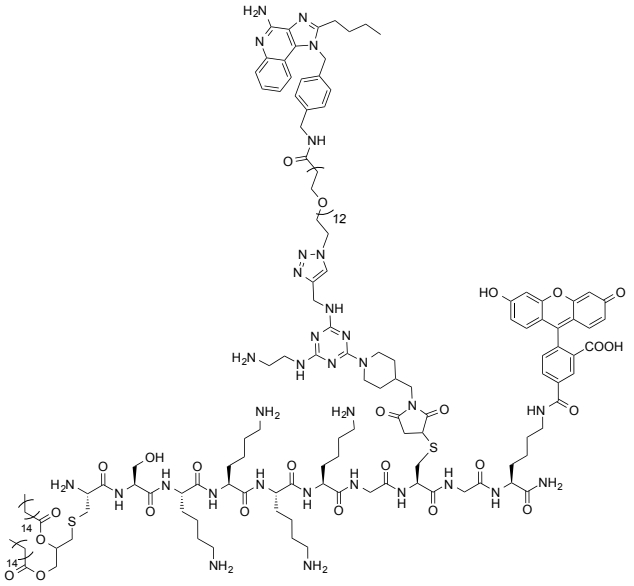

TLR2/6_7 (5.21).

The TLR2/6_Core (0.24 mg, 0.10 μmol) pre-dissolved in water (48 μL) and imidazoquinoline-PEG_{12}-N_3 (**5.10**) (0.70 mg, 1.0 μmol) in DMF (0.37 mL) were mixed. A solution of copper sulfate pentahydrate (0.50 mg, 2.0 μmol) in degassed water (63 μL) and sodium ascorbate (0.59 mg, 3.0 μmol) in degassed water (20 μL) were added to the reaction mixture in that order. The solution was allowed placed on a shaker at RT for 24 h.

The crude solution was centrifuged at 8,000 g for 10 minutes at 4 °C. The supernatant was removed and the fluorescent pellet was washed with 0.1 M EDTA (2 x 200 μL) to remove excess copper. The pellet was then re-dissolved in DMSO and purified by reverse phase HPLC using a

C8 preparatory column, where the solvent system was A: water + 0.1% TFA, B: acetonitrile + 0.1% TFA (40-90% acetonitrile/water + 0.1% TFA gradient, 0-29 minutes, $t_{retention}$: 16.5 min). The HPLC fractions were lyophilized to afford the desired product as a fluorescent yellow powder (0.33 mg recovered). MALDI-TOF: *m/z* calcd $[M+H]^+$ 3342.9, observed 3343.5.

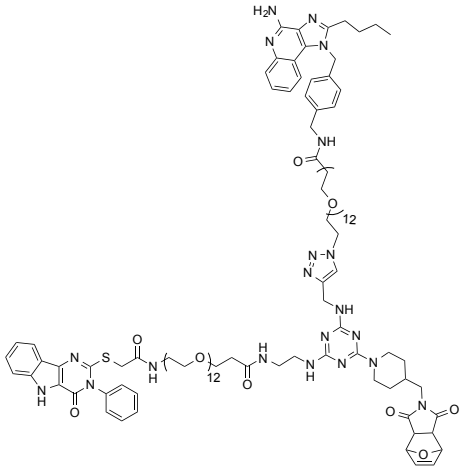

TLR4_7 (5.22).

Indole_Core (1.0 mg, 0.72 μmol) and Imidazoquinoline-PEG_{12}-N_3 (**5.10**) (0.80 mg, 0.79 μmol) were dissolved in DMF (128 μL). Copper sulfate pentahydrate (0.18 mg, 0.72 μmol) in degassed water (23 uL) and sodium ascorbate (0.28 mg, 1.4 μmol) in degassed water (20 μL) were added to the reaction mixture in that order. The reaction was placed on a shaker at RT for 24 h.

The crude solution was centrifuged at 8,000 g for 10 minutes at 4 °C. The supernatant was diluted with acetonitrile and purified by reverse phase HPLC using a C8 semi-prep column, where the solvent system is A: water + 0.1% TFA, B: acetonitrile + 0.1% TFA (40% acetonitrile/water + 0.1% TFA isocratic, 0-15 minutes, $t_{elution}$: 5.9 min). The HPLC fractions were lyophilized to afford the desired product as a white powder (1.7 mg recovered). MALDI-TOF: *m/z* calcd $[M\text{-Furan}+H]^+$ 2302.2, observed 2302.0.

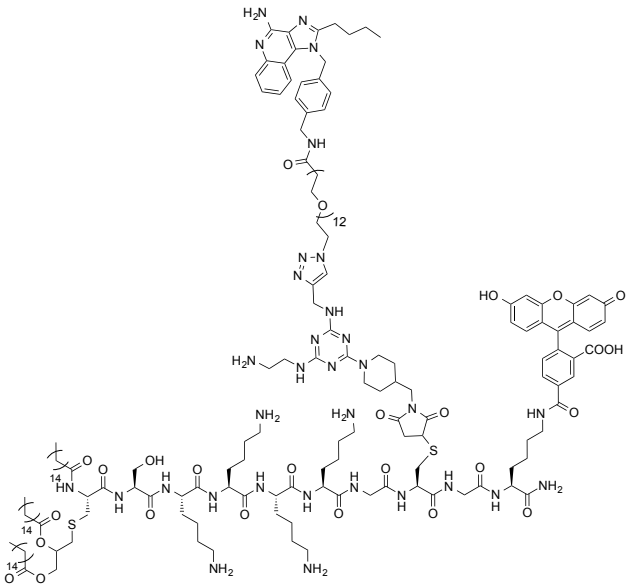

TLR1/2_7 Di-Agonist (5.23).

Pam_3CSK_4_Core (0.60 mg, 0.23 μmol) and Imidazoquinoline-PEG_{12}-N_3 (**5.10**) (1.1 mg, 1.2 μmol) were dissolved in DMF (0.13 mL). Copper sulfate pentahydrate (1.1 mg, 4.6 μmol) in degassed water (55 uL) and sodium ascorbate (1.4 mg, 6.9 μmol) in degassed water (76 μL) were added to the reaction mixture in that order. The reaction was placed on a shaker at RT for 18 h.

The crude solution was centrifuged at 8,000 g for 10 minutes at 4 °C. The supernatant was removed and the fluorescent pellet was washed with 0.1 M EDTA (2 x 200 μL) to remove excess copper. The pellet was then re-dissolved in DMSO:Acn with 0.1% TFA (1:1 v/v) and purified by reverse phase HPLC using a C8 preparatory column, where the solvent system was A: water + 0.1% TFA, B: acetonitrile + 0.1% TFA (70-90% acetonitrile/water + 0.1% TFA gradient, 0-32 minutes, $t_{retention}$: 17.3 min). The HPLC fractions were lyophilized to afford the desired product as a fluorescent yellow powder. MALDI-TOF: *m/z* calcd $[M+H]^+$ 3581.1, observed 3581.1.

Biological testing

RAW264.7 Macrophage (RAW-Blue) NF-κB Assay.

RAW-Blue cells were plated at 10 x 10^4 cells/mL density (180 μL) in 96-well plates using testing media: D-MEM High Glucose medium (Life Technologies), 10% heat inactivated FBS, 2 mM L-glutamine, and antibiotic-antimycotic (1x). RAW-Blue cells were incubated with 20 μL of each agonist for 18 h at 37 °C in a CO_2 incubator. Cell medium (50 μL) from the stimulated RAW-Blue cells was removed, placed into a 96-well plate, and incubated with QUANTI-Blue solution (InvivoGen) (150 μL) for 1.5 h at 37 °C in a CO_2 incubator. The absorbance (620 nm) was measured using a Fisher Scientific MultiSkan FC.

***In Vitro* Bone Marrow-Derived Dendritic Cell Culture and Intracellular Cytokine Staining.**

Monocytes were harvested from 6-week-old C57BL/6. Monocytes were differentiated into dendritic cells (BMDCs) using supplemented culture medium: RPMI 1640 (Life Technologies), 10% heat inactivated fetal bovine serum (Sigma), 20 ng/mL granulocyte-macrophage colony-stimulating factor (produced using "66" cell line), 2 mM L-glutamine (Life Technologies), antibiotic-antimycotic (1×) (Life Technologies), and 50 μM beta-mercaptoethanol (Sigma). After 5 days of culture, BMDCs were incubated with each agonist (0.5 μM) in culture medium for 6 h at 37 °C in a CO_2 incubator. GolgiPlug (BD Biosciences), containing Brefeldin A, was added to cell culture for the final 4 h of culture. Cells were stained for intracellular IL-12 cytokine production and analyzed using BD Accuri C6.

Immunization.

Toxicity Studies (5 days)

C57BL/6 mice were vaccinated intramuscularly (i.m.) at day 0 with TLR2/6_4_7 or TLR2/6/4/7 (1 nmol or 1 nmol of each agonist in PBS with 2% DMSO, respectively) or PBS as a control in a

total injection volume of 50 μL. Serum samples were collected from mice *via* the cheek at day 0, 3, and 5 post injection.

Vaccination Studies (21 days)

C57BL/6 mice were vaccinated i.m. at day 0 with the designated Q fever antigen and adjuvanted with TLR2/6_4_7 or TLR2/6/4/7 (1 nmol or 1 nmol of each agonist in solution, respectively) in PBS with 2% DMSO in a total injection volume of 50 μL. Mice were boosted with the same sample treatment at day 14. Serum samples were collected from mice *via* the cheek at day 0, 1, 14, 15, and 21 post injection. Spleen and lymph nodes were harvested at day 21.

Statistics.

Data was analyzed using a two-tailed t test. All values were reported as mean ± SD, unless stated otherwise.

See Chapter 4 Experimental Procedures for Probing of Protein Microarray[3,4]

***See Appendix D for supplemental figures and characterization data: NMR spectra, MALDI-TOF spectra, and HPLC traces.**

5.11 References

(1) Modulation of Innate Immune Responses via Covalently Linked TLR Agonists - ACS Central Science (ACS Publications) http://pubs.acs.org/doi/full/10.1021/acscentsci.5b00274 (accessed Oct 16, 2016).

(2) Pavot, V.; Rochereau, N.; Rességuier, J.; Gutjahr, A.; Genin, C.; Tiraby, G.; Perouzel, E.; Lioux, T.; Vernejoul, F.; Verrier, B.; et al. Cutting Edge: New Chimeric NOD2/TLR2 Adjuvant Drastically Increases Vaccine Immunogenicity. *J. Immunol.* **2014**, *193* (12), 5781–5785.

(3) Beare, P. A.; Chen, C.; Bouman, T.; Pablo, J.; Unal, B.; Cockrell, D. C.; Brown, W. C.; Barbian, K. D.; Porcella, S. F.; Samuel, J. E.; et al. Candidate Antigens for Q Fever Serodiagnosis Revealed by Immunoscreening of a Coxiella Burnetii Protein Microarray. *Clin. Vaccine Immunol. CVI* **2008**, *15* (12), 1771–1779.

(4) Vigil, A.; Chen, C.; Jain, A.; Nakajima-Sasaki, R.; Jasinskas, A.; Pablo, J.; Hendrix, L. R.; Samuel, J. E.; Felgner, P. L. Profiling the Humoral Immune Response of Acute and Chronic Q Fever by Protein Microarray. *Mol. Cell. Proteomics* **2011**, *10* (10), M110.006304.

(5) Tanji, H.; Ohto, U.; Shibata, T.; Miyake, K.; Shimizu, T. Structural Reorganization of the Toll-Like Receptor 8 Dimer Induced by Agonistic Ligands. *Science* **2013**, *339* (6126), 1426–1429.

(6) Park, B. S.; Song, D. H.; Kim, H. M.; Choi, B.-S.; Lee, H.; Lee, J.-O. The Structural Basis of Lipopolysaccharide Recognition by the TLR4–MD-2 Complex. *Nature* **2009**, *458* (7242), 1191–1195.

(7) Kanzler, H.; Barrat, F. J.; Hessel, E. M.; Coffman, R. L. Therapeutic Targeting of Innate Immunity with Toll-like Receptor Agonists and Antagonists. *Nat. Med.* **2007**, *13* (5), 552–559.

(8) Lynn, G. M.; Laga, R.; Darrah, P. A.; Ishizuka, A. S.; Balaci, A. J.; Dulcey, A. E.; Pechar, M.; Pola, R.; Gerner, M. Y.; Yamamoto, A.; et al. In Vivo Characterization of the Physicochemical Properties of Polymer-Linked TLR Agonists That Enhance Vaccine Immunogenicity. *Nat. Biotechnol.* **2015**, *33* (11), 1201–1210.

(9) Wu, C. C. N.; Hayashi, T.; Takabayashi, K.; Sabet, M.; Smee, D. F.; Guiney, D. D.; Cottam, H. B.; Carson, D. A. Immunotherapeutic Activity of a Conjugate of a Toll-like Receptor 7 Ligand. *Proc. Natl. Acad. Sci.* **2007**, *104* (10), 3990–3995.

(10) Shukla, N. M.; Mutz, C. A.; Ukani, R.; Warshakoon, H. J.; Moore, D. S.; David, S. A. Syntheses of Fluorescent Imidazoquinoline Conjugates as Probes of Toll-like Receptor 7. *Bioorg. Med. Chem. Lett.* **2010**, *20* (22), 6384–6386.

(11) Steinhagen, F.; Kinjo, T.; Bode, C.; Klinman, D. M. TLR-Based Immune Adjuvants. *Vaccine* **2011**, *29* (17), 3341–3355.

(12) Halliday, A.; Turner, J. D.; Guimarães, A.; Bates, P. A.; Taylor, M. J. The TLR2/6 Ligand PAM2CSK4 Is a Th2 Polarizing Adjuvant in Leishmania Major and Brugia Malayi Murine Vaccine Models. *Parasit. Vectors* **2016**, *9*, 96.

(13) Takeuchi, O.; Sato, S.; Horiuchi, T.; Hoshino, K.; Takeda, K.; Dong, Z.; Modlin, R. L.; Akira, S. Cutting Edge: Role of Toll-Like Receptor 1 in Mediating Immune Response to Microbial Lipoproteins. *J. Immunol.* **2002**, *169* (1), 10–14.

(14) Takeuchi, O.; Kawai, T.; Mühlradt, P. F.; Morr, M.; Radolf, J. D.; Zychlinsky, A.; Takeda, K.; Akira, S. Discrimination of Bacterial Lipoproteins by Toll-like Receptor 6. *Int. Immunol.* **2001**, *13* (7), 933–940.
(15) Jin, M. S.; Kim, S. E.; Heo, J. Y.; Lee, M. E.; Kim, H. M.; Paik, S.-G.; Lee, H.; Lee, J.-O. Crystal Structure of the TLR1-TLR2 Heterodimer Induced by Binding of a Tri-Acylated Lipopeptide. *Cell* **2007**, *130* (6), 1071–1082.
(16) Kang, J. Y.; Nan, X.; Jin, M. S.; Youn, S.-J.; Ryu, Y. H.; Mah, S.; Han, S. H.; Lee, H.; Paik, S.-G.; Lee, J.-O. Recognition of Lipopeptide Patterns by Toll-like Receptor 2-Toll-like Receptor 6 Heterodimer. *Immunity* **2009**, *31* (6), 873–884.
(17) Mogensen, T. H.; Paludan, S. R.; Kilian, M.; Østergaard, L. Live Streptococcus Pneumoniae, Haemophilus Influenzae, and Neisseria Meningitidis Activate the Inflammatory Response through Toll-like Receptors 2, 4, and 9 in Species-Specific Patterns. *J. Leukoc. Biol.* **2006**, *80* (2), 267–277.
(18) Querec, T.; Bennouna, S.; Alkan, S.; Laouar, Y.; Gorden, K.; Flavell, R.; Akira, S.; Ahmed, R.; Pulendran, B. Yellow Fever Vaccine YF-17D Activates Multiple Dendritic Cell Subsets via TLR2, 7, 8, and 9 to Stimulate Polyvalent Immunity. *J. Exp. Med.* **2006**, *203* (2), 413–424.
(19) Davies, D. H.; Liang, X.; Hernandez, J. E.; Randall, A.; Hirst, S.; Mu, Y.; Romero, K. M.; Nguyen, T. T.; Kalantari-Dehaghi, M.; Crotty, S.; et al. Profiling the Humoral Immune Response to Infection by Using Proteome Microarrays: High-Throughput Vaccine and Diagnostic Antigen Discovery. *Proc. Natl. Acad. Sci. U. S. A.* **2005**, *102* (3), 547–552.
(20) Shukla, N. M.; Malladi, S. S.; Mutz, C. A.; Balakrishna, R.; David, S. A. Structure–Activity Relationships in Human Toll-Like Receptor 7-Active Imidazoquinoline Analogues. *J. Med. Chem.* **2010**, *53* (11), 4450–4465.

Appendix A: Chapter 2

Supplemental Figures.

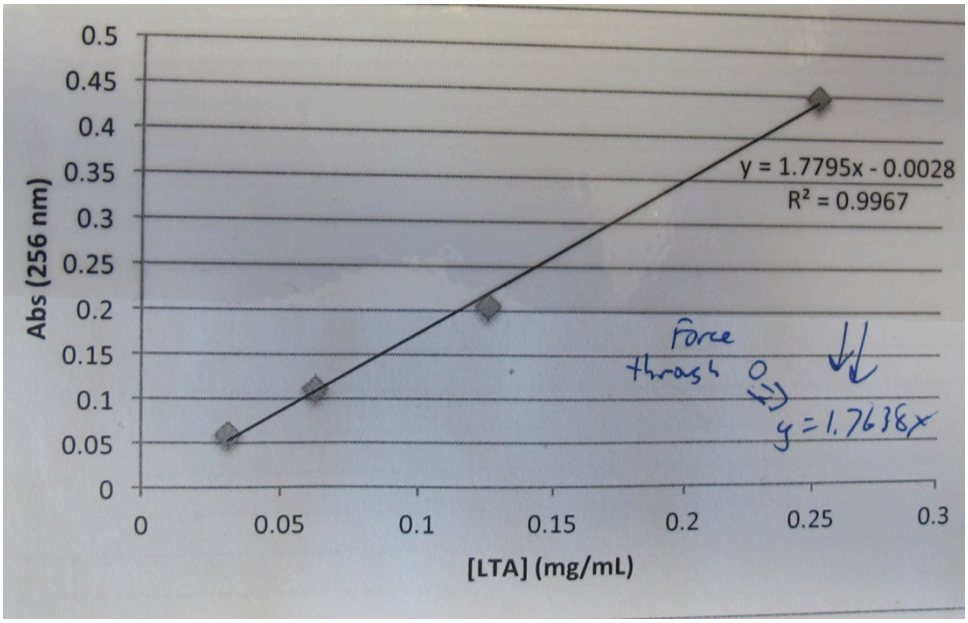

Figure S2.1. Ellman's assay cysteine calibration curve used to determine number of thiols per LTA molecule.

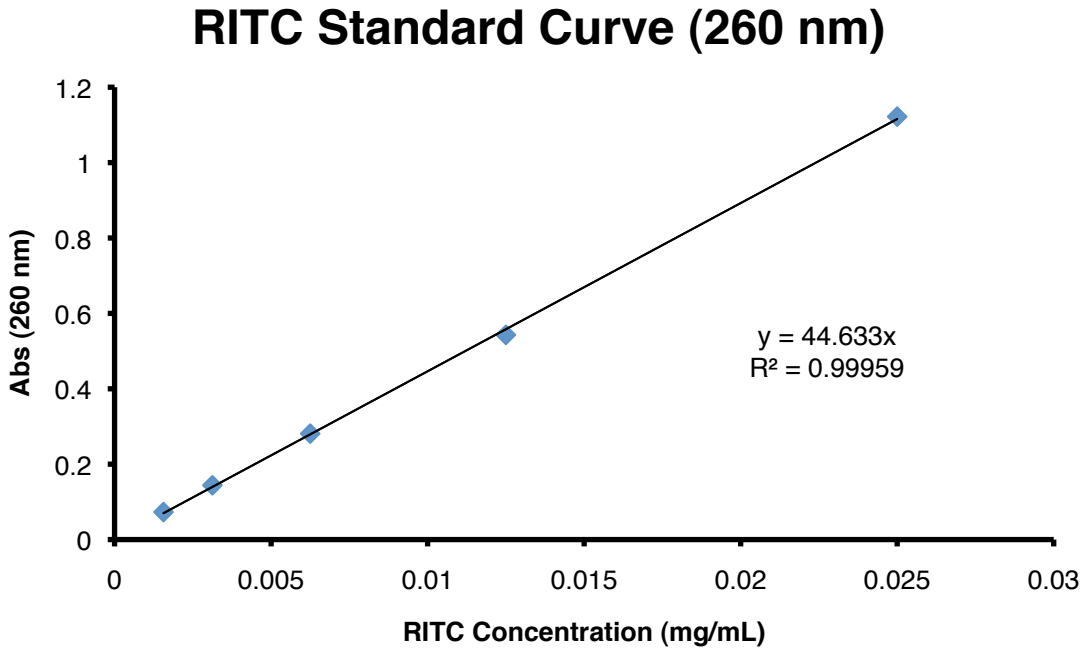

Figure S2.2. RITC standard curve at 260 nm used to quantify the number of RITC molecules conjugated to LTA.

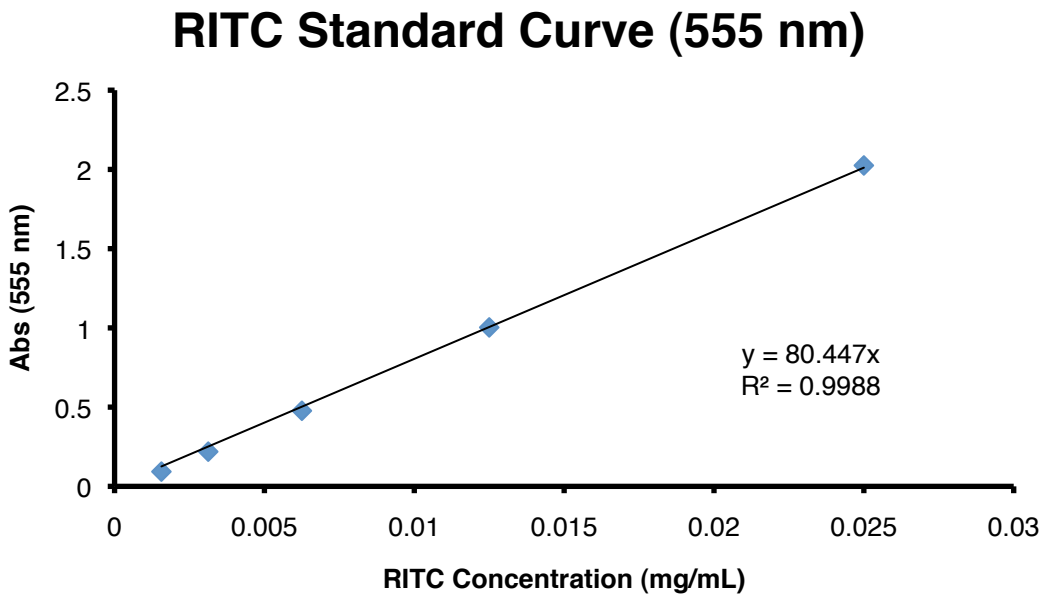

Figure S2.3. RITC standard curve at 555 nm used to quantify the number of RITC molecules conjugated to LTA.

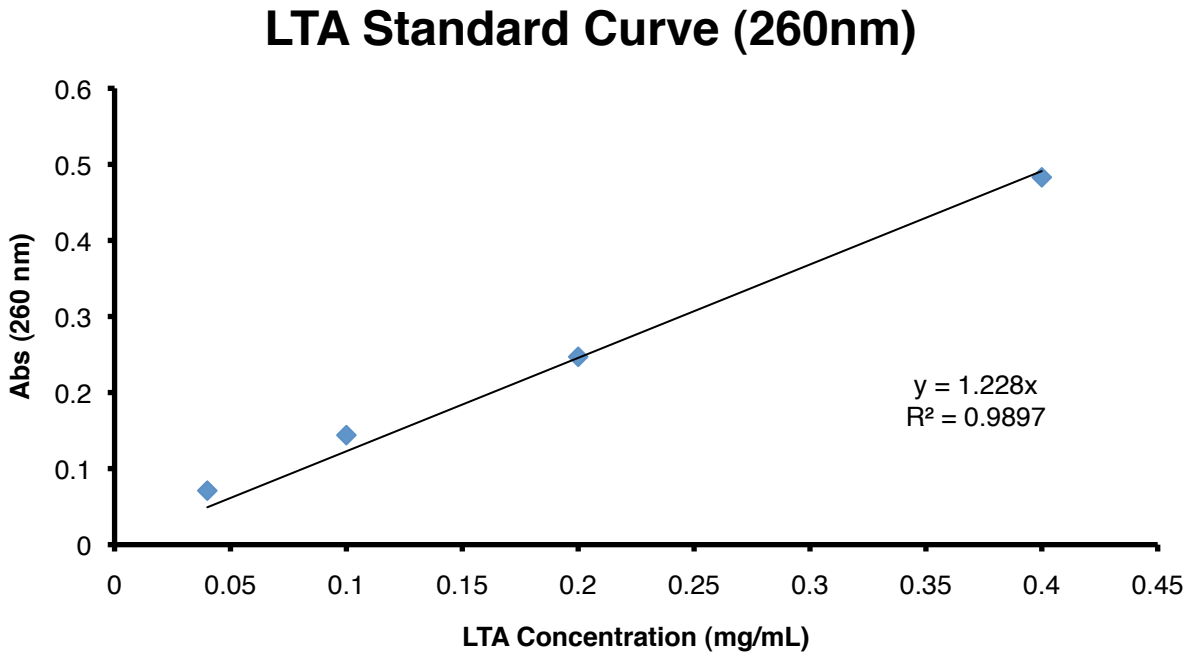

Figure S2.4. LTA standard curve at 260 nm used to quantify the number of RITC molecules conjugated to LTA.

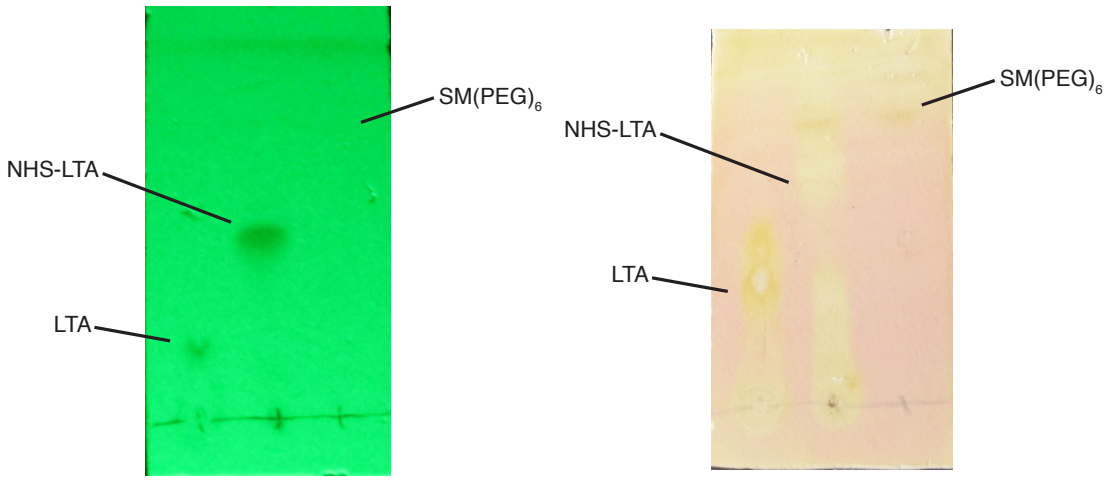

Figure S2.5. Thin-layer chromatography (in 65:25:4 $CHCl_3$:MeOH:H_2O)[5] confirming the synthesis of NHS-LTA (**2.1**): LTA (left lane), NHS-LTA (middle lane), $SM(PEG)_6$ linker (right lane) under UV light (254 nm). TLC plate under UV 254 nm (left plate) and stained with $KMnO_4$ (right plate).

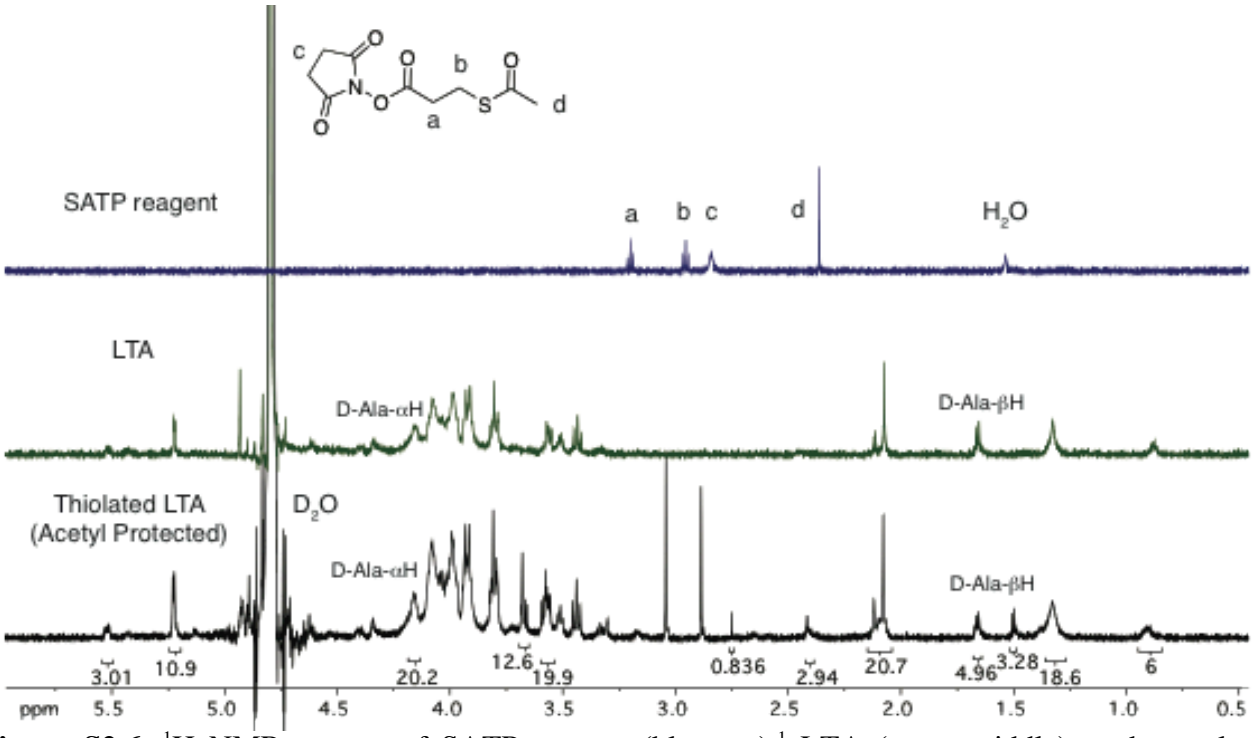

Figure S2.6. [1]H NMR spectra of SATP reagent (blue-top),[1] LTA (green-middle), and acetyl protected sulfhydryl LTA (black-bottom). LTA and thiolated LTA samples were taken in D_2O, and SATP sample was taken in $CDCl_3$.[6] (Refer to Ref. 6 for LTA structure. Peak assignment was confirmed using HSQC, data not shown. [1]H NMR of **2.1** was attempted. However, the spectrum was unclear as many of the peaks overlapped and thus was inconclusive.)

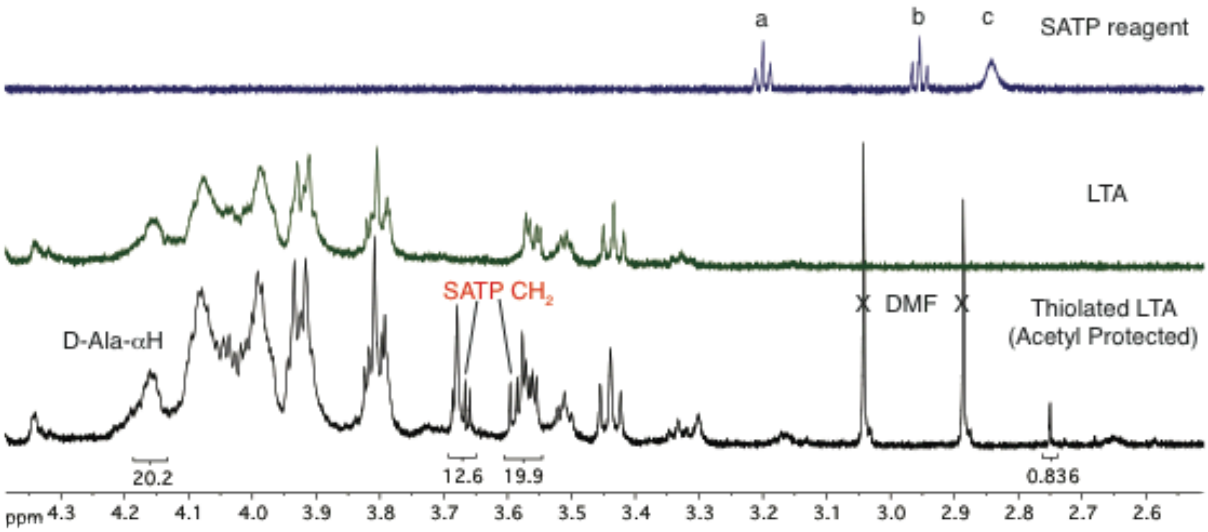

Figure S2.7. [1]H NMR spectra of SATP reagent (blue-top),[1] LTA (green-middle), and acetyl protected sulfhydryl LTA (black-bottom). LTA and thiolated LTA samples were taken in D_2O, and SATP sample was taken in $CDCl_3$. D-Ala-αH was observed at 4.16 ppm. SATP methylene protons were observed at 3.59 and 3.68 ppm.

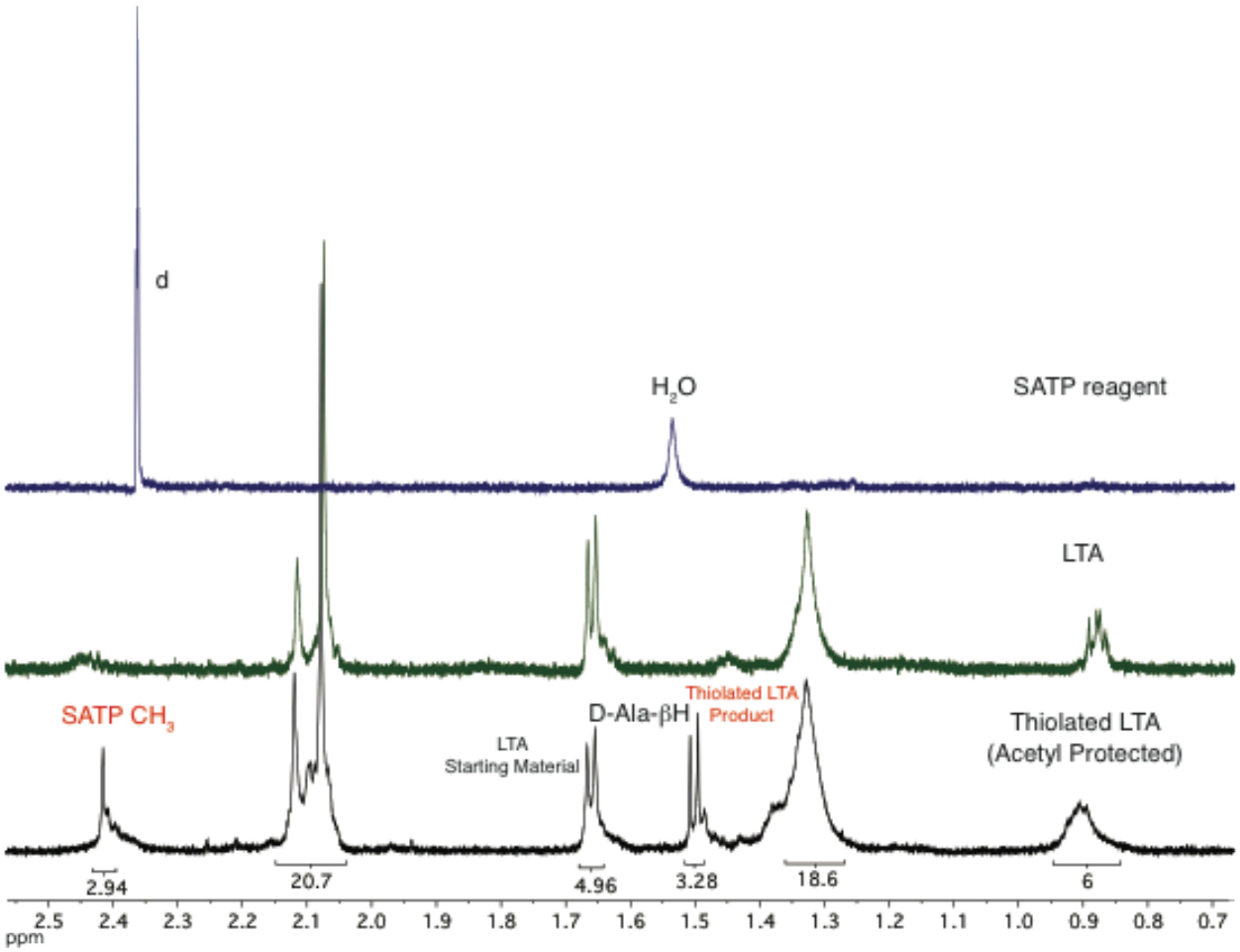

Figure S2.8. [1]H NMR spectra of SATP reagent (blue-top),[1] LTA (green-middle), and acetyl protected sulfhydryl LTA (black-bottom). LTA and thiolated LTA samples were taken in D_2O, and SATP sample was taken in $CDCl_3$. D-Ala-βH was observed at 1.50 (protected sulfhydryl LTA) and 1.66 ppm (starting material LTA). SATP methyl protons were observed at 2.42 ppm.

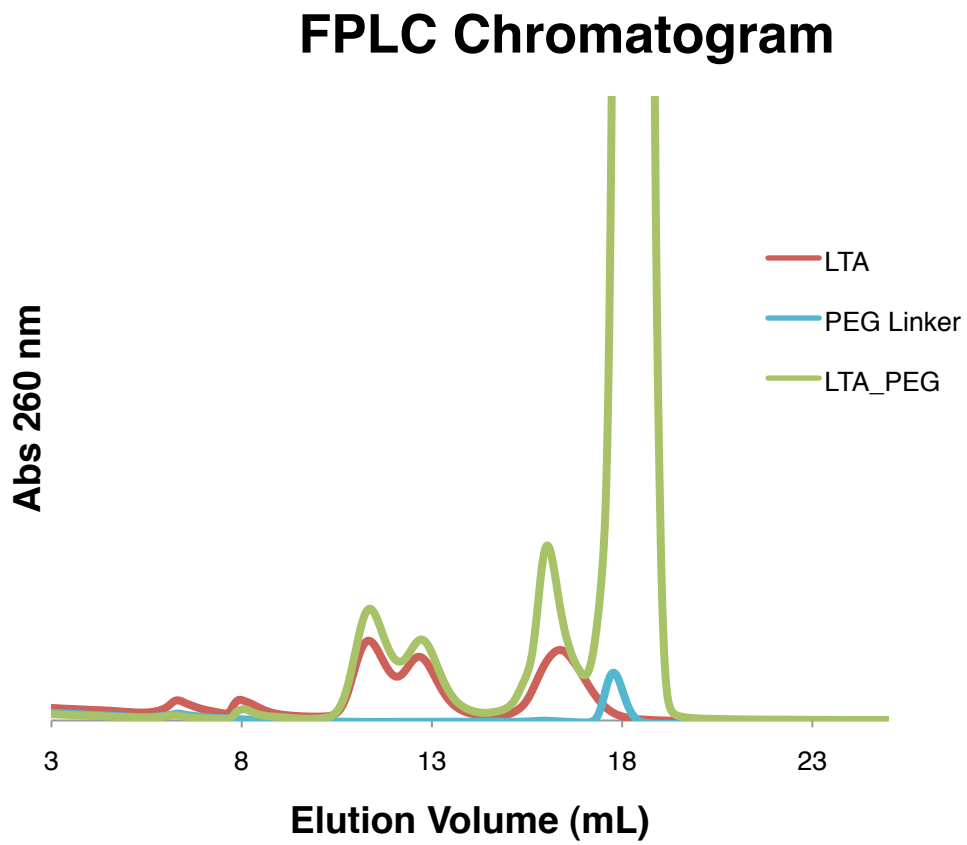

Figure S2.9. FPLC trace of LTA (red), NHS-PEG$_6$-maleimide linker (blue), and **2.1** (green) (samples run in DPBS). LTA conjugation to NHS-PEG$_6$-maleimide linker does not result in a significant shift in the FPLC trace, so **2.1** cannot be definitively confirmed using FPLC.

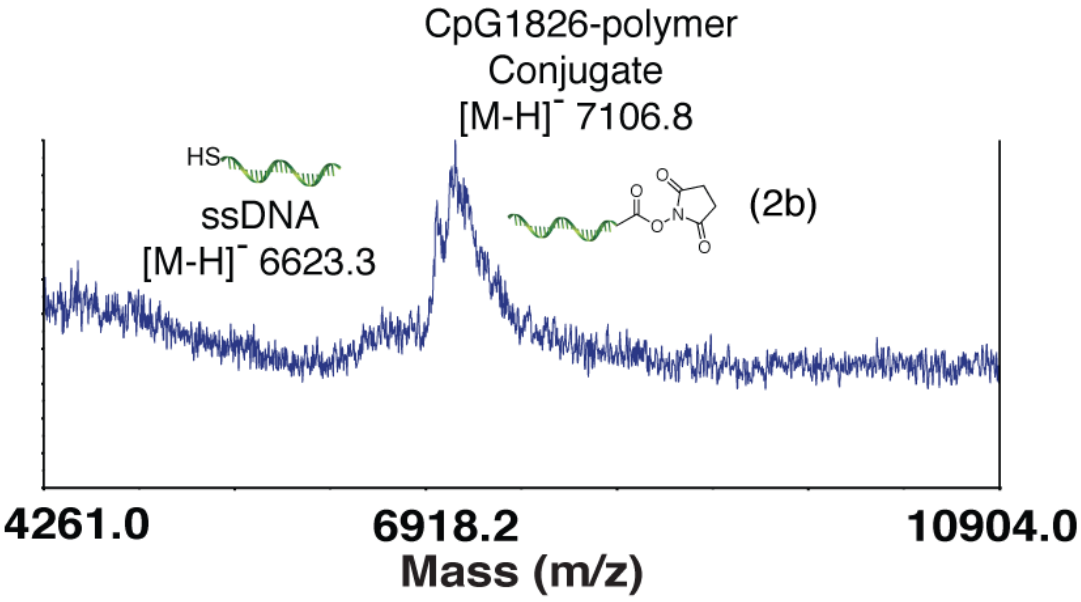

Figure S2.10. MALDI-MS confirming the synthesis of NHS-CpG-ODN (**2.2**) at m/z = 7106.8.

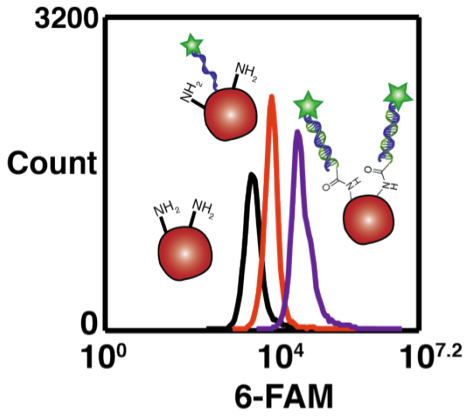

Figure S2.11. Flow cytometry confirmation of 6-FAM-labeled CpG-ODN cell surface modification of LLCs to provide **2.4**: unmodified LLCs (black), non-specific sticking of 6-FAM CpG-ODN1826 anti-sense strand (red), and 6-FAM-labeled CpG-ODN_LLCs (purple).

‡‡ After 2-5 hours, we observed disappearance of the modification from the surface of the LLCs. Endocytosis is the most likely mechanism (data not shown).

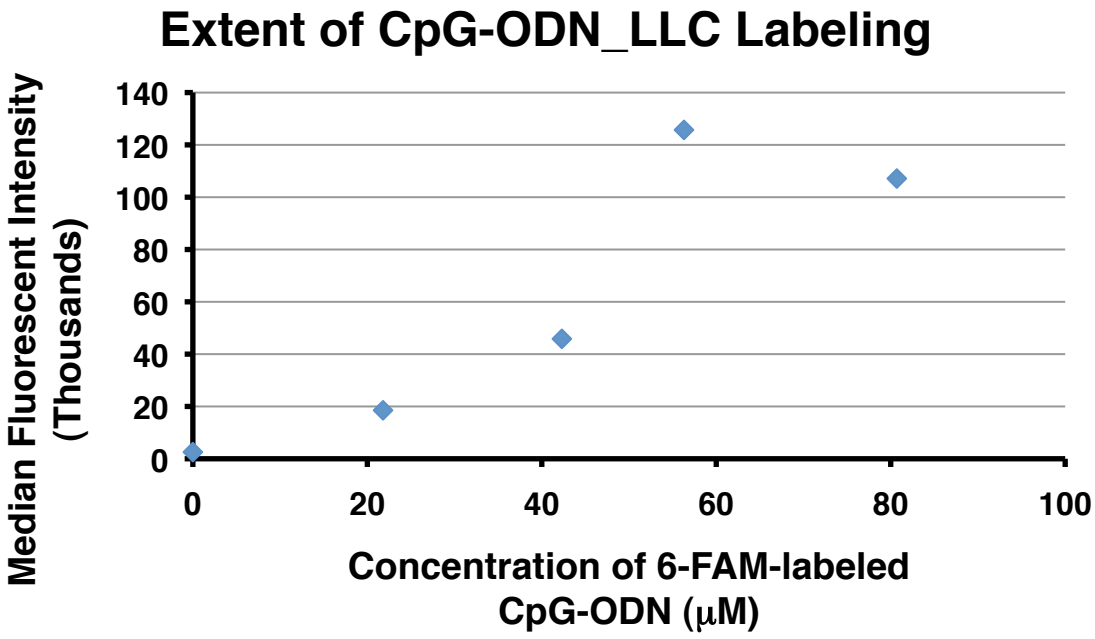

Figure S2.12. Flow cytometry quantification of 6-FAM-labeled CpG-ODN_LLCs. LLCs were incubated with varying concentrations of 6-FAM-labeled CpG-ODN1826 conjugate **2.2** for 30 min at RT.

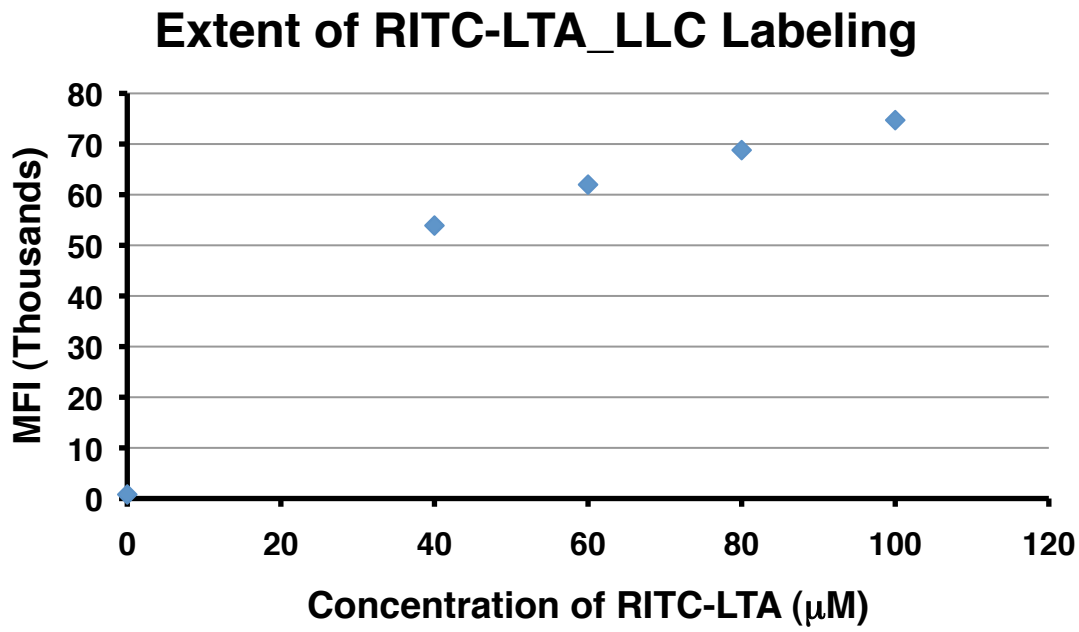

Figure S2.13. Flow cytometry quantification of RITC LTA_LLCs. LLCs were incubated with varying concentrations of RITC LTA conjugate **2.1** for 30 min at RT.

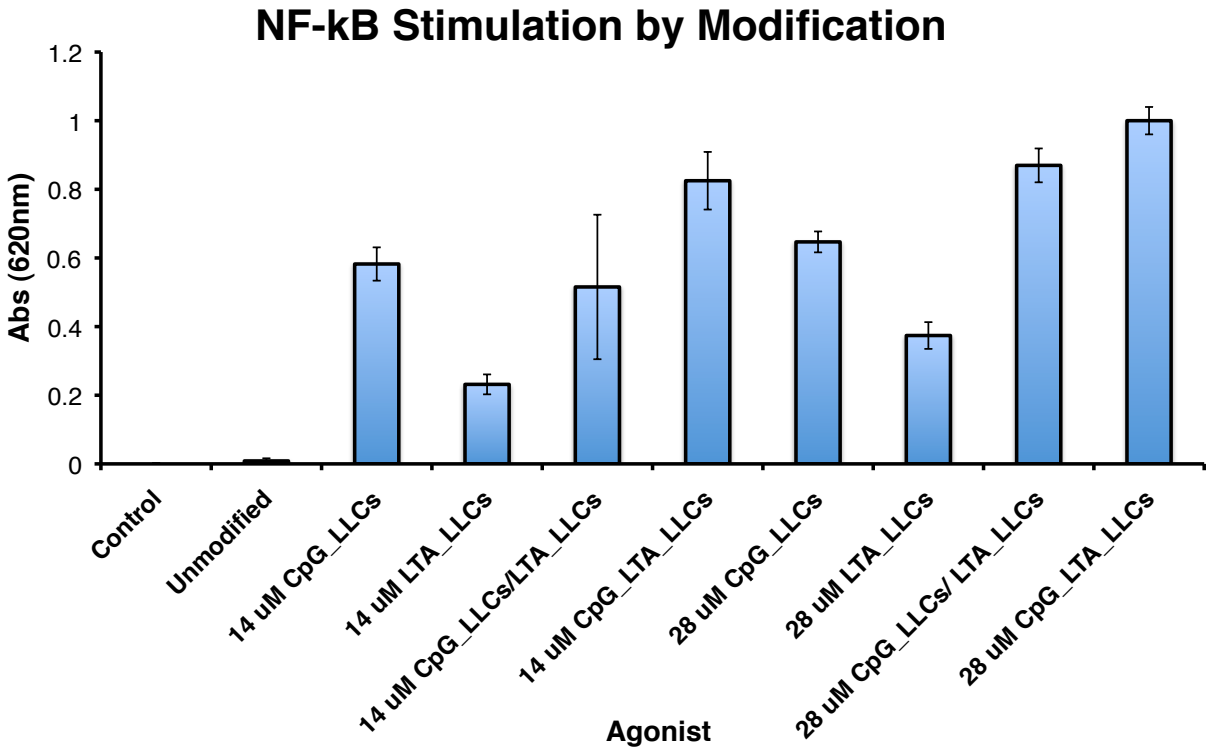

Figure S2.14. RAW264.7 macrophage NF-κB stimulation *via* alkaline phosphatase secretion. Data displays absorbance (620 nm) caused by macrophage cell incubation with TLR agonist_LLC constructs for 19 h at 37 °C, which correlates to NF-κB stimulation. LLCs were modified with half of the concentration of TLR agonist-PEG_6-NHS conjugate (14 μM) compared to the full concentration (28 μM) to determine that the activation from CpG_LTA_LLCs is more than the additive stimulation from just CpG_LLCs and LTA_LLCs. More important, the CpG_LTA_LLCs displayed the greatest stimulation over using a single TLR agonist. Data is the result of n=6, where $p < 0.05$ for CpG_LLCs relative to CpG_LTA_LLCs, $p < 0.05$ for LTA_LLCs relative to CpG_LTA_LLCs, and $p < 0.01$ for the unmodified LLCs relative to all TLR agonist_LLCs and for the CpG_LTA_LLCs relative to all other samples. Results are expressed as the mean ± SD.

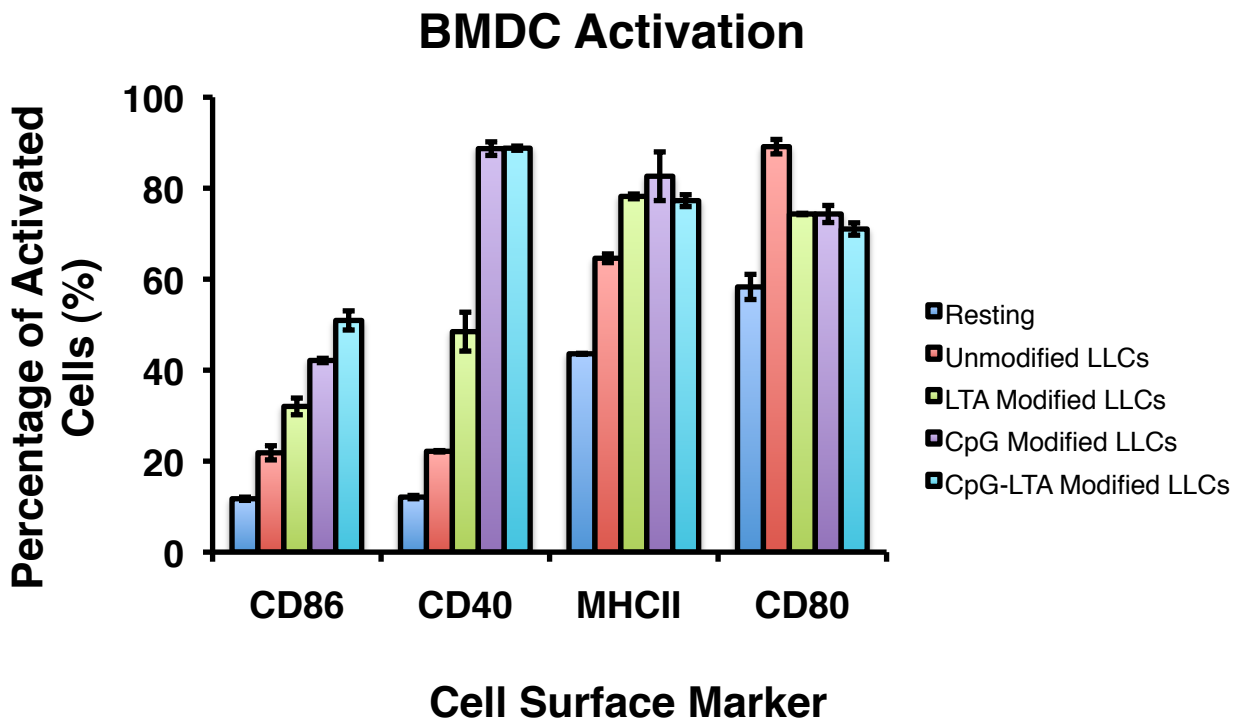

Figure S2.15. Flow cytometry analysis of BMDC cell surface marker upregulation, including CD80, using TLR agonist_LLCs: control (dark blue), unmodified LLCs (red), LTA_LLCs (green), CpG_LLCs (purple), CpG_LTA_LLCs (light blue). p values represent each TLR agonist_LLC in comparison to the resting state where $p < 0.01$ for CD86, CD40, and MHC II, $p < 0.05$ for CD80 over n=3, $p < 0.05$ for CD86 comparing unmodified LLCs to LTA_LLCs, $p < 0.01$ comparing unmodified LLCs to CpG_LLCs and CpG_LTA_LLCs, $p < 0.05$ comparing CpG_LLCs to CpG_LTA_LLCs, and $p < 0.01$ for CD40 comparing unmodified LLCs to all TLR agonist_LLCs. Results are expressed as the mean ± SD.

‡ For flow cytometry experiments, **2.3**, **2.4**, and **2.5** did not contain fluorescent tags, so that the conjugates would not interfere with quantifying the fluorescently tagged antibodies.

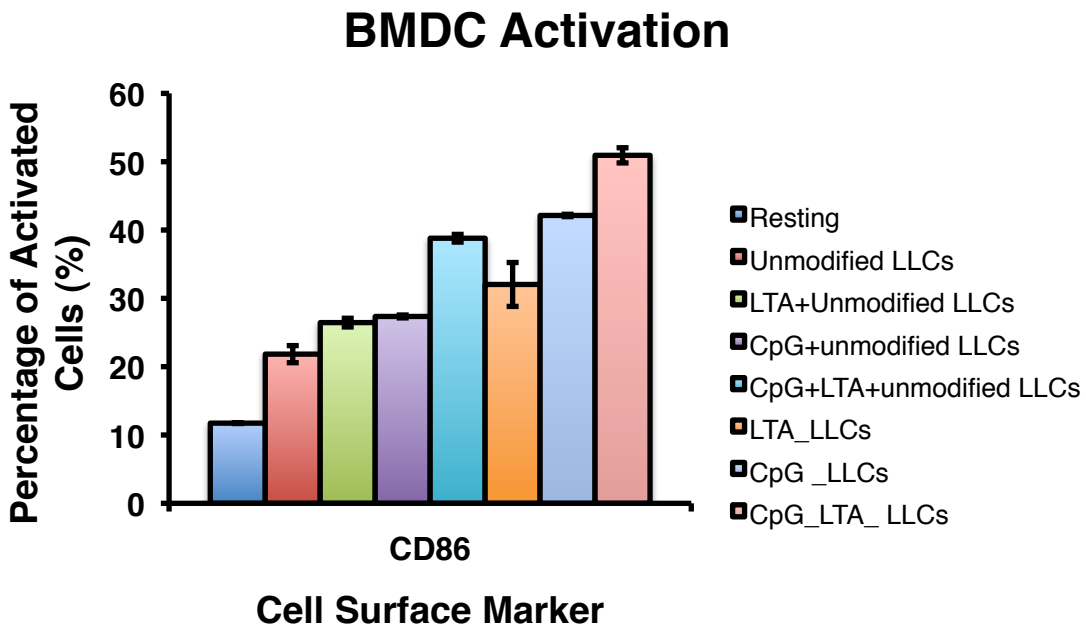

Figure S2.16. Flow cytometry analysis of BMDC CD86 upregulation, including TLR agonists free in solution (positive controls): control (dark blue), unmodified LLCs (red), LTA (1 μg/mL) and unmodified LLCs (green), CpG-ODN (5 μg/mL) and unmodified LLCs (purple), and CpG-ODN (5 μg/mL)/LTA (1 μg/mL)/unmodified LLCs (light blue), LTA_LLCs (orange), CpG_LLCs (light purple), CpG_LTA_LLCs (pink). Results are expressed as the mean ± SD and n=3.

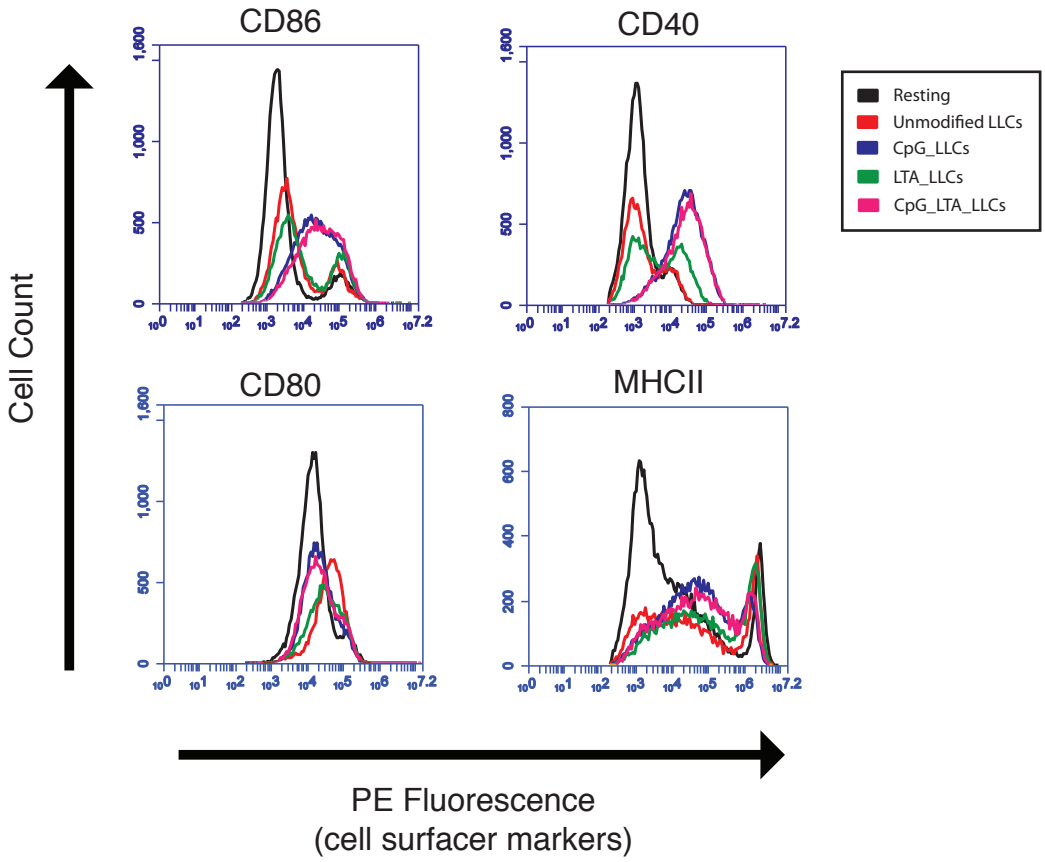

Figure S2.17. Activation of BMDCs using TLR agonist_LLCs. Expression of CD86, CD40, CD80, and MHCII was analyzed *via* flow cytometry: resting (black), unmodified LLCs (red), CpG_LLCs (blue), LTA_LLCs (green), and CpG_LTA_LLCs (pink).

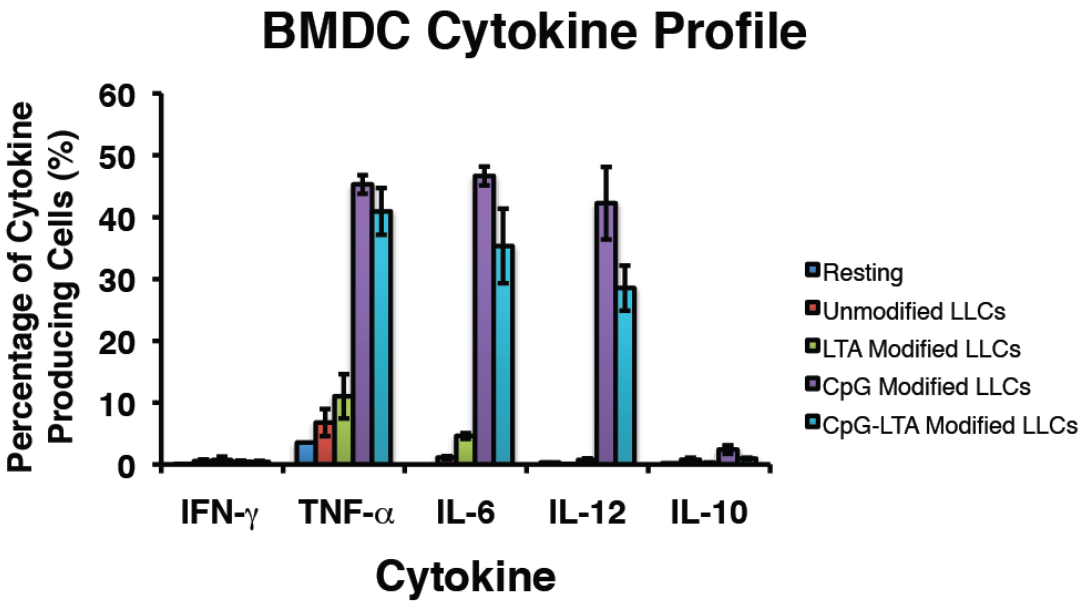

Figures S2.18. Intracellular cytokine flow cytometry analysis, including IL-10, using TLR agonist_LLCs: control (dark blue), unmodified LLCs (red), LTA_LLCs (green), CpG_LLCs (purple), CpG_LTA_LLCs (light blue). p values represent that for resting state relative to CpG_LLC and CpG_LTA_LLCs where $p < 0.01$ for TNF-α, IL-6, and IL-12 over n=3, and $p < 0.1$ for IL-6 and IL-2 comparing CpG_LTA_LLCs to CpG_LLCs. Results are expressed as the mean ± SD.

‡‡‡‡‡ Cytokines can polarize an immune response in order to elicit a specific response against a targeted pathogen. Pro-inflammatory cytokines help recruit APCs toward an infected site to eliminate a pathogen. In contrast, anti-inflammatory cytokines inhibit the recruitment of APCs and suppress an immune response, which is necessary for autoimmune diseases. A balance of the different types of immune responses is required to effectively combat foreign pathogens.

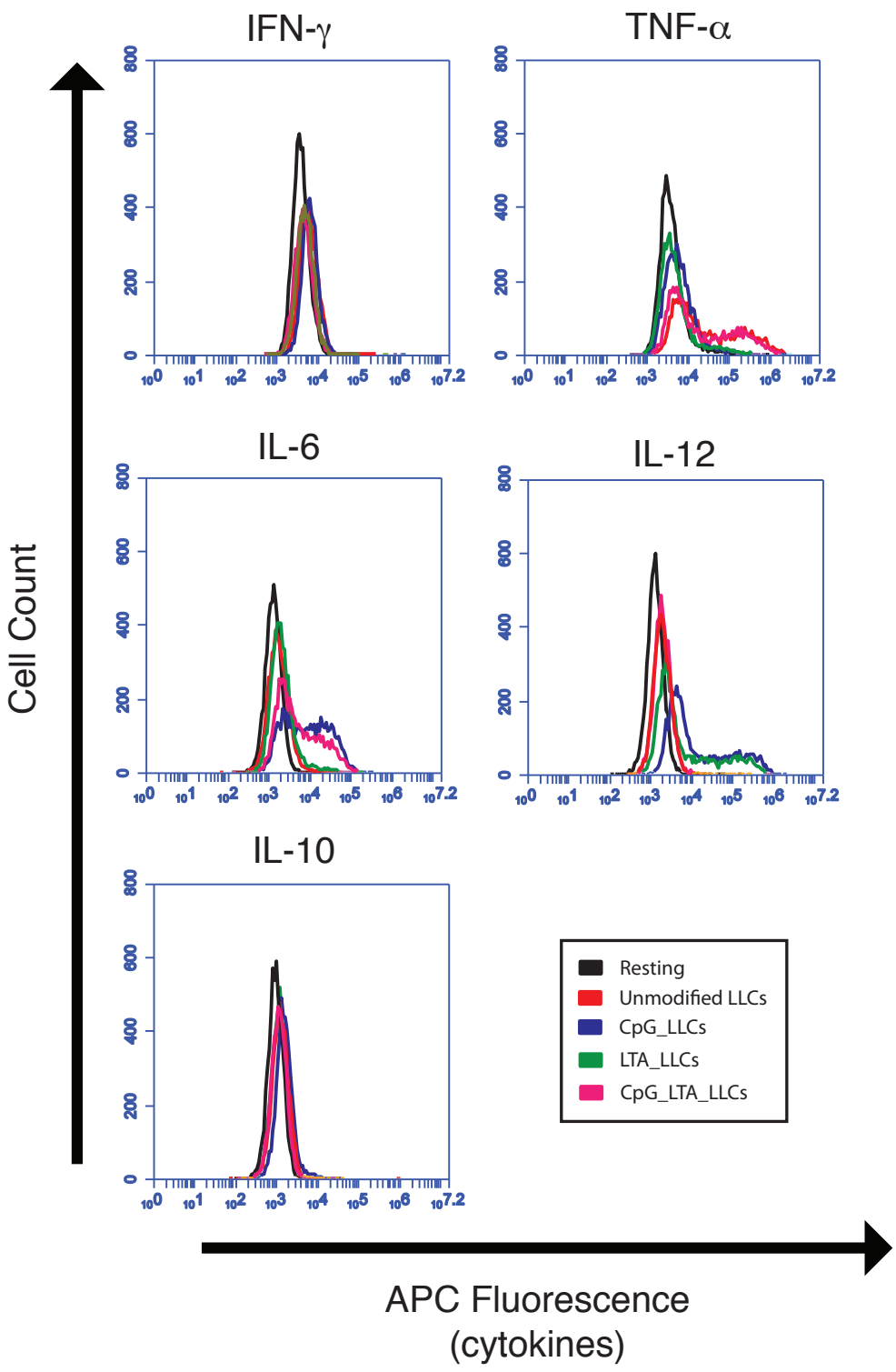

Figure S2.19. Activation of BMDCs using TLR agonist_LLCs. IFN-γ, TNF-α, IL-6, IL-12, and IL-10 cytokine production was analyzed *via* flow cytometry: resting (black), unmodified LLCs (red), CpG_LLCs (blue), LTA_LLCs (green), and CpG_LTA_LLCs (pink).

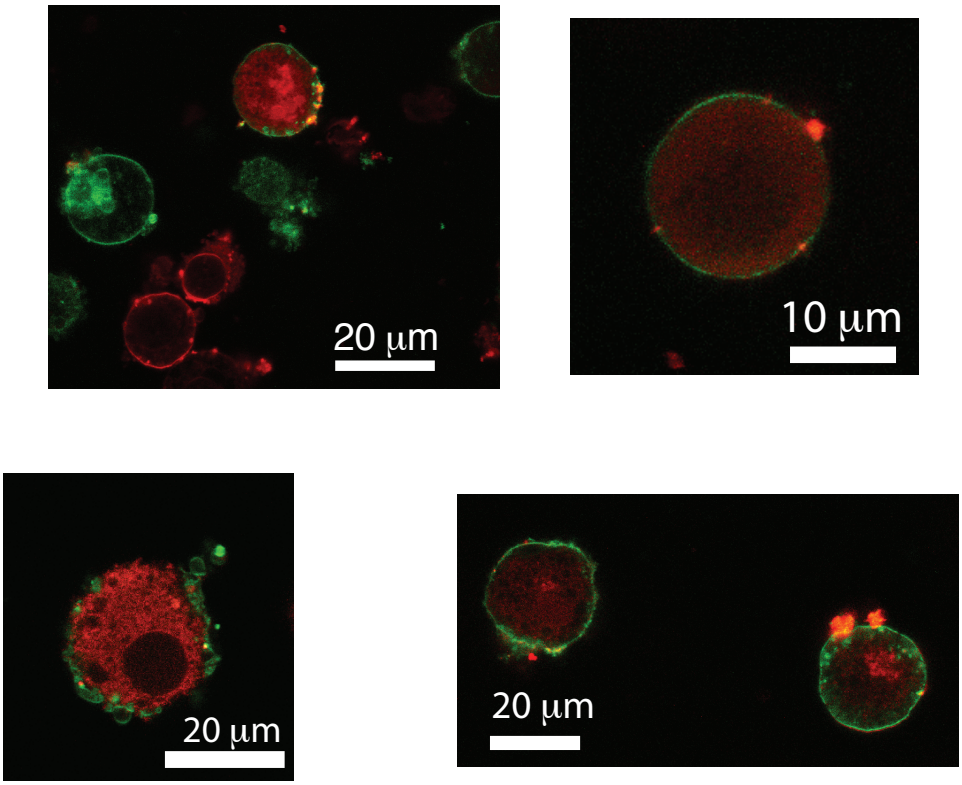

Figure S.220. Confocal microscopy image of DiI-labeled CpG_LLCs (red) macrophagocytosed by DiO-labeled dendritic cells (green).

‡‡‡ DiO is a lipophilic, membrane bound green fluorophore. DiI is a lipophilic, membrane bound red fluorophore. These lipophilic dyes are commonly used to track multiple cells. There are hypotheses that these dyes can exchange/diffuse between cells, since they embed into the cell membrane *via* lipophilic interactions. However, dialkylcarbocyanine dyes have been used for many years in the field of immunology for cell labeling and tracking experiments.[7,8] Also, no DiI-labeled CpG_LLCs were observed with DiO-labeled cell interiors and no DiI was observed on the outer cell membrane of the DCs. These results strongly suggest that the dendritic cells engulfed the CpG_LLCs and that the images were not a result of the interchange of the lipophilic dyes.

‡‡‡‡ DC stimulation using CpG-ODN recruits TLR9 from the ER through the Golgi to endosomal compartments *via* membrane fusion. TLR9 is processed and cleaved after passing through the Golgi to provide functional TLR9 in the endosome as opposed to full-length (unprocessed, non-functional) TLR9, which does not become activated by ligands.[9,10]

REFERENCES

1. N. Fuji, K. Akaji, Y. Hayashi, and H. Yajima, *Chem. Pharm. Bull.*, 1985, **33**, 362-367.
2. M. P. Matheu, D. Sen, M. D. Cahalan, and I. Parker, *J. Vis. Exp.*, 2008, **17**, e773, doi:10.3791/773 (2008).
3. http://www.invivogen.com/PDF/RAW_Blue_TDS.pdf
4. D. M. Underhill, M. Bassetti, A. Rudensky, and A. Aderem, *J. Exp. Med.*, 1999, **190**, 1909–1914.

5. A. J. Webb, M. Karatsa-Dodgson, and A. Grundling, *Mol. Microbiol.*, 2009, **74**, 299–314.
6. S. Morath, A. Geyer, I. Spreitzer, C. Hermann, and T. Hartung, *Infect. Immun.*, 2002, **70**, 938–944.
7. S. Stoll, J. Delon, T. M. Brotz, and R. N. Germain, *Science*, 2002, **296**, 1873–1876.
8. B. Ragnarson, L. Bengtsson, and A. Hægerstrand, *Histochemistry*, 1992, **97**, 329–33.
9. E. Latz, A. Schoenemeyer, A. Visintin, K. A. Fitzgerald, B. G. Monks, C. F. Knetter, E. Lien, N. J. Nilsen, T. Espevik, and D. T. Golenbock, *Nat. Immunol.*, 2004, **5**, 190–198.
10. S. E. Ewald, B. L. Lee, L. Lau, K. E. Wickliffe, G.-P. Shi, H. A. Chapman, and G. M. Barton, *Nature*, 2008, **456**, 658-662.

Appendix B: Chapter 3

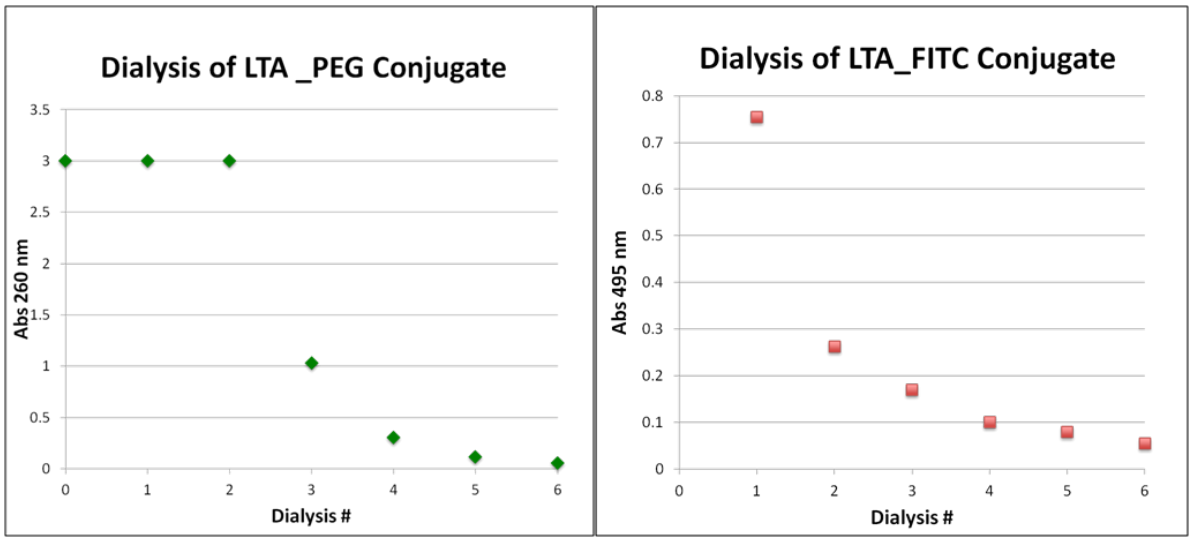

Figure S3.1. Removal of excess PEG_6 linker or FITC from LTA_PEG_6-maleimide and LTA_FITC conjugates *via* centriprep purification (3 kDa MWCO, DPBS, pH 7.4). Removal of PEG_6 linker was monitored at 260 nm (left) and removal of FITC was monitored at 495 nm (right).

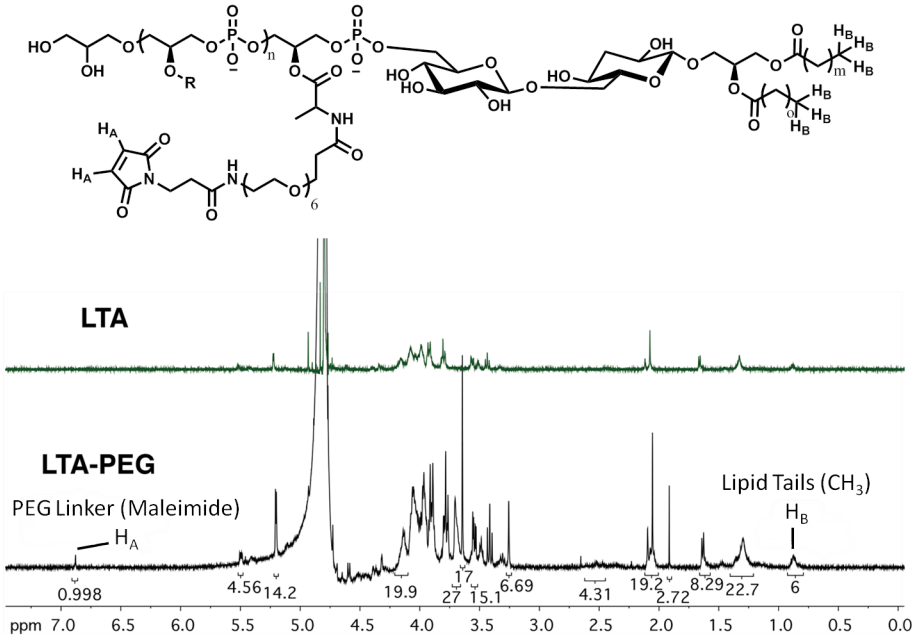

Figure S3.2. The LTA_PEG_6-maleimide conjugate was characterized by ^{1}H NMR (500 MHz, D_2O). Using the most accurate integrations (CH_3 from the lipid chains of LTA and maleimide CH from the PEG linker) a composition of 1 PEG linker to 2 LTAs was determined (50% conversion). For additional NMR assignments, see Morath *et. al.*[1]

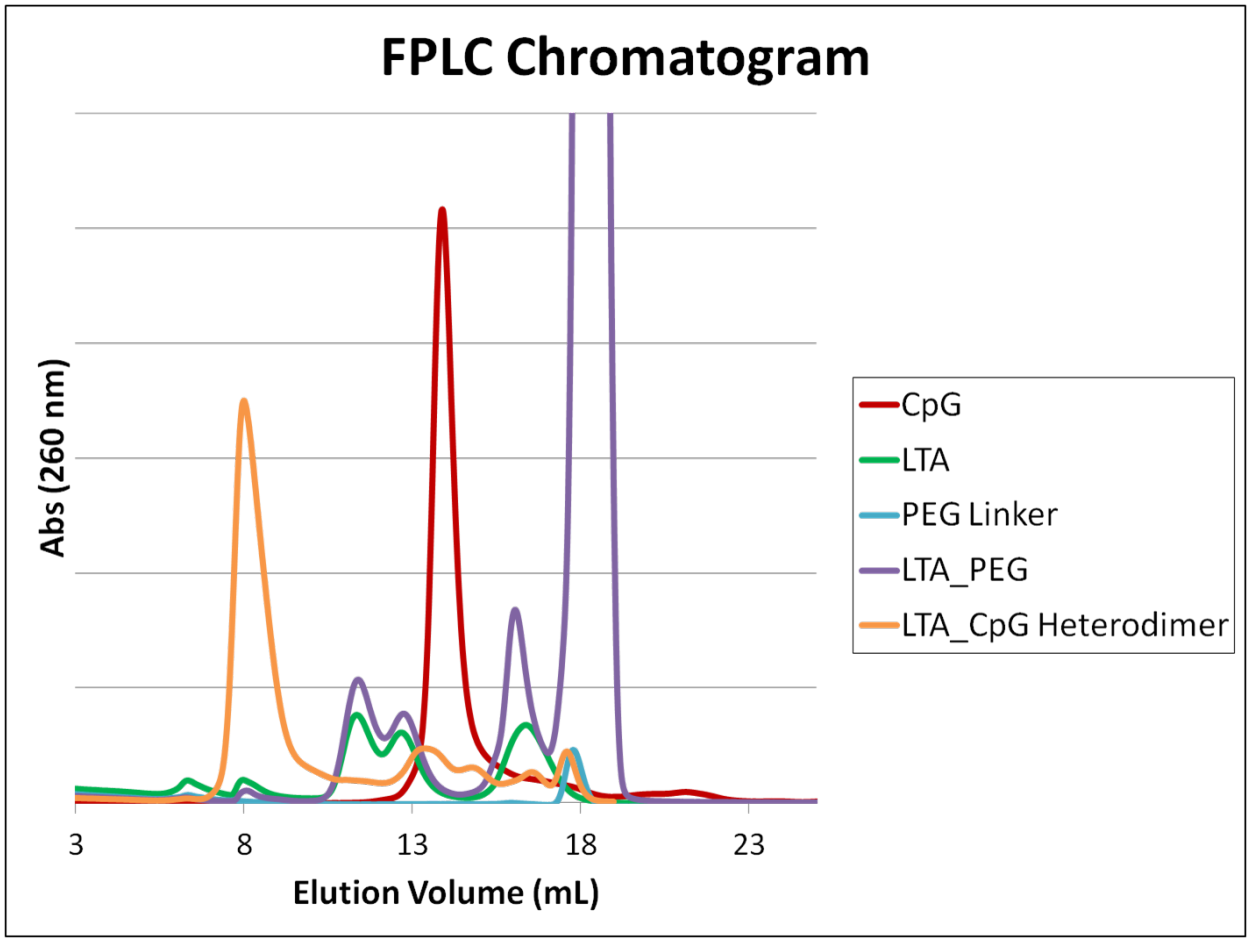

Figure S3.3. FPLC purification of the CpG_LTA di-agonist (Superdex G75, DPBS, 0.2 mL/min). Separations were conducted at 4°C, and UV/Vis absorbance was monitored at 260 nm.

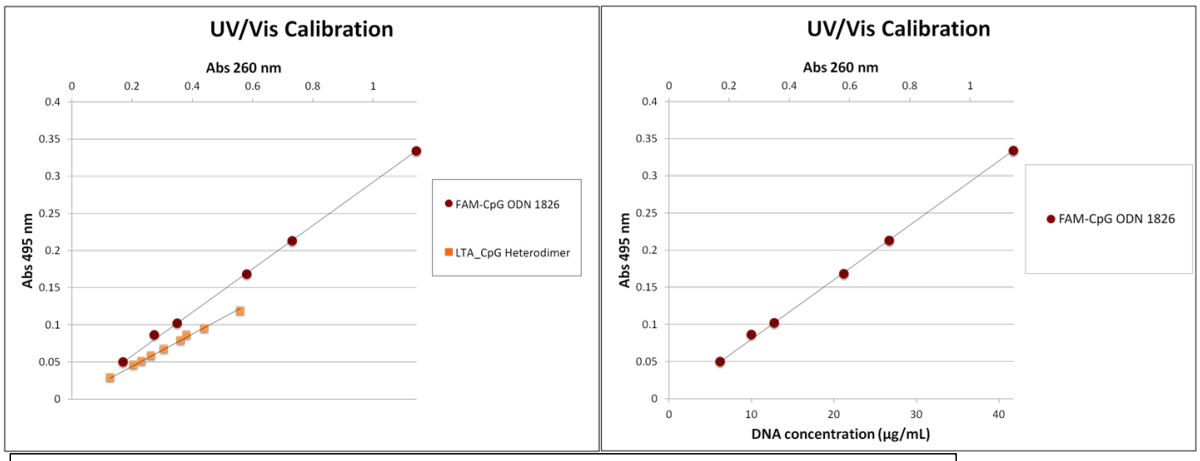

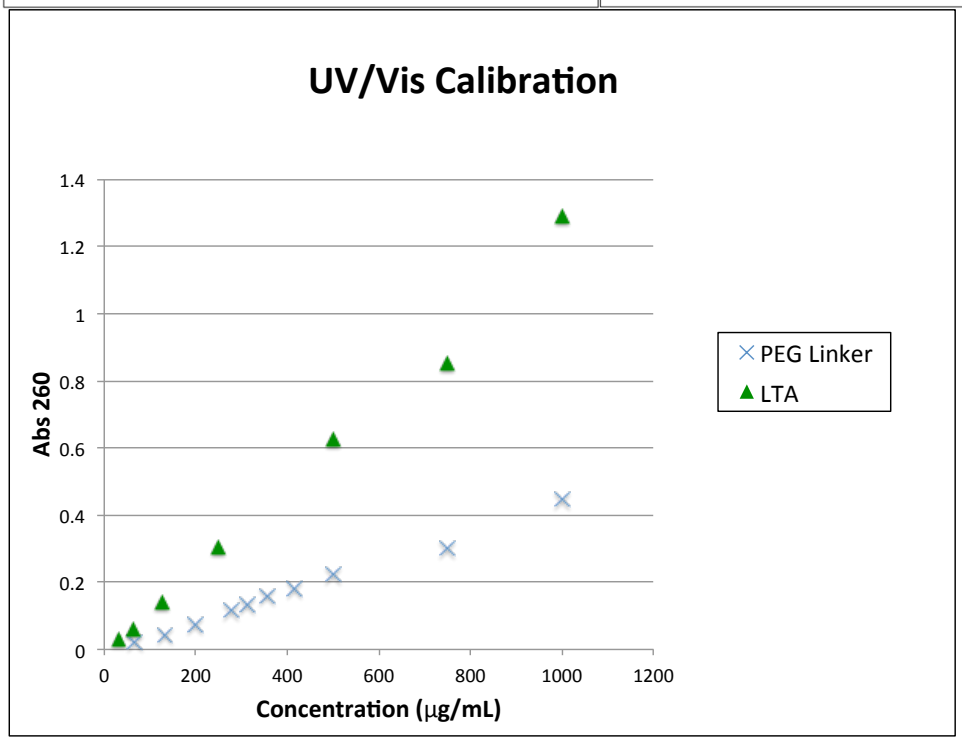

Figure S3.4: The LTA_CpG di-agonist was analyzed by UV/Vis and calibrated to 10 µg/mL with respect to CpG. Both CpG and the LTA_CpG di-agonist were diluted to an Abs_{495} of 0.086 before serial dilutions in DPBS to the relevant concentrations used in each experiment.

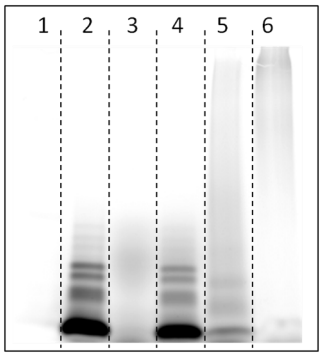

Figure S3.5. SDS-PAGE analysis of the LTA_CpG di-agonist. Lane 1: MW standard, lane 2: CpG, lane 3: FITC-LTA, lane 4: Mixture of CpG and FITC-LTA, lane 5: Crude LTA_CpG di-agonist reaction, lane 6: FPLC purified LTA_CpG di-agonist.

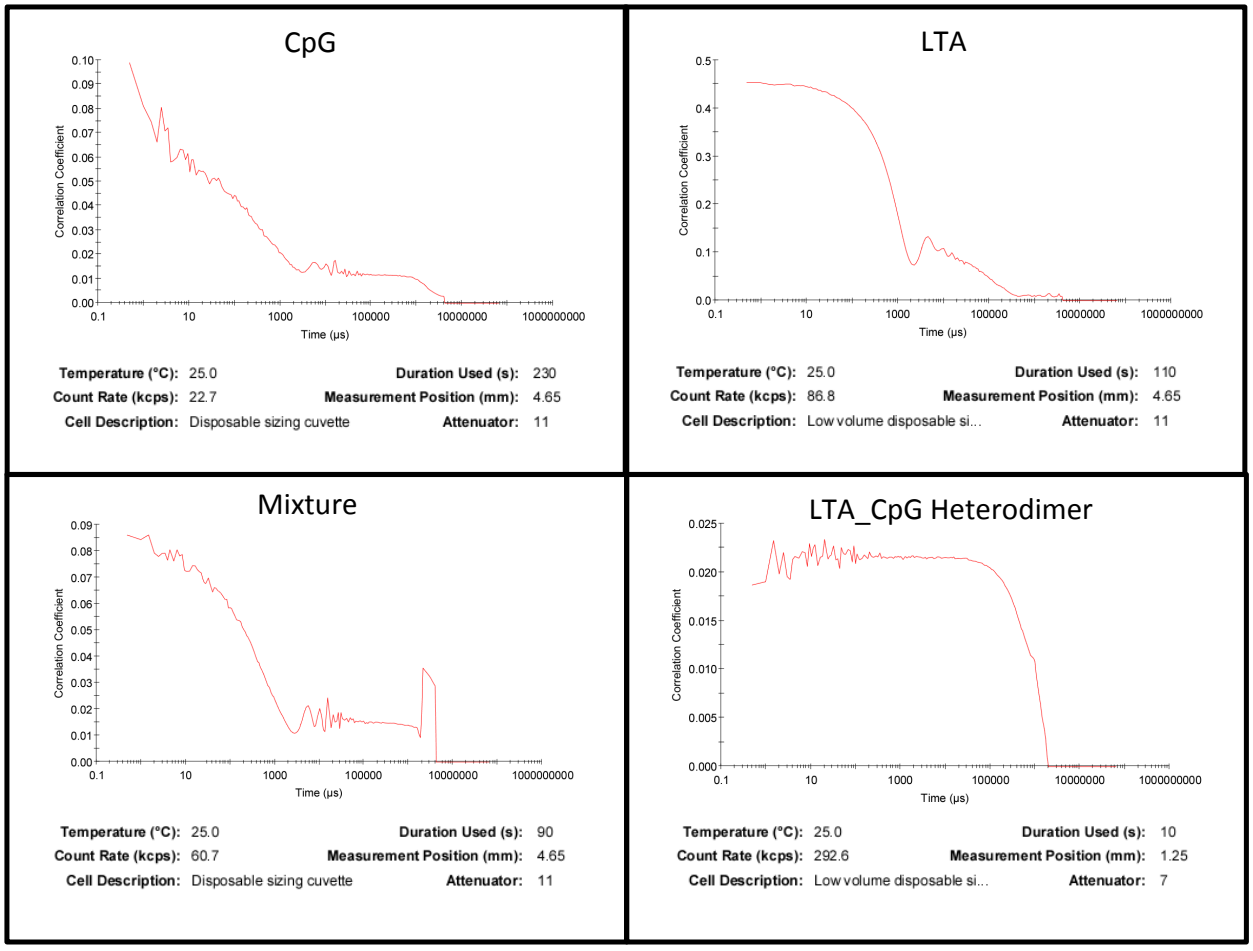

Figure S3.6. Stable particle formation was not observed by DLS and the LTA_CpG di-agonist exhibited a weak correlation coefficient. Sedimentation/agglomeration for the di-agonist was found to occur similar to LTA.

3. Immune Cell Stimulation

RAW Blue Cell Assay

The RAW-Blue cell line was cultured similarly to manufacturer's protocol in complete media (DMEM, 10% HIFBS, 2 mM glutamine, 0.1 mg/mL Zeocin). Cells between passage 5 and 15 were used for all experiments. The Quanti-Blue® assay was performed in accordance with manufacturer's specified protocol. Cells were seeded on a 96 well plate at a density of 100,000 cells/well in 200 μL of complete media per well and the cultures were allowed to incubate for 24 h. The original media was removed and the cell culture in each well was washed with 200 μL DMEM. Each well was then incubated with 190 μL of complete media and 10 μL of a 20 x solution of each sample in PBS for 15 h. Secreted Alkaline Phosphatase (SEAP) was quantified in the cell media by incubating a 10 μL aliquot of the culture media with 200 μL of the Quanti-Blue® SEAP detection reagent for 2.5 h before colorimetric assay at 620 nm. To ensure that no false positives were observed due to contaminating endotoxins, all cell culture media, PBS buffer, and FPLC buffer were also screened for endotoxins. Control studies were performed on the LTA_PEG_6-maleimide and CpG_PEG_6-NHS conjugates (LTA-PEG and CpG-PEG, respectively). In addition, 6-FAM labeled ODN1826 was compared to ODN1826 without a fluorescent tag.

Inhibitor and Antagonist Assay

In the case of samples that were tested with the inhibitor chloroquine, cells were incubated with 50 μM chloroquine for 30 minutes before addition of each the agonist. The antagonists OxPAPC and ODN2088 were added immediately prior to addition of the corresponding agonist. Samples were incubated for 15 h and subjected to the Quanti-Blue® assay as described above.

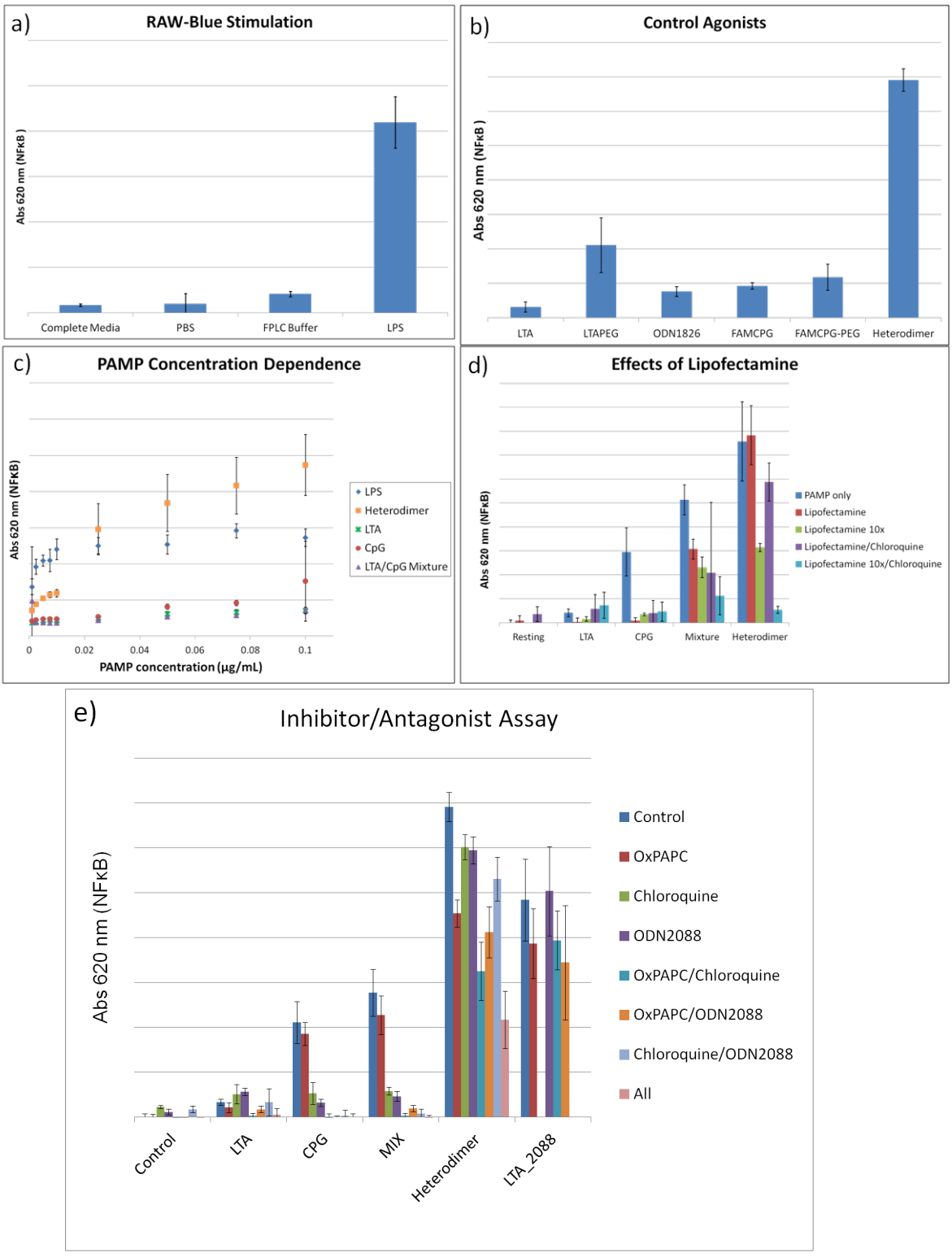

Figure S3.7. a) Endotoxin levels in the complete media used in cell culture, PBS used to dilute the TLR agonists and the FPLC buffer used to purify the di-agonist were quantified relative to LPS. b) The effect of conjugating PEG_6 or the FAM flourescent tag was examined for LTA and CpG (100 ng/mL with respect to LTA or CpG in each case). c) RAW-Blue cells were incubated

with each TLR agonist including LPS, LTA, CpG, a mixture of LTA and CpG, or the LTA_CpG di-agonist. After 15 h, NF-κB activation was quantified using the Quanti-Blue Assay. Experiments were performed in sextuplet. d) Effect of lipofectamine on RAW-Blue stimulation. Lipofectamine (5 μL lipofectamine 2000/μg TLR agonist), lipofectamine 10x (50 μL lipofectamine/μg TLR agonist), lipofectamine/chloroquine (the cells were first incubated with 50 μM chloroquine for 30 min) e) The effects of the antagonists OxPAPC (TLR2) and ODN2088 (TLR9) were screened along with the endosomal protease inhibitor chloroquine. LTA conjugated to the antagonist ODN2088 (LTA_2088) was also included in selected experiments.
Results are expressed as the mean ± SD and n=6.

4. Murine Bone-Marrow Derived Dendritic Cells (BMDC)

BMDC Harvest and Culture
Monocytes were harvested from mouse femurs and cultured as described previously.[2] Briefly, the monocytes were plated in 8.5 mL of complete media (RPMI, 10% heat inactivated FBS, 2 mM glutamine, 20 ng/mL GMCSF) at a density of $1x10^6$ cells/mL in a Petri dish and were incubated for 3 days. On day 3, the volume of the cell culture was doubled by addition of complete media, and the cells were cultured for an additional 3 days before use. Cells were released from the surface by pipetting and suspended in 10 mL of RPMI media. Cells were centrifuged, media removed, and fresh complete RPMI media was added before seeding at a density of $6x10^5$ cells/well on 24/well plates. BMDCs were used immediately in subsequent stimulation procedures.

BMDC Stimulation
The cells were immediately stimulated by addition of a 20x solution of CpG, LTA, the LTA_CpG di-agonist or a mixture of LTA and CpG at final concentrations of 100 ng/mL in the cell media. For cytokine experiments lipopolysacharide (LPS) was employed as a positive control. To measure cytokine expression, cytokine secretion was inhibited. 1.2 μL of the Golgi Plug protein transport inhibitor was added to each well in experiments for measuring cytokines. Cells used to screen for cell-adhesion and antigen presentation proteins were stimulated for 15 h. Cells used to measure cytokine production were stimulated for 10 h.

BMDC Antibody Staining
The BMDCs were released from the 24/well plates by rapidly pipetting the cell media for 1 min before transferring the released cells to 1.5 mL centrifuge tubes kept at 0°C. The cells were centrifuged and the media was removed. All centrifuge steps were performed at 300 rcf, 10 min, 4°C. The pellets were re-suspended in 300 μL FACS (10% HIFBS, PBS, 0.01% sodium azide) and incubated with 1.2 μL of the blocking antibody for 20 min before centrifugation. The blocking mixture was removed and the pellet was re-suspended in 300 μL FACS with 1.2 μL of FITC anti-CD11c.

Antigen Presentation and Cell Adhesion Proteins
In screens that involved cell adhesion or antigen presentation proteins the corresponding antibody (PE anti-MHCII, CD40, CD80, or CD86) was added with the FITC anti-CD11c. The cell mixture was incubated at 0 °C for 30 min before centrifuging and washing 2 times with 300

μL FACS buffer. The cells were re-suspended in 200 μL FACS buffer before analysis by flow cytometry.

Cytokine Production

In screens that involved cytokine production, the FITC anti-CD11c labeled cells were incubated for 30 min at 0 °C. The samples were then centrifuged, and the cells were permeabilized/fixed by re-suspending the pellets in 300 μL of the BD cytoperm buffer at 0 °C for 20 min. The cells were then incubated with antibodies for the corresponding cytokines (APC anti-TNF α, Interferon γ, IL-6, IL-10, or IL-12) for 20 min before washing (2 x 300 μL) of the BD wash buffer. The cells were then centrifuged, re-suspended in 200 μL FACS buffer and analyzed by flow cytometry.

5. Flow Cytometry

Flow cytometry was performed, and cells were gated according to control cell samples. Positive $CD11c^+$ gating was performed relative to the unlabeled cell culture. In the case of cell surface proteins, $3x10^4$ total cells per experiment were counted, and for the cytokine profiling experiments $1x10^4$ cells displaying the $CD11c^+$ phenotype were counted in each experiment. For fluorescence measurements of labeled cell-surface proteins and cytokines, samples were compared relative to isotype controls (**Fig. S8**).

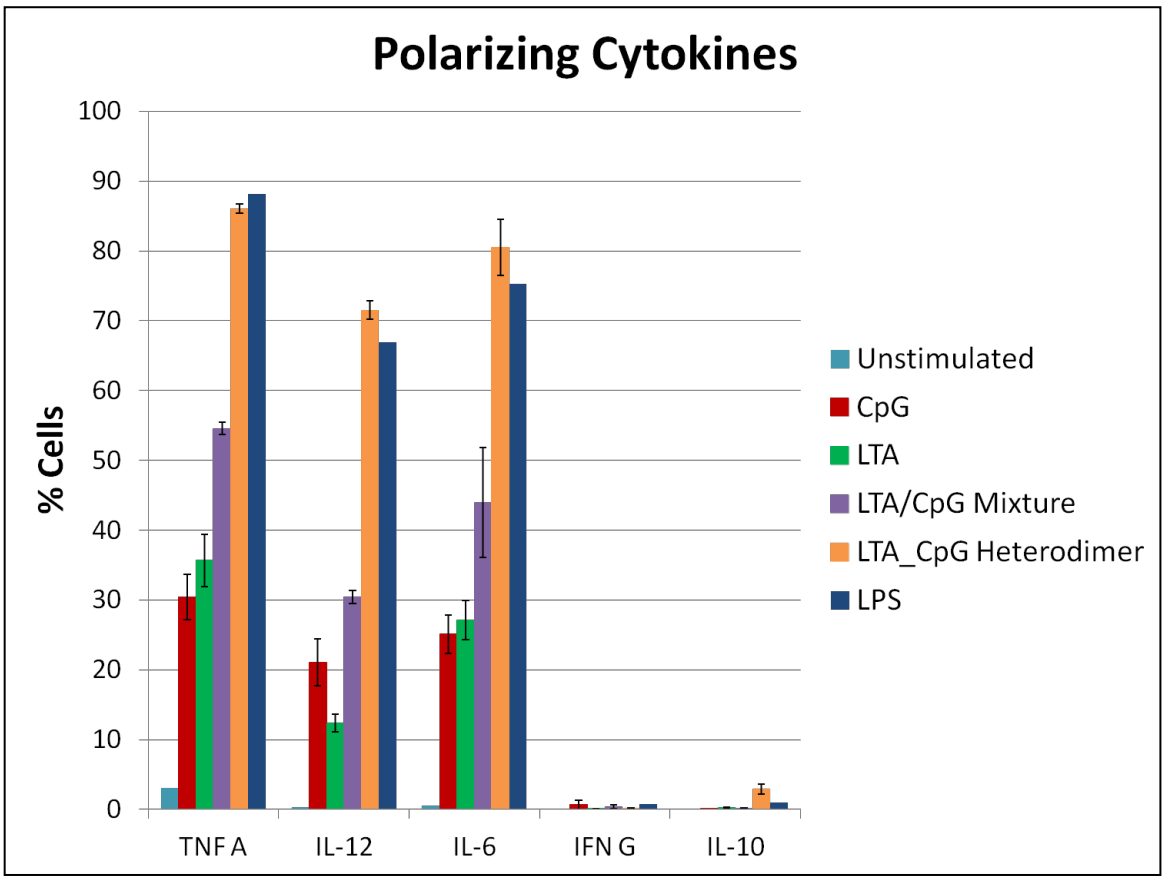

Figure S3.8. Polarizing cytokines screened in BMDCs included TNF-α, L-12, IL-6, Interferon-γ, and IL-10. Stimulation by the LTA_CpG di-agonist was screened relative to stimulation with LTA, CpG, a mixture of the two TLR agonists or lipopolysacharide (LPS). Results are expressed as the mean ± SD and n=3.

6. Confocal Microscopy

Sample Preparation

RAW-Blue Cells were cultured as described above. Passages between 5 and 10 were used for all confocal microscopy experiments. Cells were seeded at a density of 700,000 cells/dish on glass bottomed petri dishes. Complete DMEM media (3 mL) was added to each cell culture and the petri dishes were incubated for 24h before further use. The media was removed and the cells were washed 3 times with confocal buffer (10 mM HEPES buffer containing 250 mM glucose). For control samples the cells were treated with 500 μL of PBS. For stimulated samples 100 μL of the TLR agonist (10 μg/mL, DPBS) was added. Samples included cells stimulated by CpG or

the LTA_CpG di-agonist. In time-lapse experiments, cell binding was observed to occur over the course of 30 min for both CpG and the di-agonist. The di-agonist showed greater binding to the cell surface likely due to the LTA and punctuated clustering was observed for both samples consistent with CpG trafficking (**Fig. S9**).

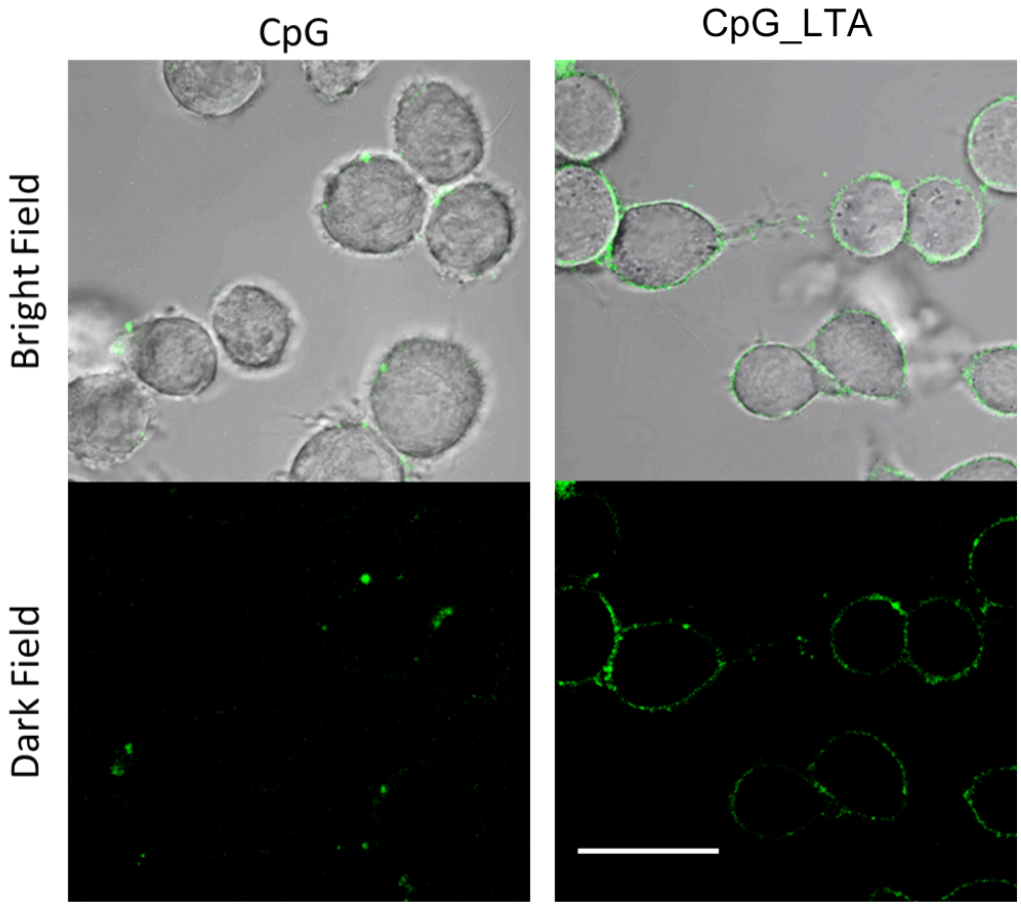

Figure S3.9. Confocal microscopy of RAW-Blue cells treated FAM labeled CpG or the CpG_LTA di-agonist/heterodimer at 10 μg/mL with respect to CpG. Scale bar = 20 μm.

Cytokine Flow Cytometry Data: FL1-H corresponds to anti-CD11c+ labeling, FL2-H corresponds to cell surface protein labeling, and FL4-H corresponds to cytokine labeling.

CELL SURFACE PROTEINS

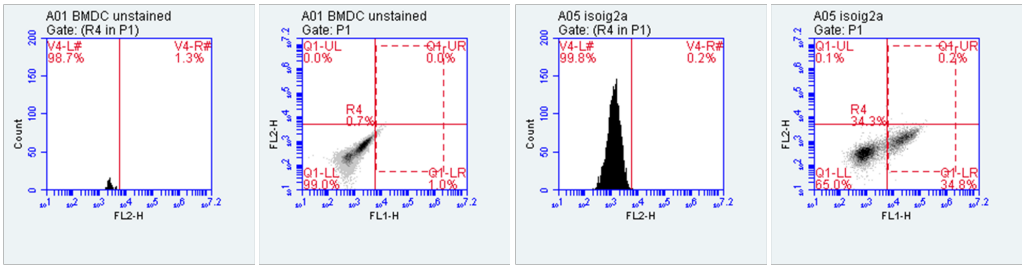

CD86

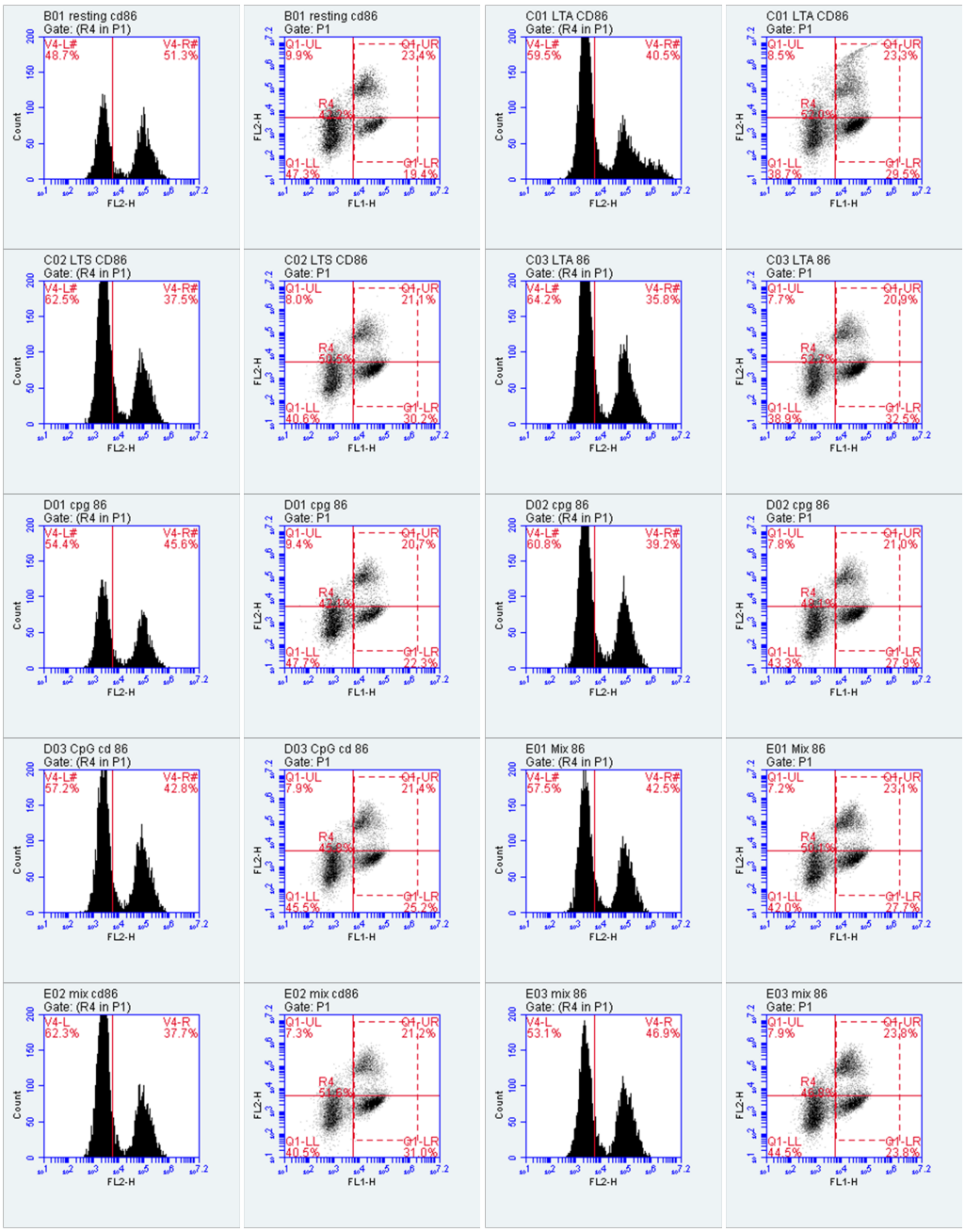
B01 resting cd86
Gate: (R4 in P1)
V4-L# 48.7%
V4-R# 51.3%
B01 resting cd86
Gate: P1
Q1-UL 9.9%
Q1-UR 23.4%
R4 46.8%
Q1-LL 47.3%
Q1-LR 19.4%
C01 LTA CD86
Gate: (R4 in P1)
V4-L# 59.5%
V4-R# 40.5%
C01 LTA CD86
Gate: P1
Q1-UL 8.5%
Q1-UR 23.3%
R4 52.0%
Q1-LL 38.7%
Q1-LR 29.5%
C02 LTS CD86
Gate: (R4 in P1)
V4-L# 62.5%
V4-R# 37.5%
C02 LTS CD86
Gate: P1
Q1-UL 8.0%
Q1-UR 21.1%
R4 50.6%
Q1-LL 40.6%
Q1-LR 30.2%
C03 LTA 86
Gate: (R4 in P1)
V4-L# 64.2%
V4-R# 35.8%
C03 LTA 86
Gate: P1
Q1-UL 7.7%
Q1-UR 20.9%
R4 52.3%
Q1-LL 38.9%
Q1-LR 32.5%
D01 cpg 86
Gate: (R4 in P1)
V4-L# 54.4%
V4-R# 45.6%
D01 cpg 86
Gate: P1
Q1-UL 9.4%
Q1-UR 20.7%
R4 47.1%
Q1-LL 47.7%
Q1-LR 22.3%
D02 cpg 86
Gate: (R4 in P1)
V4-L# 60.8%
V4-R# 39.2%
D02 cpg 86
Gate: P1
Q1-UL 7.8%
Q1-UR 21.0%
R4 49.1%
Q1-LL 43.3%
Q1-LR 27.9%
D03 CpG cd 86
Gate: (R4 in P1)
V4-L# 57.2%
V4-R# 42.8%
D03 CpG cd 86
Gate: P1
Q1-UL 7.9%
Q1-UR 21.4%
R4 48.2%
Q1-LL 45.5%
Q1-LR 25.2%
E01 Mix 86
Gate: (R4 in P1)
V4-L# 57.5%
V4-R# 42.5%
E01 Mix 86
Gate: P1
Q1-UL 7.2%
Q1-UR 23.1%
R4 50.1%
Q1-LL 42.0%
Q1-LR 27.7%
E02 mix cd86
Gate: (R4 in P1)
V4-L 62.3%
V4-R 37.7%
E02 mix cd86
Gate: P1
Q1-UL 7.3%
Q1-UR 21.2%
R4 51.5%
Q1-LL 40.5%
Q1-LR 31.0%
E03 mix 86
Gate: (R4 in P1)
V4-L 53.1%
V4-R 46.9%
E03 mix 86
Gate: P1
Q1-UL 7.9%
Q1-UR 23.8%
R4 48.8%
Q1-LL 44.5%
Q1-LR 23.8%
Count
FL2-H
FL1-H

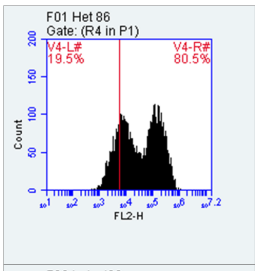
F01 Het 86
Gate: (R4 in P1)
V4-L#
19.5%
V4-R#
80.5%
Count
FL2-H

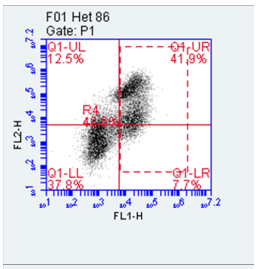
F01 Het 86
Gate: P1
Q1-UL
12.5%
Q1-UR
41.9%
R4
Q1-LL
37.8%
G1-LR
7.7%
FL2-H
FL1-H

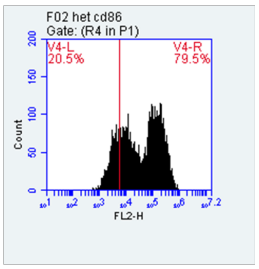
F02 het cd86
Gate: (R4 in P1)
V4-L
20.5%
V4-R
79.5%
Count
FL2-H

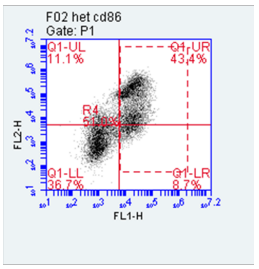
F02 het cd86
Gate: P1
Q1-UL
11.1%
Q1-UR
43.4%
R4
Q1-LL
36.7%
G1-LR
8.7%
FL2-H
FL1-H

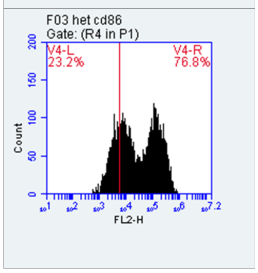
F03 het cd86
Gate: (R4 in P1)
V4-L
23.2%
V4-R
76.8%
Count
FL2-H

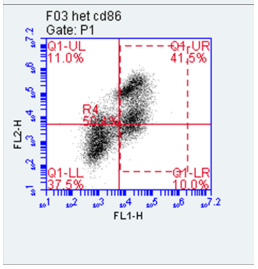
F03 het cd86
Gate: P1
Q1-UL
11.0%
Q1-UR
41.5%
R4
Q1-LL
37.5%
G1-LR
10.0%
FL2-H
FL1-H

CD80

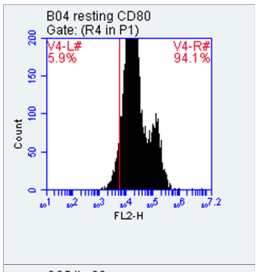
B04 resting CD80
Gate: (R4 in P1)
V4-L#
5.9%
V4-R#
94.1%
Count
FL2-H

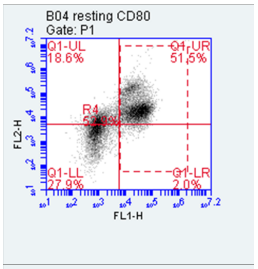
B04 resting CD80
Gate: P1
Q1-UL
18.6%
Q1-UR
51.5%
R4
Q1-LL
27.9%
G1-LR
2.0%
FL2-H
FL1-H

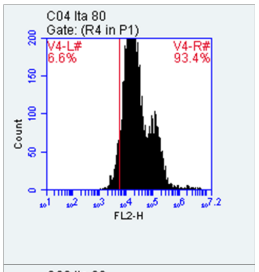
C04 Ita 80
Gate: (R4 in P1)
V4-L#
6.6%
V4-R#
93.4%
Count
FL2-H

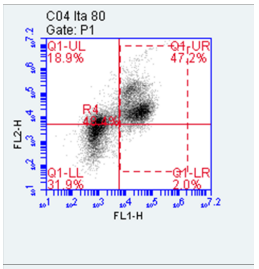
C04 Ita 80
Gate: P1
Q1-UL
18.9%
Q1-UR
47.2%
R4
Q1-LL
31.9%
G1-LR
2.0%
FL2-H
FL1-H

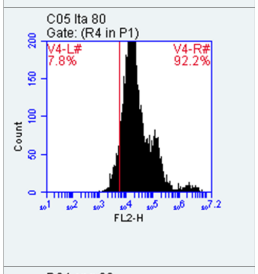
C05 Ita 80
Gate: (R4 in P1)
V4-L#
7.8%
V4-R#
92.2%
Count
FL2-H

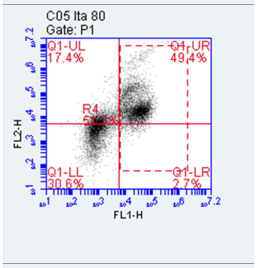
C05 Ita 80
Gate: P1
Q1-UL
17.4%
Q1-UR
49.4%
R4
Q1-LL
30.6%
G1-LR
2.7%
FL2-H
FL1-H

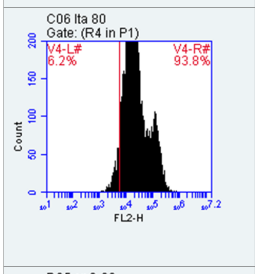
C06 Ita 80
Gate: (R4 in P1)
V4-L#
6.2%
V4-R#
93.8%
Count
FL2-H

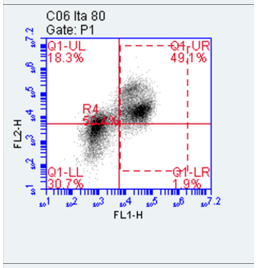
C06 Ita 80
Gate: P1
Q1-UL
18.3%
Q1-UR
49.1%
R4
Q1-LL
30.7%
G1-LR
1.9%
FL2-H
FL1-H

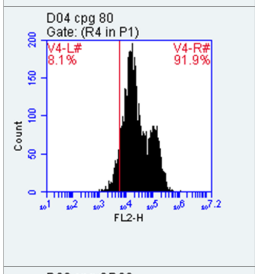
D04 cpg 80
Gate: (R4 in P1)
V4-L#
8.1%
V4-R#
91.9%
Count
FL2-H

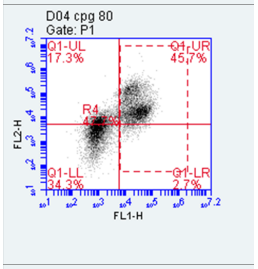
D04 cpg 80
Gate: P1
Q1-UL
17.3%
Q1-UR
45.7%
R4
Q1-LL
34.3%
G1-LR
2.7%
FL2-H
FL1-H

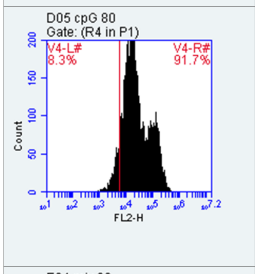
D05 cpG 80
Gate: (R4 in P1)
V4-L#
8.3%
V4-R#
91.7%
Count
FL2-H

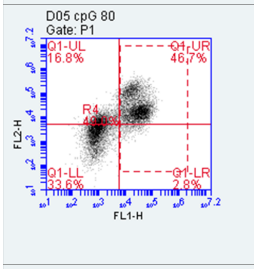
D05 cpG 80
Gate: P1
Q1-UL
16.8%
Q1-UR
46.7%
R4
Q1-LL
33.6%
G1-LR
2.8%
FL2-H
FL1-H

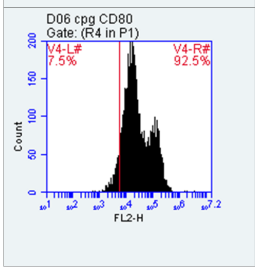
D06 cpg CD80
Gate: (R4 in P1)
V4-L#
7.5%
V4-R#
92.5%
Count
FL2-H

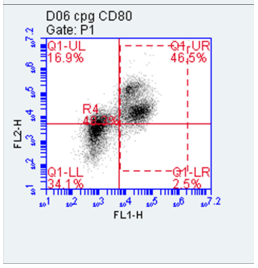
D06 cpg CD80
Gate: P1
Q1-UL
16.9%
Q1-UR
46.5%
R4
Q1-LL
34.1%
G1-LR
2.5%
FL2-H
FL1-H

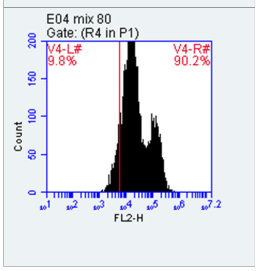
E04 mix 80
Gate: (R4 in P1)
V4-L#
9.8%
V4-R#
90.2%
Count
FL2-H

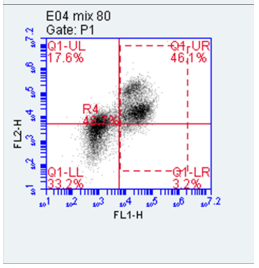
E04 mix 80
Gate: P1
Q1-UL
17.6%
Q1-UR
46.1%
R4
Q1-LL
33.2%
G1-LR
3.2%
FL2-H
FL1-H

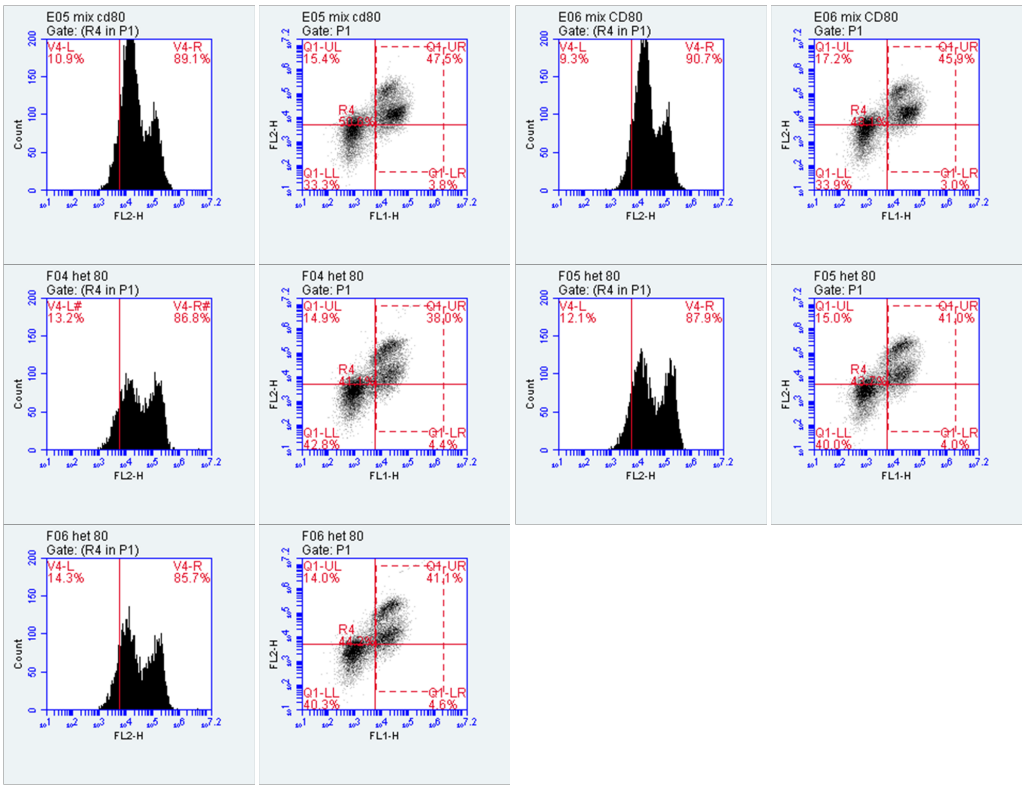
E05 mix cd80
Gate: (R4 in P1)
V4-L
10.9%
V4-R
89.1%
Count
FL2-H
E05 mix cd80
Gate: P1
Q1-UL
15.4%
Q1-UR
47.5%
R4
Q1-LL
33.3%
G1-LR
3.8%
FL2-H
FL1-H
E06 mix CD80
Gate: (R4 in P1)
V4-L
9.3%
V4-R
90.7%
Count
FL2-H
E06 mix CD80
Gate: P1
Q1-UL
17.2%
Q1-UR
45.9%
R4
Q1-LL
33.9%
G1-LR
3.0%
FL2-H
FL1-H
F04 het 80
Gate: (R4 in P1)
V4-L#
13.2%
V4-R#
86.8%
Count
FL2-H
F04 het 80
Gate: P1
Q1-UL
14.9%
Q1-UR
38.0%
R4
Q1-LL
42.8%
G1-LR
4.4%
FL2-H
FL1-H
F05 het 80
Gate: (R4 in P1)
V4-L
12.1%
V4-R
87.9%
Count
FL2-H
F05 het 80
Gate: P1
Q1-UL
15.0%
Q1-UR
41.0%
R4
Q1-LL
40.0%
G1-LR
4.0%
FL2-H
FL1-H
F06 het 80
Gate: (R4 in P1)
V4-L
14.3%
V4-R
85.7%
Count
FL2-H
F06 het 80
Gate: P1
Q1-UL
14.0%
Q1-UR
41.1%
R4
Q1-LL
40.3%
G1-LR
4.6%
FL2-H
FL1-H

MHCII

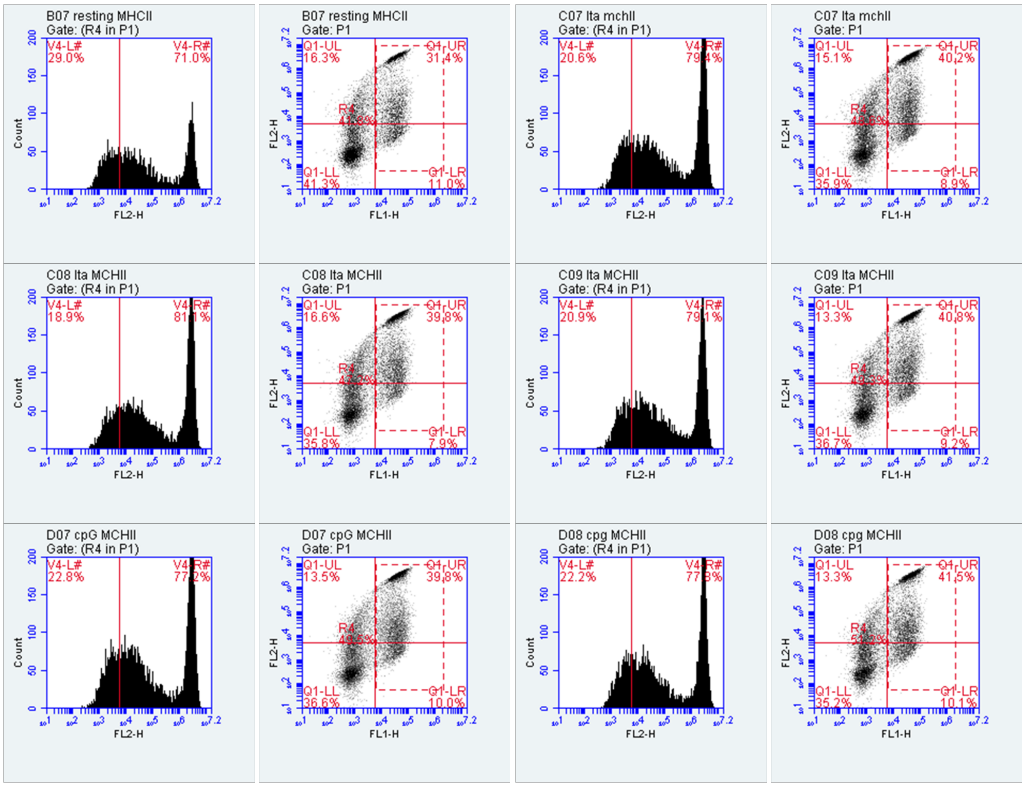
B07 resting MHCII
Gate: (R4 in P1)
V4-L#
29.0%
V4-R#
71.0%
Count
FL2-H
B07 resting MHCII
Gate: P1
Q1-UL
16.3%
Q1-UR
31.4%
R4
Q1-LL
41.3%
G1-LR
11.0%
FL2-H
FL1-H
C07 Ita mchII
Gate: (R4 in P1)
V4-L#
20.6%
V4-R#
79.4%
Count
FL2-H
C07 Ita mchII
Gate: P1
Q1-UL
15.1%
Q1-UR
40.2%
R4
Q1-LL
35.9%
G1-LR
8.9%
FL2-H
FL1-H
C08 Ita MCHII
Gate: (R4 in P1)
V4-L#
18.9%
V4-R#
81.1%
Count
FL2-H
C08 Ita MCHII
Gate: P1
Q1-UL
16.6%
Q1-UR
39.8%
R4
Q1-LL
35.8%
G1-LR
7.9%
FL2-H
FL1-H
C09 Ita MCHII
Gate: (R4 in P1)
V4-L#
20.9%
V4-R#
79.1%
Count
FL2-H
C09 Ita MCHII
Gate: P1
Q1-UL
13.3%
Q1-UR
40.8%
R4
Q1-LL
36.7%
G1-LR
9.2%
FL2-H
FL1-H
D07 cpG MCHII
Gate: (R4 in P1)
V4-L#
22.8%
V4-R#
77.2%
Count
FL2-H
D07 cpG MCHII
Gate: P1
Q1-UL
13.5%
Q1-UR
39.8%
R4
Q1-LL
36.6%
G1-LR
10.0%
FL2-H
FL1-H
D08 cpg MCHII
Gate: (R4 in P1)
V4-L#
22.2%
V4-R#
77.8%
Count
FL2-H
D08 cpg MCHII
Gate: P1
Q1-UL
13.3%
Q1-UR
41.5%
R4
Q1-LL
35.2%
G1-LR
10.1%
FL2-H
FL1-H

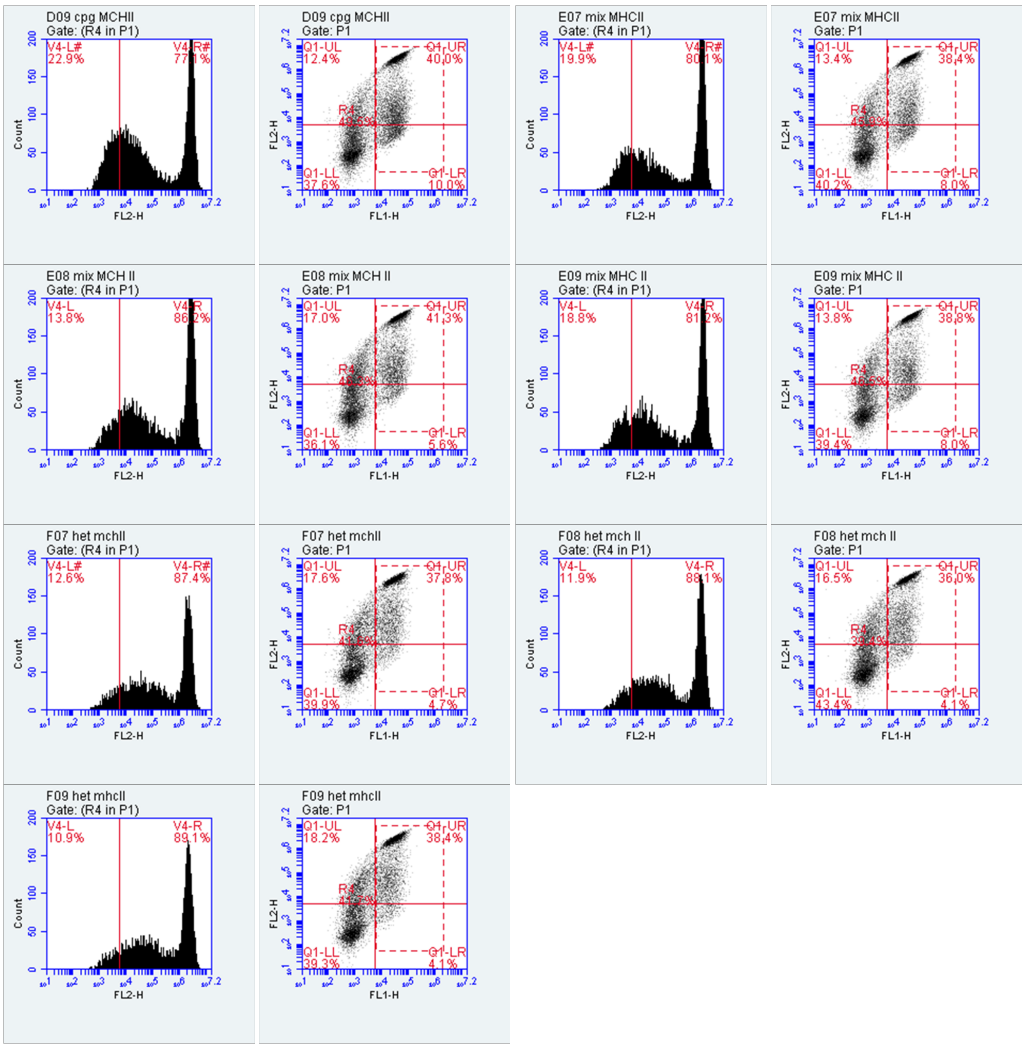
D09 cpg MCHII
Gate: (R4 in P1)
V4-L# 22.9%
V4-R# 77.1%
D09 cpg MCHII
Gate: P1
Q1-UL 12.4%
Q1-UR 40.0%
R4 47.6%
Q1-LL 37.6%
G1-LR 10.0%
E07 mix MHCII
Gate: (R4 in P1)
V4-L# 19.9%
V4-R# 80.1%
E07 mix MHCII
Gate: P1
Q1-UL 13.4%
Q1-UR 38.4%
R4 48.2%
Q1-LL 40.2%
G1-LR 8.0%
E08 mix MCH II
Gate: (R4 in P1)
V4-L 13.8%
V4-R 86.2%
E08 mix MCH II
Gate: P1
Q1-UL 17.0%
Q1-UR 41.3%
R4 41.6%
Q1-LL 36.1%
G1-LR 5.6%
E09 mix MHC II
Gate: (R4 in P1)
V4-L 18.8%
V4-R 81.2%
E09 mix MHC II
Gate: P1
Q1-UL 13.8%
Q1-UR 38.8%
R4 48.6%
Q1-LL 39.4%
G1-LR 8.0%
F07 het mchII
Gate: (R4 in P1)
V4-L# 12.6%
V4-R# 87.4%
F07 het mchII
Gate: P1
Q1-UL 17.6%
Q1-UR 37.8%
R4 43.6%
Q1-LL 39.9%
G1-LR 4.7%
F08 het mch II
Gate: (R4 in P1)
V4-L 11.9%
V4-R 88.1%
F08 het mch II
Gate: P1
Q1-UL 16.5%
Q1-UR 36.0%
R4 43.4%
Q1-LL 43.4%
G1-LR 4.1%
F09 het mhcII
Gate: (R4 in P1)
V4-L 10.9%
V4-R 89.1%
F09 het mhcII
Gate: P1
Q1-UL 18.2%
Q1-UR 38.4%
R4 43.4%
Q1-LL 39.3%
G1-LR 4.1%
Count
FL2-H
FL1-H

CD40

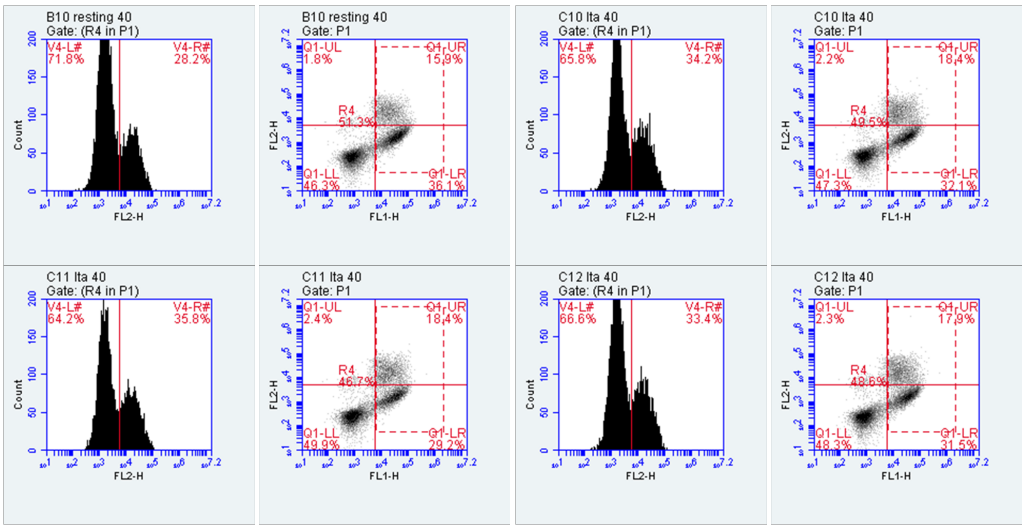
B10 resting 40
Gate: (R4 in P1)
V4-L# 71.8%
V4-R# 28.2%
B10 resting 40
Gate: P1
Q1-UL 1.8%
Q1-UR 15.9%
R4 51.3%
Q1-LL 46.3%
G1-LR 36.1%
C10 Ita 40
Gate: (R4 in P1)
V4-L# 65.8%
V4-R# 34.2%
C10 Ita 40
Gate: P1
Q1-UL 2.2%
Q1-UR 18.4%
R4 49.5%
Q1-LL 47.3%
G1-LR 32.1%
C11 Ita 40
Gate: (R4 in P1)
V4-L# 64.2%
V4-R# 35.8%
C11 Ita 40
Gate: P1
Q1-UL 2.4%
Q1-UR 18.4%
R4 46.7%
Q1-LL 49.9%
G1-LR 29.7%
C12 Ita 40
Gate: (R4 in P1)
V4-L# 66.6%
V4-R# 33.4%
C12 Ita 40
Gate: P1
Q1-UL 2.3%
Q1-UR 17.9%
R4 49.6%
Q1-LL 48.2%
G1-LR 31.5%
Count
FL2-H
FL1-H

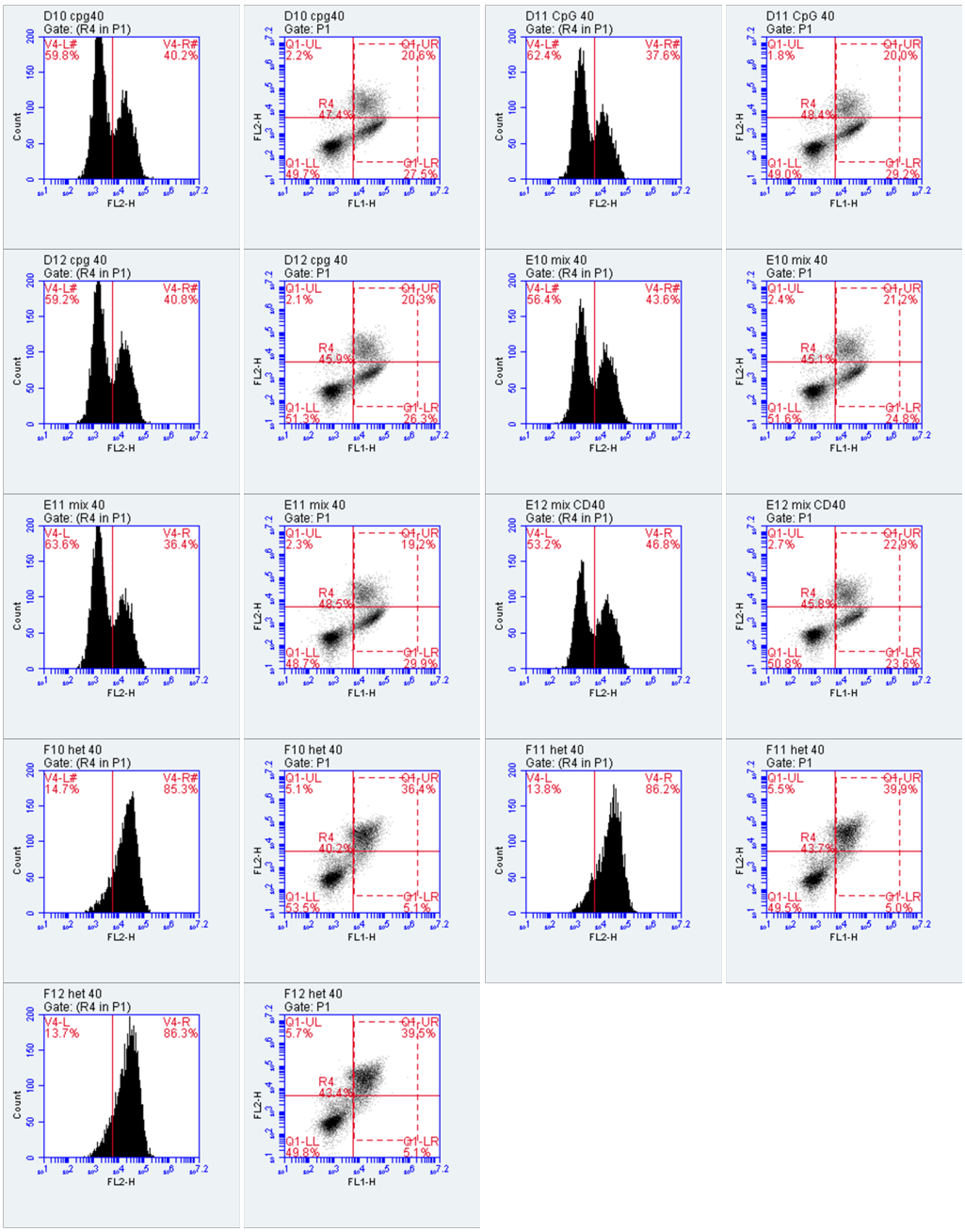

CYTOKINE PROFILES

Interferon-γ

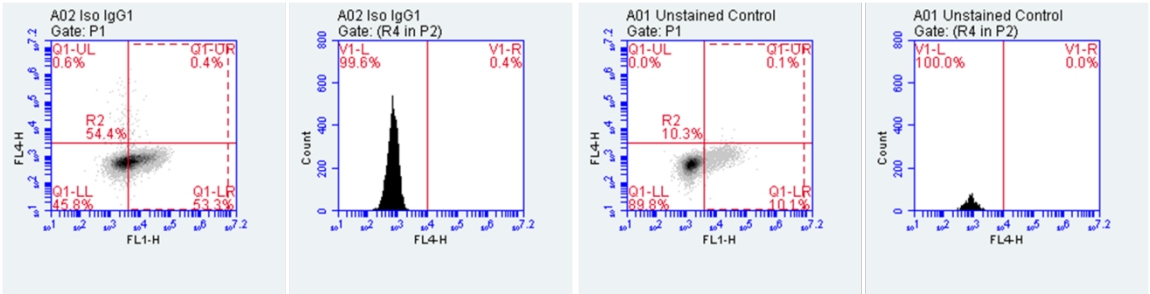

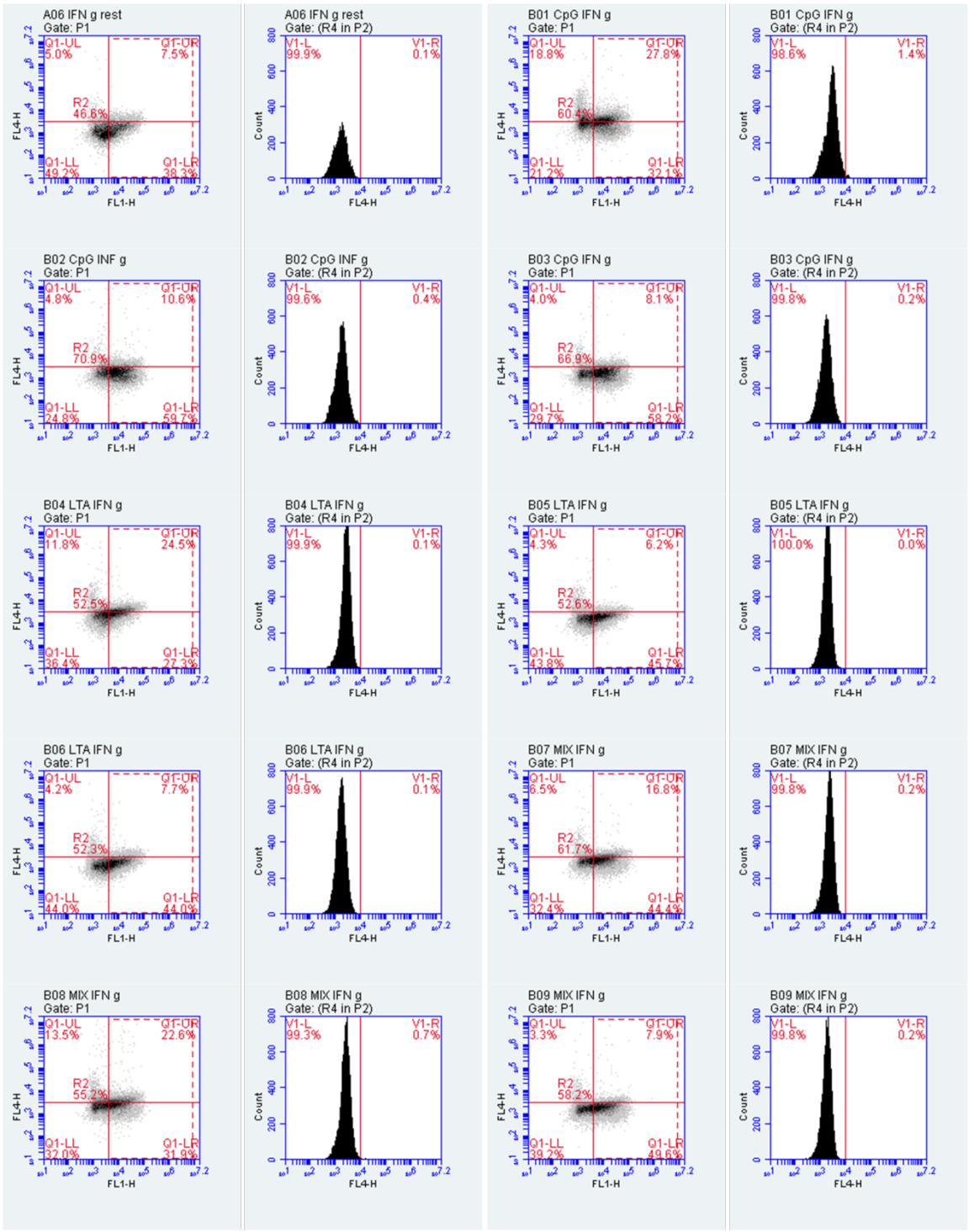
A06 IFN g rest
Gate: P1
Q1-UL 5.0%
Q1-UR 7.5%
R2 46.6%
Q1-LL 49.2%
Q1-LR 38.3%
A06 IFN g rest
Gate: (R4 in P2)
V1-L 99.9%
V1-R 0.1%
B01 CpG IFN g
Gate: P1
Q1-UL 18.8%
Q1-UR 27.8%
R2 60.4%
Q1-LL 21.2%
Q1-LR 32.1%
B01 CpG IFN g
Gate: (R4 in P2)
V1-L 98.6%
V1-R 1.4%
B02 CpG INF g
Gate: P1
Q1-UL 4.8%
Q1-UR 10.6%
R2 70.9%
Q1-LL 24.8%
Q1-LR 59.7%
B02 CpG INF g
Gate: (R4 in P2)
V1-L 99.6%
V1-R 0.4%
B03 CpG IFN g
Gate: P1
Q1-UL 4.0%
Q1-UR 8.1%
R2 66.8%
Q1-LL 29.7%
Q1-LR 58.2%
B03 CpG IFN g
Gate: (R4 in P2)
V1-L 99.8%
V1-R 0.2%
B04 LTA IFN g
Gate: P1
Q1-UL 11.8%
Q1-UR 24.5%
R2 52.5%
Q1-LL 36.4%
Q1-LR 27.3%
B04 LTA IFN g
Gate: (R4 in P2)
V1-L 99.9%
V1-R 0.1%
B05 LTA IFN g
Gate: P1
Q1-UL 4.3%
Q1-UR 6.2%
R2 52.6%
Q1-LL 43.8%
Q1-LR 45.7%
B05 LTA IFN g
Gate: (R4 in P2)
V1-L 100.0%
V1-R 0.0%
B06 LTA IFN g
Gate: P1
Q1-UL 4.2%
Q1-UR 7.7%
R2 52.3%
Q1-LL 44.0%
Q1-LR 44.0%
B06 LTA IFN g
Gate: (R4 in P2)
V1-L 99.9%
V1-R 0.1%
B07 MIX IFN g
Gate: P1
Q1-UL 6.5%
Q1-UR 16.8%
R2 61.7%
Q1-LL 32.4%
Q1-LR 44.4%
B07 MIX IFN g
Gate: (R4 in P2)
V1-L 99.8%
V1-R 0.2%
B08 MIX IFN g
Gate: P1
Q1-UL 13.5%
Q1-UR 22.6%
R2 55.2%
Q1-LL 32.0%
Q1-LR 31.9%
B08 MIX IFN g
Gate: (R4 in P2)
V1-L 99.3%
V1-R 0.7%
B09 MIX IFN g
Gate: P1
Q1-UL 3.3%
Q1-UR 7.9%
R2 58.2%
Q1-LL 39.2%
Q1-LR 49.6%
B09 MIX IFN g
Gate: (R4 in P2)
V1-L 99.8%
V1-R 0.2%
FL1-H
FL4-H
Count

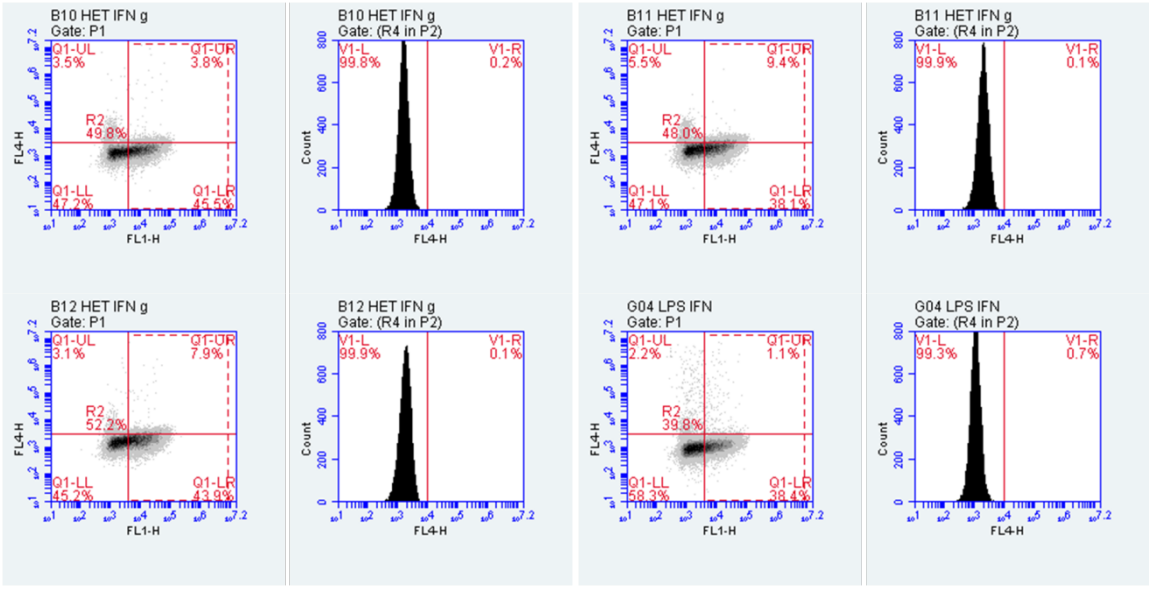
B10 HET IFN g
Gate: P1
Q1-UL 3.5%
Q1-UR 3.8%
R2 49.8%
Q1-LL 47.2%
Q1-LR 45.5%
FL4-H
FL1-H
B10 HET IFN g
Gate: (R4 in P2)
V1-L 99.8%
V1-R 0.2%
Count
FL4-H
B11 HET IFN g
Gate: P1
Q1-UL 5.5%
Q1-UR 9.4%
R2 48.0%
Q1-LL 47.1%
Q1-LR 38.1%
FL4-H
FL1-H
B11 HET IFN g
Gate: (R4 in P2)
V1-L 99.9%
V1-R 0.1%
Count
FL4-H
B12 HET IFN g
Gate: P1
Q1-UL 3.1%
Q1-UR 7.9%
R2 52.2%
Q1-LL 45.2%
Q1-LR 43.9%
FL4-H
FL1-H
B12 HET IFN g
Gate: (R4 in P2)
V1-L 99.9%
V1-R 0.1%
Count
FL4-H
G04 LPS IFN
Gate: P1
Q1-UL 2.2%
Q1-UR 1.1%
R2 39.8%
Q1-LL 58.3%
Q1-LR 38.4%
FL4-H
FL1-H
G04 LPS IFN
Gate: (R4 in P2)
V1-L 99.3%
V1-R 0.7%
Count
FL4-H

TNF-α

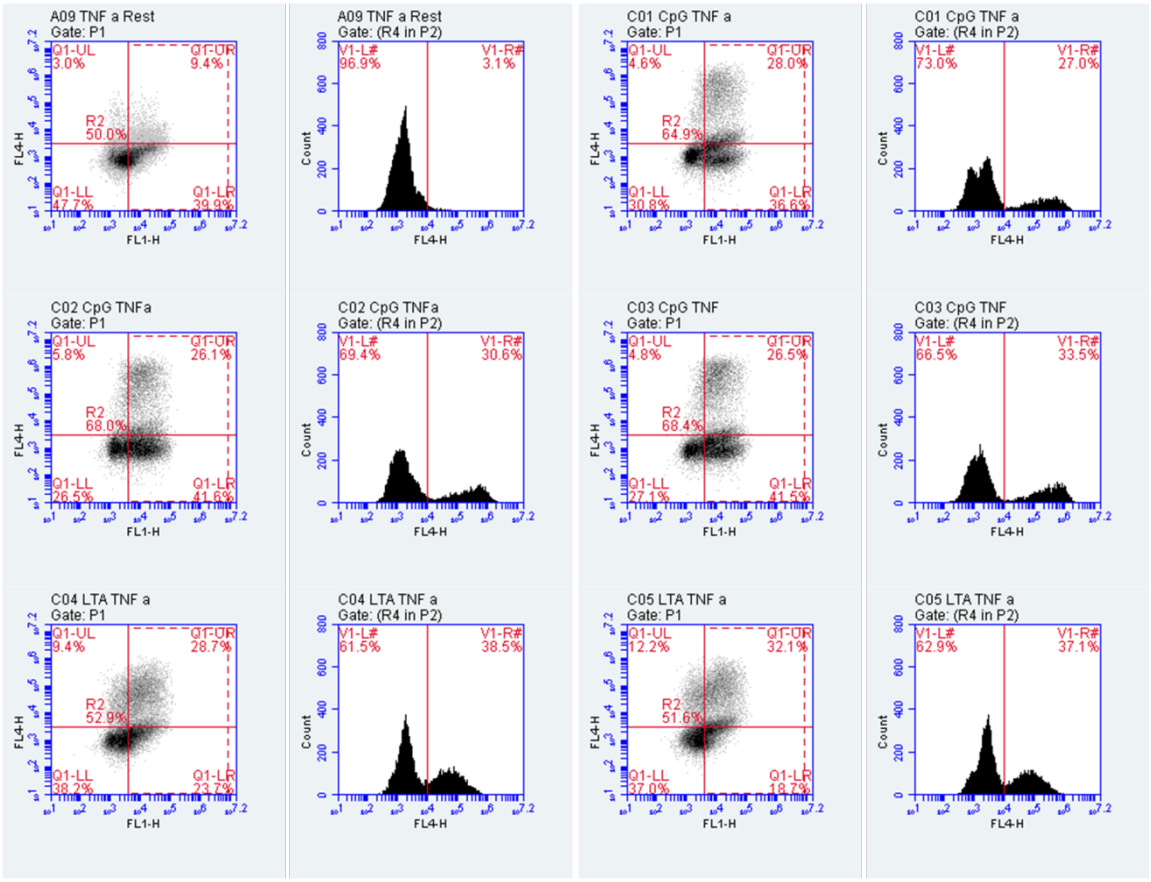
A09 TNF a Rest
Gate: P1
Q1-UL 3.0%
Q1-UR 9.4%
R2 50.0%
Q1-LL 47.7%
Q1-LR 39.9%
FL4-H
FL1-H
A09 TNF a Rest
Gate: (R4 in P2)
V1-L# 96.9%
V1-R# 3.1%
Count
FL4-H
C01 CpG TNF a
Gate: P1
Q1-UL 4.6%
Q1-UR 28.0%
R2 64.9%
Q1-LL 30.8%
Q1-LR 36.6%
FL4-H
FL1-H
C01 CpG TNF a
Gate: (R4 in P2)
V1-L# 73.0%
V1-R# 27.0%
Count
FL4-H
C02 CpG TNFa
Gate: P1
Q1-UL 5.8%
Q1-UR 26.1%
R2 68.0%
Q1-LL 26.5%
Q1-LR 41.6%
FL4-H
FL1-H
C02 CpG TNFa
Gate: (R4 in P2)
V1-L# 69.4%
V1-R# 30.6%
Count
FL4-H
C03 CpG TNF
Gate: P1
Q1-UL 4.8%
Q1-UR 26.5%
R2 68.4%
Q1-LL 27.1%
Q1-LR 41.5%
FL4-H
FL1-H
C03 CpG TNF
Gate: (R4 in P2)
V1-L# 66.5%
V1-R# 33.5%
Count
FL4-H
C04 LTA TNF a
Gate: P1
Q1-UL 9.4%
Q1-UR 28.7%
R2 52.9%
Q1-LL 38.2%
Q1-LR 23.7%
FL4-H
FL1-H
C04 LTA TNF a
Gate: (R4 in P2)
V1-L# 61.5%
V1-R# 38.5%
Count
FL4-H
C05 LTA TNF a
Gate: P1
Q1-UL 12.2%
Q1-UR 32.1%
R2 51.6%
Q1-LL 37.0%
Q1-LR 18.7%
FL4-H
FL1-H
C05 LTA TNF a
Gate: (R4 in P2)
V1-L# 62.9%
V1-R# 37.1%
Count
FL4-H

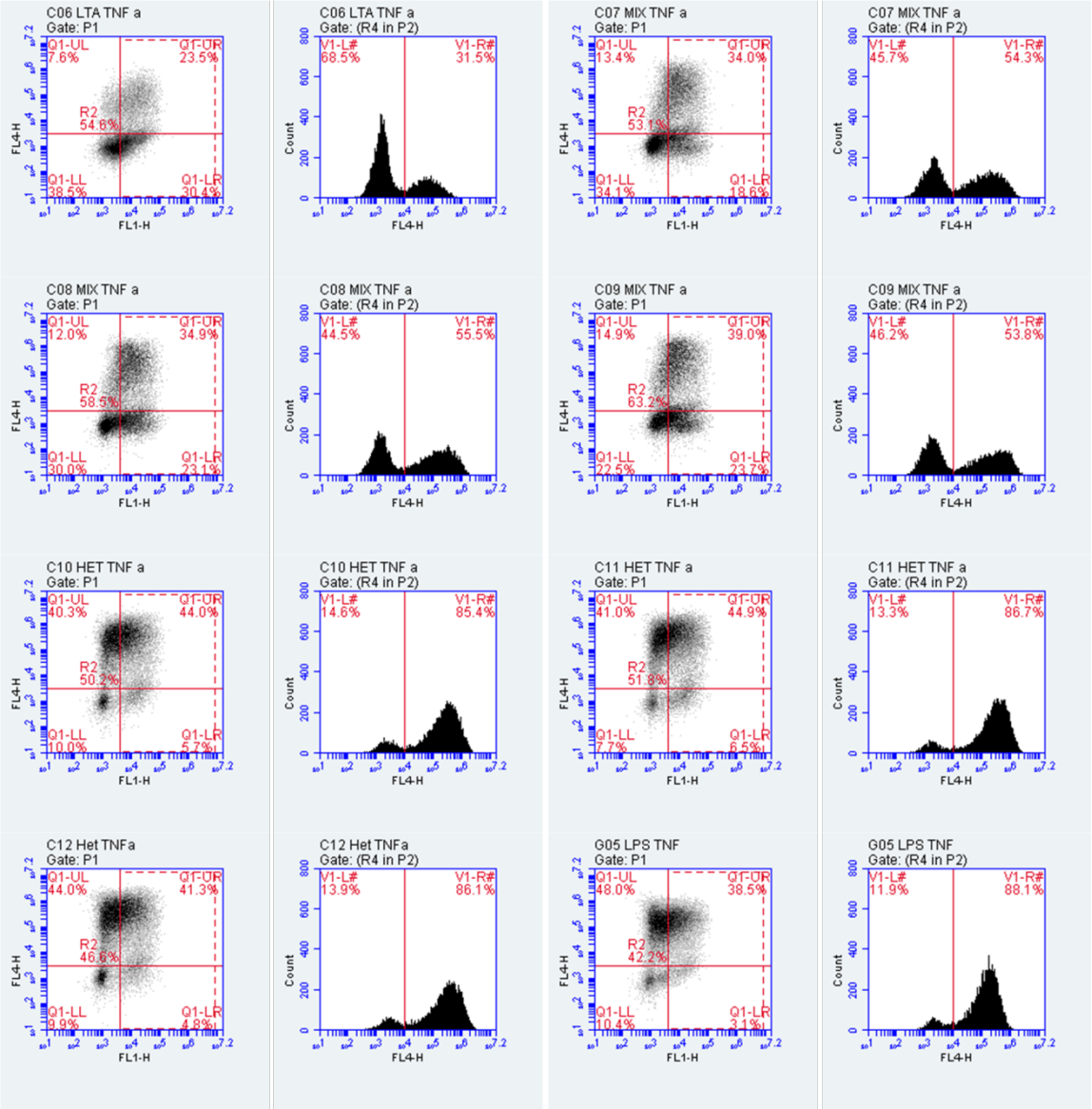
C06 LTA TNF a
Gate: P1
Q1-UL 7.6%
Q1-UR 23.5%
R2 54.8%
Q1-LL 38.5%
Q1-LR 30.4%
C06 LTA TNF a
Gate: (R4 in P2)
V1-L# 68.5%
V1-R# 31.5%
C07 MIX TNF a
Gate: P1
Q1-UL 13.4%
Q1-UR 34.0%
R2 53.1%
Q1-LL 34.1%
Q1-LR 18.6%
C07 MIX TNF a
Gate: (R4 in P2)
V1-L# 45.7%
V1-R# 54.3%
C08 MIX TNF a
Gate: P1
Q1-UL 12.0%
Q1-UR 34.9%
R2 58.5%
Q1-LL 30.0%
Q1-LR 23.1%
C08 MIX TNF a
Gate: (R4 in P2)
V1-L# 44.5%
V1-R# 55.5%
C09 MIX TNF a
Gate: P1
Q1-UL 14.9%
Q1-UR 39.0%
R2 63.2%
Q1-LL 22.5%
Q1-LR 23.7%
C09 MIX TNF a
Gate: (R4 in P2)
V1-L# 46.2%
V1-R# 53.8%
C10 HET TNF a
Gate: P1
Q1-UL 40.3%
Q1-UR 44.0%
R2 50.2%
Q1-LL 10.0%
Q1-LR 5.7%
C10 HET TNF a
Gate: (R4 in P2)
V1-L# 14.6%
V1-R# 85.4%
C11 HET TNF a
Gate: P1
Q1-UL 41.0%
Q1-UR 44.9%
R2 51.8%
Q1-LL 7.7%
Q1-LR 6.5%
C11 HET TNF a
Gate: (R4 in P2)
V1-L# 13.3%
V1-R# 86.7%
C12 Het TNFa
Gate: P1
Q1-UL 44.0%
Q1-UR 41.3%
R2 46.6%
Q1-LL 9.9%
Q1-LR 4.8%
C12 Het TNFa
Gate: (R4 in P2)
V1-L# 13.9%
V1-R# 86.1%
G05 LPS TNF
Gate: P1
Q1-UL 48.0%
Q1-UR 38.5%
R2 42.2%
Q1-LL 10.4%
Q1-LR 3.1%
G05 LPS TNF
Gate: (R4 in P2)
V1-L# 11.9%
V1-R# 88.1%
FL4-H
FL1-H
Count

IL-12

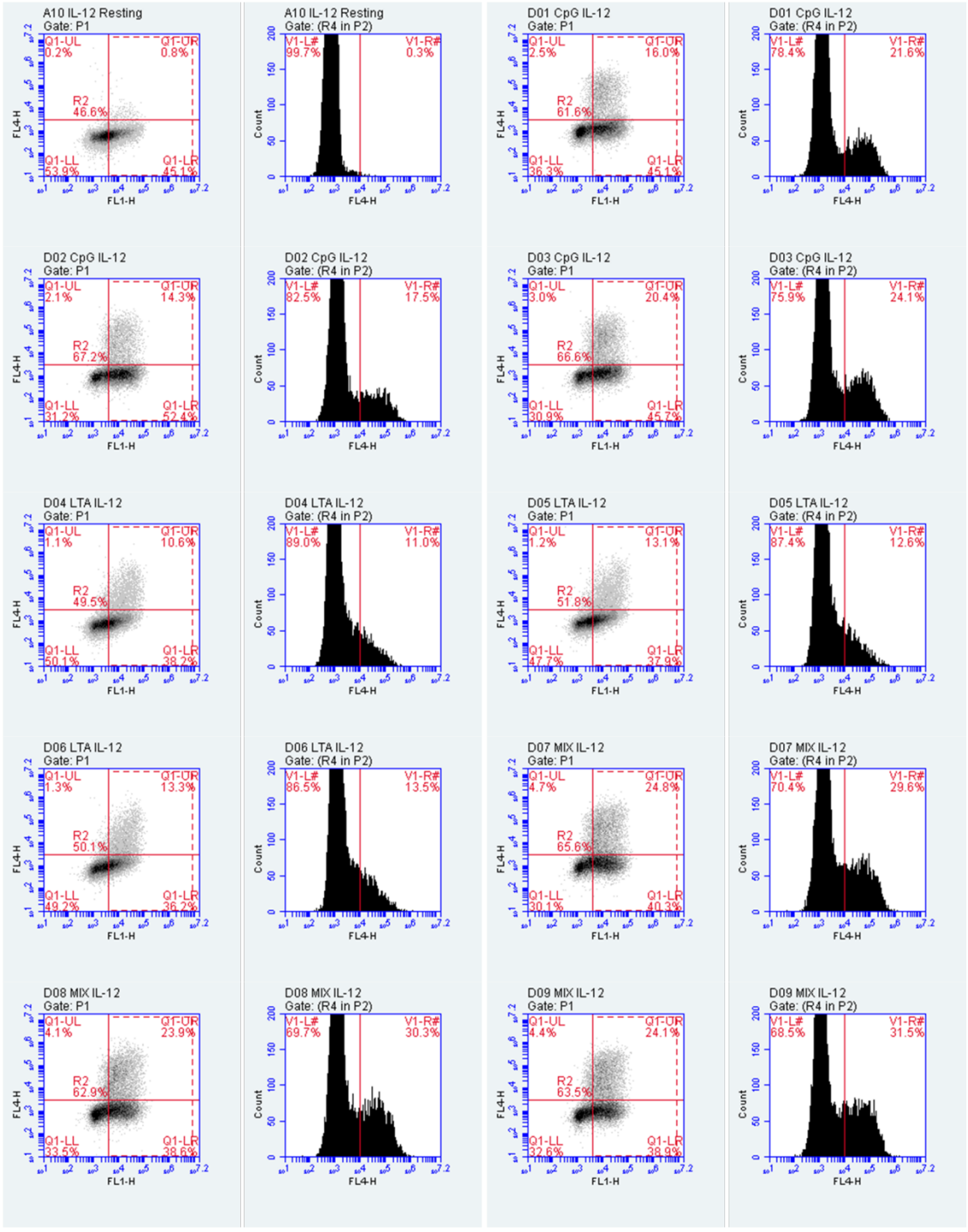
A10 IL-12 Resting
Gate: P1
Q1-UL 0.2%
Q1-UR 0.8%
R2 46.6%
Q1-LL 53.9%
Q1-LR 45.1%
FL1-H
FL4-H
A10 IL-12 Resting
Gate: (R4 in P2)
V1-L# 99.7%
V1-R# 0.3%
Count
D01 CpG IL-12
Gate: P1
Q1-UL 2.5%
Q1-UR 16.0%
R2 61.6%
Q1-LL 36.3%
Q1-LR 45.1%
D01 CpG IL-12
Gate: (R4 in P2)
V1-L# 78.4%
V1-R# 21.6%
D02 CpG IL-12
Gate: P1
Q1-UL 2.1%
Q1-UR 14.3%
R2 67.2%
Q1-LL 31.2%
Q1-LR 52.4%
D02 CpG IL-12
Gate: (R4 in P2)
V1-L# 82.5%
V1-R# 17.5%
D03 CpG IL-12
Gate: P1
Q1-UL 3.0%
Q1-UR 20.4%
R2 66.6%
Q1-LL 30.9%
Q1-LR 45.7%
D03 CpG IL-12
Gate: (R4 in P2)
V1-L# 75.9%
V1-R# 24.1%
D04 LTA IL-12
Gate: P1
Q1-UL 1.1%
Q1-UR 10.6%
R2 49.5%
Q1-LL 50.1%
Q1-LR 38.2%
D04 LTA IL-12
Gate: (R4 in P2)
V1-L# 89.0%
V1-R# 11.0%
D05 LTA IL-12
Gate: P1
Q1-UL 1.2%
Q1-UR 13.1%
R2 51.8%
Q1-LL 47.7%
Q1-LR 37.9%
D05 LTA IL-12
Gate: (R4 in P2)
V1-L# 87.4%
V1-R# 12.6%
D06 LTA IL-12
Gate: P1
Q1-UL 1.3%
Q1-UR 13.3%
R2 50.1%
Q1-LL 49.2%
Q1-LR 36.2%
D06 LTA IL-12
Gate: (R4 in P2)
V1-L# 86.5%
V1-R# 13.5%
D07 MIX IL-12
Gate: P1
Q1-UL 4.7%
Q1-UR 24.8%
R2 65.6%
Q1-LL 30.1%
Q1-LR 40.3%
D07 MIX IL-12
Gate: (R4 in P2)
V1-L# 70.4%
V1-R# 29.6%
D08 MIX IL-12
Gate: P1
Q1-UL 4.1%
Q1-UR 23.9%
R2 62.9%
Q1-LL 33.5%
Q1-LR 38.6%
D08 MIX IL-12
Gate: (R4 in P2)
V1-L# 69.7%
V1-R# 30.3%
D09 MIX IL-12
Gate: P1
Q1-UL 4.4%
Q1-UR 24.1%
R2 63.5%
Q1-LL 32.6%
Q1-LR 38.9%
D09 MIX IL-12
Gate: (R4 in P2)
V1-L# 68.5%
V1-R# 31.5%

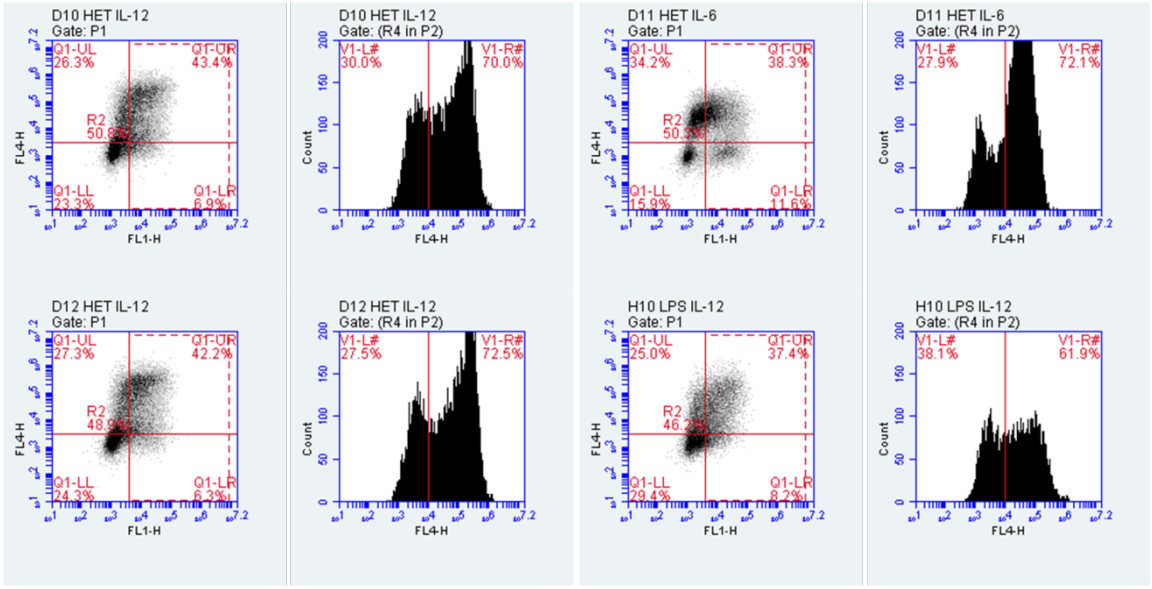
D10 HET IL-12
Gate: P1
Q1-UL 26.3%
Q1-UR 43.4%
R2 50.8%
Q1-LL 23.3%
Q1-LR 6.9%
FL4-H
FL1-H
D10 HET IL-12
Gate: (R4 in P2)
V1-L# 30.0%
V1-R# 70.0%
Count
FL4-H
D11 HET IL-6
Gate: P1
Q1-UL 34.2%
Q1-UR 38.3%
R2 50.5%
Q1-LL 15.9%
Q1-LR 11.6%
FL4-H
FL1-H
D11 HET IL-6
Gate: (R4 in P2)
V1-L# 27.9%
V1-R# 72.1%
Count
FL4-H
D12 HET IL-12
Gate: P1
Q1-UL 27.3%
Q1-UR 42.2%
R2 48.9%
Q1-LL 24.3%
Q1-LR 6.3%
FL4-H
FL1-H
D12 HET IL-12
Gate: (R4 in P2)
V1-L# 27.5%
V1-R# 72.5%
Count
FL4-H
H10 LPS IL-12
Gate: P1
Q1-UL 25.0%
Q1-UR 37.4%
R2 46.2%
Q1-LL 29.4%
Q1-LR 8.2%
FL4-H
FL1-H
H10 LPS IL-12
Gate: (R4 in P2)
V1-L# 38.1%
V1-R# 61.9%
Count
FL4-H

IL-6

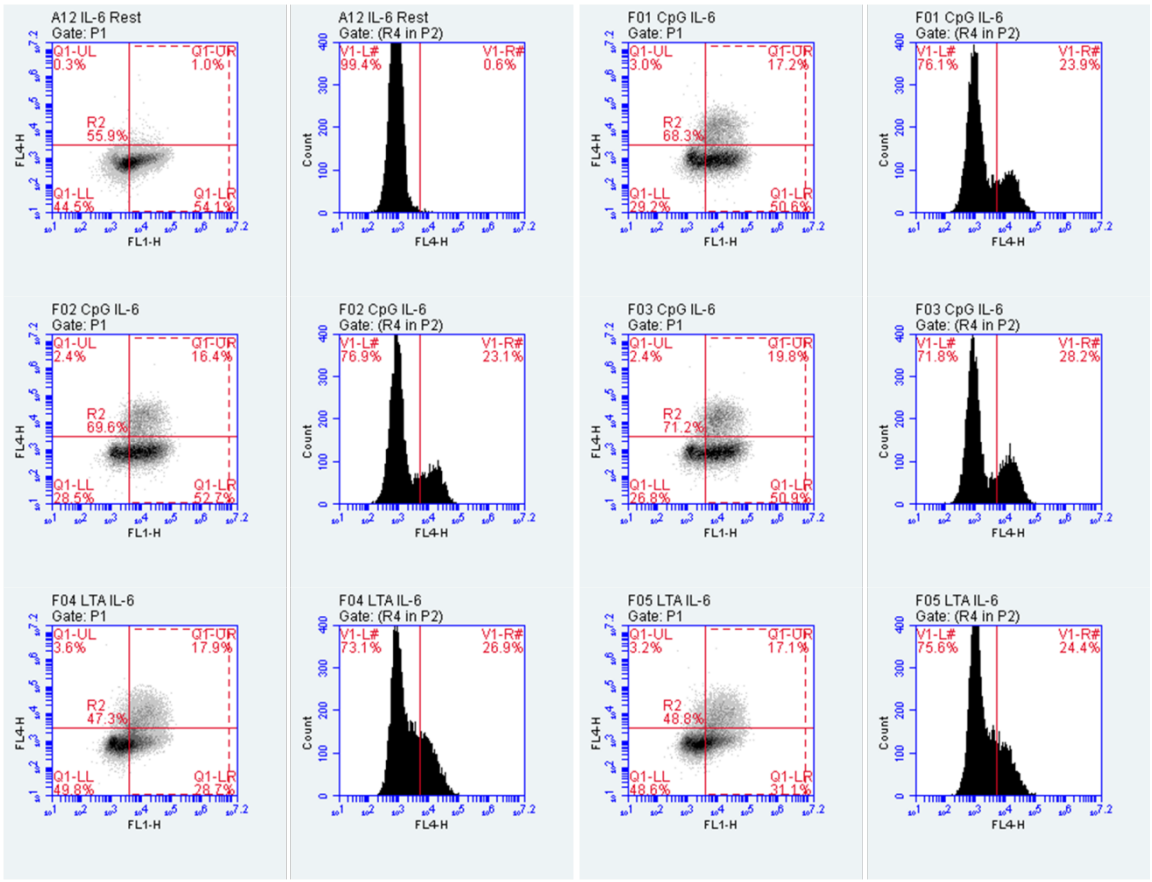
A12 IL-6 Rest
Gate: P1
Q1-UL 0.3%
Q1-UR 1.0%
R2 55.9%
Q1-LL 44.5%
Q1-LR 54.1%
FL4-H
FL1-H
A12 IL-6 Rest
Gate: (R4 in P2)
V1-L# 99.4%
V1-R# 0.6%
Count
FL4-H
F01 CpG IL-6
Gate: P1
Q1-UL 3.0%
Q1-UR 17.2%
R2 68.3%
Q1-LL 29.2%
Q1-LR 50.6%
FL4-H
FL1-H
F01 CpG IL-6
Gate: (R4 in P2)
V1-L# 76.1%
V1-R# 23.9%
Count
FL4-H
F02 CpG IL-6
Gate: P1
Q1-UL 2.4%
Q1-UR 16.4%
R2 69.6%
Q1-LL 28.5%
Q1-LR 52.7%
FL4-H
FL1-H
F02 CpG IL-6
Gate: (R4 in P2)
V1-L# 76.9%
V1-R# 23.1%
Count
FL4-H
F03 CpG IL-6
Gate: P1
Q1-UL 2.4%
Q1-UR 19.8%
R2 71.2%
Q1-LL 26.8%
Q1-LR 50.9%
FL4-H
FL1-H
F03 CpG IL-6
Gate: (R4 in P2)
V1-L# 71.8%
V1-R# 28.2%
Count
FL4-H
F04 LTA IL-6
Gate: P1
Q1-UL 3.6%
Q1-UR 17.9%
R2 47.3%
Q1-LL 49.8%
Q1-LR 28.7%
FL4-H
FL1-H
F04 LTA IL-6
Gate: (R4 in P2)
V1-L# 73.1%
V1-R# 26.9%
Count
FL4-H
F05 LTA IL-6
Gate: P1
Q1-UL 3.2%
Q1-UR 17.1%
R2 48.8%
Q1-LL 48.6%
Q1-LR 31.1%
FL4-H
FL1-H
F05 LTA IL-6
Gate: (R4 in P2)
V1-L# 75.6%
V1-R# 24.4%
Count
FL4-H

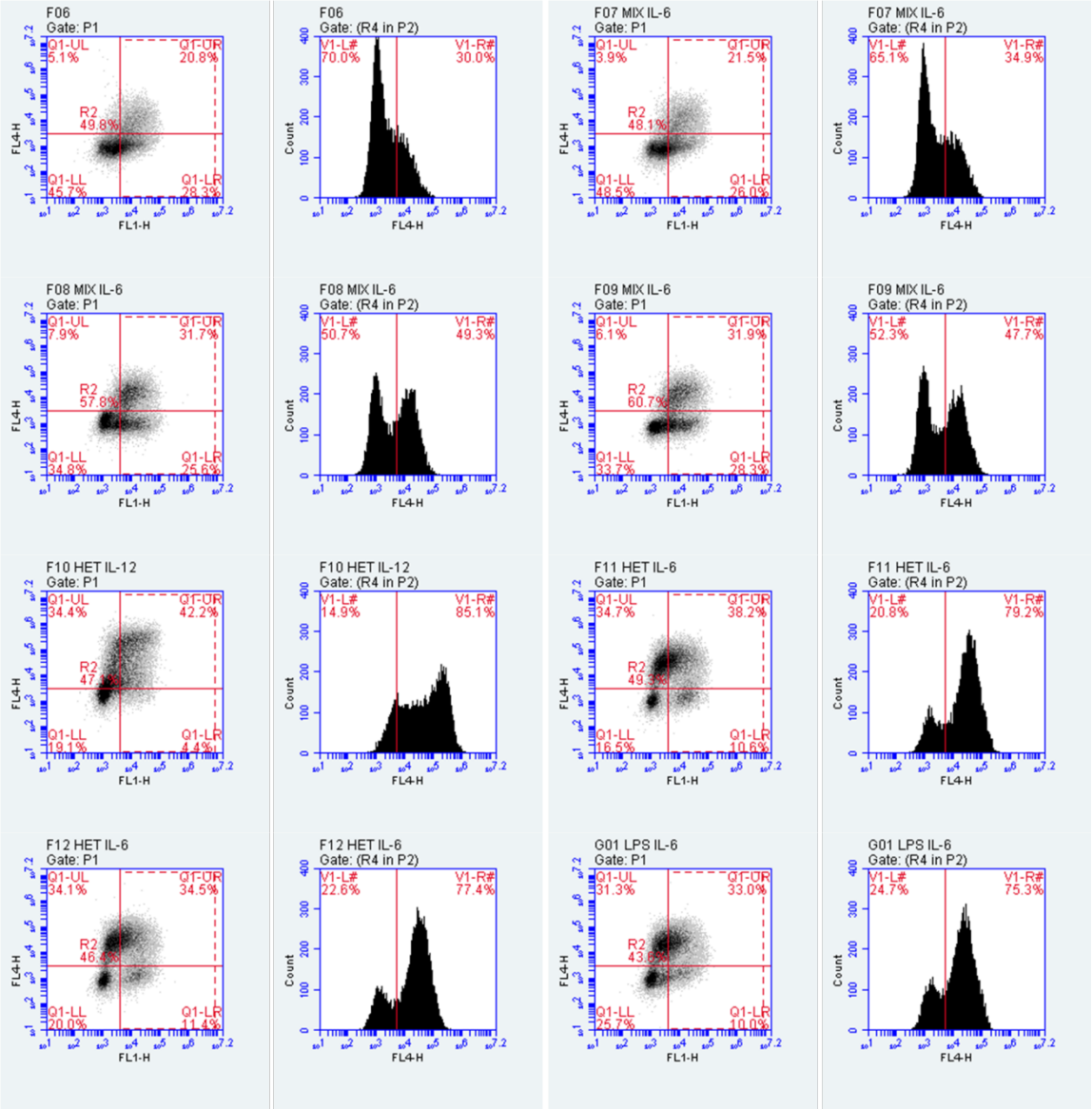
F06
Gate: P1
Q1-UL 5.1%
Q1-UR 20.8%
R2 49.8%
Q1-LL 45.7%
Q1-LR 28.3%
FL4-H
FL1-H
F06
Gate: (R4 in P2)
V1-L# 70.0%
V1-R# 30.0%
Count
FL4-H
F07 MIX IL-6
Gate: P1
Q1-UL 3.9%
Q1-UR 21.5%
R2 48.1%
Q1-LL 48.5%
Q1-LR 26.0%
FL4-H
FL1-H
F07 MIX IL-6
Gate: (R4 in P2)
V1-L# 65.1%
V1-R# 34.9%
Count
FL4-H
F08 MIX IL-6
Gate: P1
Q1-UL 7.9%
Q1-UR 31.7%
R2 57.8%
Q1-LL 34.8%
Q1-LR 25.6%
FL4-H
FL1-H
F08 MIX IL-6
Gate: (R4 in P2)
V1-L# 50.7%
V1-R# 49.3%
Count
FL4-H
F09 MIX IL-6
Gate: P1
Q1-UL 6.1%
Q1-UR 31.9%
R2 60.7%
Q1-LL 33.7%
Q1-LR 28.3%
FL4-H
FL1-H
F09 MIX IL-6
Gate: (R4 in P2)
V1-L# 52.3%
V1-R# 47.7%
Count
FL4-H
F10 HET IL-12
Gate: P1
Q1-UL 34.4%
Q1-UR 42.2%
Q1-LL 19.1%
Q1-LR 4.4%
FL4-H
FL1-H
F10 HET IL-12
Gate: (R4 in P2)
V1-L# 14.9%
V1-R# 85.1%
Count
FL4-H
F11 HET IL-6
Gate: P1
Q1-UL 34.7%
Q1-UR 38.2%
Q1-LL 16.5%
Q1-LR 10.6%
FL4-H
FL1-H
F11 HET IL-6
Gate: (R4 in P2)
V1-L# 20.8%
V1-R# 79.2%
Count
FL4-H
F12 HET IL-6
Gate: P1
Q1-UL 34.1%
Q1-UR 34.5%
Q1-LL 20.0%
Q1-LR 11.4%
FL4-H
FL1-H
F12 HET IL-6
Gate: (R4 in P2)
V1-L# 22.6%
V1-R# 77.4%
Count
FL4-H
G01 LPS IL-6
Gate: P1
Q1-UL 31.3%
Q1-UR 33.0%
Q1-LL 25.7%
Q1-LR 10.0%
FL4-H
FL1-H
G01 LPS IL-6
Gate: (R4 in P2)
V1-L# 24.7%
V1-R# 75.3%
Count
FL4-H

IL-10

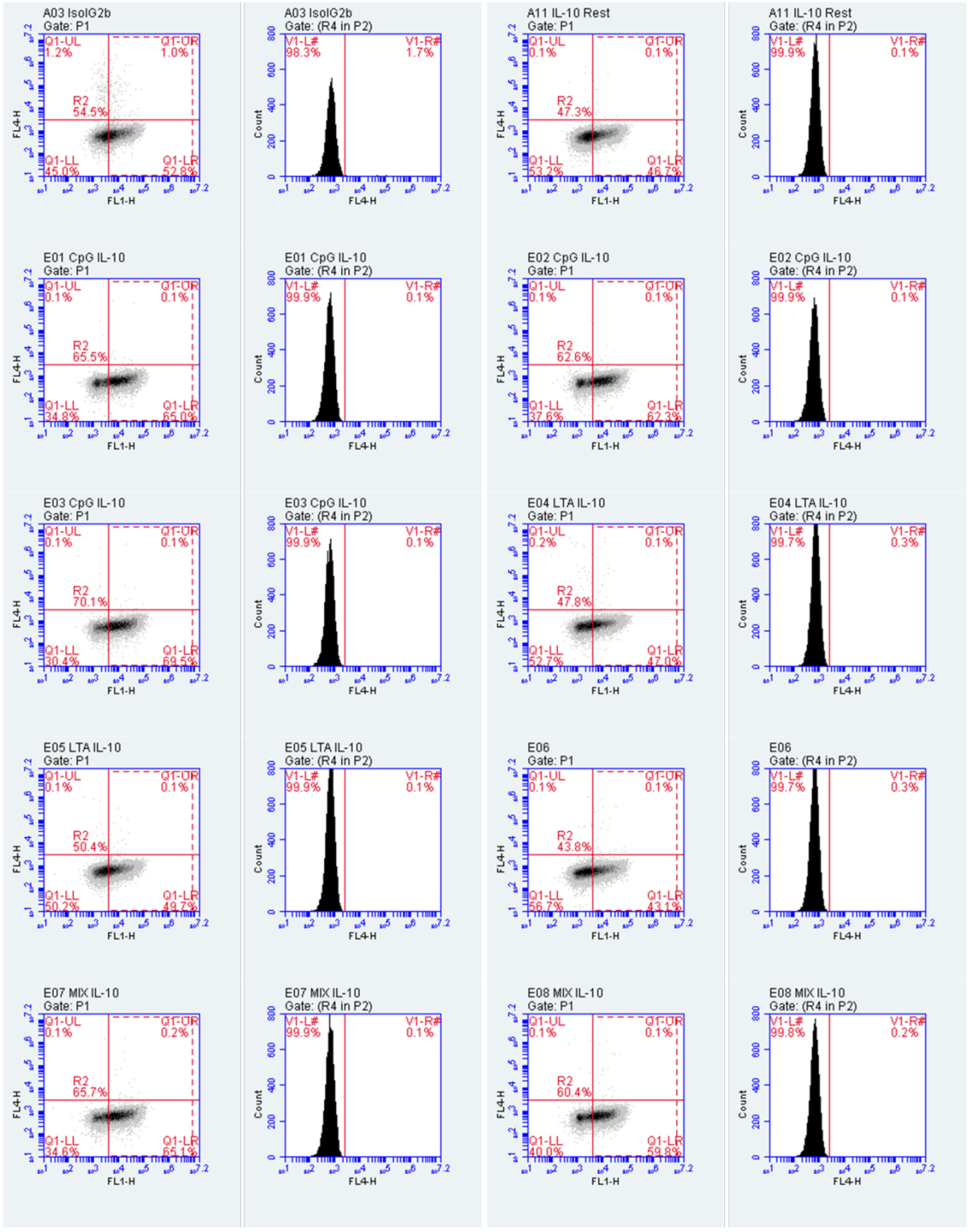
A03 IsoIG2b
Gate: P1
Q1-UL 1.2%
Q1-UR 1.0%
R2 54.5%
Q1-LL 45.0%
Q1-LR 52.8%
FL4-H
FL1-H
A03 IsoIG2b
Gate: (R4 in P2)
V1-L# 98.3%
V1-R# 1.7%
Count
FL4-H
A11 IL-10 Rest
Gate: P1
Q1-UL 0.1%
Q1-UR 0.1%
R2 47.3%
Q1-LL 53.2%
Q1-LR 46.7%
FL4-H
FL1-H
A11 IL-10 Rest
Gate: (R4 in P2)
V1-L# 99.9%
V1-R# 0.1%
Count
FL4-H
E01 CpG IL-10
Gate: P1
Q1-UL 0.1%
Q1-UR 0.1%
R2 65.5%
Q1-LL 34.8%
Q1-LR 65.0%
FL4-H
FL1-H
E01 CpG IL-10
Gate: (R4 in P2)
V1-L# 99.9%
V1-R# 0.1%
Count
FL4-H
E02 CpG IL-10
Gate: P1
Q1-UL 0.1%
Q1-UR 0.1%
R2 62.6%
Q1-LL 37.6%
Q1-LR 62.3%
FL4-H
FL1-H
E02 CpG IL-10
Gate: (R4 in P2)
V1-L# 99.9%
V1-R# 0.1%
Count
FL4-H
E03 CpG IL-10
Gate: P1
Q1-UL 0.1%
Q1-UR 0.1%
R2 70.1%
Q1-LL 30.4%
Q1-LR 69.5%
FL4-H
FL1-H
E03 CpG IL-10
Gate: (R4 in P2)
V1-L# 99.9%
V1-R# 0.1%
Count
FL4-H
E04 LTA IL-10
Gate: P1
Q1-UL 0.2%
Q1-UR 0.1%
R2 47.8%
Q1-LL 52.7%
Q1-LR 47.0%
FL4-H
FL1-H
E04 LTA IL-10
Gate: (R4 in P2)
V1-L# 99.7%
V1-R# 0.3%
Count
FL4-H
E05 LTA IL-10
Gate: P1
Q1-UL 0.1%
Q1-UR 0.1%
R2 50.4%
Q1-LL 50.2%
Q1-LR 49.7%
FL4-H
FL1-H
E05 LTA IL-10
Gate: (R4 in P2)
V1-L# 99.9%
V1-R# 0.1%
Count
FL4-H
E06
Gate: P1
Q1-UL 0.1%
Q1-UR 0.1%
R2 43.8%
Q1-LL 56.7%
Q1-LR 43.1%
FL4-H
FL1-H
E06
Gate: (R4 in P2)
V1-L# 99.7%
V1-R# 0.3%
Count
FL4-H
E07 MIX IL-10
Gate: P1
Q1-UL 0.1%
Q1-UR 0.2%
R2 65.7%
Q1-LL 34.6%
Q1-LR 65.1%
FL4-H
FL1-H
E07 MIX IL-10
Gate: (R4 in P2)
V1-L# 99.9%
V1-R# 0.1%
Count
FL4-H
E08 MIX IL-10
Gate: P1
Q1-UL 0.1%
Q1-UR 0.1%
R2 60.4%
Q1-LL 40.0%
Q1-LR 59.8%
FL4-H
FL1-H
E08 MIX IL-10
Gate: (R4 in P2)
V1-L# 99.8%
V1-R# 0.2%
Count
FL4-H

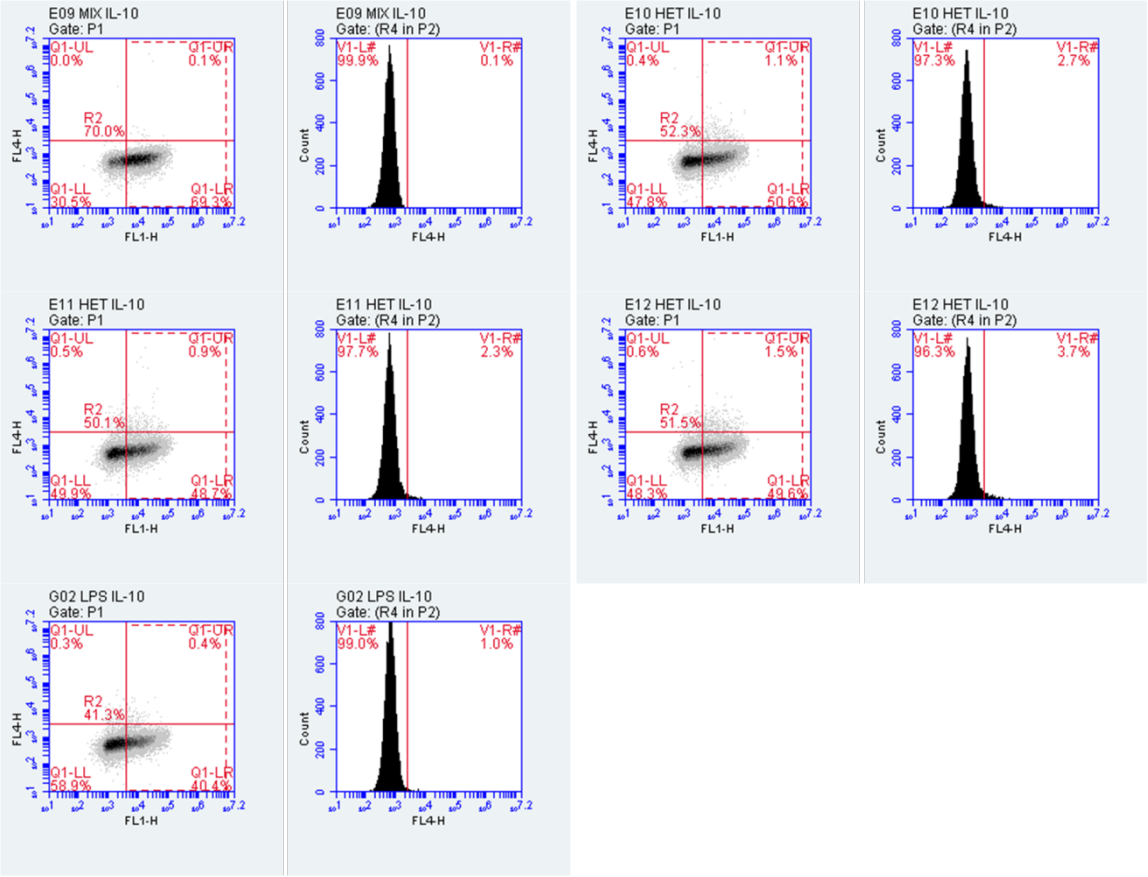

References

(1) Morath, S.; Geyer, A.; Spreitzer, I.; Hermann, C.; Hartung, T. Structural Decomposition and Heterogeneity of Commercial Lipoteichoic Acid Preparations. *Infect. Immun.* **2002**, *70* (2), 938–944.

(2) Matheu, M. P.; Sen, D.; Cahalan, M. D.; Parker, I. Generation of Bone Marrow Derived Murine Dendritic Cells for Use in 2-Photon Imaging. *J. Vis. Exp. JoVE* **2008**, No. 17.

Appendix C: Chapter 4

Synthetic Schemes.

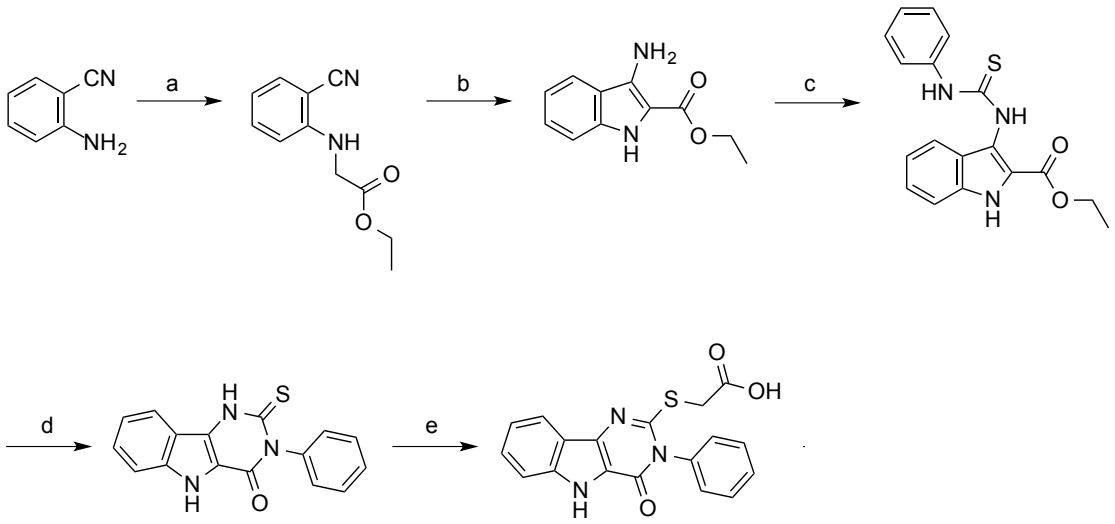

Scheme S4.1. Synthetic scheme of pyrimido-indole by Chan, M. *et al*.[1] a) $BrCH_2COOEt$, $NaHCO_3$, EtOH, reflux; b) potassium tert-butoxide, THF, <30 °C; c) phenyl-NCS, EtOH, reflux; d) PPA, 110 °C; e) $ClCH_2COOH$, KOH/EtOH, reflux.

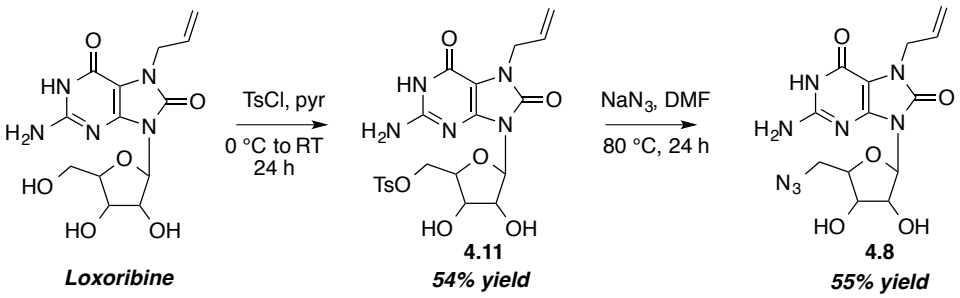

Loxoribine **4.11** ***54% yield*** **4.8** ***55% yield***

Scheme S4.2. Synthesis of azide-modified loxoribine.

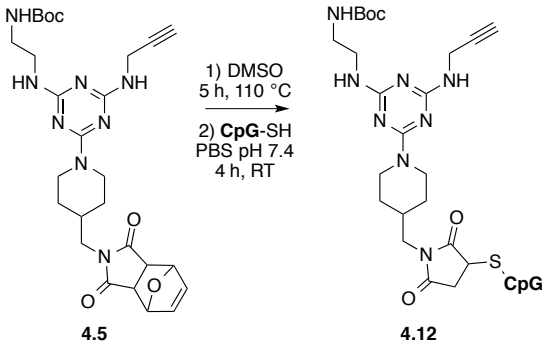

Scheme S4.3. Synthesis of CpG_core.

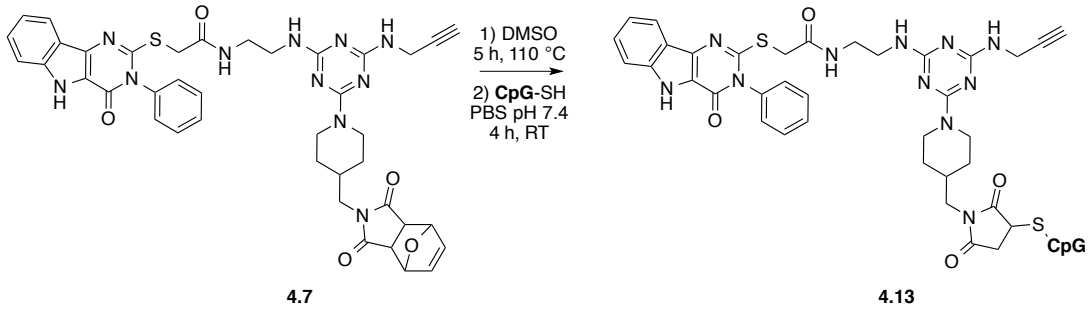

Scheme S4.4. Synthesis of Indole_CpG.

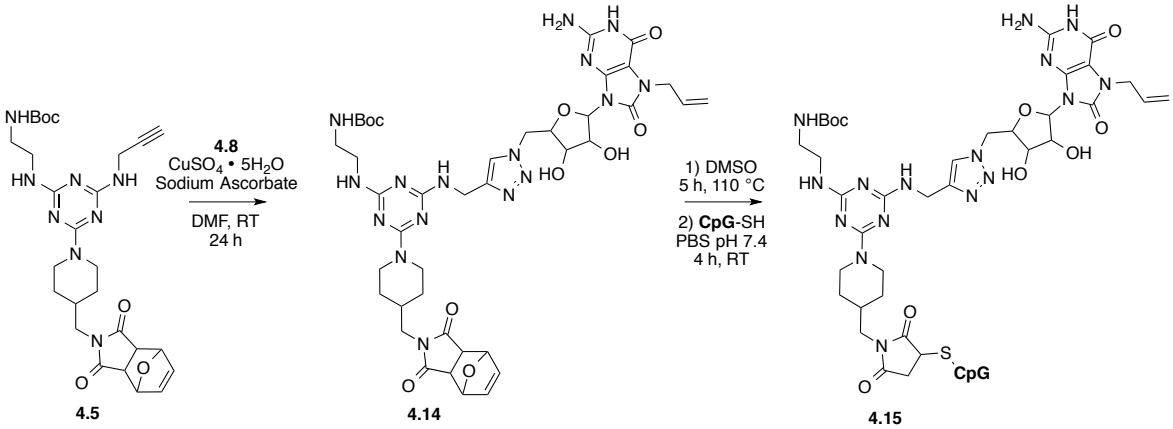

Scheme S4.5. Synthesis of Lox_CpG.

Supplemental Figures.

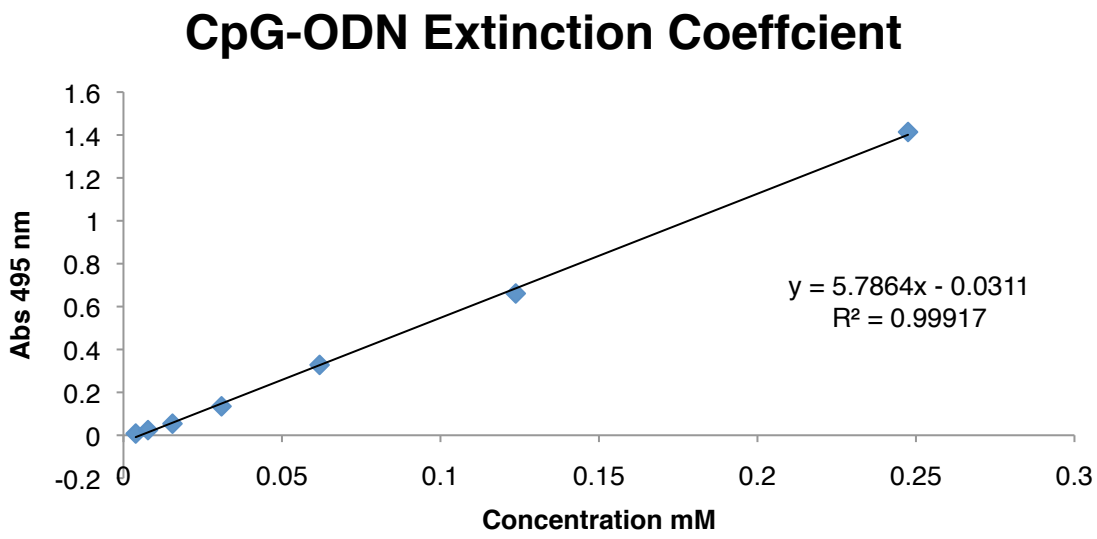

Figure S4.1. Calibration line for the extinction coefficient of 5'-C6 thiol modified CpG-ODN1826-6-FAM-3' using a NanoDrop spectrophotometer at 495 nm.

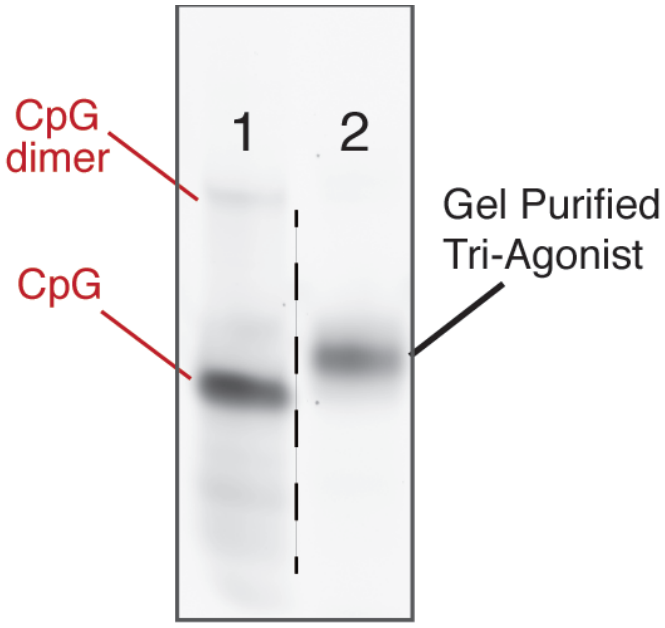

Figure S4.2. Gel of extracted, purified tri-agonist (lane 2) in comparison to CpG reference (lane 1), showing the isolated product as one band.

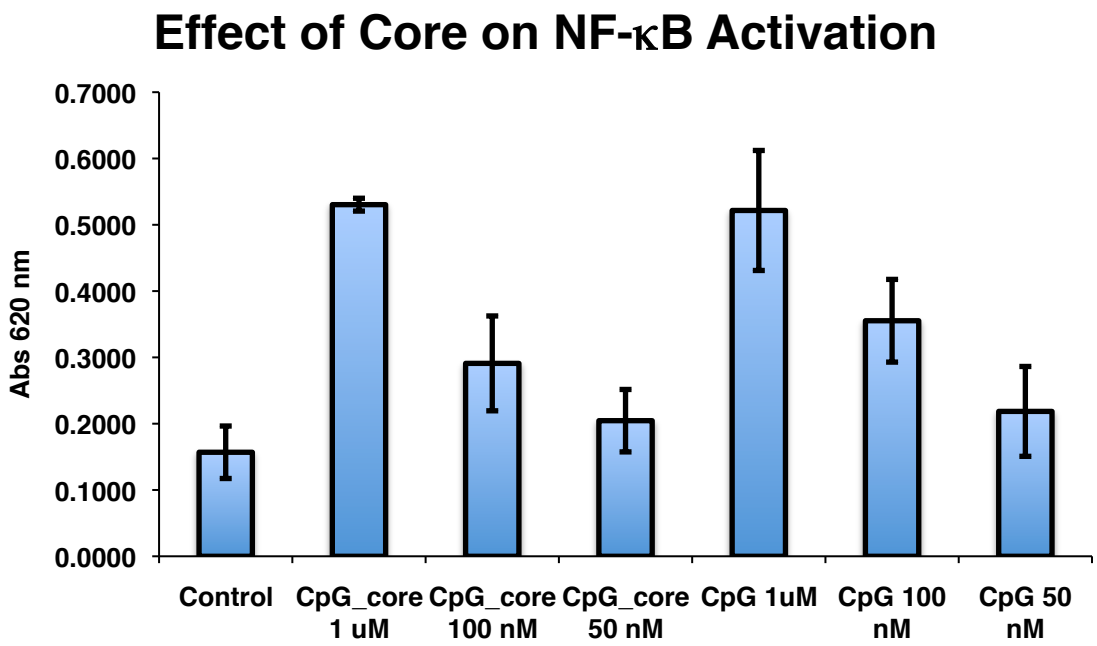

Figure S4.3. RAW264.7 macrophage NF-κB stimulation measured *via* alkaline phosphatase secretion. RAW-Blue cells were treated with each compound for 18 h at 37 °C. Supernatant was then incubated with Quanti-Blue solution for 1 h at 37 °C and analyzed at 620 nm, demonstrating that the core did not affect CpG NF-κB activity. Data is a result of n=3. Results are expressed as the mean ± SD.

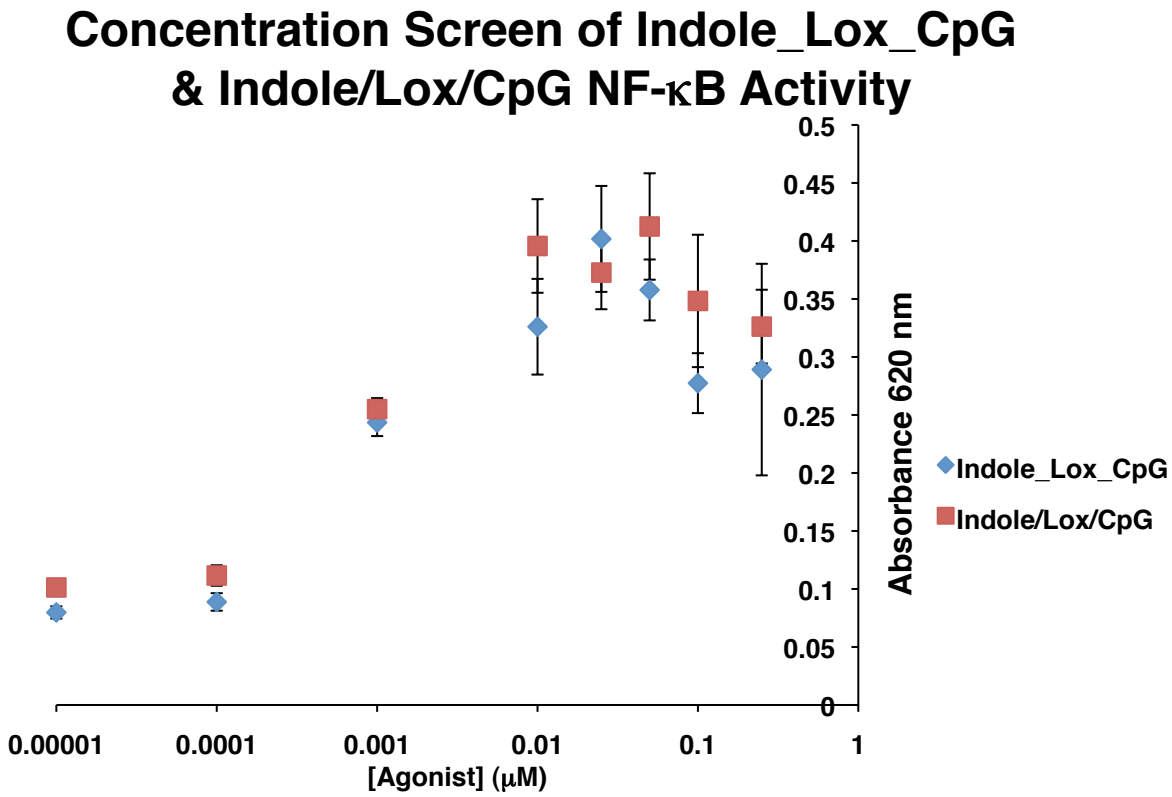

Figure S4.4. RAW264.7 macrophage NF-κB stimulation measured *via* alkaline phosphatase secretion. RAW-Blue cells were treated with the tri-agonist at concentrations ranging from 10 pM to 0.25 μM for 18 h at 37 °C. Supernatant was then incubated with Quanti-Blue solution for 1 h at 37 °C and analyzed at 620 nm. Data is a result of n=3. Results are expressed as the mean ± SD.

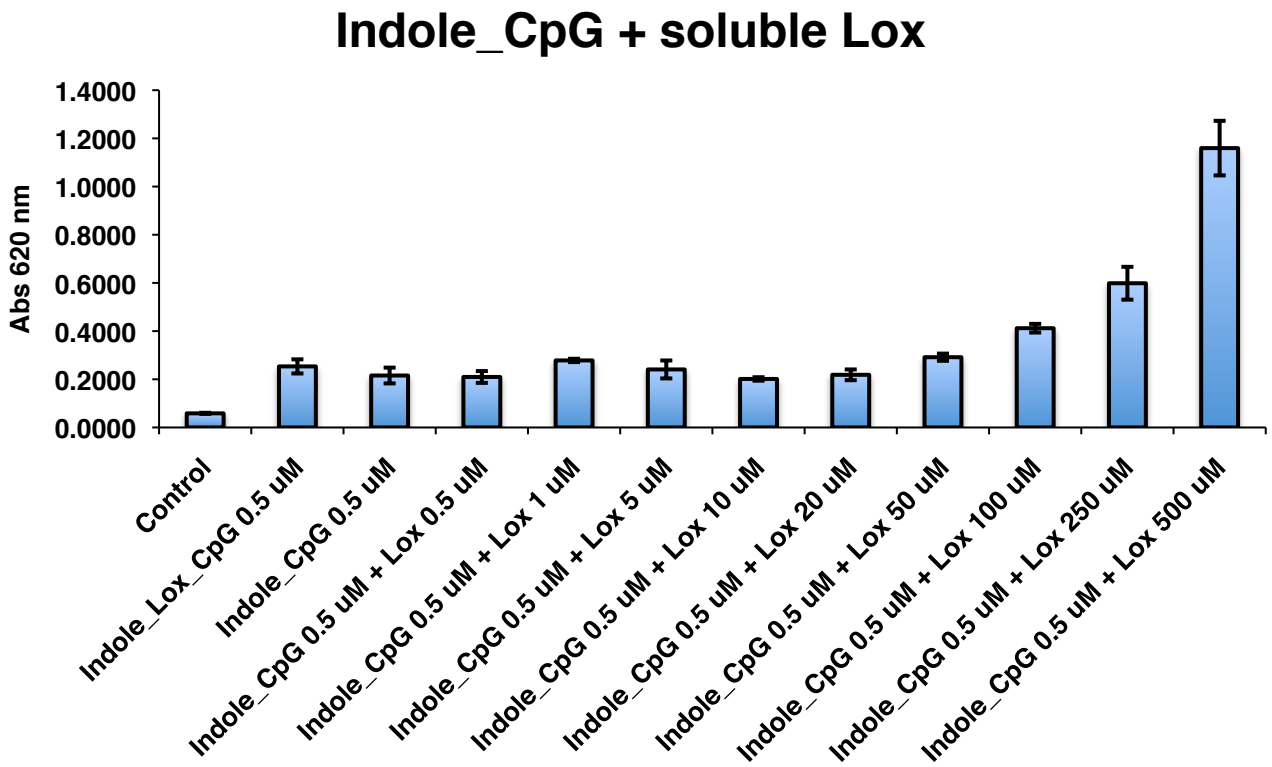

Figure S4.5. RAW264.7 macrophage NF-κB stimulation measured *via* alkaline phosphatase secretion. RAW-Blue cells were treated with the tri-agonist (0.5 μM) or Indole_CpG (0.5 μM) with soluble Lox (at designated concentration) for 18 h at 37 °C. Supernatant was then incubated with Quanti-Blue solution for 1 h at 37 °C and analyzed at 620 nm. An increase in NF-κB activity compared to Indole_CpG (0.5 μM) was not observed until adding in a high concentration of Lox (at least 50 μM, *$p < 0.05$) to Indole_CpG (0.5 μM). These results demonstrated how Lox is a weak agonist, so little effect should be expected from the mixture of three agonists. Data is the result of n=3. Results are expressed as the mean ± SD.

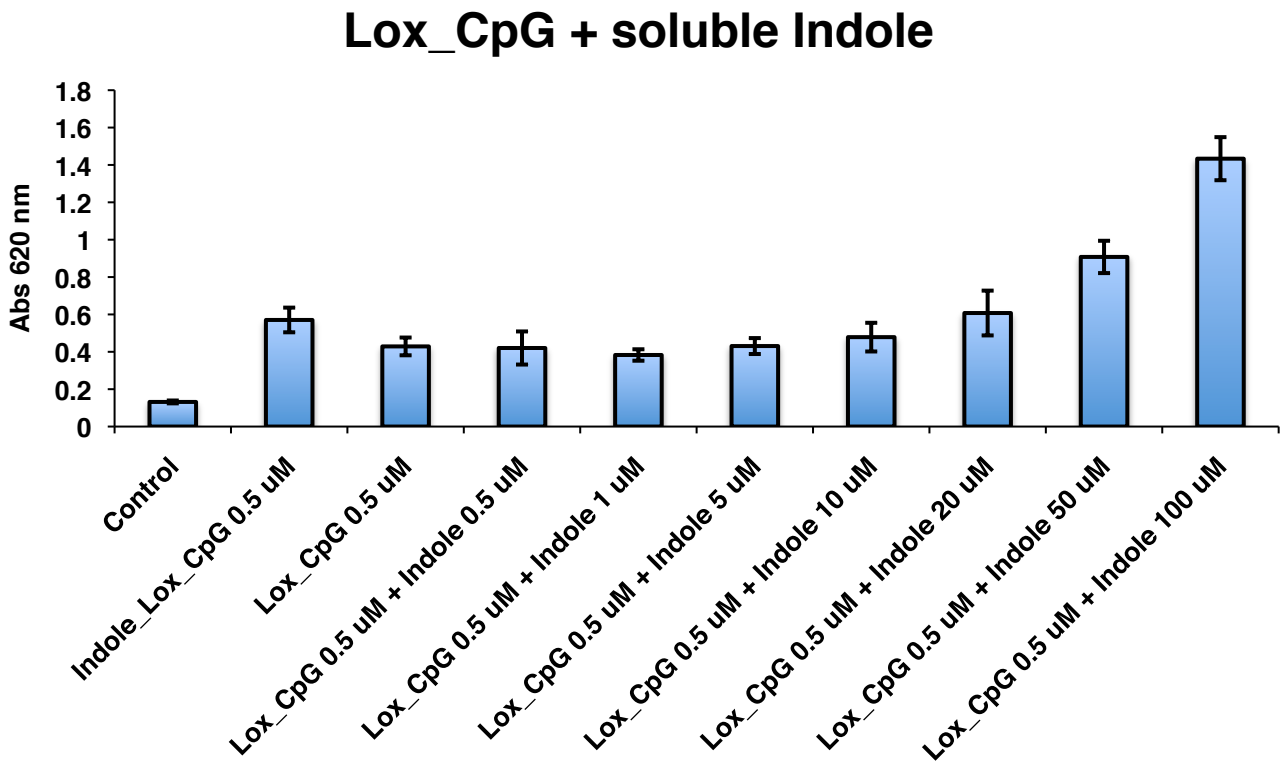

Figure S4.6. RAW264.7 macrophage NF-κB stimulation measured *via* alkaline phosphatase secretion. RAW-Blue cells were treated with the tri-agonist (0.5 μM) or Lox_CpG (0.5 μM) with soluble Indole (at designated concentration) for 18 h at 37 °C. Supernatant was then incubated with Quanti-Blue solution for 1 h at 37 °C and analyzed at 620 nm. An increase of NF-κB activity compared to Lox_CpG (0.5 μM) was not observed until adding in a high concentration of Indole (at least 50 μM, $^{**}p < 0.01$) to Lox_CpG (0.5 μM). These results demonstrated the importance of covalently linking the three agonists. Data is the result of n=3. Results are expressed as the mean ± SD.

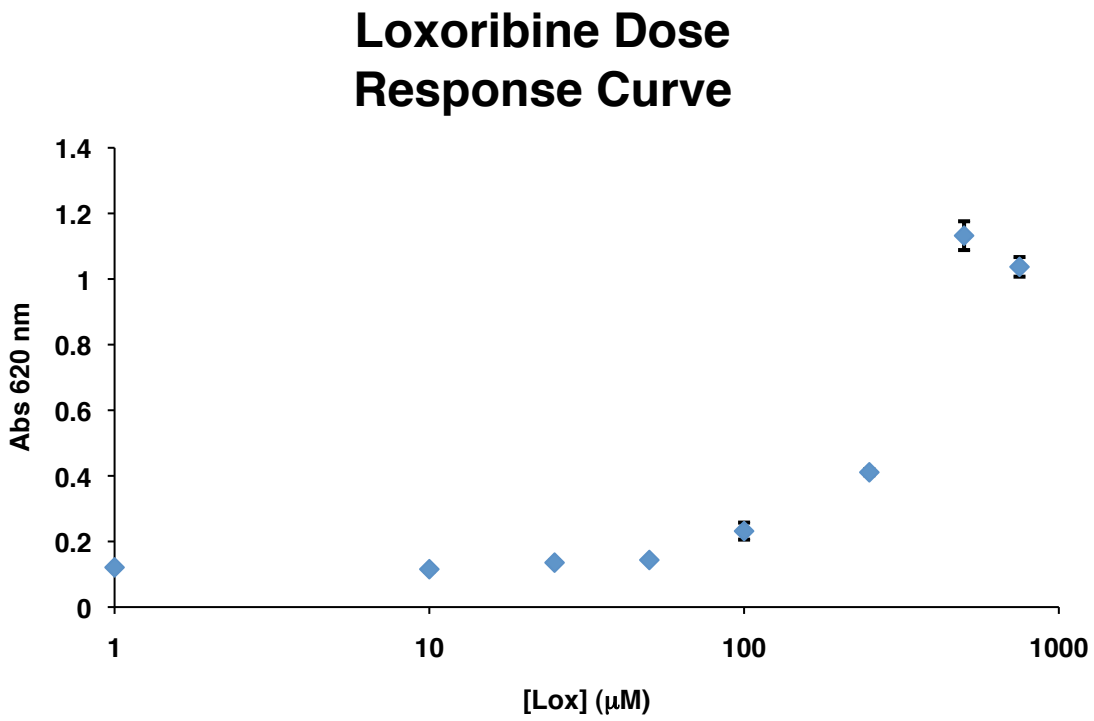

Figure S4.7. RAW264.7 macrophage NF-κB stimulation measured *via* alkaline phosphatase secretion. RAW-Blue cells were treated with increasing concentrations of loxoribine for 18 h at 37 °C. Supernatant was then incubated with Quanti-Blue solution for 1 h at 37 °C and analyzed at 620 nm. Data is the result of n=3. Results are expressed as the mean ± SD.

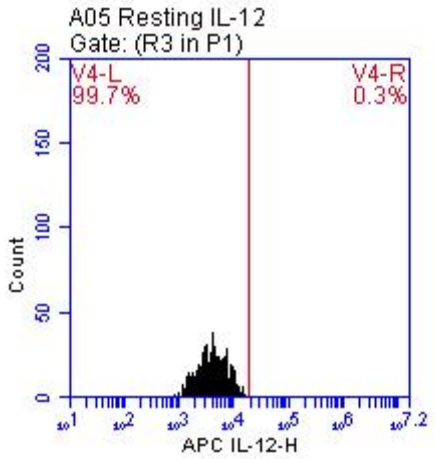
A05 Resting IL-12
Gate: (R3 in P1)
V4-L
99.7%
V4-R
0.3%
Count
APC IL-12-H

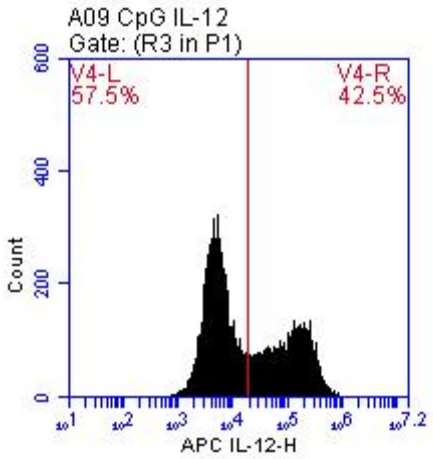
A09 CpG IL-12
Gate: (R3 in P1)
V4-L
57.5%
V4-R
42.5%
Count
APC IL-12-H

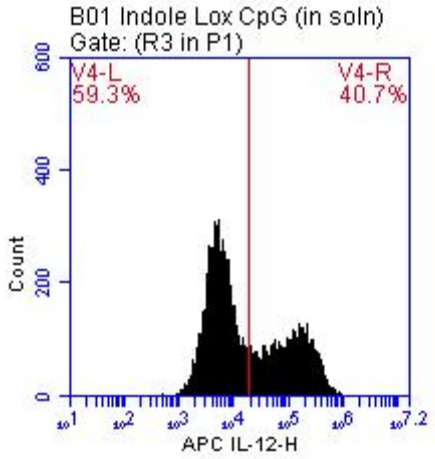
B01 Indole Lox CpG (in soln)
Gate: (R3 in P1)
V4-L
59.3%
V4-R
40.7%
Count
APC IL-12-H

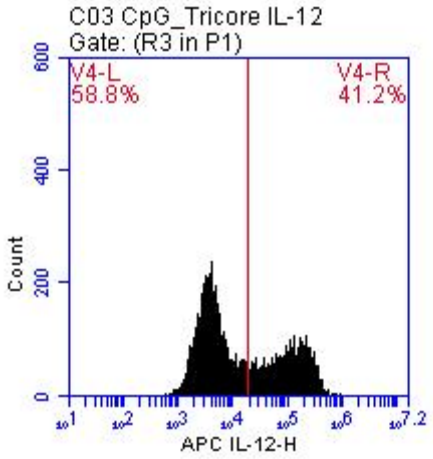
C03 CpG_Tricore IL-12
Gate: (R3 in P1)
V4-L
58.8%
V4-R
41.2%
Count
APC IL-12-H

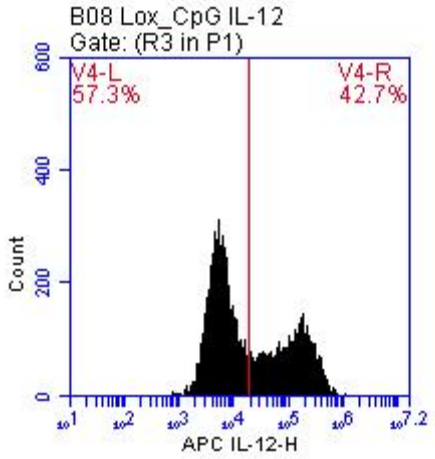
B08 Lox_CpG IL-12
Gate: (R3 in P1)
V4-L
57.3%
V4-R
42.7%
Count
APC IL-12-H

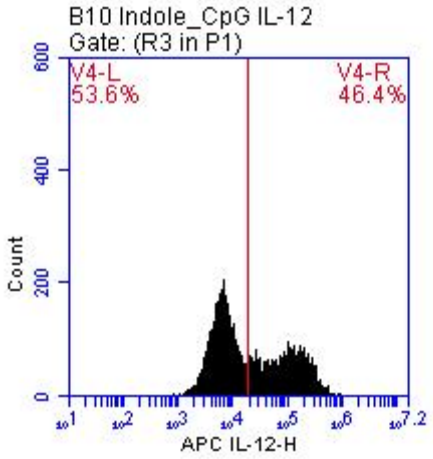
B10 Indole_CpG IL-12
Gate: (R3 in P1)
V4-L
53.6%
V4-R
46.4%
Count
APC IL-12-H

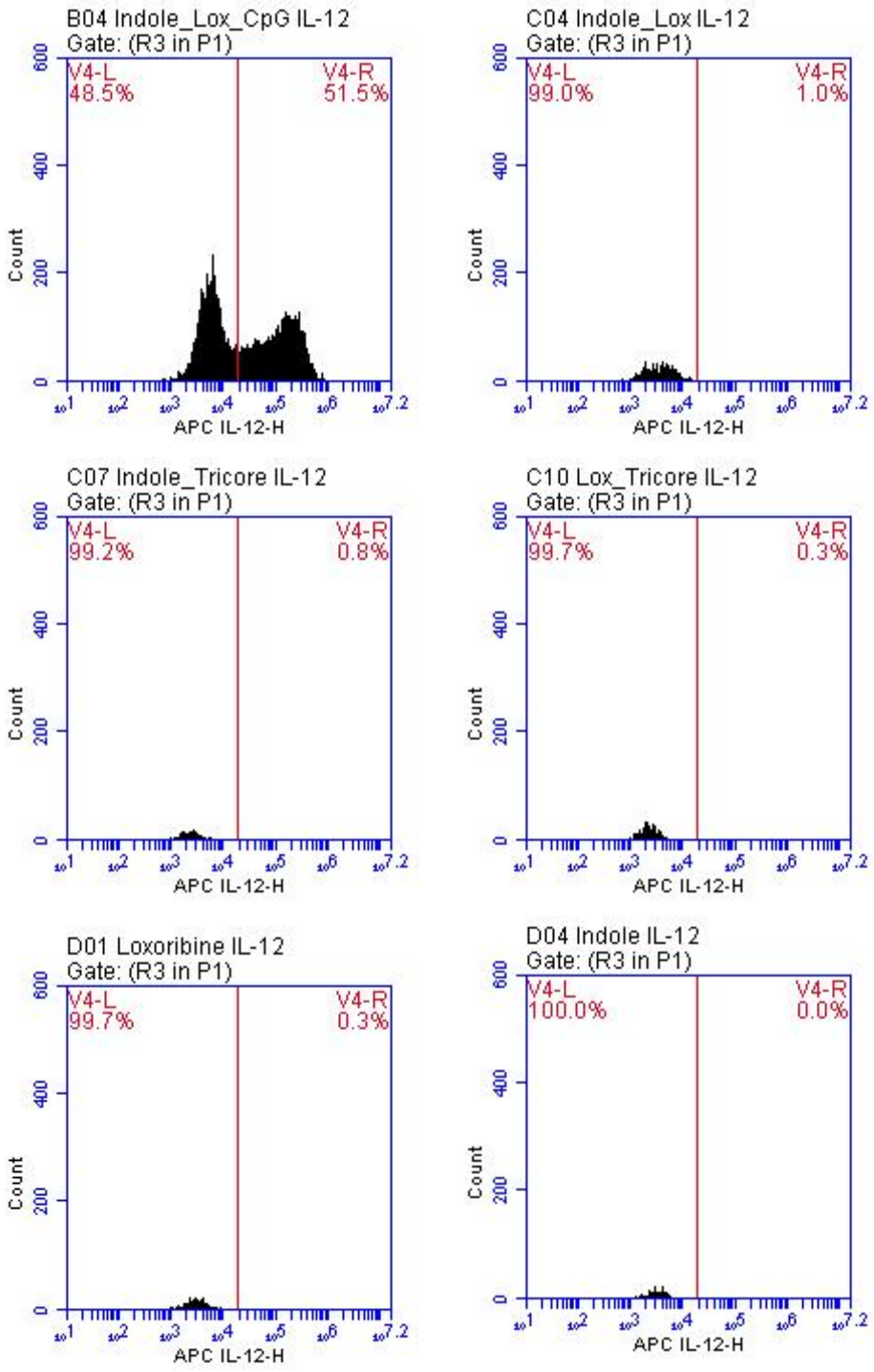

Figure S4.8. Representative FACS histograms of BMDC IL-12 production when incubated with no agonist (Resting), CpG-ODN, Indole/Lox/CpG, CpG_core, Lox_CpG, Indole_CpG (page S6), Indole_Lox_CpG, Indole_Lox, Indole_core, Lox_core, Loxoribine, and Indole (page S18) at 0.5 μM. BMDCs were incubated with the designated agonist for 6 h at 37 °C and subsequently stained with FITC CD11c and APC IL-12 (ICS). Data was obtained over three independent experiments.

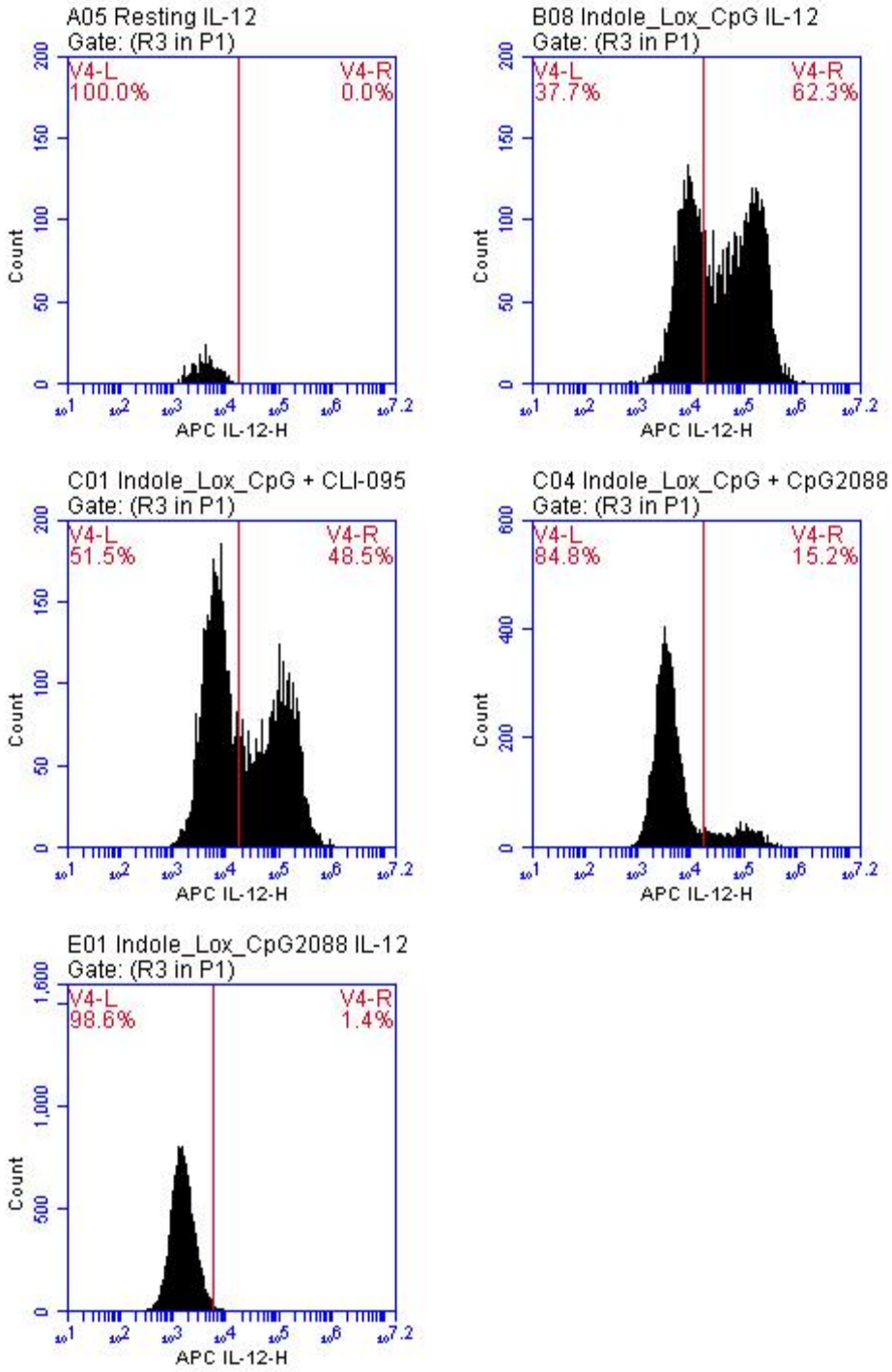

Figure S4.9. Representative FACS histograms of BMDC IL-12 production when incubated with no agonist (Resting), Indole_Lox_CpG, Indole_Lox_CpG with CLI-095 (100 nM), Indole_Lox_CpG with CpG2088 (100nM), and Indole_Lox_CpG2088 at 0.5 μM. BMDCs were incubated with the designated inhibitor for 1 h at 37 °C and then the designated agonist for an additional 6 h at 37 °C. Cells were subsequently stained with FITC CD11c and APC IL-12 (ICS). Data was obtained over three independent experiments.

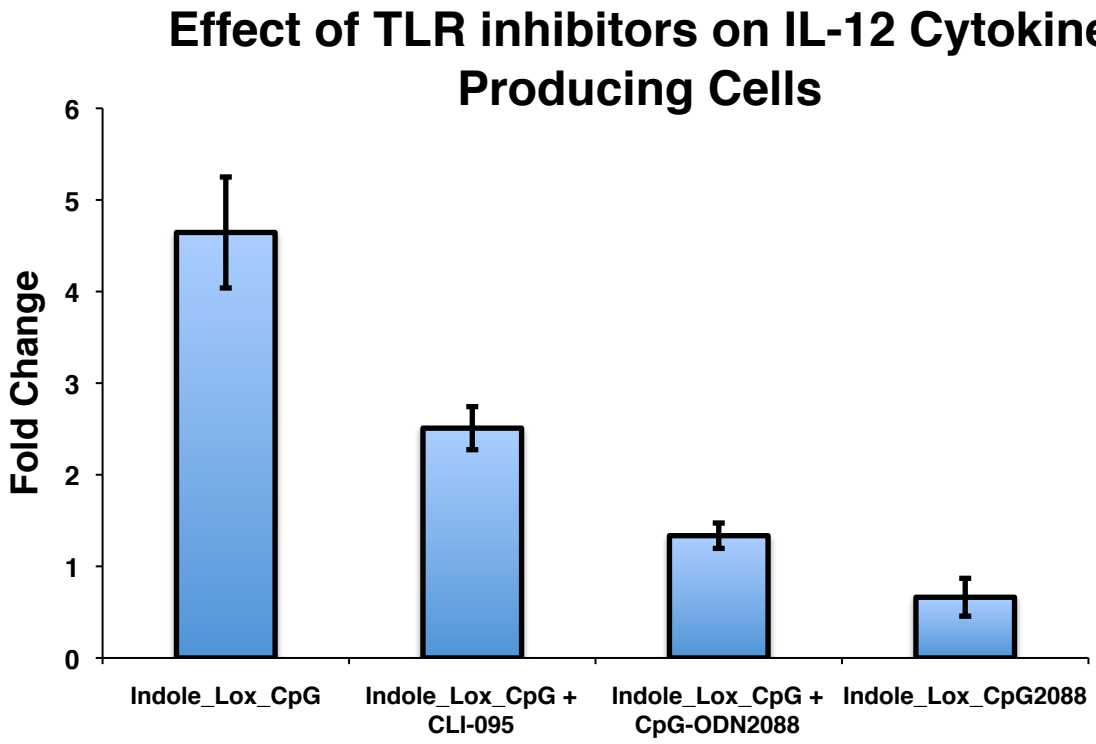

Figure S4.10. Flow Cytometry analysis of IL-12 producing BMDCs when incubated with Indole_Lox_CpG (0.5 μM) and TLR signaling inhibitors, TLR4 inhibitor CLI-095 (100 nM) or TLR9 antagonist CpG-ODN2088 (100 nM) as well as tri-antagonist, Indole_Lox_CpG2088 (0.5 μM). Tri-antagonist (Indole_Lox_CpG2088) exhibited nearly resting level (no agonist) IL-12 cytokine production. BMDCs were incubated with the designated inhibitor for 1 h at 37 °C. Then, the agonist was added and incubated with BMDCs for an additional 6 h at 37 °C. Cells were subsequently stained with FITC CD11c and APC IL-12 (ICS). Data is the result of n=3. Results are expressed as the mean ± SD.

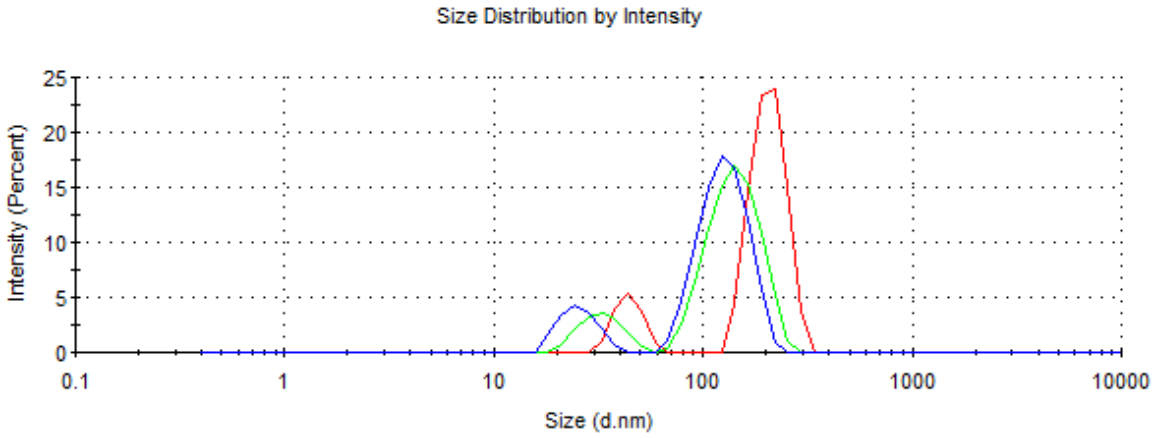

Figure S4.11. Dynamic light scattering (DLS) spectra of CpG-ODN1826 at 0.5 μM in PBS. Spectrum displays three measurements (measurement 1- red, 2-green, 3-blue) of a CpG-ODN1826 solution. The measurements showed that two different sized aggregates formed in solution with diameters of 160 nm ± 42 and 34.2 nm ± 9.4.

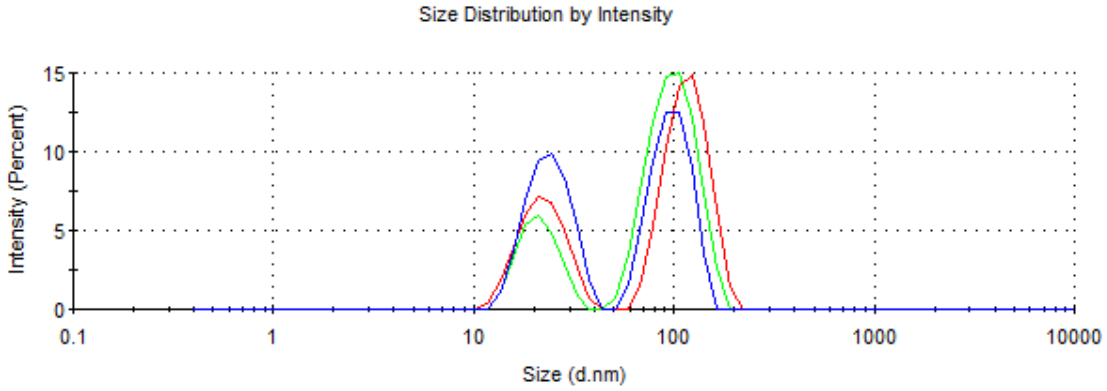

Figure S4.12. Dynamic light scattering (DLS) spectra of Indole_Lox_CpG at 0.5 μM in PBS. Spectrum displays three measurements (measurement 1- red, 2-green, 3-blue) of a Indole-Lox_CpG solution. The measurements showed that two different sized aggregates, comparable to that of CpG-ODN1826, formed in solution with diameters of 106 nm ± 11 and 22.6 nm ± 1.4.

NMR Spectra

4.4 Maleimide Functional Handle

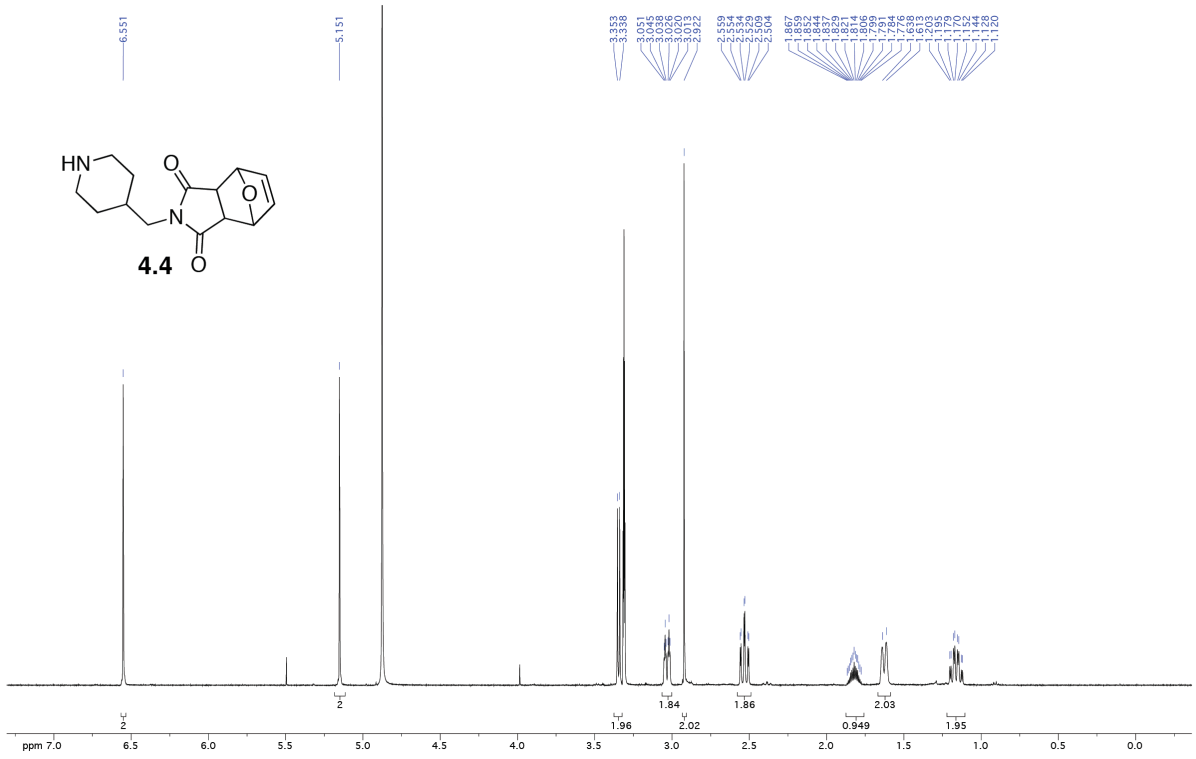

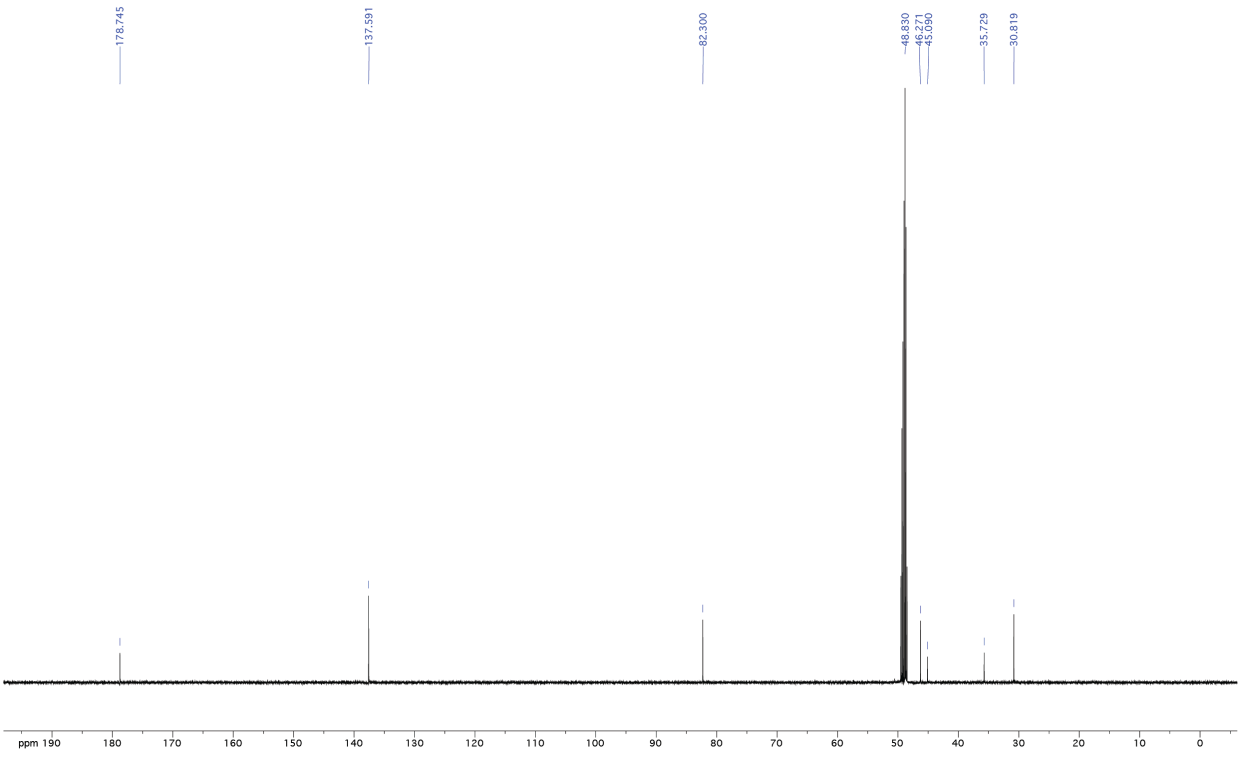

4.5 Tri-Functional Core

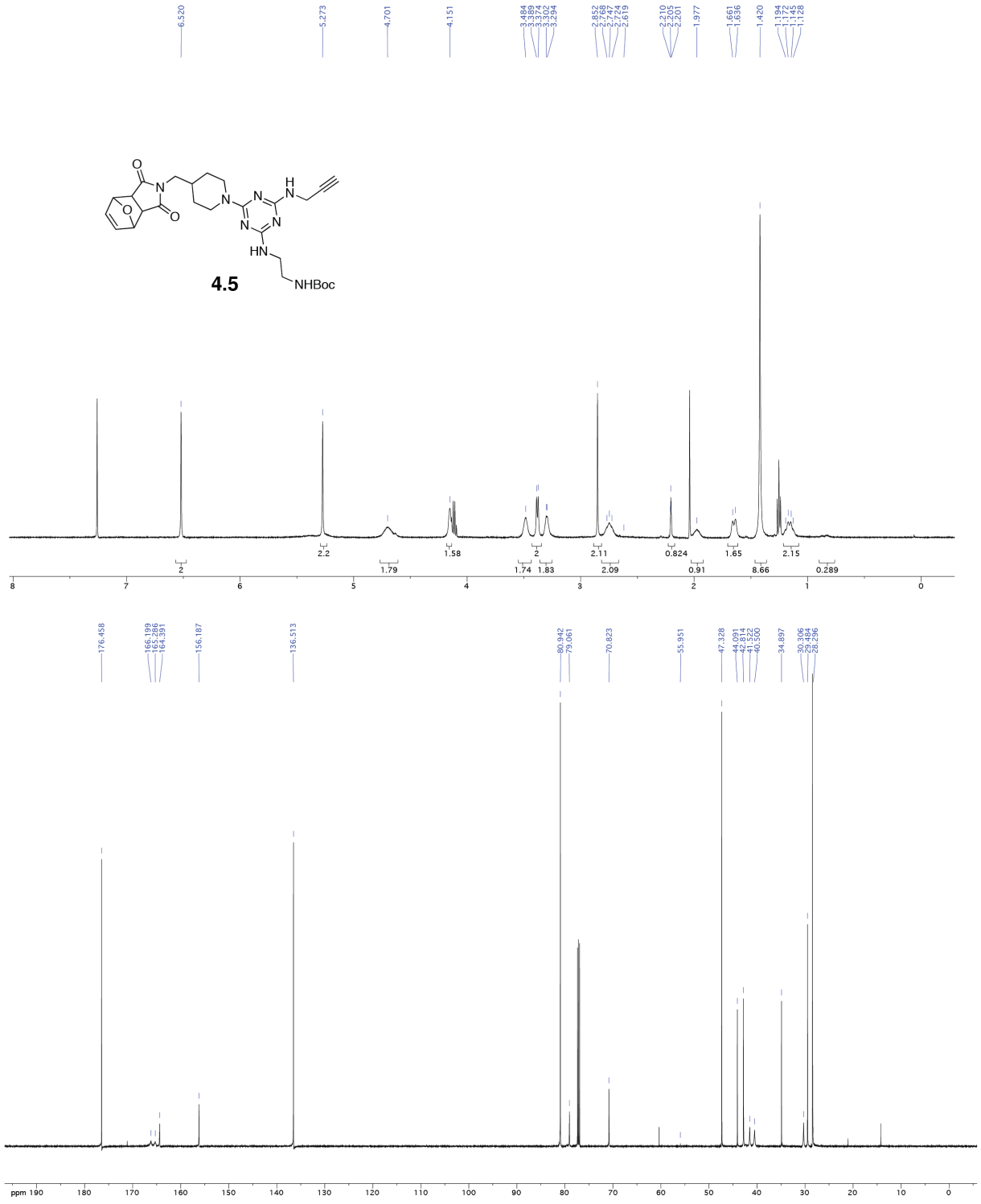

4.7 Indole_Core‡

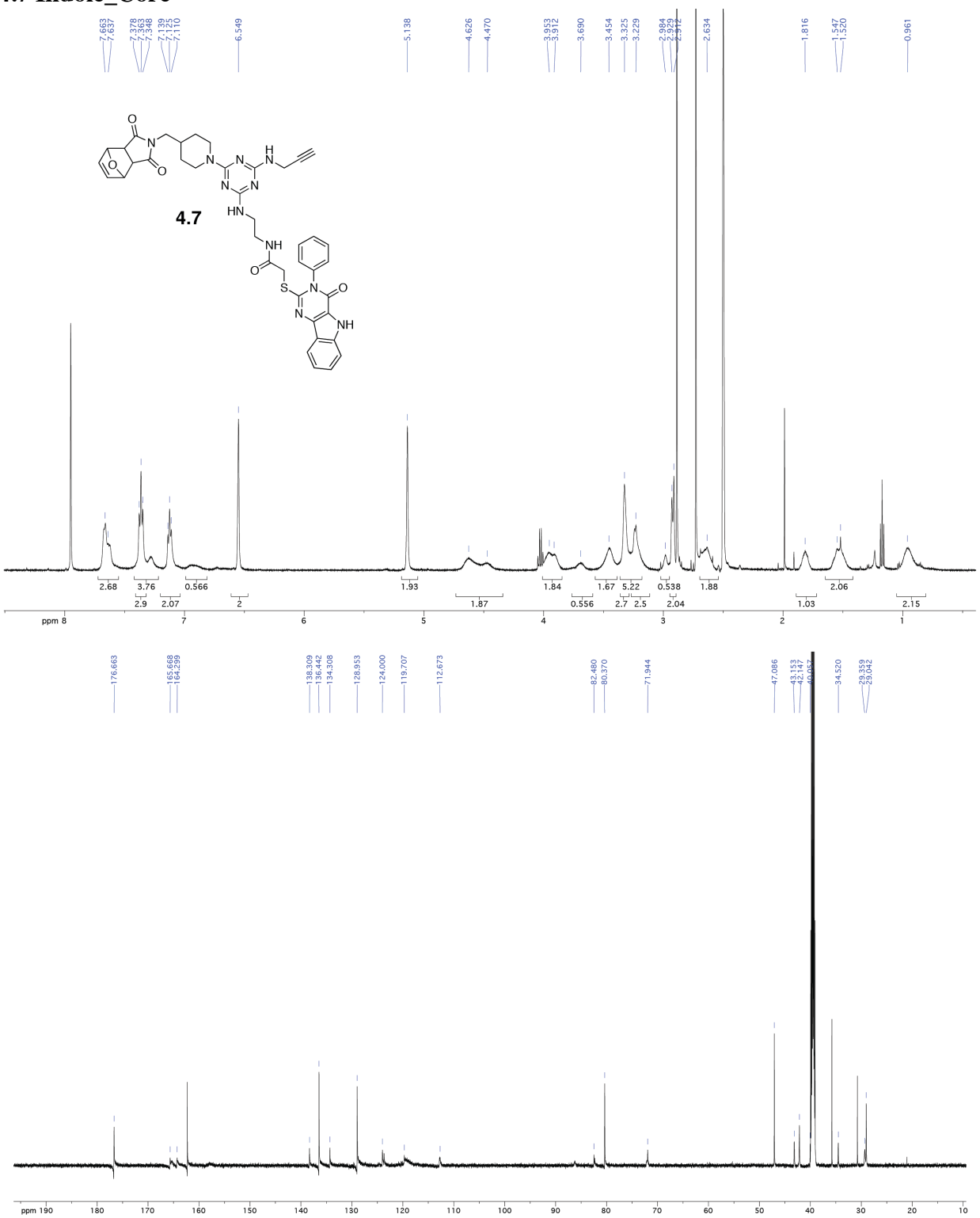

‡Extraction, column purification, and lyophilization were performed to attempt removal of residual solvent. Due to solubility and viscous nature of the product, residual solvent was still present, and the product was taken on to the next step.

4.8 Lox-N_3

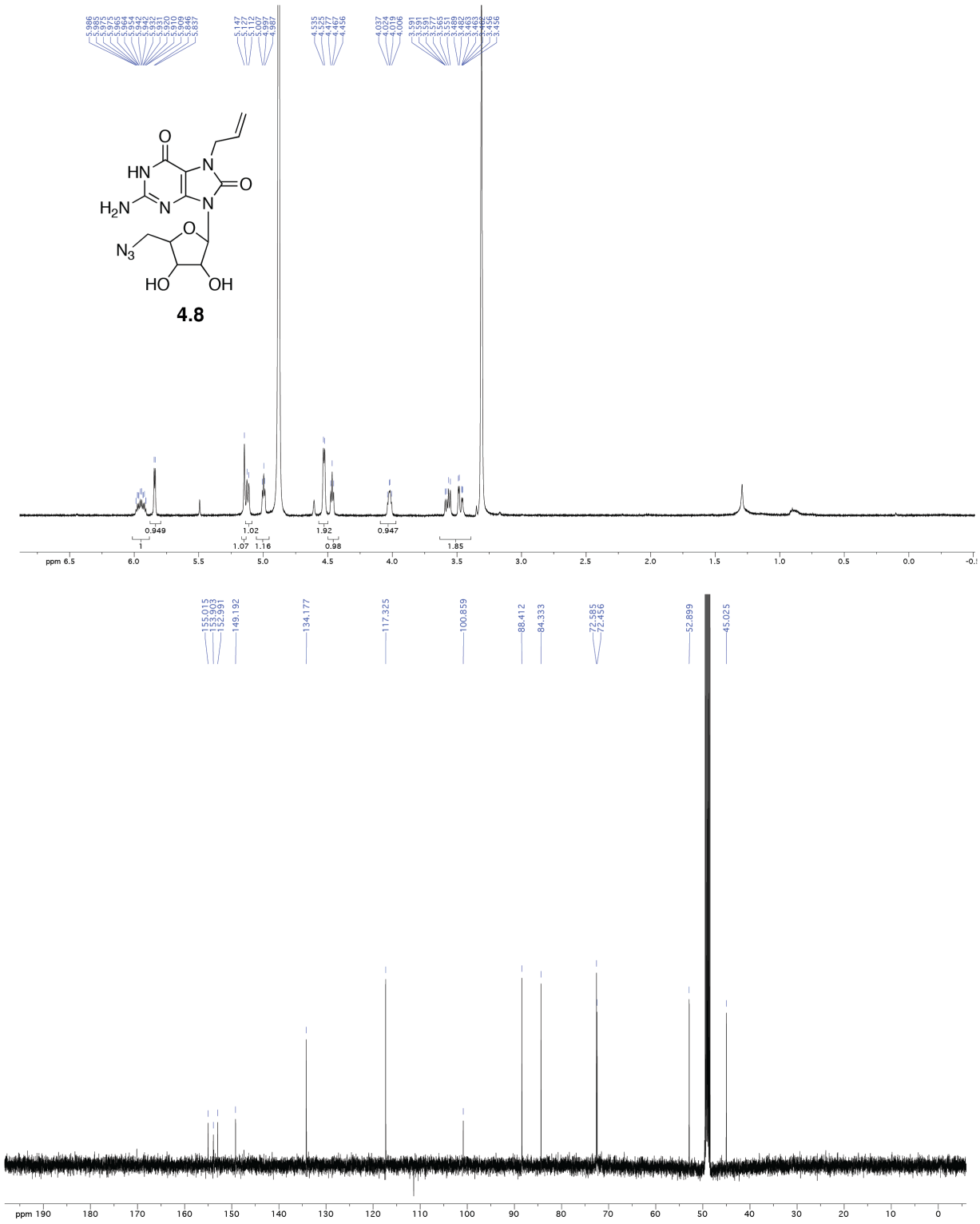
5.986
5.985
5.975
5.973
5.965
5.964
5.954
5.942
5.941
5.932
5.931
5.930
5.910
5.909
5.846
5.837
5.147
5.127
5.112
5.107
4.997
4.987
4.535
4.525
4.477
4.467
4.456
4.037
4.024
4.019
4.006
3.591
3.581
3.577
3.565
3.551
3.489
3.482
3.463
3.456
3.456
HN
N
O
O
H_2N
N
N
O
N_3
HO
OH
4.8
0.949
1
1.02
1.07
1.16
1.92
0.98
0.947
1.85
ppm 6.5
6.0
5.5
5.0
4.5
4.0
3.5
3.0
2.5
2.0
1.5
1.0
0.5
0.0
155.015
153.603
152.991
149.192
134.177
117.325
100.859
88.412
84.333
72.585
72.456
52.899
45.025
ppm 190
180
170
160
150
140
130
120
110
100
90
80
70
60
50
40
30
20
10
0

4.9 Indole_Lox[‡]

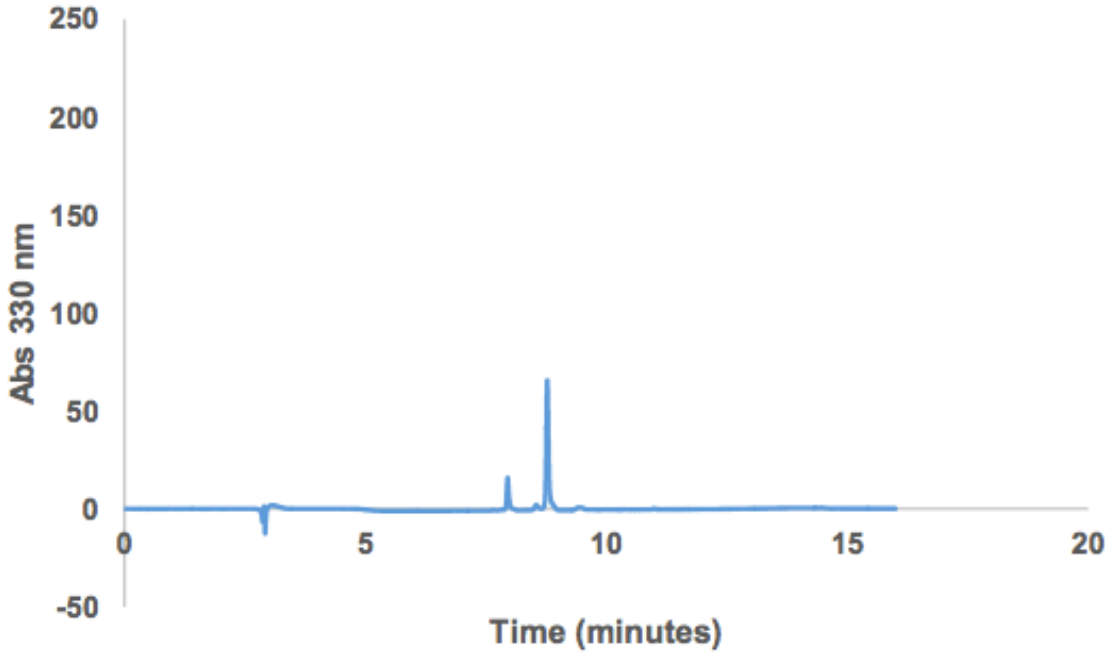

[‡]The desired m/z of Indole_Lox was the only mass observed in both large and small peaks. A clear ^{1}H NMR was difficult to obtain and analyze due to solubility and broad, overlapping peaks.

4.11 Lox-OTs

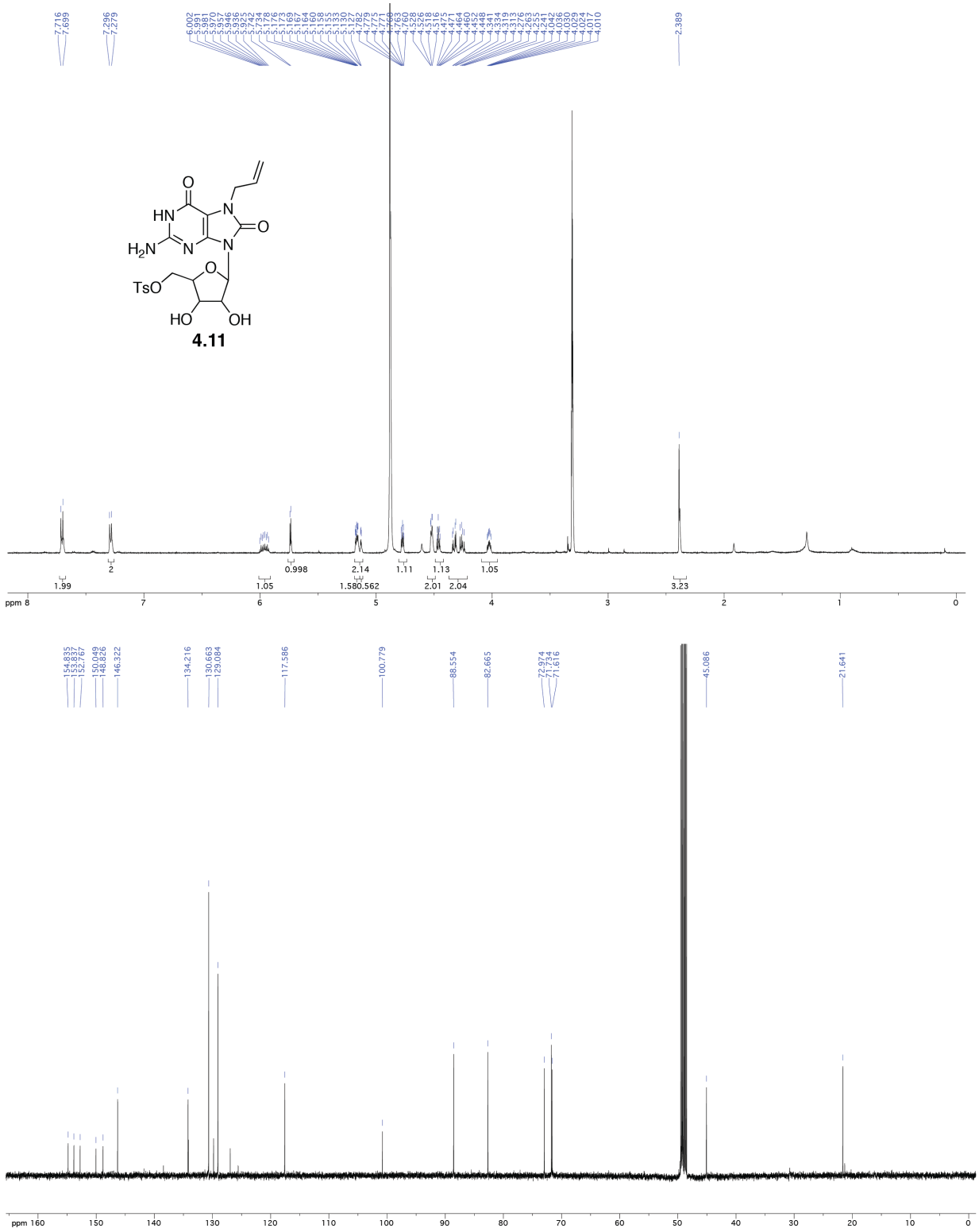

4.14 Lox_Core[‡]

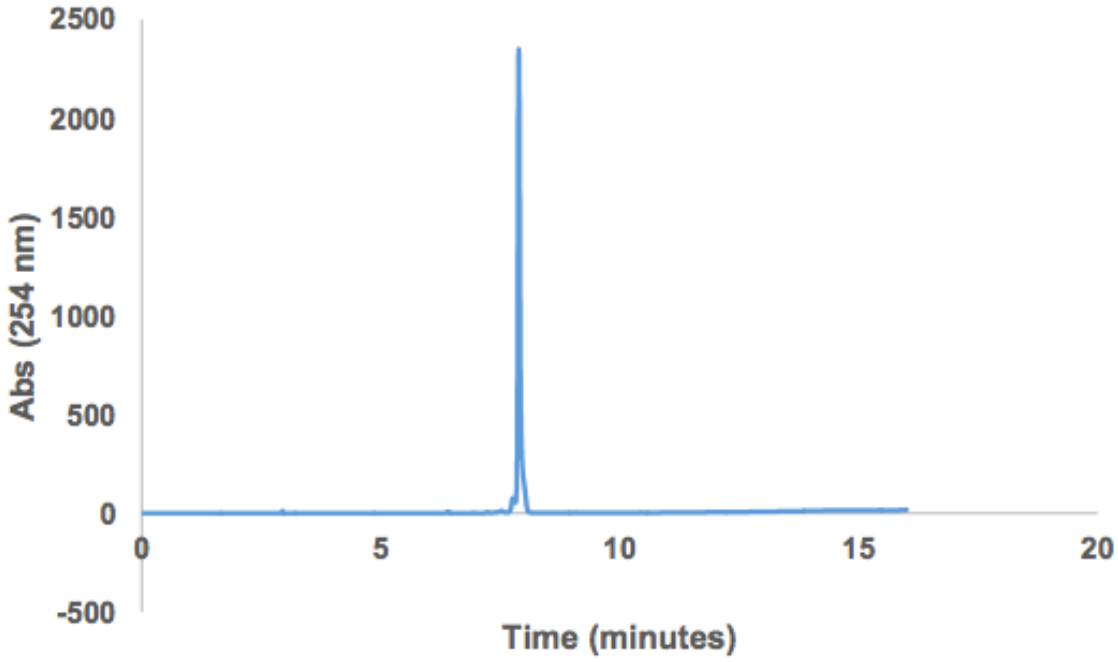

[‡]A clear ^{1}H NMR of Lox_Core was difficult to obtain and analyze due to solubility and broad, overlapping peaks.

References:

(1) Chan, M.; Hayashi, T.; Mathewson, R. D.; Nour, A.; Hayashi, Y.; Yao, S.; Tawatao, R. I.; Crain, B.; Tsigelny, I. F.; Kouznetsova, V. L.; et al. Identification of Substituted Pyrimido[5,4-B]indoles as Selective Toll-Like Receptor 4 Ligands. *J. Med. Chem.* **2013**, *56* (11), 4206–4223.

Appendix D: Chapter 5

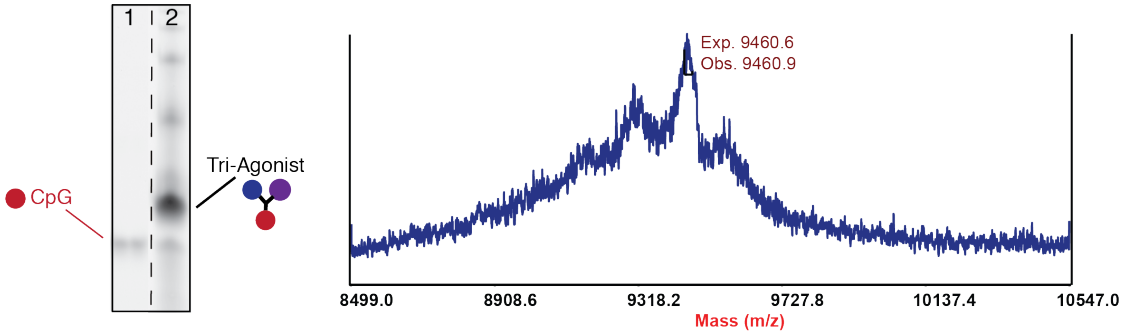

Figure S5.1. TBE-urea gel electrophoresis of CpG-DNA (Lane 1, left) and crude reaction mixture containing TLR4_7_9 tri-agonist (Lane 2, right). MALDI-TOF of TLR4_7_9 tri-agonist using THAP matrix in reflector negative mode.

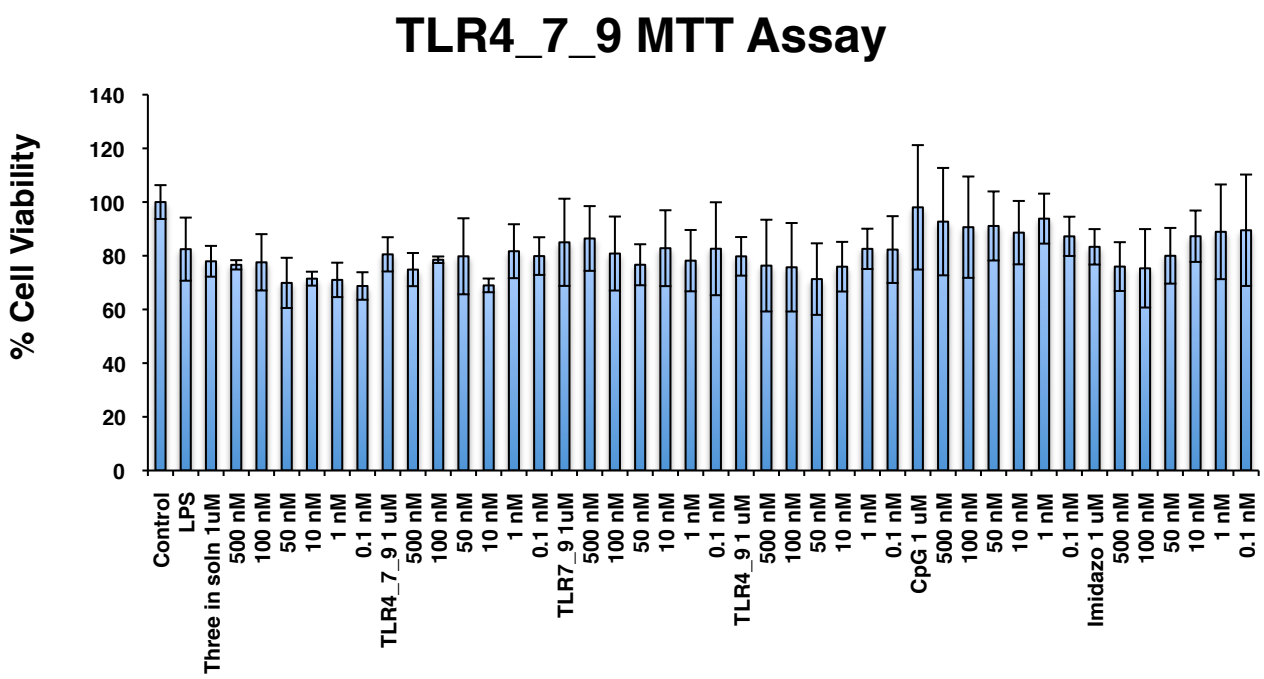

Figure S5.2. RAW-Blue macrophage cells were treated with each compound at concentrations ranging from 1 μM to 0.1 nM for 18 h at 37 °C. Then, the MTT assay was performed on the RAW-Blue cells to assess cell viability. Each bar is the result of n=3. Results are expressed as the mean ± SD.

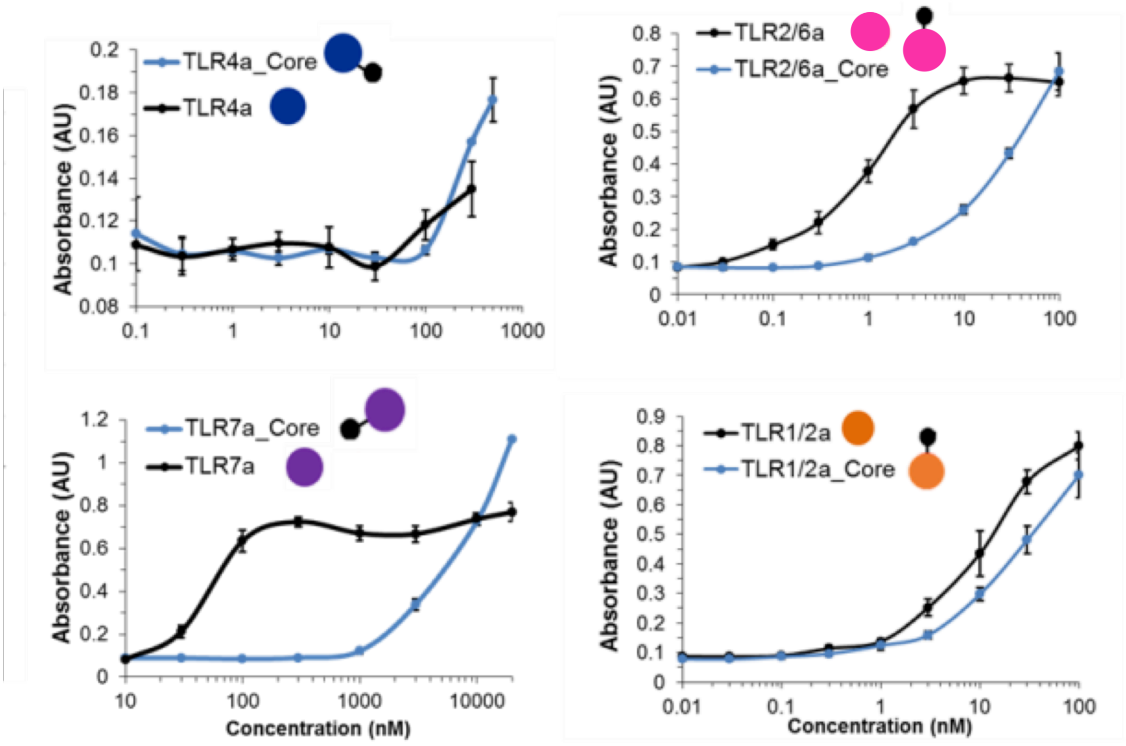

Figure S5.3. RAW-Blue macrophage cells were treated with each compound at varying concentrations for 18 h at 37 °C to compare the native agonists to their corresponding TLR agonist_Core conjugate. Results are expressed as the mean ± SD and n=6.

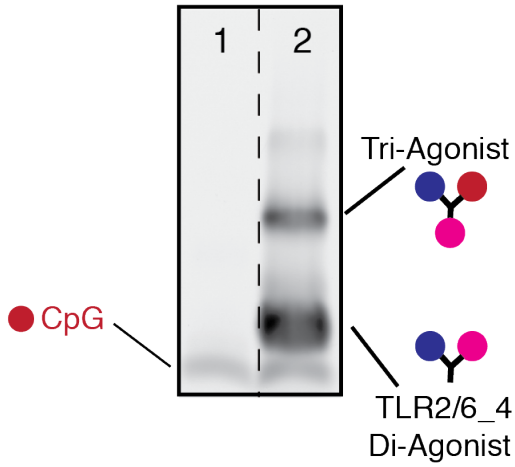

Figure S5.4. SDS-PAGE of CpG-DNA (Lane 1, left) and crude reaction mixture containing TLR2/6_4_9 tri-agonist (Lane 2, right).

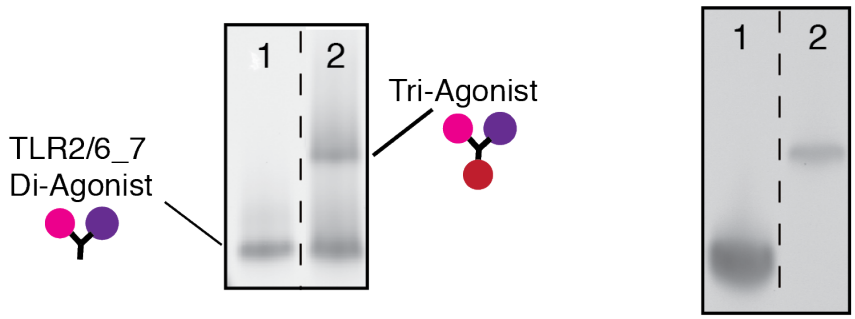

Figure S5.5. SDS-PAGE of TLR2/6_7 di-agonist (Lane 1, left) and crude reaction mixture containing TLR2/6_4_9 tri-agonist (Lane 2, right) [left image-crude reaction mixture]. SDS-PAGE of TLR2/6_7 di-agonist (Lane 1, left) and purified TLR2/6_4_9 tri-agonist (Lane 2, right) [right image-post gel extraction purification].

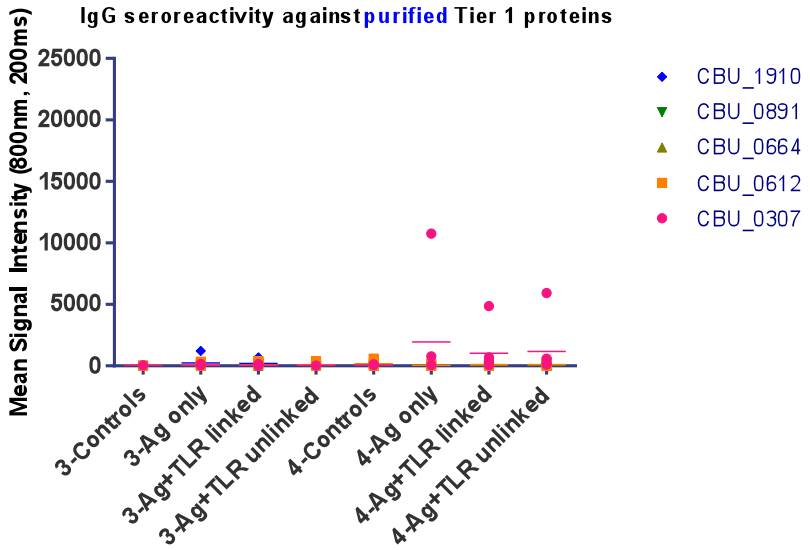

Figure S5.6. CBU_0307 Specific IgG Antibodies Probed by Microarray Chip Technology. Detection of IgG antibodies specific to CBU_0307 expressed as mean signal intensity. Sera were drawn from C57/BL6 mice vaccinated with PBS (Control), CBU_0307 (Ag only), CBU_0307 plus unlinked TLR2/6/4/7 (1 nmol of each agonists unconjugated), or CBU_0307 plus linked TLR2/6_4_7 (1 nmol of conjugated agonists). Each bar is the result of n=6. Results are expressed as the mean ± SEM.

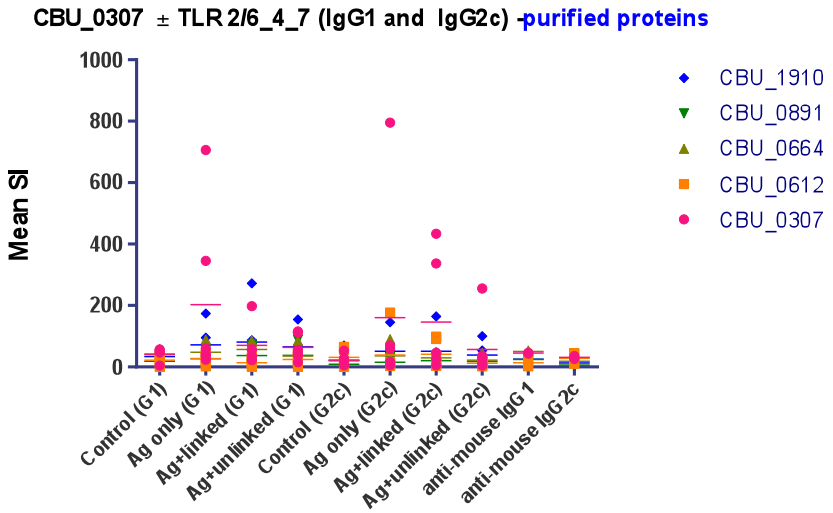

Figure S5.7. CBU_0307 Specific IgG1 and IgG2c Antibodies Probed by Microarray Chip Technology. Detection of IgG1 or IgG2c antibodies specific to CBU_0307 expressed as mean signal intensity. Sera were drawn from C57/BL6 mice vaccinated with PBS (Control), CBU_0307 (Ag only), CBU_0307 plus unlinked TLR2/6/4/7 (1 nmol of each agonists unconjugated), or CBU_0307 plus linked TLR2/6_4_7 (1 nmol of conjugated agonists). Each bar is the result of n=5. Results are expressed as the mean ± SEM.

NMR Spectra and HPLC Traces

5.1 Carboxylic Acid Core ^{1}H NMR‡ and HPLC Trace

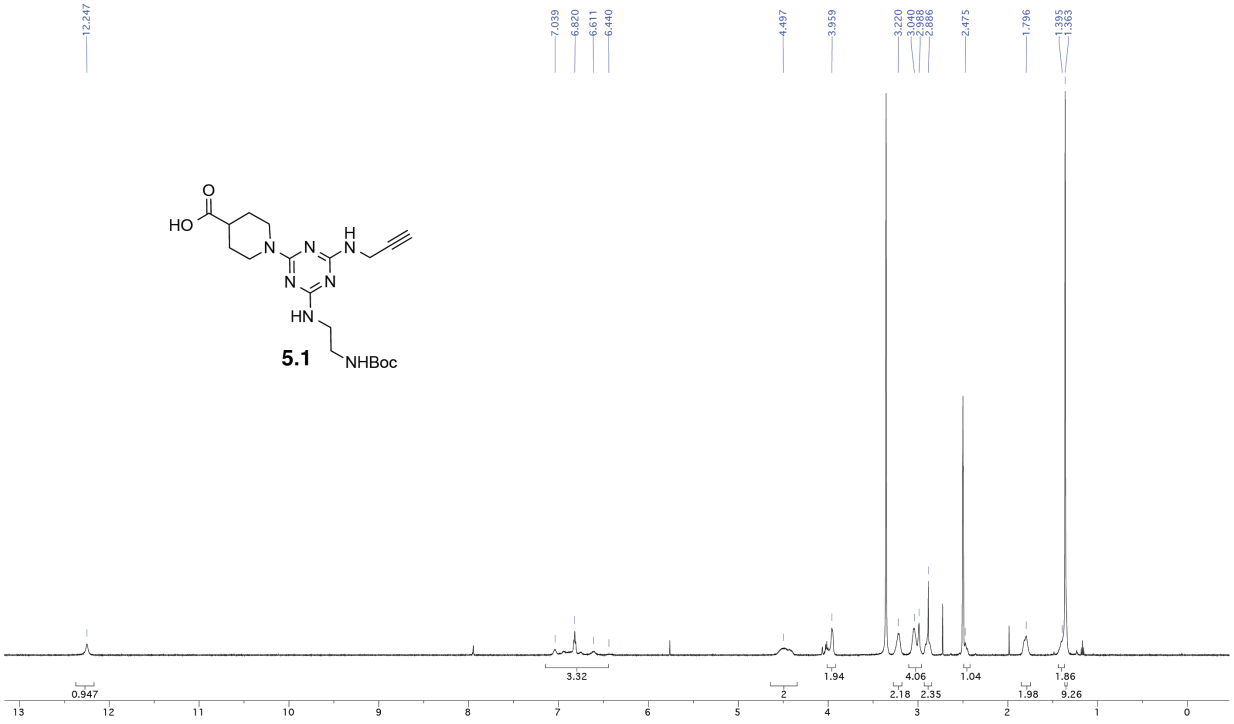

‡A clear ^{13}C NMR of the carboxylic acid core was difficult to obtain and analyze due to the insoluble nature of the product.

b) HPLC trace of Carboxylic Acid Core **5.1**

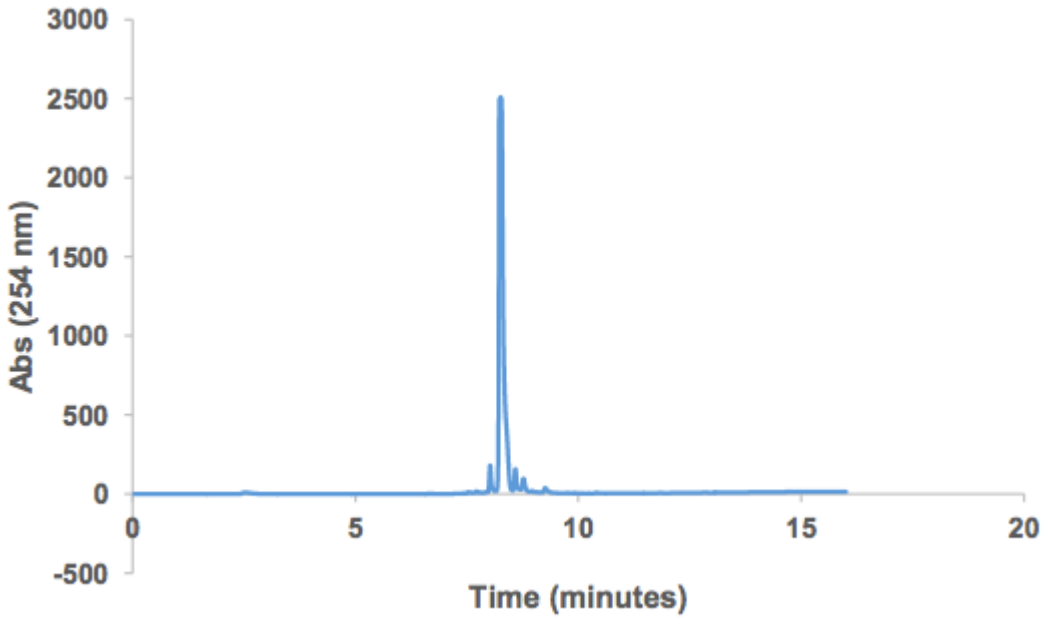

HPLC trace at 254 nm on a C8 analytical column. Solvent A: 0.1 % TFA water, Solvent B: 0.1% TFA acetonitrile. Gradient: t 0-1 min hold 10% B, t 1-11 min ramp to 90% B, t 11-16 min hold 90% B.

5.2 Imidazoquinoline ^{1}H NMR Spectra

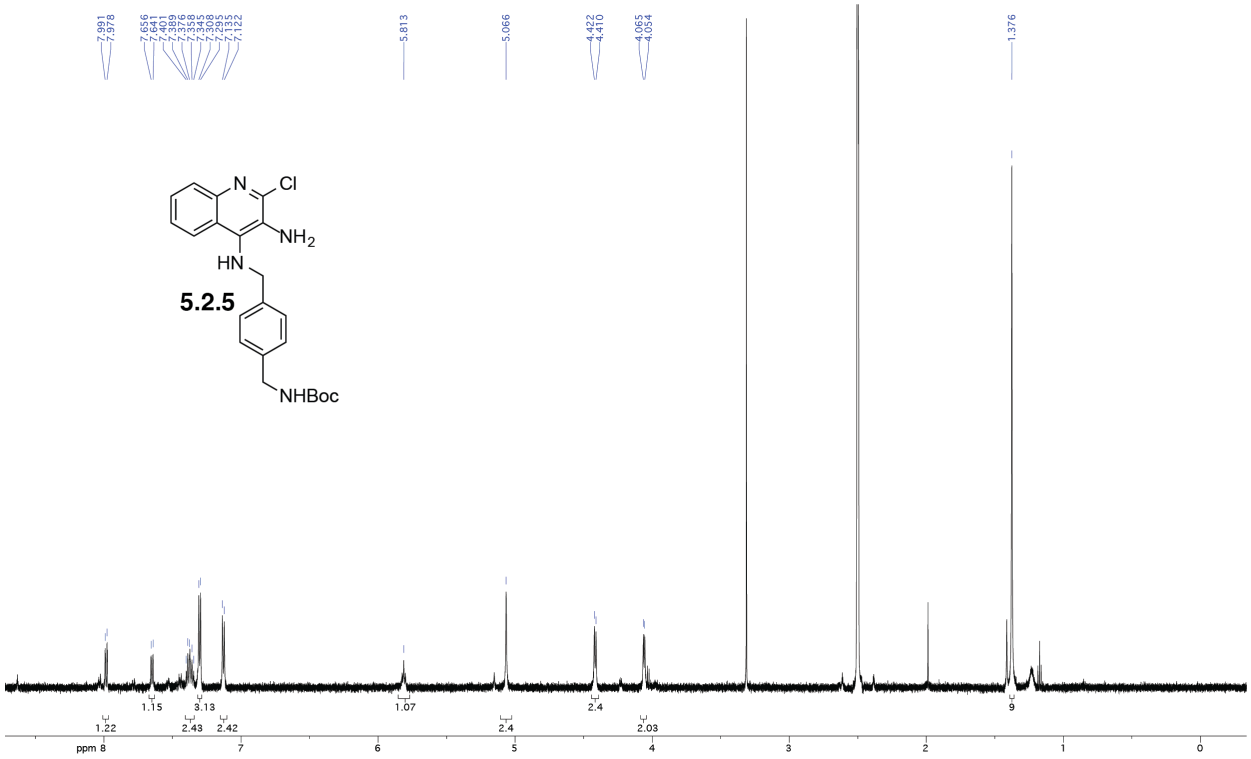

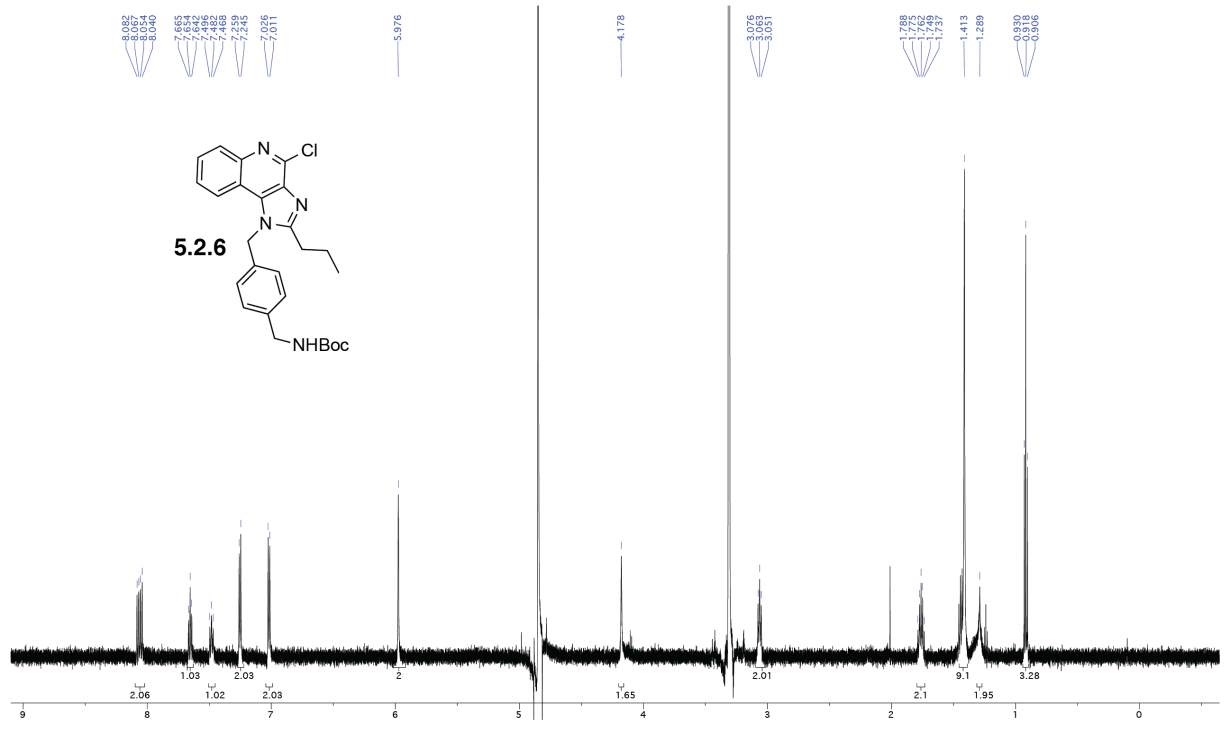

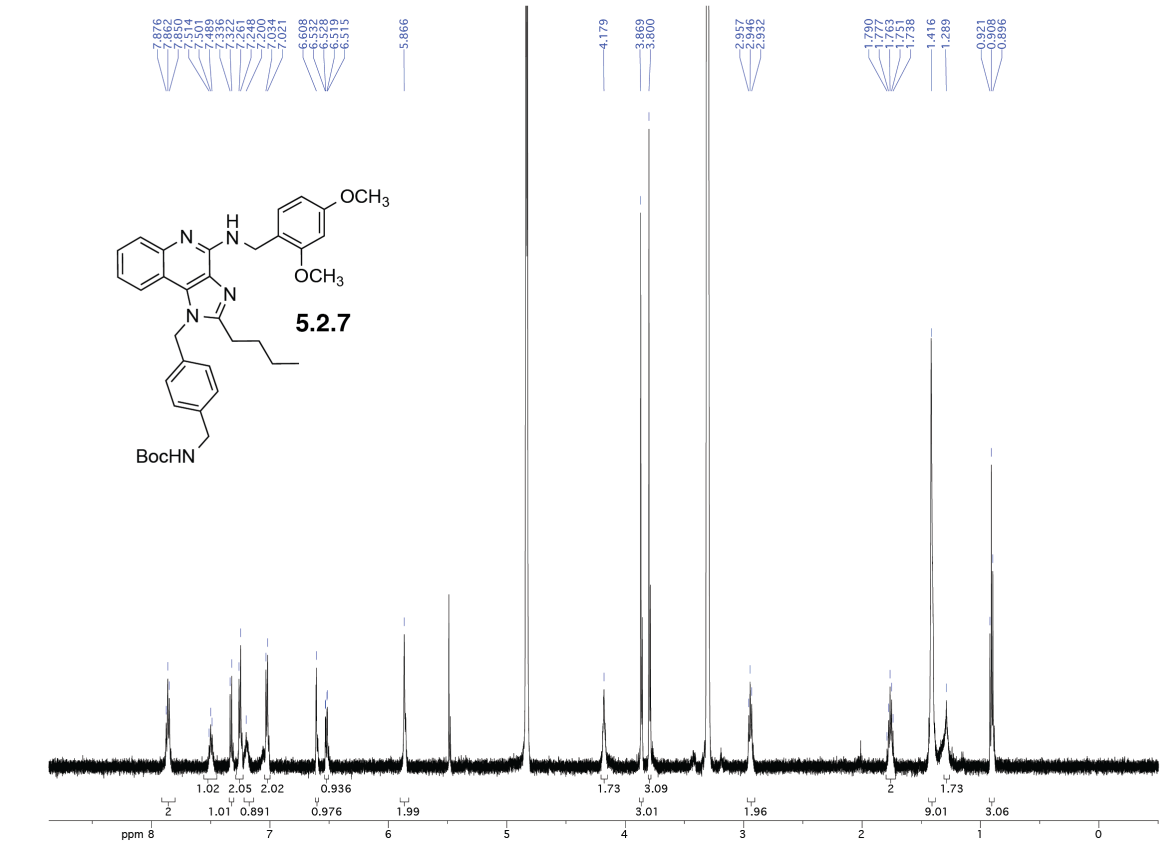
7.876
7.862
7.850
7.514
7.501
7.489
7.336
7.332
7.261
7.248
7.200
7.084
7.021
6.608
6.532
6.528
6.519
6.515
5.866
4.179
3.869
3.800
2.957
2.946
2.932
1.790
1.777
1.763
1.751
1.738
1.416
1.289
0.921
0.908
0.896
OCH3
OCH3
H
N
N
N
N
5.2.7
BocHN
1.02
2.05
2.02
0.936
1.73
3.09
2
1.73
2
1.01
0.891
0.976
1.99
3.01
1.96
9.01
3.06
ppm 8
7
6
5
4
3
2
1
0

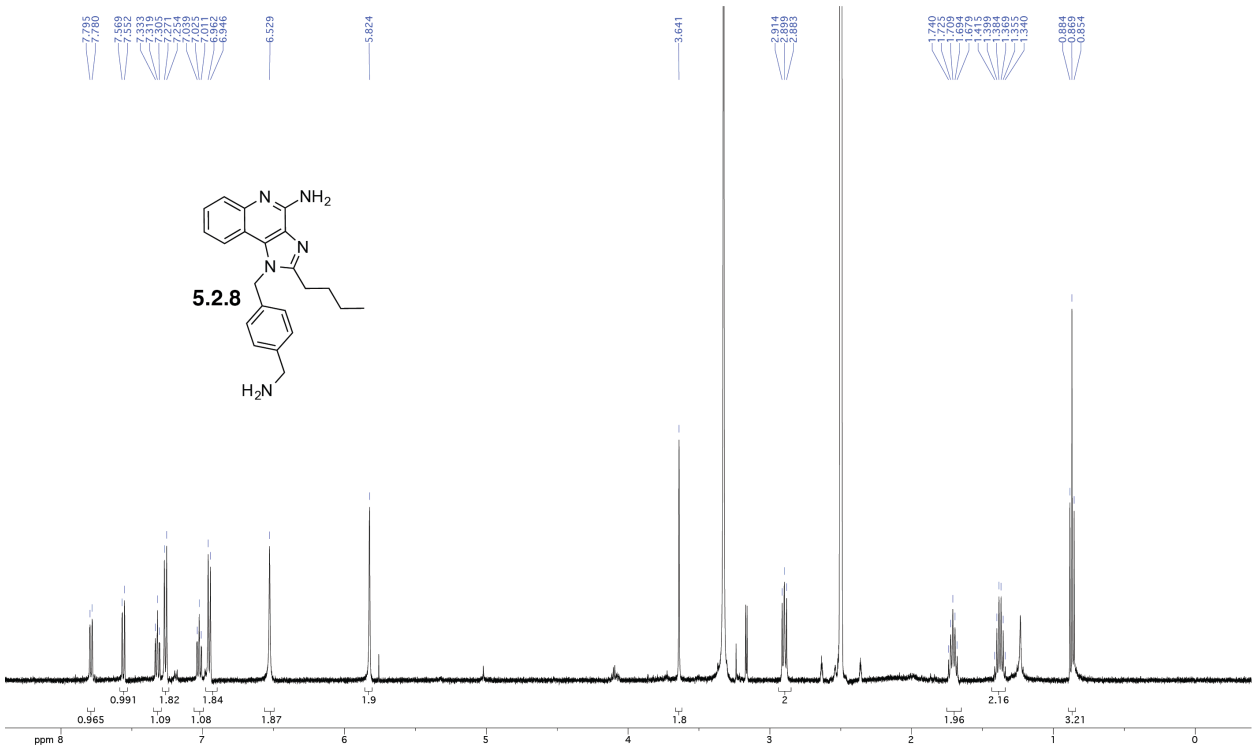
7.795
7.780
7.569
7.552
7.333
7.319
7.315
7.271
7.254
7.239
7.025
7.011
6.962
6.946
6.529
5.824
3.641
2.914
2.899
2.883
1.740
1.725
1.709
1.694
1.679
1.415
1.399
1.384
1.369
1.355
1.340
0.884
0.869
0.854
NH2
N
N
N
5.2.8
H2N
0.965
0.991
1.09
1.82
1.08
1.84
1.87
1.9
1.8
2
2.16
1.96
3.21
ppm 8
7
6
5
4
3
2
1
0

5.3 TLR7_PEG$_{12}$-NH-Fmoc NMR Spectra

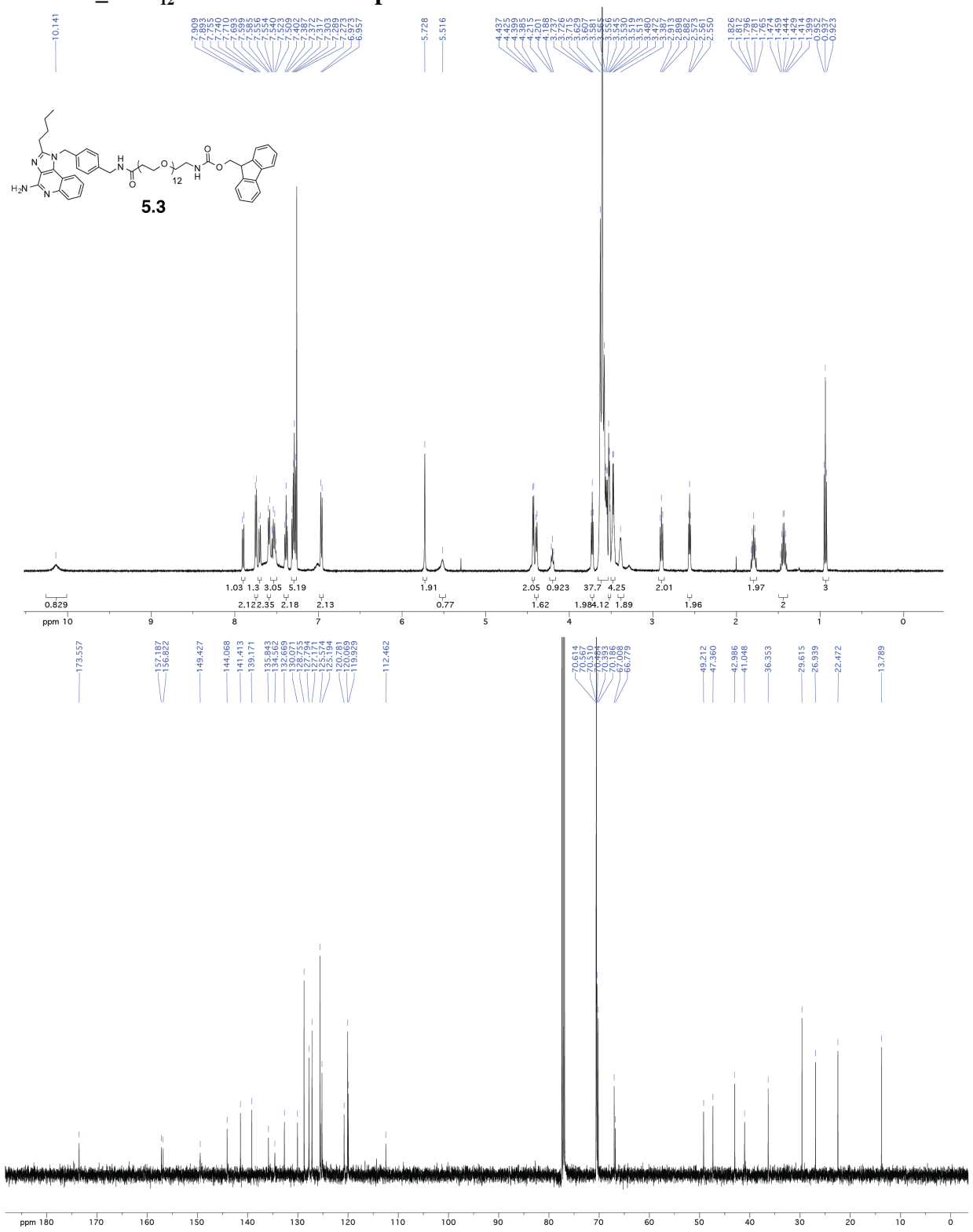

5.4 TLR7_PEG$_{12}$_Core NMR Spectra

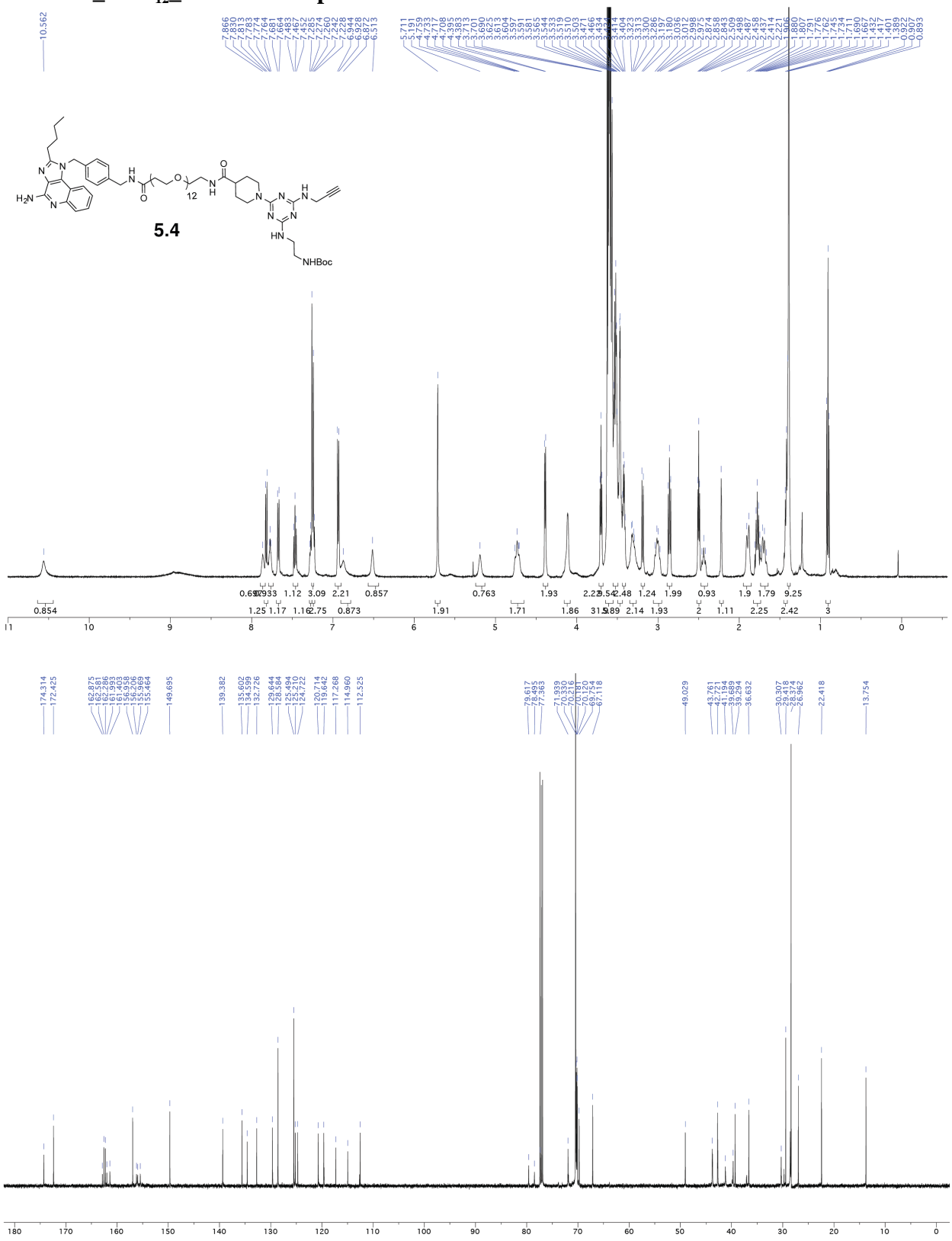

5.5 TLR7_PEG$_{12}$_Core_PEG$_{12}$-NH-Fmoc NMR Spectra

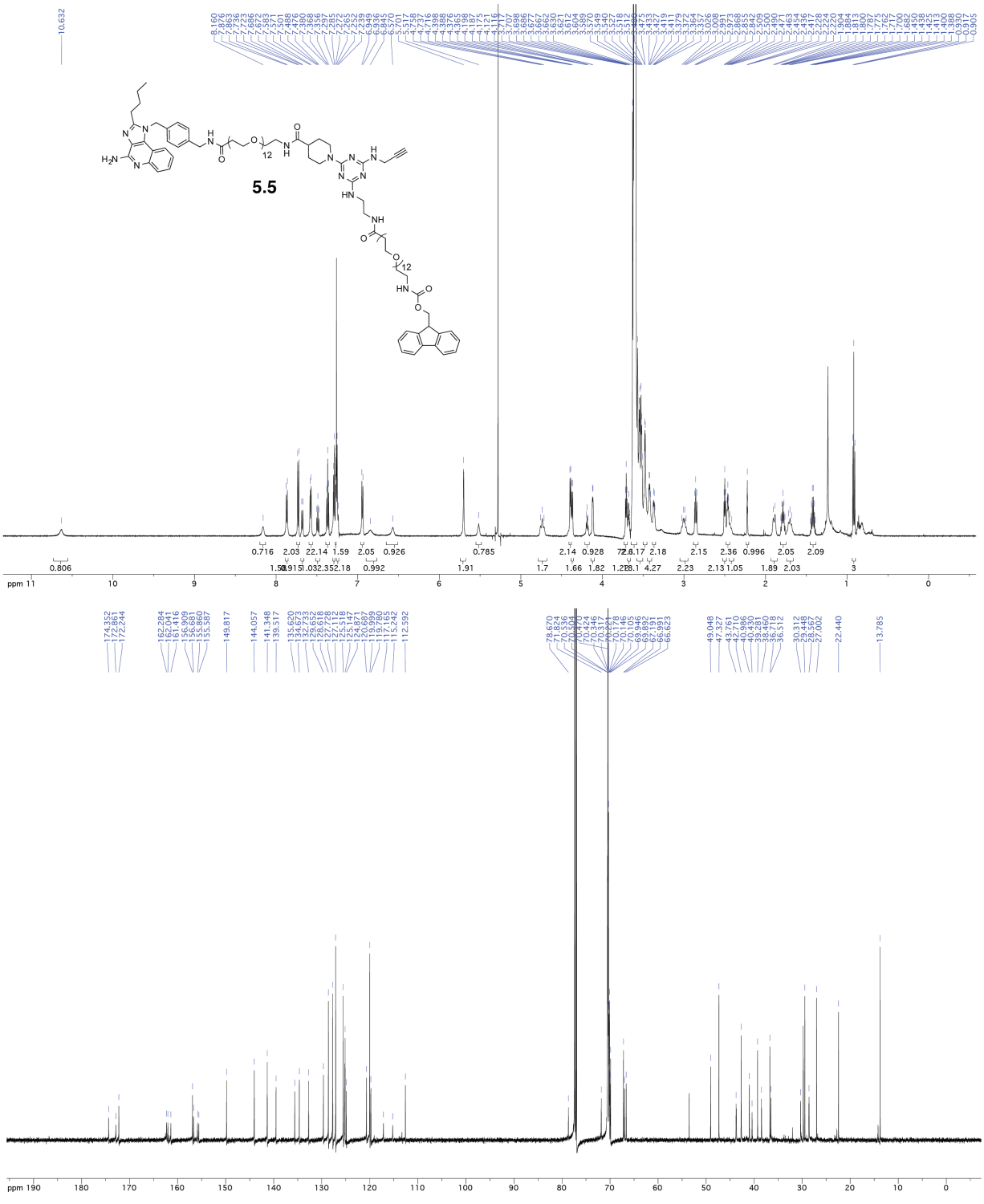

5.6 TLR4_7 ^{1}H NMR and HPLC Trace

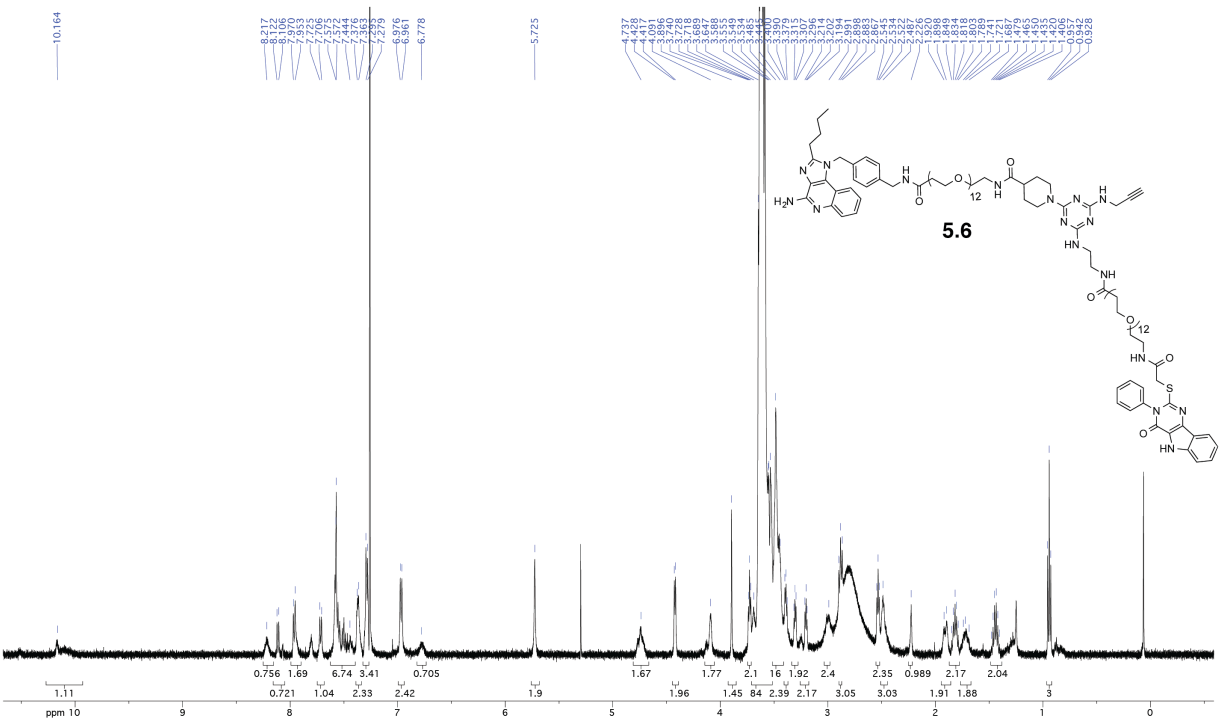

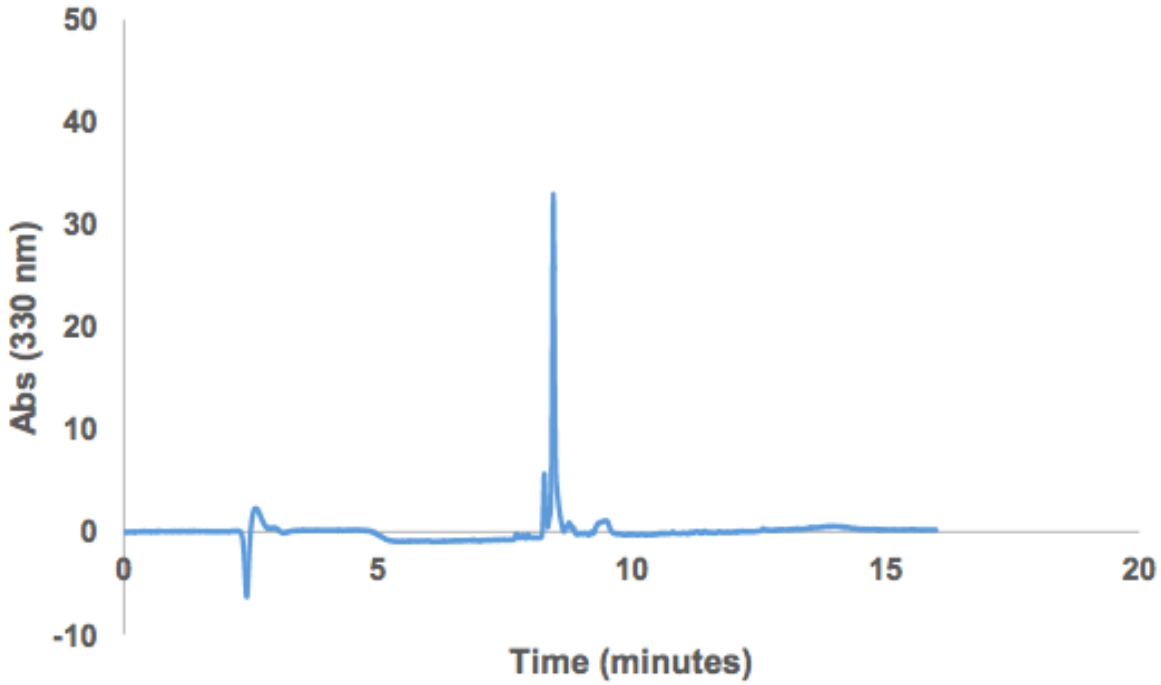

HPLC trace at 330 nm on a C8 analytical column. Solvent A: 0.1 % TFA water, Solvent B: 0.1% TFA acetonitrile. Gradient: t 0-1 min hold 10% B, t 1-11 min ramp to 90% B, t 11-16 min hold 90% B.

5.8 Indole_PEG$_{12}$_Core NMR Spectra (*provided by Tyler Albin)*

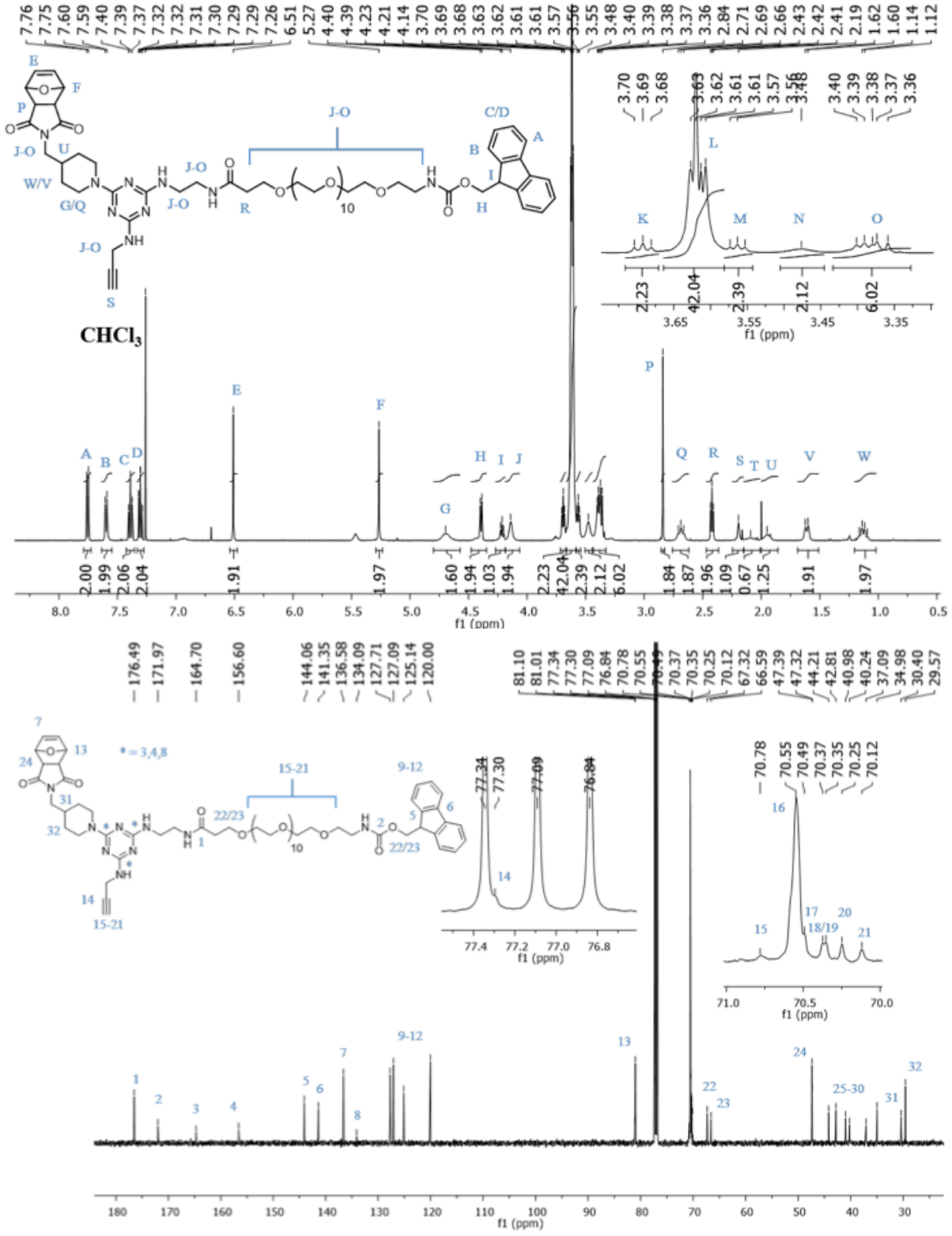

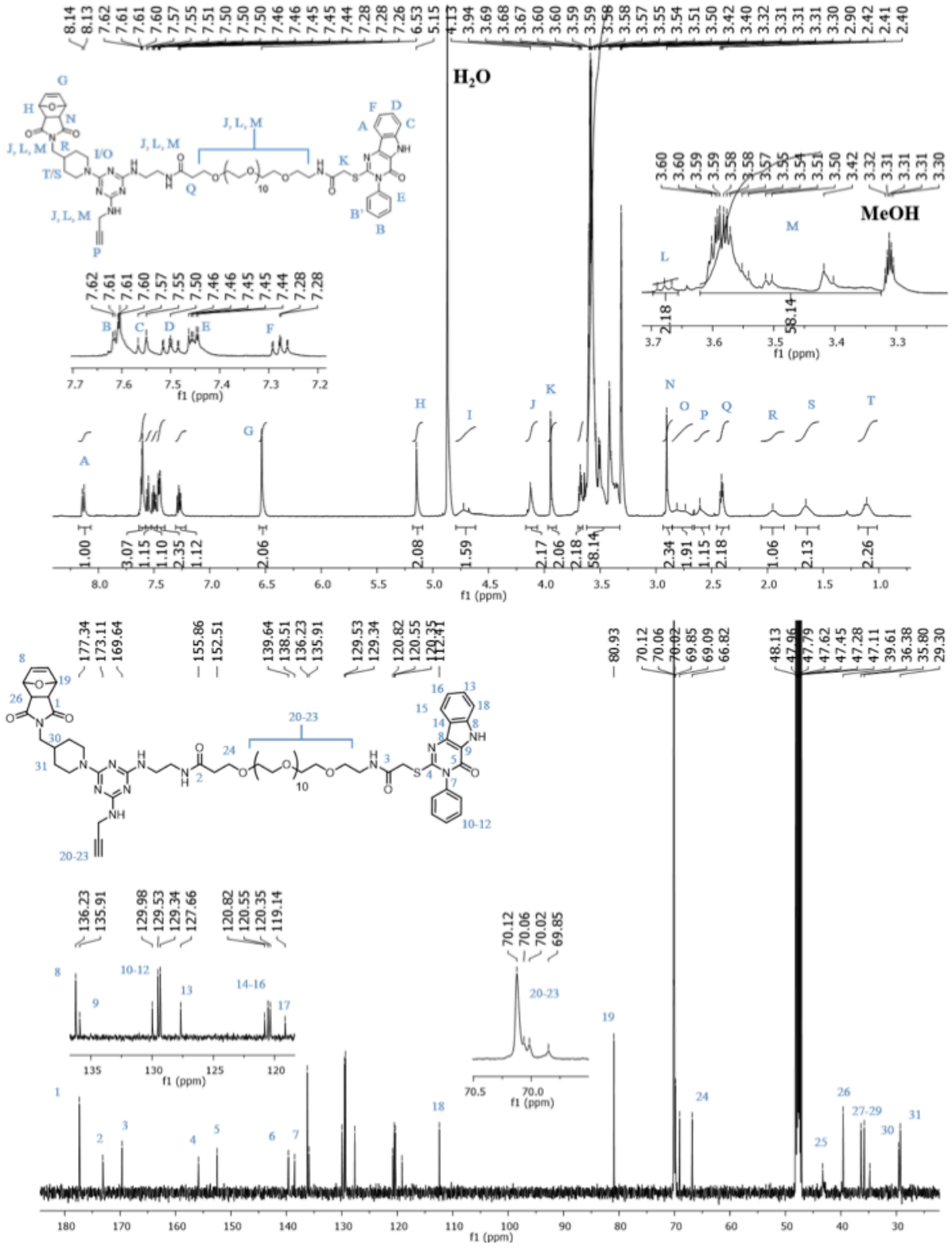
H2O
MeOH
f1 (ppm)

5.9 TLR2/6 _4 HPLC Trace and MALDI-TOF (*provided by Tyler Albin)*

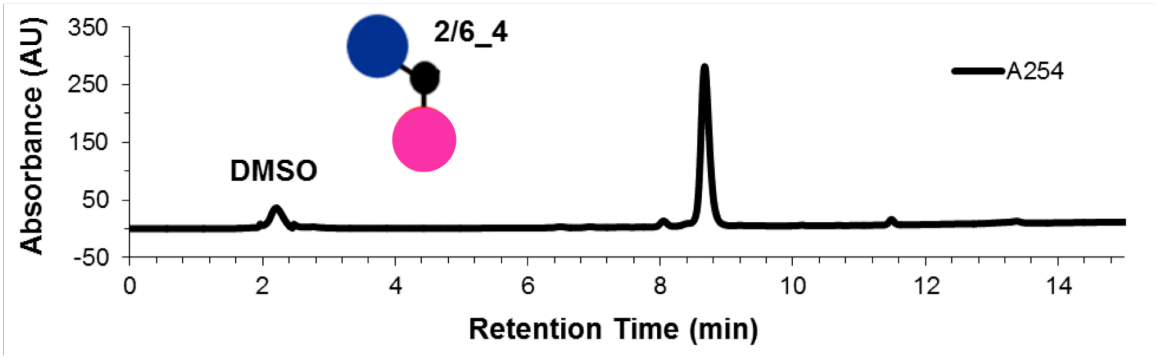

HPLC trace at 254 nm on a C8 analytical column. Solvent A: 0.1 % TFA water, Solvent B: 0.1% TFA acetonitrile. Gradient: t 0-1 min hold 50% B, t 1-11 min ramp to 90% B, t 11-15 min hold 90% B.

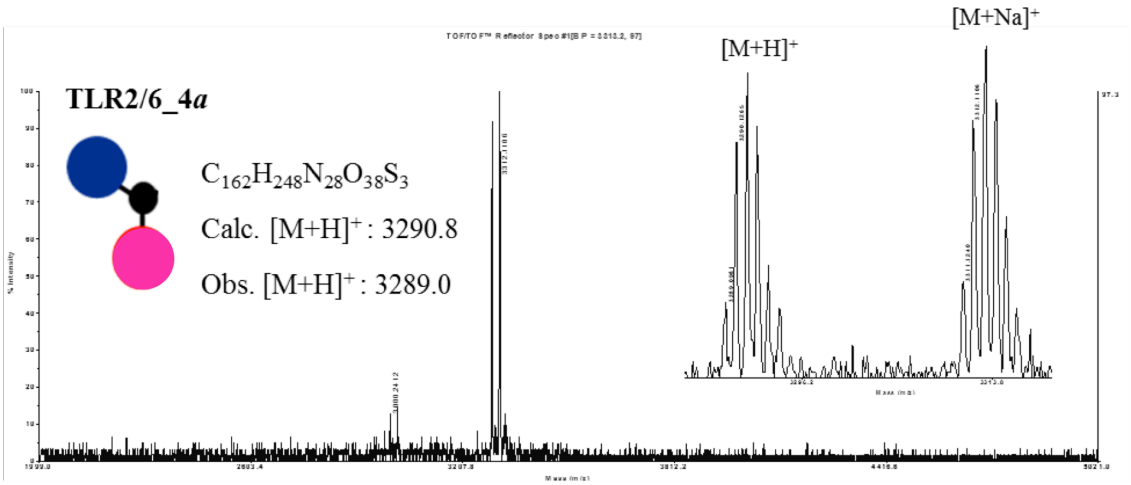

5.9.1 TLR2/6 _Core HPLC Trace and MALDI-TOF (*provided by Tyler Albin)*

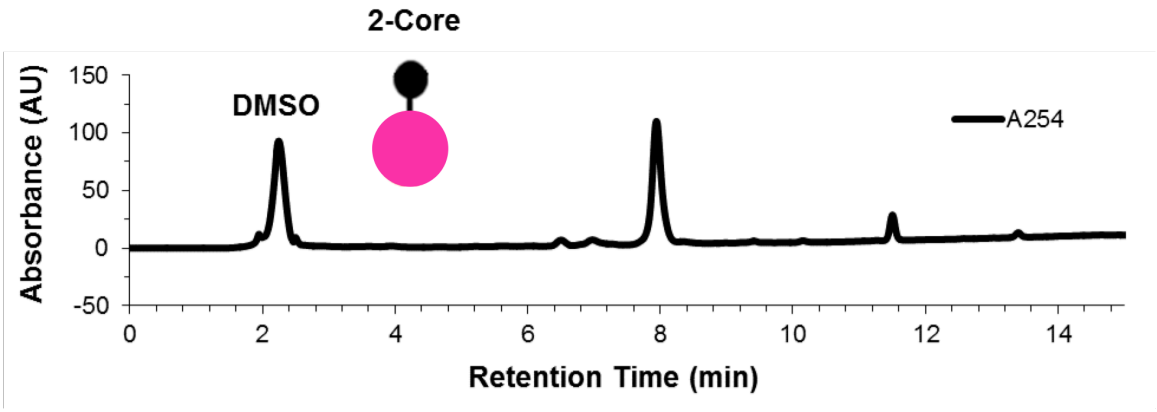

HPLC trace at 254 nm on a C8 analytical column. Solvent A: 0.1 % TFA water, Solvent B: 0.1% TFA acetonitrile. Gradient: t 0-1 min hold 50% B, t 1-11 min ramp to 90% B, t 11-16 min hold 90% B.

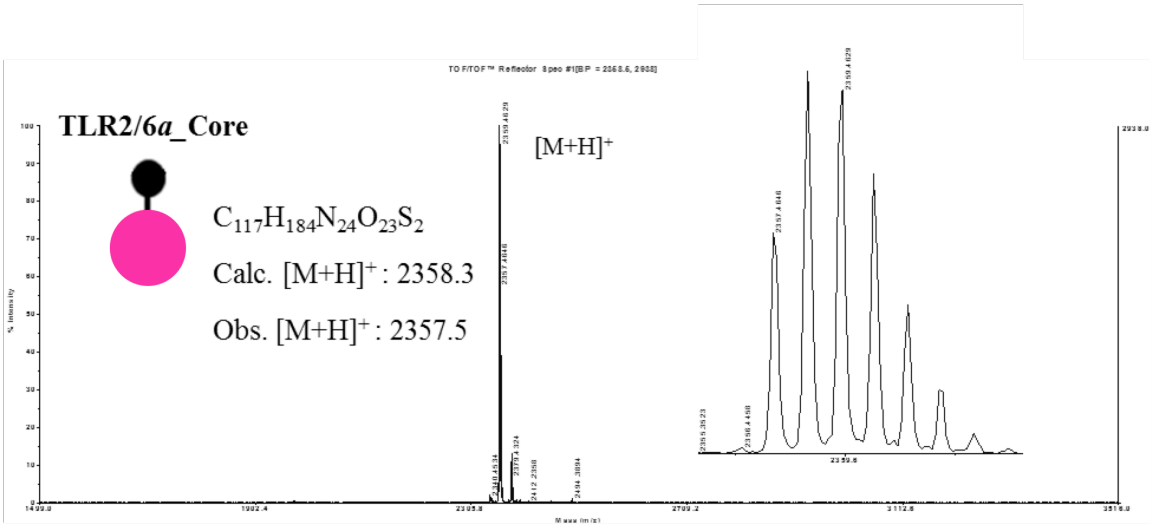

5.10 Imidazoquinoline-N_3 NMR Spectra

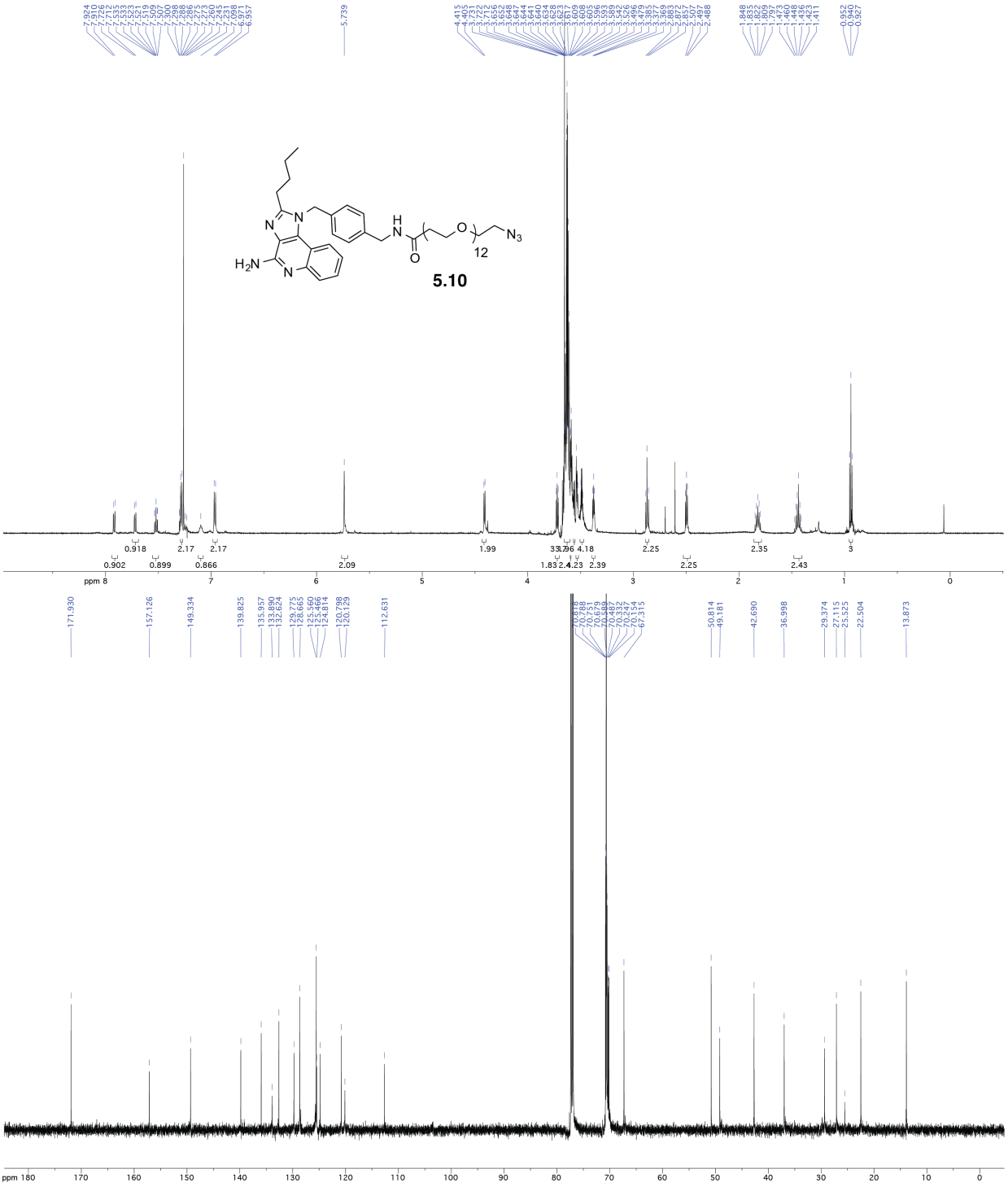

5.11 TLR2/6_4_7 HPLC Trace and MALDI-TOF

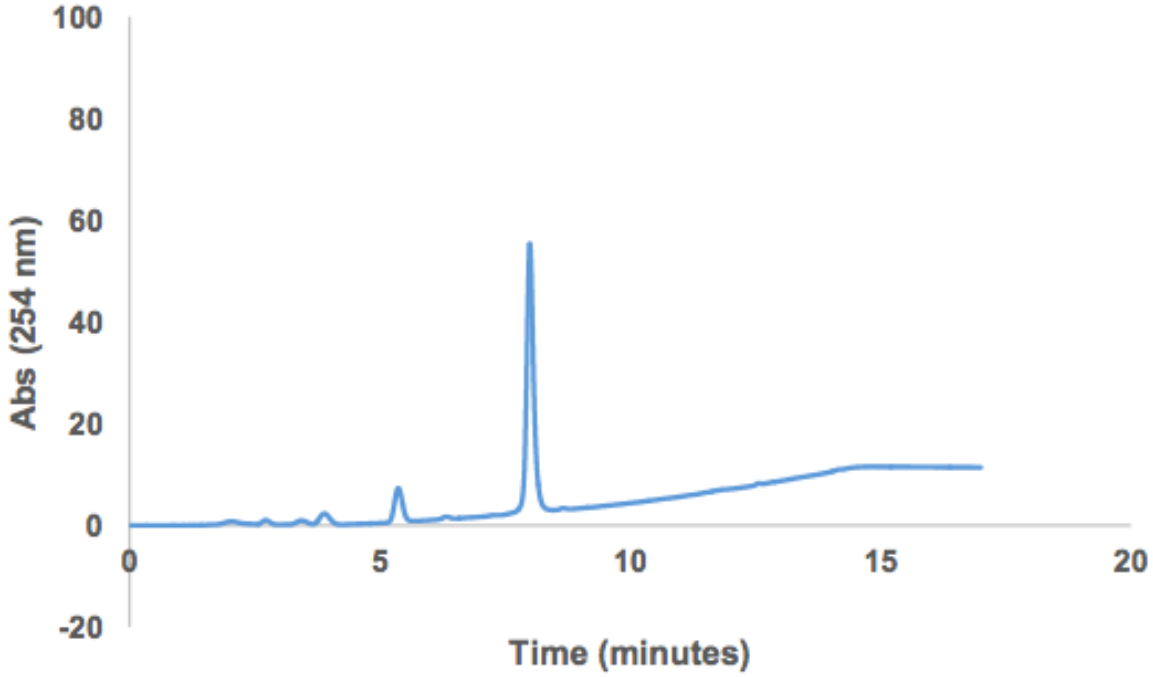

HPLC trace at 254 nm on a C8 analytical column. Solvent A: 0.1 % TFA water, Solvent B: 0.1% TFA acetonitrile. Gradient: t 0-1 min hold 50% B, t 1-11 min ramp to 90% B, t 11-16 min hold 90% B.

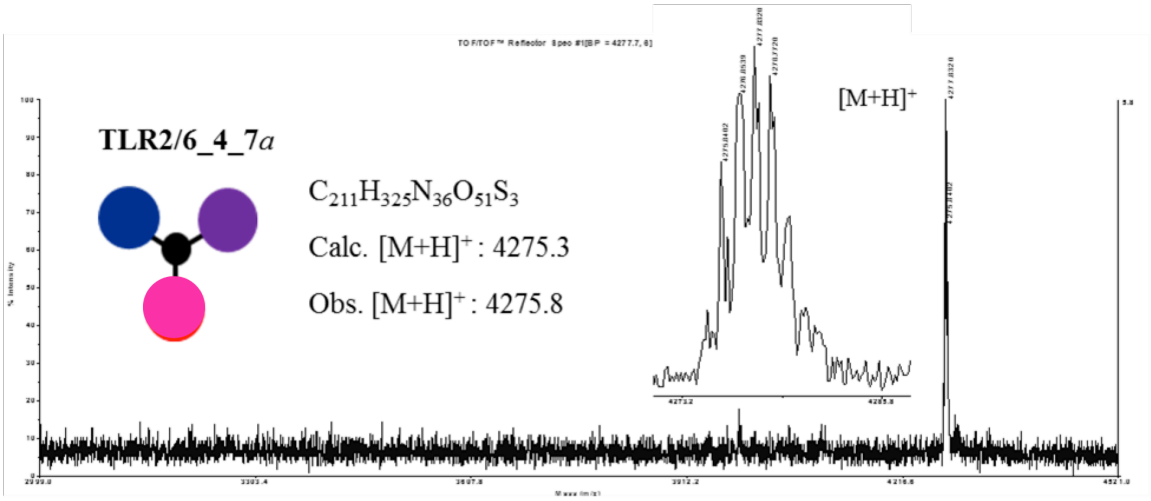

5.11 TLR1/2_Core HPLC Trace and MALDI-TOF (*provided by Tyler Albin)*

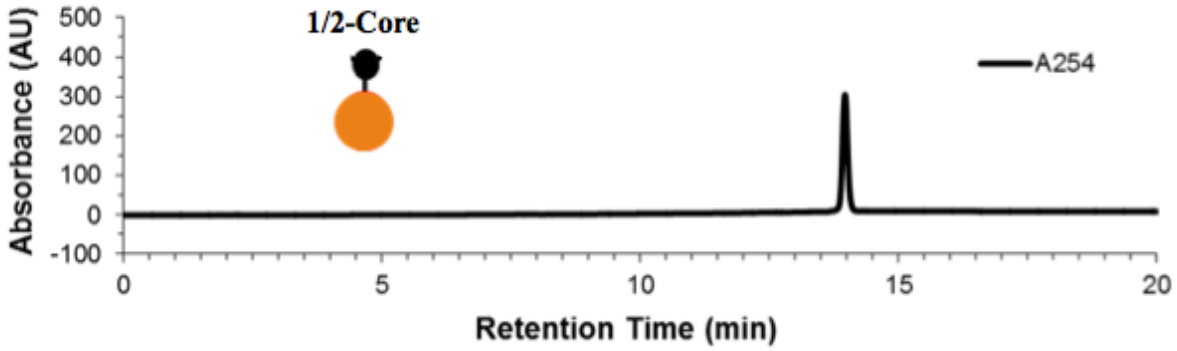

HPLC trace at 254 nm on a C8 analytical column. Solvent A: 0.1 % TFA water, Solvent B: 0.1% TFA acetonitrile. Gradient: t 0-1 min hold 50% B, t 1-11 min ramp to 90% B, t 11-20 min hold 90% B.

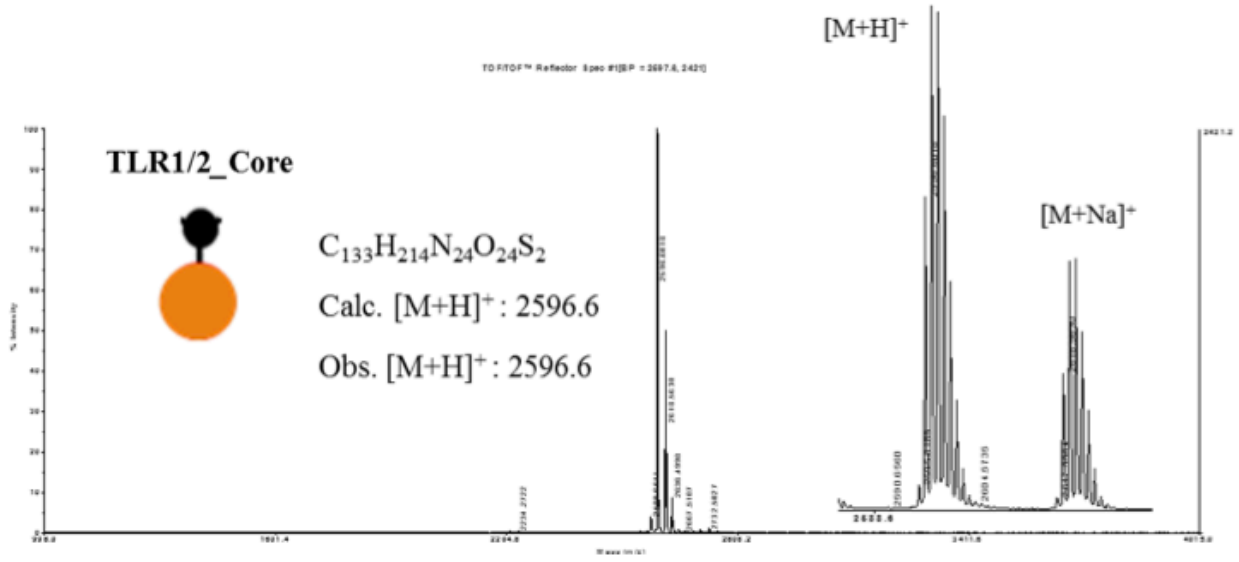

5.12 TLR1/2_4 HPLC Trace and MALDI-TOF (*provided by Tyler Albin*)

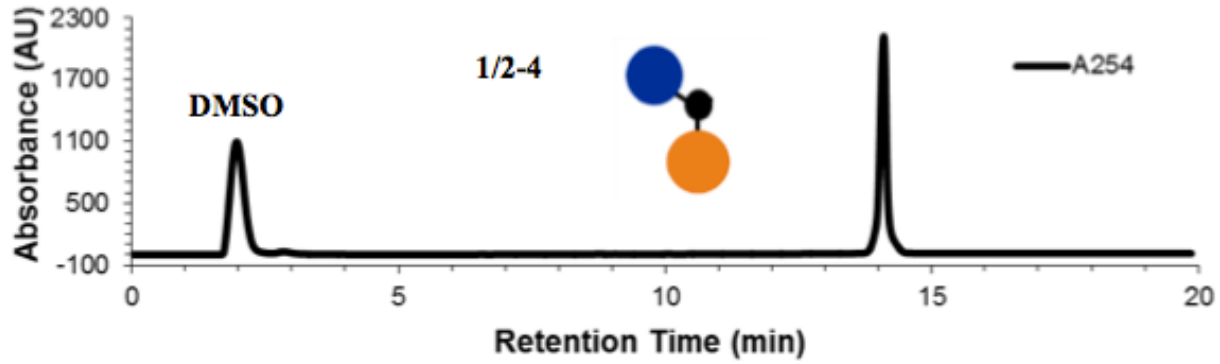

HPLC trace at 254 nm on a C8 analytical column. Solvent A: 0.1 % TFA water, Solvent B: 0.1% TFA acetonitrile. Gradient: t 0-1 min hold 50% B, t 1-11 min ramp to 90% B, t 11-20 min hold 90% B.

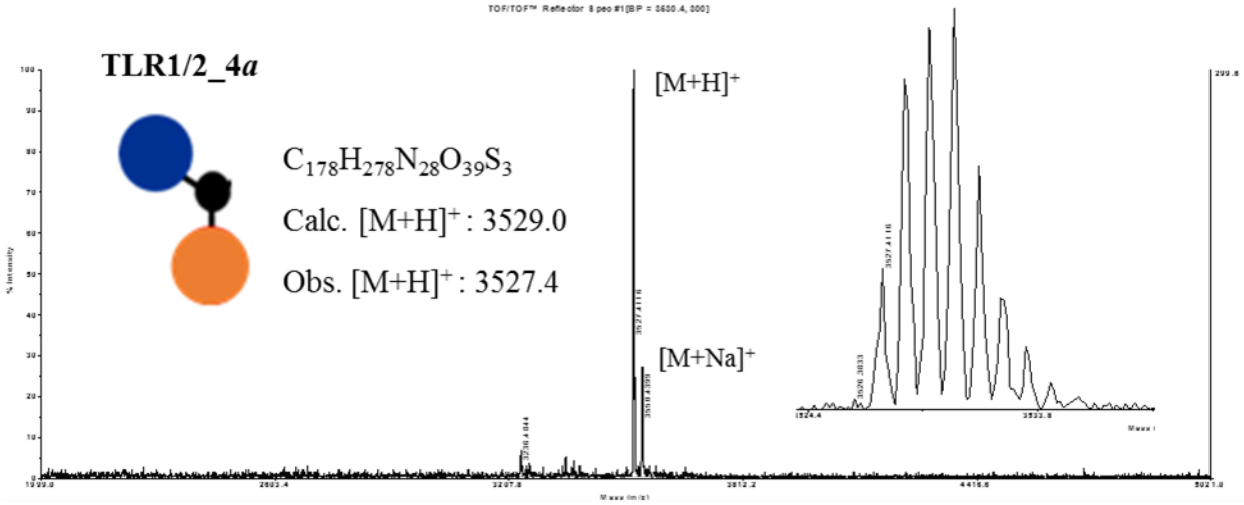

5.13 TLR1/2_4_7 Tri-Agonist HPLC Trace and MALDI-TOF

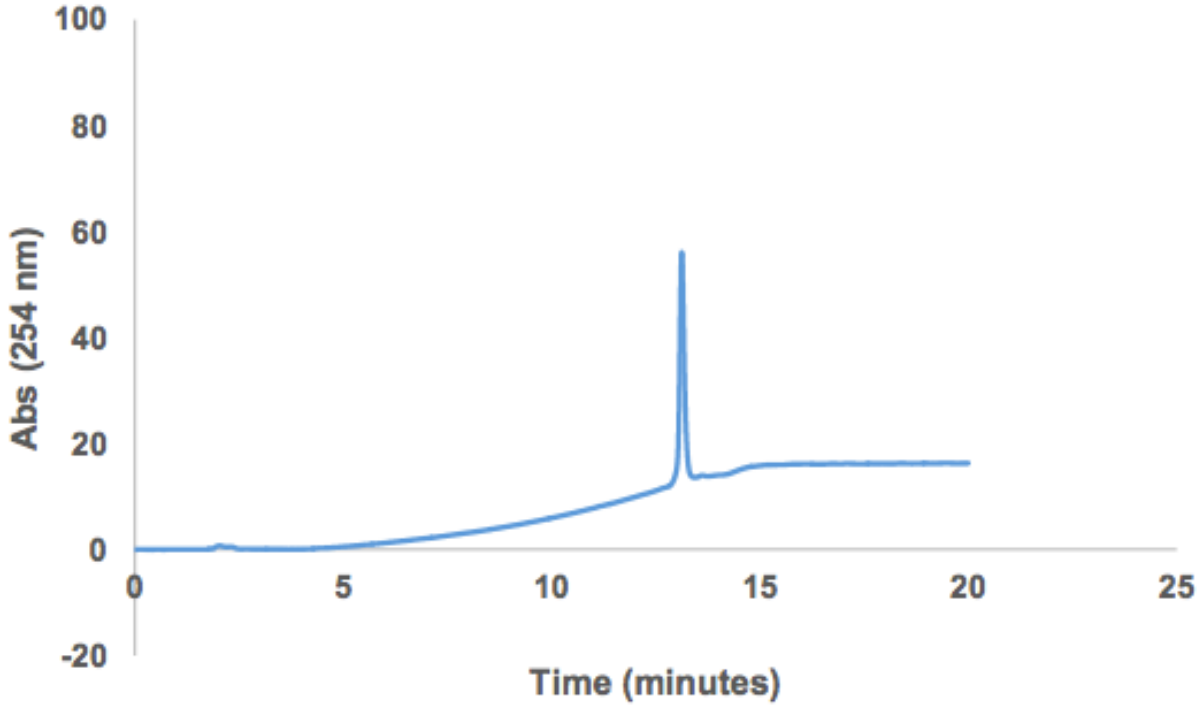

HPLC trace at 254 nm on a C8 analytical column. Solvent A: 0.1 % TFA water, Solvent B: 0.1% TFA acetonitrile. Gradient: t 0-1 min hold 50% B, t 1-11 min ramp to 90% B, t 11-20 min hold 90% B.

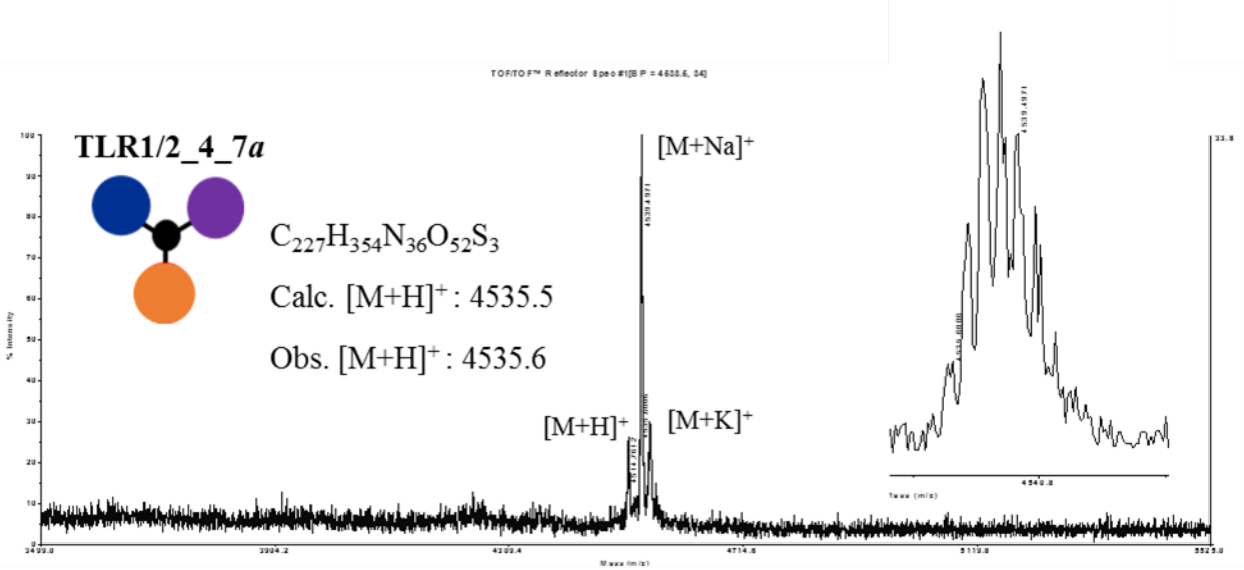

5.15 TLR2/6_7 MALDI-TOF

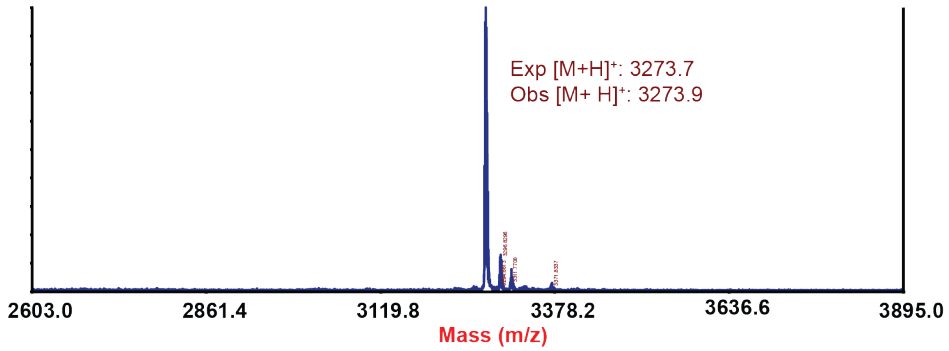

5.18 Acid Core_PEG$_{12}$-NH-Fmoc NMR Spectra

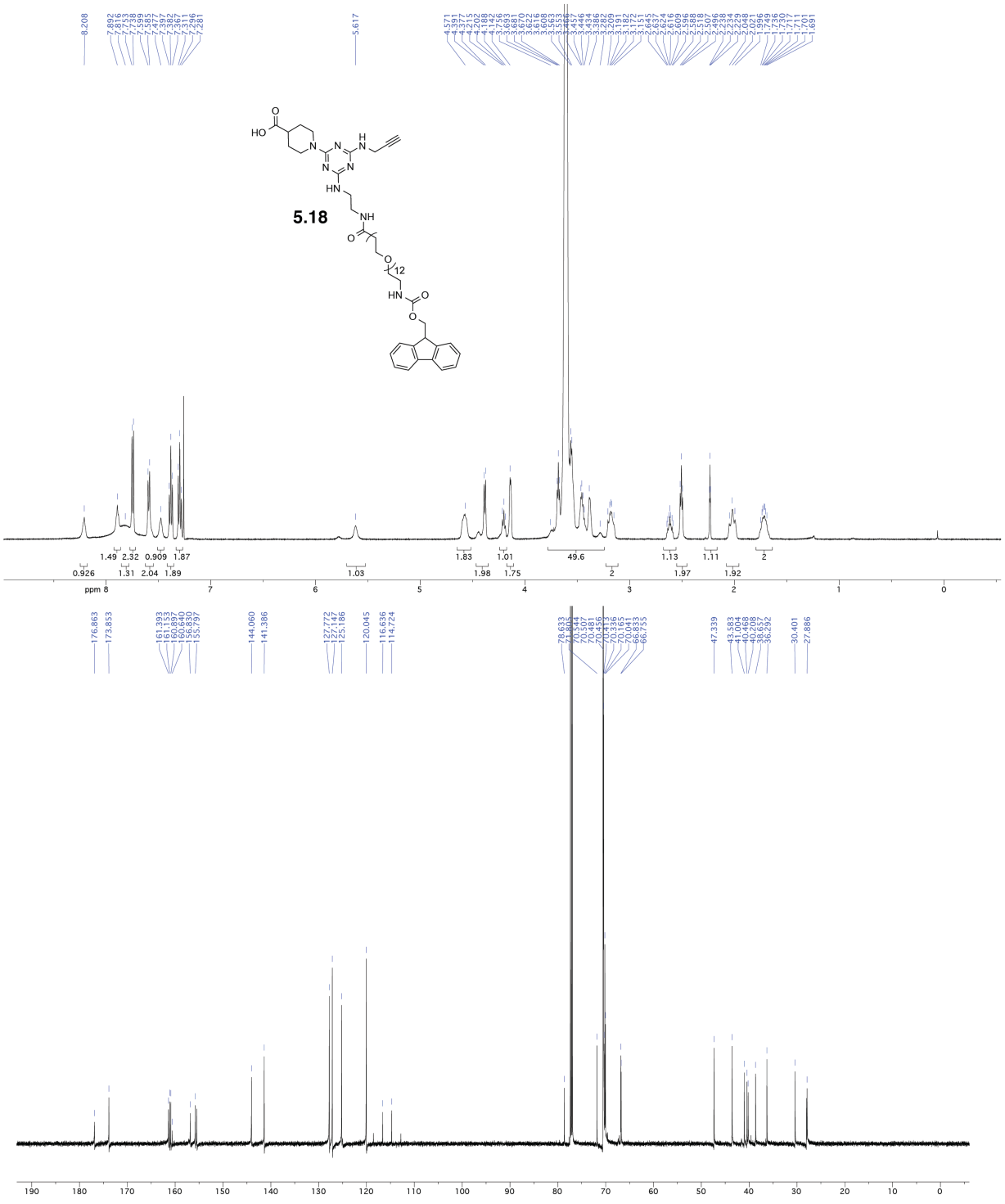

5.19 TLR4_acid core NMR Spectra and HPLC Trace

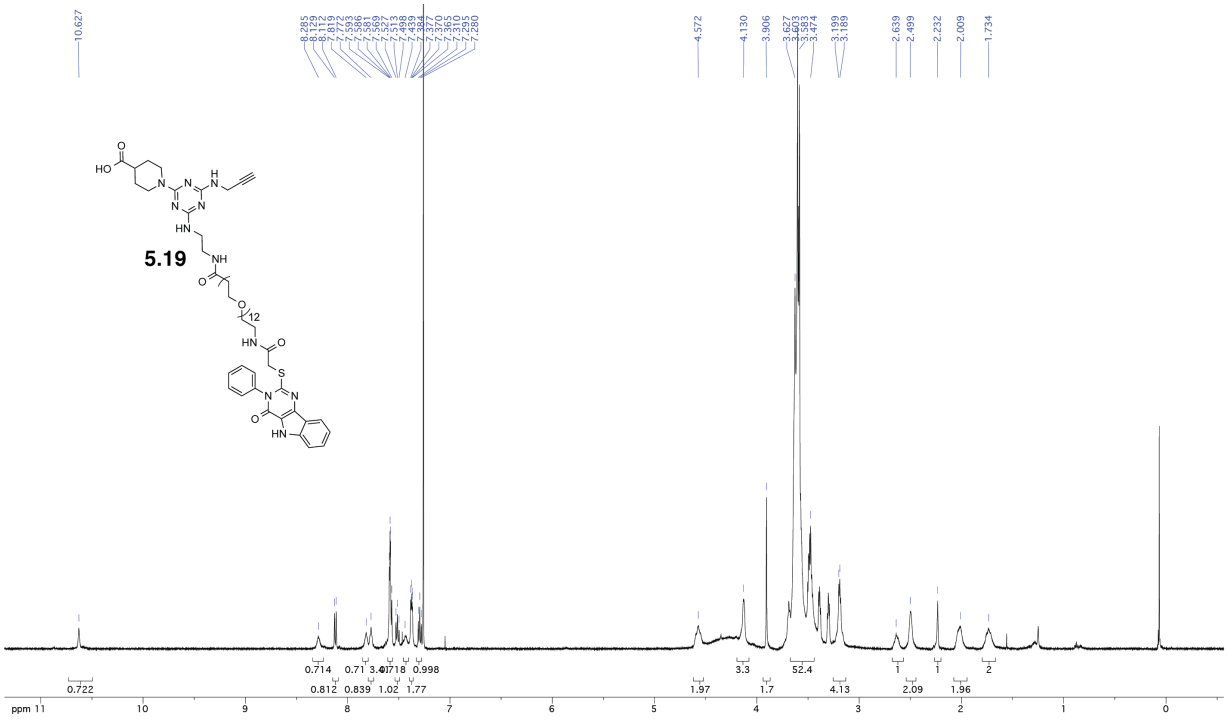

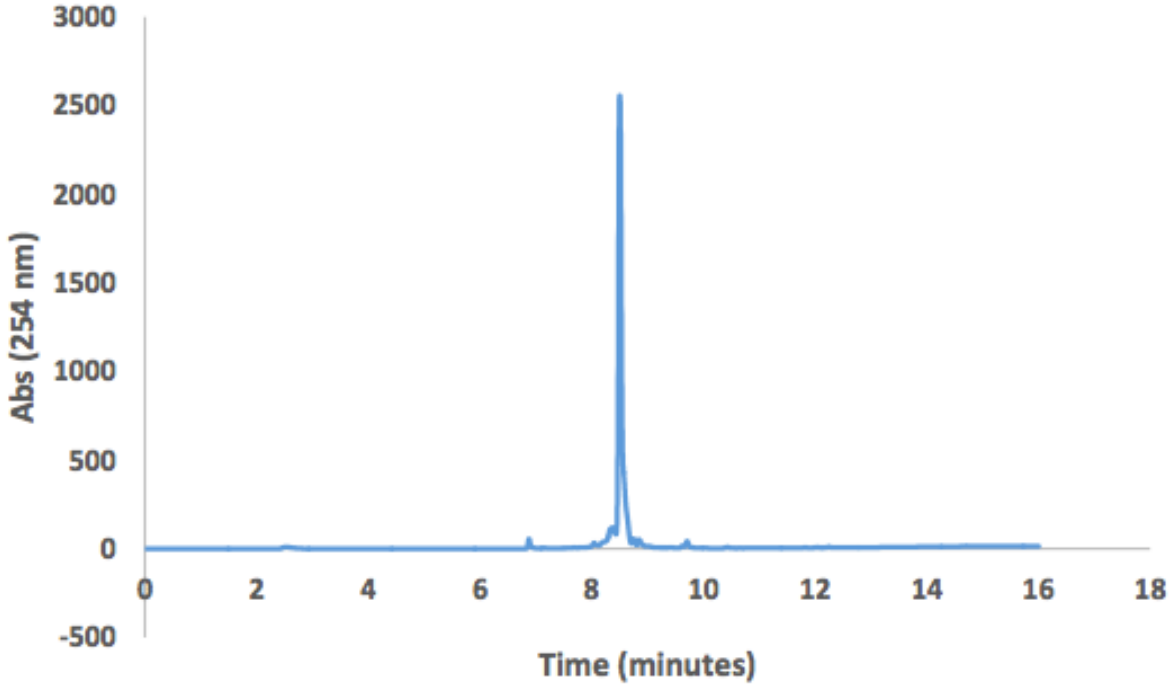

HPLC trace at 254 nm on a C8 analytical column. Solvent A: 0.1 % TFA water, Solvent B: 0.1% TFA acetonitrile. Gradient: t 0-1 min hold 10% B, t 1-11 min ramp to 90% B, t 11-16 min hold 90% B.

5.21 TLR2/6_7 HPLC Trace and MALDI-TOF

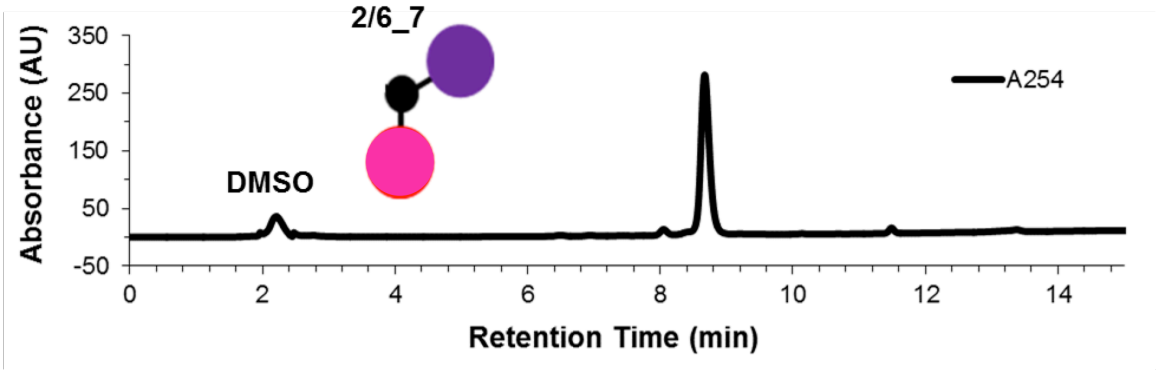

HPLC trace at 254 nm on a C8 analytical column. Solvent A: 0.1 % TFA water, Solvent B: 0.1% TFA acetonitrile. Gradient: t 0-1 min hold 50% B, t 1-11 min ramp to 90% B, t 11-15 min hold 90% B.

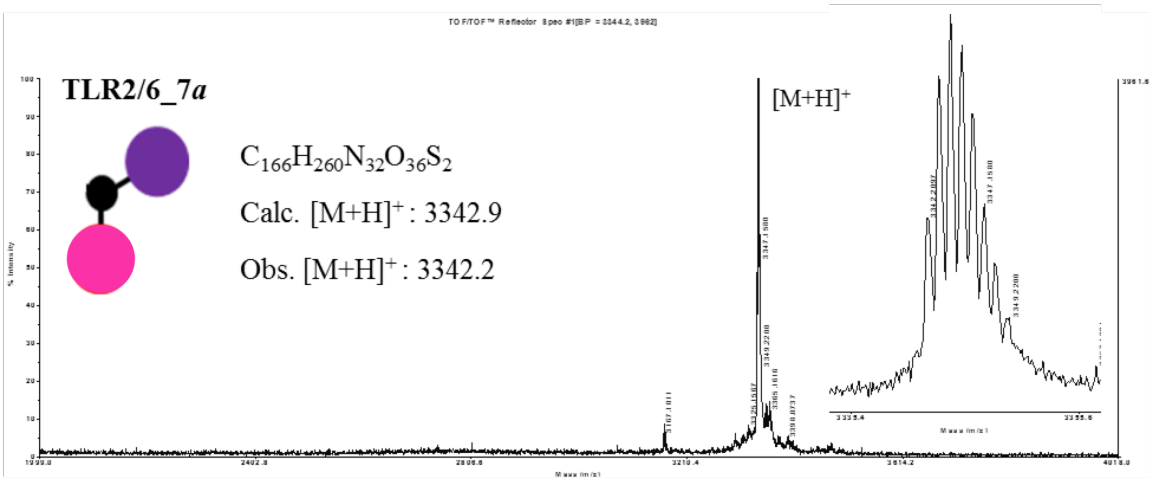

5.22 TLR4_7 HPLC Trace and MALDI-TOF

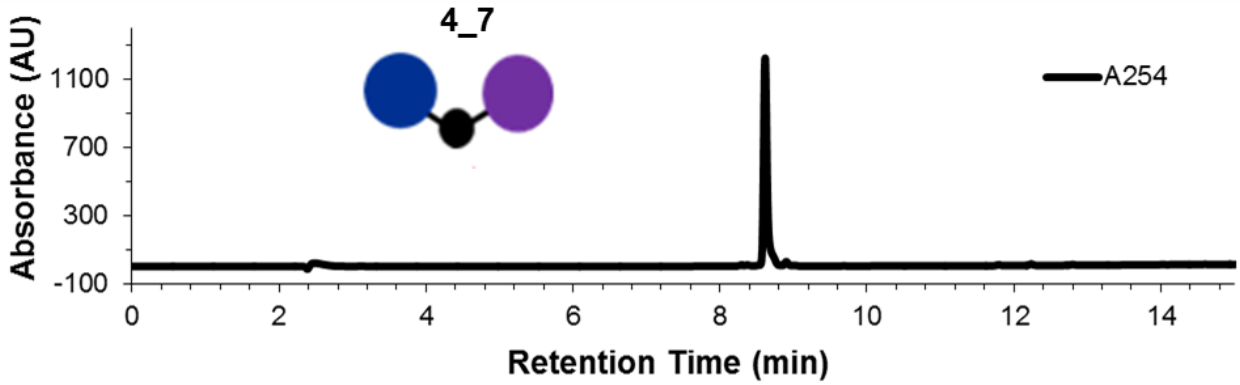

HPLC trace at 254 nm on a C8 analytical column. Solvent A: 0.1 % TFA water, Solvent B: 0.1% TFA acetonitrile. Gradient: t 0-1 min hold 10% B, t 1-11 min ramp to 90% B, t 11-15 min hold 90% B.

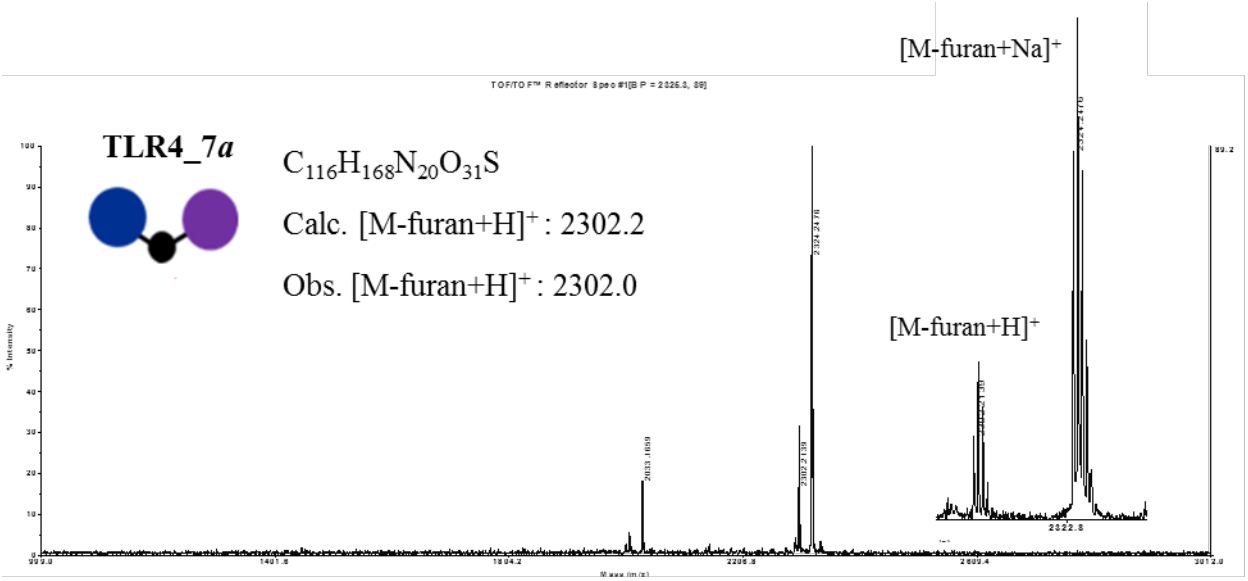

5.23 TLR1/2_7 HPLC Trace and MALDI-TOF

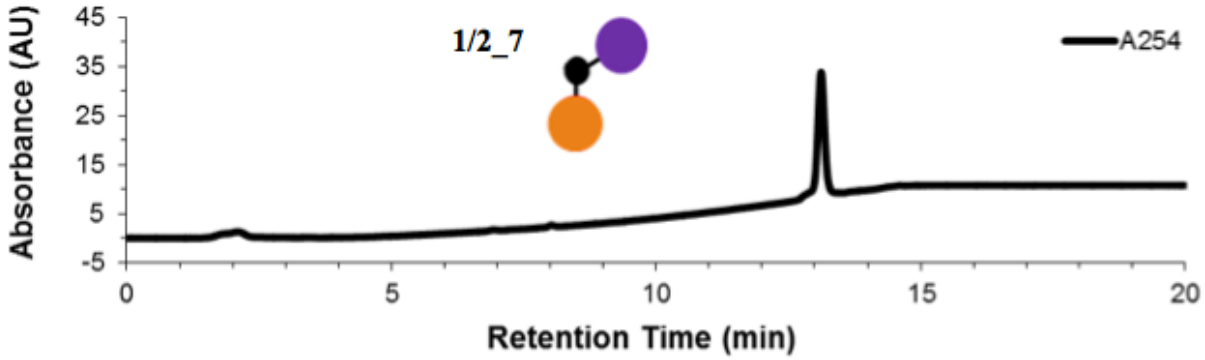

HPLC trace at 254 nm on a C8 analytical column. Solvent A: 0.1 % TFA water, Solvent B: 0.1% TFA acetonitrile. Gradient: t 0-1 min hold 50% B, t 1-11 min ramp to 90% B, t 11-20 min hold 90% B.